Regulatory roles of the cytochrome b6f complex in redox sensing and state transitions in Chlamydomonas reinhardtii

Louis Dumas

UNIVERSITÉ D'AIX-MARSEILLE

ÉCOLE DOCTORALE DES SCIENCES DE LA VIE ET DE LA SANTÉ

UMR 7265 – Institut de Biosciences et Biotechnologies d'Aix-Marseille (BIAM)

Laboratoire de Bioénergétique et Biotechnologie des Bactéries et Microalgues (LB^{3}M)

Thèse Présentée pour Obtenir le Grade Universitaire de Docteur

Discipline : Biologie

Spécialité : Biologie Végétale

Louis Dumas

Regulatory roles of the cytochrome *b*$_6$*f* complex in redox sensing and state transitions in *Chlamydomonas reinhardtii* – A structure-function study –

Soutenue le 24 Janvier 2018 devant le jury :

Michel GOLDSCHMIDT-CLERMONT – Université de Genève	Rapporteur
Francis-André WOLLMAN – IBPC Paris, CNRS UMR 7141	Rapporteur
Alison SMITH – University of Cambridge	Examinatrice
Wolfgang NITSCHKE – AMU, CNRS UMR 7281	Président du jury
Jean ALRIC – CEA, CNRS UMR 7265	Co-directeur de thèse
Gilles PELTIER – CEA, CNRS UMR 7265	Directeur de thèse
Francesca ZITO – IBPC Paris, CNRS UMR 7099	Membre invité

Abstract

Sunlight is a powerful but fluctuating energy source used by photosynthetic organisms to power the assimilation of atmospheric CO_2 into reduced carbon compounds. To optimize photosynthetic efficiency in ever-changing light conditions, organisms of the green lineage regulate the distribution of energy input between the two photosystems through state transitions. This process is governed by the redox state of the membrane pool of quinones, liposoluble electron carriers. Through a yet unknown mechanism, the cytochrome (cyt) b_6f complex detects these redox changes and transmits a signal to the state transition kinase Stt7 for its activation. In order to decipher the role of the cyt b_6f, we devised a novel experimental strategy in *Chlamydomonas reinhardtii* combining the random mutagenesis of a chloroplast gene (*petD* coding for cyt b_6f subunit IV) by error-prone PCR, chloroplast transformation and selection of clones on phototrophic growth. Analysis of variant sequences allowing proper assembly and function of cyt b_6f revealed some interesting features on the mutational robustness of this subunit in the context of its large transmembrane protein complex. Transformants were then screened by chlorophyll fluorescence emission imaging on their ability to perform state transitions. Several state transition mutants were isolated, and sequencing revealed that mutations concentrated in the stromal fg loop of subunit IV. Site-directed mutagenesis of key fg loop residues showed that substitutions of Asn122, Tyr124 and Arg125 produced mutants that are blocked in State I independently of the redox state of the PQ pool and with no adverse effects on cyt b_6f assembly and electron transfer activity. Protein-protein interaction studies provided evidence that the kinase domain of Stt7 interacts with the subunit IV fg loop and that its autophosphorylation activity depends on Arg125. We propose a model for the interaction between these two proteins as well as for the cyt b_6f-mediated mechanism of Stt7 activation.

Keywords: photosynthetic efficiency, Chlamydomonas reinhardtii, state transitions, Stt7 kinase, cytochrome b_6f complex, structure-function, random mutagenesis, error-prone PCR, chlorophyll fluorescence, protein interactions, kinase activation, Rieske/cyt b evolution.

Résumé

La lumière du Soleil est une source d'énergie puissante mais fluctuante utilisée par les organismes photosynthétiques pour permettre l'assimilation du CO_2 atmosphérique en espèces carbonées réduites. Pour optimiser l'efficacité photosynthétique en conditions de lumière changeantes, les organismes de la lignée verte régulent la distribution de l'excitation lumineuse entre les deux photosystèmes grâce aux transitions d'état. Ce processus est modulé par l'état redox du réservoir membranaire de quinones, des transporteurs d'électrons liposolubles. Par un mécanisme encore inconnu, le cytochrome (cyt) *b_6f* détecte ces changements redox et transmet un signal d'activation à la kinase des transitions d'état, Stt7. Afin de comprendre le rôle du cyt *b_6f*, nous avons mis au point une nouvelle stratégie expérimentale chez *Chlamydomonas reinhardtii* combinant la mutagénèse aléatoire d'un gène chloroplastique (*petD* codant pour la sous-unité IV du cyt *b_6f*) par PCR error-prone, la transformation chloroplastique et la sélection des clones sur leur croissance phototrophe. L'analyse des séquences variantes permettant l'assemblage et le fonctionnement du cyt *b_6f* a révélé certaines caractéristiques intéressantes de la robustesse aux mutations de cette sous-unité dans le contexte du complexe protéique transmembranaire auquel elle appartient. Les transformants ont ensuite été criblés par imagerie de l'émission de fluorescence de la chlorophylle sur leur capacité à réaliser des transitions d'état. Plusieurs mutants de transitions d'état ont été ainsi isolés, et le séquençage a révélé que les mutations impliquées étaient concentrées sur la boucle stromale fg de la sous-unité IV. La mutagénèse dirigée de plusieurs résidus clés de la boucle fg a montré que les substitutions des résidus Asn122, Tyr124 et Arg215 généraient des mutants bloqués à l'état I indépendamment de l'état redox du pool de quinones et sans effets défavorables sur l'assemblage et l'activité de transfert d'électrons du complexe. Des expériences d'interaction protéine-protéine ont ensuite servi à prouver que le domaine kinase de Stt7 interagit avec la boucle fg de la sous-unité IV et que son activité d'autophosphorylation dépend du résidu Arg125. Nous proposons un modèle de l'interaction entre ces deux protéines ainsi que du mécanisme d'activation de la kinase médié par le cyt *b_6f*.

Mots-clés : efficacité photosynthétique, Chlamydomonas reinhardtii, transitions d'état, kinase Stt7, complexe cytochrome b_6f, structure-fonction, mutagénèse aléatoire, PCR error-prone, fluorescence de la chlorophylle, interactions protéiques, activation de kinase, évolution des complexes Rieske/cyt b.

Acknowledgments – Remerciements

Ces trois dernières années ont été une période très enrichissante pour moi, pendant laquelle j'ai énormément appris sur le plan scientifique autant que sur le plan personnel ; j'ai beaucoup de personnes à remercier pour cela !

Tout d'abord, merci à ***David****, mais aussi* ***Camille*** *et* ***Catherine****, du LBC de m'avoir accueilli et formé au printemps 2013 pendant mon stage de M1. Cela m'a permis de découvrir la Provence, le CEA et la biologie moléculaire et a beaucoup joué dans ma décision de poursuivre en thèse par la suite. Merci à David également de m'avoir conseillé au moment du choix du sujet de thèse, je lui en suis très reconnaissant.*

Gilles*, merci de m'avoir accueilli au sein du laboratoire et de m'avoir suivi tout au long de la thèse. Cela peut paraitre évident, mais on l'oublie facilement : tout ce travail n'aurait pas été possible sans les ressources humaines qu'a la chance de posséder ce laboratoire. Je pense en particulier aux personnes qui font tourner le labo : merci à toi* ***Stéphane****, de toujours trouver le temps d'aider et pour ta capacité à garder ton calme en situation de crise ;* ***Pierre****, pour tes blagues généreuses et ta bonne humeur ;* ***Stéphanie*** *pour toute ton aide et ta capacité à supporter à la fois le froid et moi-même pendant de longues heures de purif,* ***Pascaline*** *pour ton aide et tes conseils, mais aussi* ***Véronique*** *et* ***Audrey*** *qui, entre autres, s'assurent que le labo fonctionne en continu.*

J'aimerais remercier ***Bernard*** *et* ***Pascal*** *d'avoir participé à mon comité de thèse et d'avoir toujours été disponibles pour discuter de sciences et de tout et n'importe quoi. Un grand merci également aux membres du* ***jury*** *pour l'attention qu'ils ont portée à mon travail.*

Au cours de ces trois dernières années, j'ai pu me rendre compte de l'importance fondamentale de l'environnement humain dans le succès d'une thèse ou de tout travail scientifique. Pour cela, je m'estime très chanceux et je vous remercie infiniment, ***Jean*** *et* ***Xenie****, de m'avoir accueilli dans votre univers et aidé à construire ma propre vision de ce processus fabuleux qu'est la photosynthèse.*

J'aimerais te remercier tout particulièrement, ***Jean****, de m'avoir très vite fait confiance et laissé une grande liberté, tout en sachant précisément comment me conseiller ou me recentrer quand cela était nécessaire. J'ai beaucoup appris de toi autant sur la science pure que sur la méthode scientifique, la communication, la présentation de résultats, la rédaction… des outils qui me serviront toute ma vie. Tu valorises la rigueur dans l'expérimentation et l'analyse des résultats, tout en laissant une liberté totale aux idées nouvelles et au fait de suivre ses intuitions ; je pense que c'est une bonne recette et je compte m'y tenir par la suite. On a fait bonne équipe, j'espère que l'aventure ne s'arrêtera pas là !*

Cara ***Francesca****, grazie infinite ! Une grande part de ce travail, si ce n'est l'ensemble de ce travail, n'aurait pas été possible sans ta collaboration. J'ai beaucoup apprécié travailler avec*

toi à Paris et découvrir l'univers de l'IBPC. En parlant de ces manips, je me dois de te remercier ***Sandrine*** *de nous avoir plusieurs fois épaulés (en échange de quelques éclairs au chocolat, bien sûr ! ...). Merci aussi à toi* ***Daniel*** *d'avoir plusieurs fois pris le temps de discuter avec moi et de nous avoir donné certains détails structuraux cruciaux !*

Merci à vous bien sûr, collègues et amis, pour tous les joyeux moments, les nombreuses soirées et les quelques vacances partagées. Sans vous, ces trois années ne seraient pas remplies d'autant de souvenirs : ***Fred****,* ***Camille****,* ***Ivana****,* ***Margot****,* ***Marie****,* ***Inès****,* ***Ludo****,* ***Charlie****, ainsi que toute la* ***section plongée*** *de Cadarache avec qui j'ai passé de nombreux dimanches dans les calanques à bord de Cas'Cad !*

Merci à mes sœurs ***Juliette*** *et* ***Marion*** *et surtout à mes* ***parents*** *qui m'ont toujours apporté le soutien nécessaire pour pouvoir entreprendre mes projets, et inculqué la curiosité et l'éthique de travail requises pour en arriver à présenter ma thèse. Merci à toi, ma* ***Claire****, pour ta patience et tes encouragements pendant toute cette dernière année.*

Enfin, merci ***Chlamy****, pour ta coopération et ton efficacité. J'espère qu'on va pouvoir continuer à collaborer…*

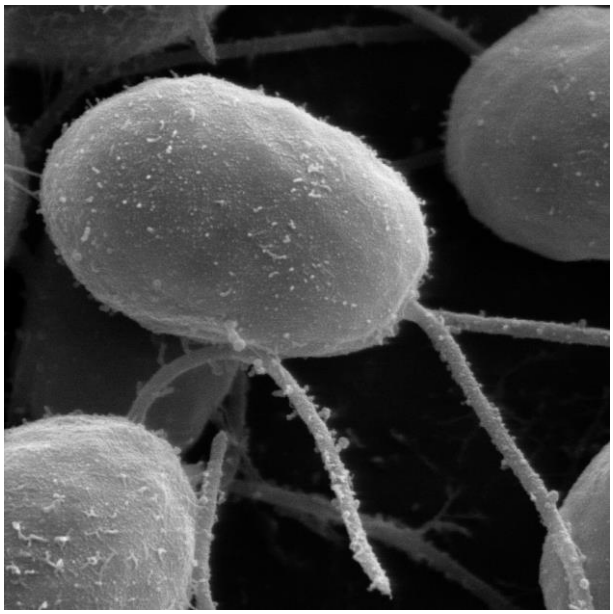

Table of contents

Foreword and Context

Ideas emerge when a part of the real or imagined world is studied for its own sake.

– E. O. Wilson

Solar irradiance is the main power source on our planet, representing 137 000 TW compared to the 47 TW of heat flow from the Earth core to the surface. A significant part of the solar spectrum ranges from 400 to 700 nm and is also denoted "visible region" or PAR for "Photosynthetically Active Radiation" (Figure 1A). The development of life on Earth as we know it was made possible by the emergence of organisms that evolved the ability to harvest and convert sunlight energy. The entire photosynthetic process, in prokaryotes or eukaryotes, relies on a few common principles (Figure 1B) whose functions were given by the evolution of complex molecular structures embedded in highly organized lipid membranes: light harvesting complexes (pigment-containing proteins), photochemistry and charge separation (reaction centers), long-range electron transport (soluble electron carriers), coupling of electron transfer to proton translocation to generate a membrane electrochemical potential (Rieske/cytochrome *b*) used for ATP synthesis (ATP synthase), and synthesis of carbohydrates (Calvin-Benson-Bassham cycle enzymes). Of the 5 x 10^{24} J of solar energy received by the Earth per year, 5% (2.8 x 10^{23} J) is absorbed by photosynthetic pigments and 0.5% (4.0 x 10^{21} J) is converted and stored as reduced carbon molecules (Antal et al. 2013).

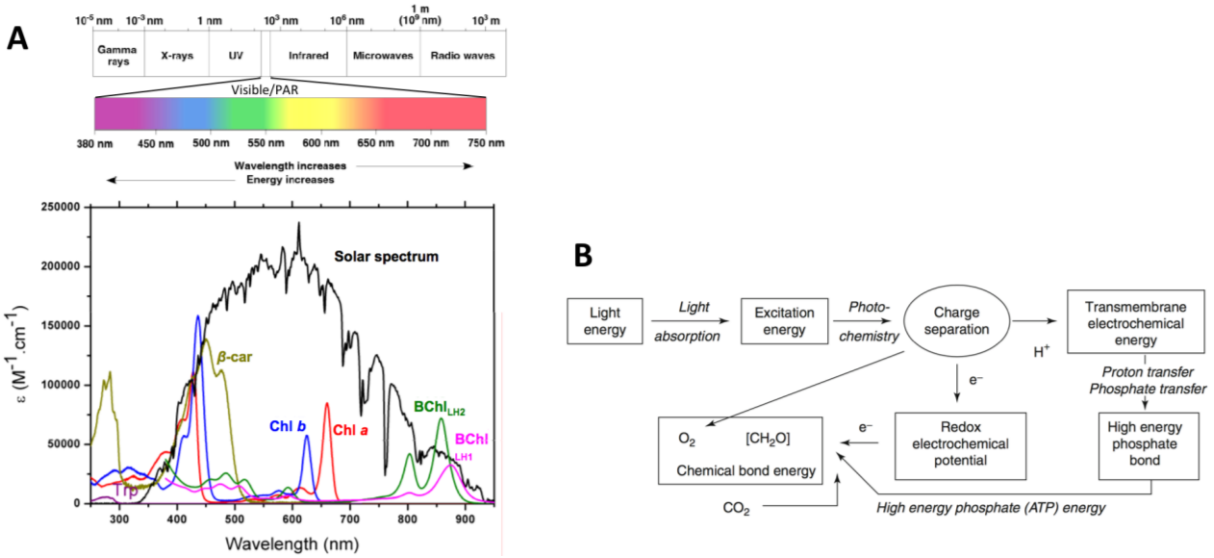

Figure 1. Photosynthesis converts solar energy through conserved mechanisms.
(A) Solar irradiance spectrum and absorption spectra of various pigments of oxygenic (chlorophyll, carotene) and anoxygenic (bacteriochlorophylls) photosynthesis. (B) Common principles of energy transformation in photosynthesis (from (Bjorn 2015)).

Over recent years, the apparent inefficiency of the system has prompted researchers to look at each of these core functions and determine which components could be redesigned in order to improve photosynthetic efficiency in an effort to “meet global food and energy demand” (Ort et al. 2015). This was also the context of my Ph.D. project when I first embarked on this journey: to re-engineer a photosynthetic complex, the cytochrome b_6f complex, in order to generate mutants with a higher photosynthetic efficiency. However, as I was drowning into the abundant literature on photosynthesis in general and on the cytochrome b_6f in particular, I got a grasp of the complexity of the system and soon realized that unbridling photosynthetic electron and proton transfer would probably take more time than what is available in a 3-year Ph.D. I also started to look for "grey areas" in our knowledge of the cytochrome b_6f complex, other than the thoroughly-studied electron transfer functions that it shares with its ancestors, the bacterial and mitochondrial cytochrome bc_1 complexes. The cytochrome b_6f complex is implicated in several sensing and acclimation mechanisms of photosynthesis, functions acquired through the evolution of a quinol oxido-reductase (ancestral *b*-type cytochrome) in the driving belt fitted to the two photosystems of oxygenic photosynthesis found in cyanobacteria and chloroplasts. In particular, I noticed that there was still a big gap in our understanding of how the cytochrome b_6f senses the redox state of the quinone pool and activates the Stt7 kinase during state transitions. Jean agreed that his idea of performing a random mutagenesis of the complex coupled to a chlorophyll fluorescence emission screen could be used to probe the regions involved in an interaction or signal transduction toward Stt7 and, with the help of Francesca, we set off on this path.

This Ph.D. thesis is therefore a fundamental study of the sensing and regulatory roles of the cytochrome b_6f complex during state transitions in *Chlamydomonas reinhardtii*. A thorough understanding of this mechanism could have important implications because state transitions are a central regulator of energy flow in photosynthesis and control the balance of excitation energy between PSII and PSI, which in turn directly influences the maximal quantum yield of the entire process.

CHAPTER I – Introduction

A. Photosynthesis

1. General aspects, origin and evolution

Photosynthetic organisms form the base of the food chain on Earth as the major contributors to primary productivity. On a global scale, photosynthesis and respiration represent massive carbon fluxes among the many biogeochemical processes that participate in the carbon cycle. Oxygenic phototrophs transform solar irradiance into chemical energy in the form of reduced organic compounds by reducing atmospheric CO_2 using electrons taken from the photolysis of water which releases oxygen:

$$6CO_2 + 6H_2O + h\nu \rightarrow C_6H_{12}O_6 + 6O_2$$

Their ancestors, anoxygenic phototrophs, use compounds other than water as their primary electron donor (Blankenship 2013). Green-sulfur bacteria, for example, oxidize compounds such as hydrogen sulfide and do not generate oxygen in the process.

Our understanding of the origin and evolution of life on Earth largely depends on our knowledge of how the first energy-converting mechanisms emerged. Haldane's long-standing "primordial soup" theory, which hailed fermentation as the first mechanism of energy generation (Haldane 1929), has been put aside in favor of the "chemiosmotic-alkaline hydrothermal vent" hypothesis (Lane et al. 2010) which hails chemiosmotic coupling (see Section I.A.3.) as the founder of bioenergetic systems. The first autonomous cells most likely used energy conversion mechanisms akin to chemiosmosis and sulfur respiration. Later on came photosynthesis and oxidative phosphorylation, whose emergence necessitated many (phylogenetically diverse) enzymes.

Although photosynthesis came "late", the advent of oxygenic photosynthesis in the ancestors of modern cyanobacteria around 3.5 Gya was the most impactful biological innovation in Earth's history (Figure I.1). The use of water as a primary donor for energy conversion and reducing power meant that life no longer depended on geochemically-derived reductants.

Global primary productivity surged and the oxygen released through water oxidation completely transformed the redox state of the Earth's atmosphere and oceans, leading to a permanent reorganization of the global biogeochemical cycles. The evolutionary trajectory of life's major metabolic pathways was also greatly influenced because aerobic conditions favored organisms that adapted their bioenergetics to resist and utilize oxygen (i.e. aerobic respiration and fermentation).

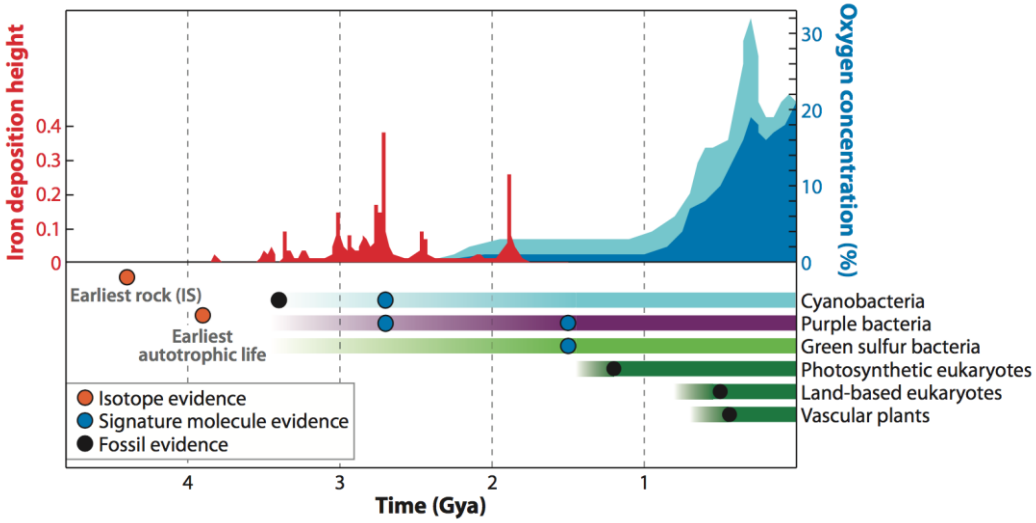

Figure I.1. The Earth's geological history is linked to the emergence and evolution of photosynthesis. As labelled in the original publication (Hohmann-Marriott and Blankenship 2011), "*minimum and maximum estimates for oxygen concentration are indicated by dark blue and light blue areas, respectively*".

In turn, the Earth's physical and chemical environment shaped the evolution of the molecular structures, electron carriers, redox cofactors, light-harvesting pigments and carbon fixation modes of photosynthesis throughout its history. The evolutionary history of photosynthetic organisms is a matter of great debate. The complexity of reconstructing it stems from the fact that different components of the photosynthetic process seem to have followed independent evolutionary pathways (Hohmann-Marriott and Blankenship 2011), and that there is evidence for extensive lateral gene transfer between organisms and phyla (Raymond et al. 2002). There is therefore no single conserved evolutionary history among phototrophs, although several models have been proposed to explain the phylogenetic distribution of phototrophy (reviewed in (Fischer et al. 2016). A central question is to determine the distinct paths of FeS-type reaction centers (RC1) and Q-type reaction centers (RCII) and to understand how they gave rise to the PSII-PSI setup of oxygenic photosynthesis in Cyanobacteria. Anoxygenic phototrophs are found in seven different bacterial phyla that are scattered throughout the tree of life: Proteobacteria (purple bacteria, RCII), Chloroflexi (filamentous green non-sulfur bacteria,

RCII), Chlorobi (green sulfur bacteria, RCI), Firmicutes (Heliobacteria, RCI), Acidobacteria (RCI), Gemmatimonadetes (RCII), and Cyanobacteria (RCII + RCI) (Figure I.2). Phylogenetic analysis reveals that each photosynthetic group emerged late within these phyla, suggesting that none of the latter stemmed from a photosynthetic ancestor.

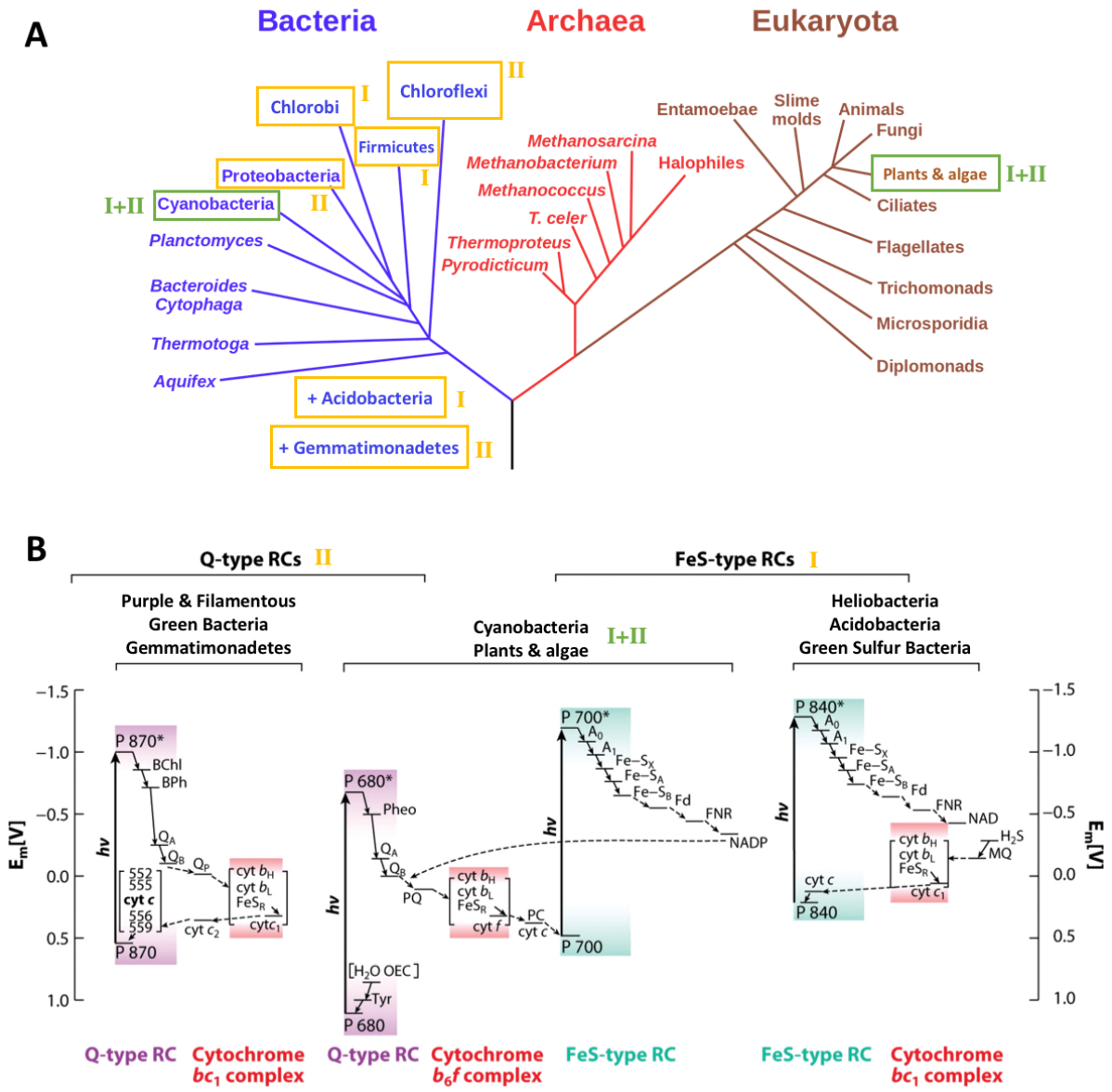

Figure I.2. Phylogenetic distribution and diversity of photosynthetic organisms.
(A) Evolutionary tree of life with anoxygenic (orange) and oxygenic (green) phototrophs boxed. The recently identified Acidobacteria (Bryant et al. 2007) and Gemmatimonadetes (Zeng et al. 2014) phyla were not present in the original figure (adapted from (Blankenship 2002)). The type of RC (I, II or I+II) found in each phylum is indicated. **(B)** Overview of the various combinations of RC and cyt *b* complexes forming the electron transport chains of anoxygenic-RCII (left), anoxygenic-RCI (right) and oxygenic PSII+PSI (middle) phototrophs. Cofactors are placed according to their redox midpoint potentials. Adapted from (Hohmann-Marriott and Blankenship 2011).

The chloroplast of eukaryotic oxygenic photosynthetic organisms emerged through endosymbiosis, when a heterotrophic (proto?)eukaryotic host cell captured and stably integrated a cyanobacterium that ultimately turned into a plastid (Schimper 1883; Mereschkowsky 1905; Margulis 1981; Martin and Kowallik 1999). This primary endosymbiosis event may have happened around 1-1.5 Gya and was followed by secondary endosymbiosis events that gave rise to the three known lines of photosynthetic eukaryotes: Glaucophytes, Rhodopythes and Chlorophytes. These successive endosymbiotic events played a crucial role in distributing photosynthesis throughout Eukarya (Keeling 2010). Most genes of the plastid ancestors have been either lost or transferred to the nucleus of the host cell (Martin et al. 1998). For example, the chloroplast genome of Chlorophytes (also called "green lineage") has retained about 3% of the genes of its cyanobacterial ancestor (~100 of ~3000), which code for photosynthetic complex subunits and regulators of chloroplast gene expression (Figure I.3). As a result, eukaryotic phototrophs possess complex networks of gene expression that coordinate the nuclear, chloroplast and mitochondrial genomes. Among other things, this relies on post-transcriptional regulations by nucleus-encoded factors (Choquet and Wollman 2002), regulation of subunit accumulation through the Control by Epistasy of Synthesis (CES, (Choquet and Wollman 2009)), and various protein import pathways.

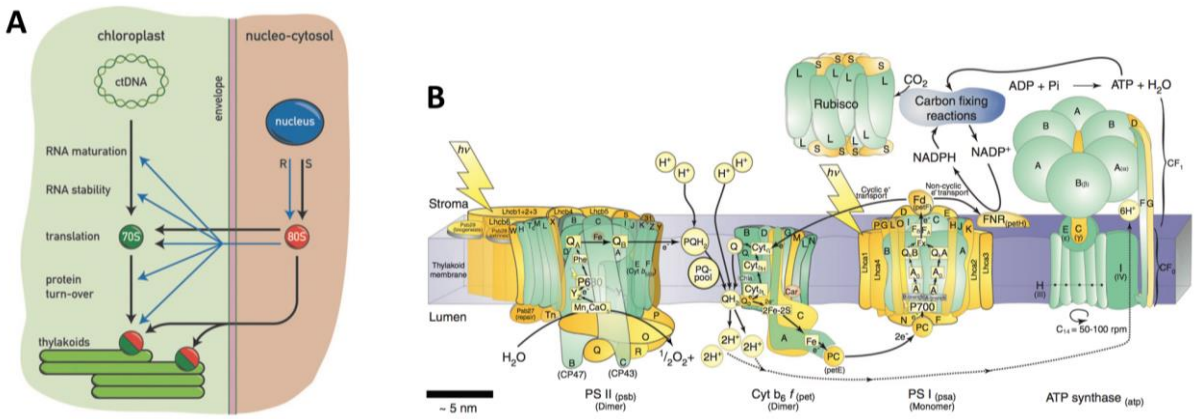

Figure I.3. The endosymbiotic origin of eukaryotic phototrophs accounts for the complexity of the biogenesis and assembly of their photosynthetic apparatus.
(A) Scheme of the cooperation between the chloroplast and nucleocytosolic compartments, depicting the chloroplast- and nucleus-encoded subunits (S, black arrows) and the nucleus-encoded factors (R, blue arrows) required for post-transcriptional regulation of chloroplast gene expression (Rochaix 2013). **(B)** Photosynthetic apparatus of eukaryotic phototrophs (nomenclature for *A. thaliana*), with chloroplast- and nuclear-encoded subunits colored in green and yellow, respectively (Allen et al. 2011).

2. *Localization and composition of the photosynthetic machinery*

The photosynthetic machinery of oxygenic photosynthetic eukaryotes is localized in the chloroplast, a 5-10 µm plastid-type organelle (Figure I.4). The chloroplast is surrounded by an envelope of two membrane bilayers separated by an intermembrane space. The space inside the chloroplast inner membrane is called the stroma and contains the chloroplast genome, the ribosomal protein synthesis machinery, some components of the cell's carotenoid, chlorophyll and lipid biosynthesis pathways, the enzymes of the Calvin-Benson-Bassham (CBB) cycle involved in carbon fixation and other components such as proteases, chaperones and assembly factors. Inside the chloroplast are also found highly organized membrane structures called thylakoids that form a closed compartment with a lumenal space and house all the components that make up the electron transport chain.

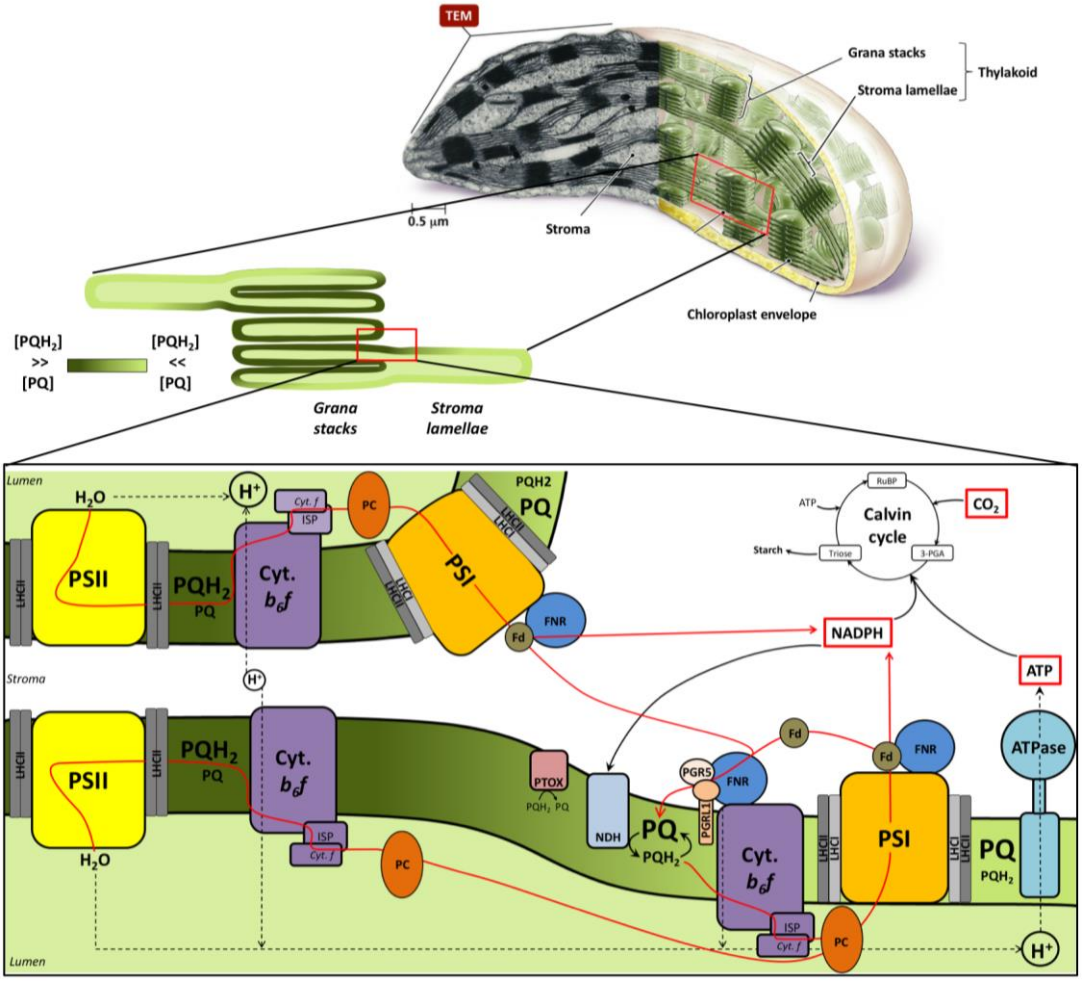

Figure I.4. The chloroplast is where the magic *(of oxygenic photosynthesis)* happens.
Exploding diagram of the chloroplast, thylakoid membrane unit and photosynthetic chain components. The network of thylakoid membranes is arranged in appressed stacks ("grana", containing PSII and cyt b_6f, and a more reduced PQ pool) linked by non-appressed membranes ("stroma lamellae", containing PSI, cyt b_6f, and ATP synthase, and a more oxidized PQ pool). Red arrows: electron transport; dashed lines: proton influx and efflux. Adapted from (Dumas et al. 2016).

The “light reactions” of photosynthesis, as opposed to the “dark reactions” of the CBB cycle, make use of large membrane protein complexes (PSII, cyt b_6f, PSI and ATP synthase) containing pigments (chlorophylls and carotenoids) and cofactors (hemes and metal clusters), as well as liposoluble electron carriers (quinones) and hydrosoluble proteins (plastocyanin (PC), ferredoxin (Fd), ferredoxin-$NADP^+$ reductase (FNR)). Before getting into the molecular mechanisms of oxygenic photosynthesis, a brief description of the major complexes of the electron transport chain is provided, except for the cyt b_6f that will be described in detail in a separate section.

PS II (water-plastoquinol oxidoreductase) is a homodimeric supercomplex composed of both transmembrane proteins and extrinsic (lumenal) proteins. Depending on the organism, the ~350 kDa PSII monomer is composed of ~20 subunits and many cofactors: 35 chlorophylls, 12 carotenoids, 2 pheophytines, one non-hemic iron, two calcium ions, four manganese ions, two chloride ions, 2 quinones, 2 hemes and 25 lipids. These numbers are based on a recent structure of a cyanobacterial PSII (Guskov et al. 2009) and can serve as references for PSII complexes of green lineage organisms. The complex encompasses the PSII core, the water-oxidation or oxygen-evolution complex (OEC) and the LHCII antenna system. The core and LHCII proteins are embedded in the membrane, whereas the OEC is extrinsic to the membrane. The complex is often viewed as three modules: the electron-donor side in the lumen containing the Mn_4Ca cluster of the OEC protected and stabilized several by extrinsic proteins, the electron-acceptor side containing the quinone binding pockets Q_A and Q_B on the stromal side of the membrane, and the central transmembrane module containing the necessary components for charge separation (including the P_{680} chlorophyll special pair) and electron transfer from the donor to the acceptor side. PS II are mostly found in the appressed grana of thylakoids.

PSI (plastocyanin-ferredoxin oxidoreductase) is a chlorophyll-protein complex composed of 14 polypeptides. The PSI core is formed by a heterodimer of the two paralogous PsaA et PsaB proteins (~83 kDa each) and is associated to other smaller peripheral subunits. At variance with PSII, its core complex binds ~80-100 Chl *a* and ~20 β-carotene molecules, as well as the other electron transfer cofactors, classifying it as a fused antenna/reaction center system. The core proteins and cofactors form two potential electron transfer chains from plastocyanin to ferredoxin, along three Chl *a* pairs (including the P_{700} special pair), a phylloquinone pair and

three iron-sulfur clusters. PSI are mostly found in the non-appressed stroma lamellae of thylakoids.

The ATP synthase is a 600 kDa protein complex formed by 9 subunits organized in two domains that couples the translocation of protons from the lumen to the stroma to the phosphorylation of ADP into ATP. The CF_0 domain is embedded in the thylakoid membrane and composed of four subunits, and the CF_1 domain exposed to the stroma and composed of five subunits. Subunits from each of these domains form the "rotor" and "stator" parts of this enzyme that has been likened to a rotary motor. The number of units forming the ring-like structure of subunit III of the CF_0 domain determines the ratio of translocated proton to synthesized ATP molecule, and it can vary between 8 to 15 depending on the organism. In all cases, one full rotation of the subunits forming the rotor leads to the synthesis of three ATP molecules.

3. Molecular mechanisms and regulations of oxygenic photosynthesis

Proton motive force and chemiosmotic coupling

At the time when the notions of oxidative phosphorylation (work by Kalckar, Belitzer and many others in the first half of the 20th century (Prebble 2010)) and photophosphorylation (Arnon et al. 1954) were being conceptualized, there was no clear understanding of what could be the intermediate between electron flow and ATP synthesis, *i.e.* how the energetically unfavorable phosphorylation of ADP to ATP was achieved. It was proposed that electron transfer could produce high-energy intermediates that would promote the direct transfer of phosphoryl groups to form ATP (Slater 1953). In 1961, realizing that only membrane-enclosed organelles catalyzed these phosphorylations, Peter Mitchell formulated a radically new idea: a chemiosmotic-type mechanism could couple electron and proton transfer to the phosphorylation of ADP (Mitchell 1961). In this model, the energy potential created by electrochemical ion gradients across the bioenergetic membrane is sufficient to drive an uphill reaction. The membrane harbors two types of proton pumps: one that builds up the proton gradient across the membrane as it transfers electrons along the membrane, and one that dissipates the proton gradient while converting its energy into the energy-rich bonds of ATP using ADP and inorganic phosphate.

As its name indicates, two components make up the *electrochemical* proton gradient $\Delta\mu H^+$:

- the difference in proton concentration across the membrane (ΔpH, osmotic force) generated by the release of protons into the lumen during water oxidation at PSII and the translocation of protons from the stroma to the lumen in the Q-cycle of the cyt b_6f (see Section I.B.4.).
- the difference in electrical potential between the stroma and the lumen ($\Delta\Psi$) due to the charged nature of protons and to the charge separation in the photochemical reaction centers.

The electrochemical proton gradient, or *proton motive force* (*pmf*), is related to the pH and electric potential differences across the membrane by the following equation:

$$\Delta\mu H^+ = -F\Delta\Psi + 2.3RT\Delta pH$$

where F is the Faraday constant, R the gas constant, and T the temperature in Kelvin.

Electron flow and regulations

Light energy in the visible and near-infrared regions of the solar spectrum is absorbed by pigments (chlorophylls and carotenoids) bound by transmembrane proteins forming the light-harvesting complexes (LHC) of PSII and PSI. The protein scaffolds optimize the spatial arrangement of pigments and favor the funneling of excitation energy toward the reaction centers. Excitation of the PSII P_{680} and PSI P_{700} chlorophyll special pairs transform them transiently into strong reductants that enable a sequential electron transfer reaction from water to $NAPD^+$ through gradually increasing redox potentials following the Z-scheme (Figure I.5) (Hill and Bendall 1960). This electron transfer pathway is called linear electron flow (LEF).

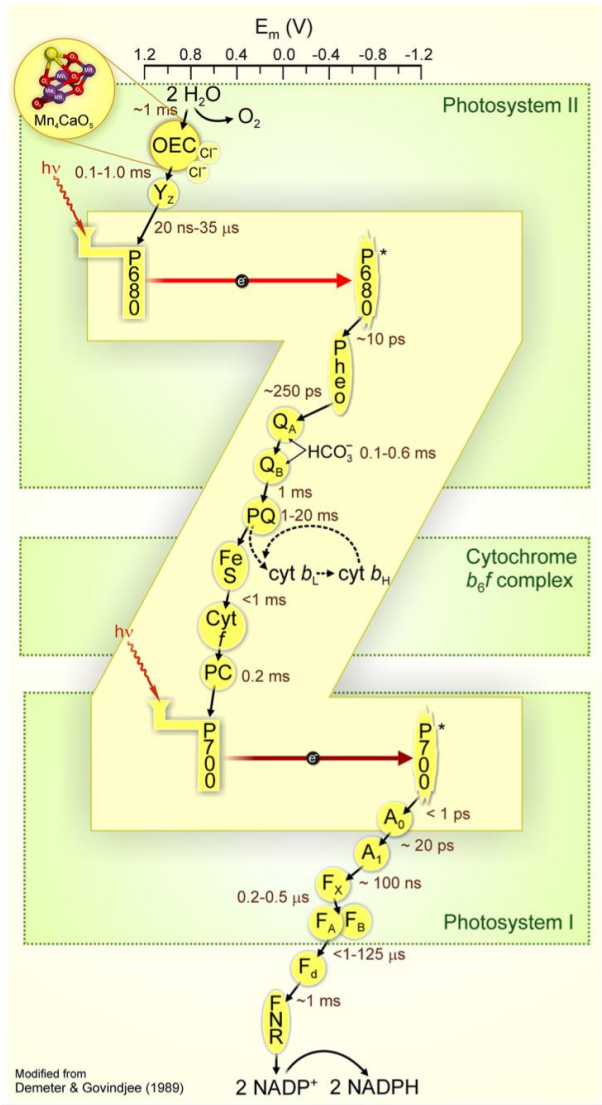

Figure I.5. The Z-scheme of electron transport in photosynthesis.
The electron carriers are placed horizontally according to their midpoint redox potentials at pH 7.0 ($E_{m,7}$). See in-text description below. From (Govindjee et al. 2017).

In the PSII reaction center, excited state P_{680} (P_{680}*) donates an electron to pheophytin which leads to a stable charge separation (P_{680}^+ $Pheo^-$). This electron is further transferred to Q_A and Q_B, forming the (Q_A Q_B^-) state. At each charge separation, P_{680} is regenerated from P_{680}^+ by the OEC of the PSII donor side that oxidizes water and transfers an electron to P_{680}^+ via the Y_Z tyrosine of the D1 subunit. A second charge separation doubly reduces Q_B into PQH_2 that unbinds from PSII and diffuses toward the cyt *b*$_6$*f*. The latter doubly oxidizes PQH_2 at the lumenal Q_o site and the two electrons are bifurcated: one is transferred to the lumenal, copper-containing protein PC and the other is transferred to the lumenal Q_i site of the cyt *b*$_6$*f* where it is used to reduce a plastoquinone into plastosemiquinone (Q-cycle). A second turnover of PQH_2 oxidation is needed to fully reduce the semiquinone into PQH_2. For each electron transferred from PSII to PSI (each PQH_2 oxidation), two protons are released into the lumen, thus participating in the build-up of the *pmf*. In PSI, light absorbed by the antenna system and funneled to the reaction center leads to the formation of P_{700}* and a charge separation (P_{700}^+ Chl A_0^-). The electron is then transferred to ferredoxin (Fd) through three 4Fe-4S centers (F_X, F_A and F_B). The P_{700}^+ special pair resulting from the charge separation oxidizes PC to regenerate P_{700}. Reduced Fd transfers its electrons to Fd-$NADP^+$ reductase (FNR) which catalyzes the reduction of $NADP^+$ into NADPH.

Overall, the transfer of four electrons from H_2O to $NADP^+$ through LEF generates two NAPDH molecules. This electron transfer is coupled to the translocation of 12 protons from the stroma to the lumen, which for Chlamydomonas translates into only ~2.77 ATP molecules due to the 13 subunit III modules of the ATP synthase rotor (Allen 2003). However, the CBB cycle requires 2 NADPH and 3 ATP molecules to reduce one CO_2 molecule. This slight stoichiometric disequilibrium can lead to the build-up of NADPH relative to ATP and inhibit photosynthetic carbon fixation because a lack of $NADP^+$ regeneration by the CBB cycle (*i.e.* a lack of electron acceptors) also blocks LEF and ATP synthesis. This accumulation of excessive reducing power is known as the PSI acceptor-side limitation (Chaux et al. 2015) and can lead to the formation of ROS through the reduction of molecular oxygen. Several regulatory mechanisms that help equilibrate the relative production and consumption of ATP and NAPDH have been described. They all rely on the modulation of the proton gradient to ensure that the reducing power generated by the electron transport chain does not exceed metabolic needs. These include photosynthetic control and non-photochemical quenching (NPQ), both regulated by the proton gradient, as well as cyclic electron flow (CEF) around PSI that generates additional proton gradient. These *pmf*-dependent mechanisms are discussed in the section on the regulatory functions of the cyt b_6f, as it is the main contributor to the proton gradient. Other major processes that help buffer excessive reducing power include the various pathways of oxygen photoreduction (Melher reactions, chlororespiration, flavodiiron proteins and photorespiration). These are outside the scope of this work and will not be addressed here.

B. The cytochrome b_6f complex

Cytochrome proteins are ubiquitous metalloproteins that perform redox reactions essential to all cellular life. Their use of iron, an environmental transition metal, to form their heme cofactors, much like proteins containing nickel-iron centers and molybdenum/tungsten compounds, has placed them on the list of key players in the origin and evolution of bioenergetic systems. The cyt b_6f complex belongs to the Rieske/cyt *b* family of cytochrome proteins.

1. The ubiquitous Rieske/cyt b complexes

The use of energy potential stored in ion gradients across biological membranes to power endergonic reactions is the basis of the chemiosmotic theory proposed by Peter Mitchell in 1961 (Mitchell 1961). Chemiosmosis is a prime candidate in theories on the origin of life (Koch and Schmidt 1991), and LUCA is believed to have obtained its energy by chemiosmotic coupling (Lane et al. 2010). In such energy converting mechanisms, Rieske/cyt *b* complexes (quinol:cyt *c*/plastocyanin oxidoreductases) play a key role by generating the electrochemical proton gradient required for the formation of the energy-rich phosphate bonds of ATP. As such, they are ubiquitous proteins found in all domains of life and are fundamental components of the electron-transport chains of oxygen respiration, photosynthesis, nitrate and nitrite respiration, sulfide oxidation and hydrogen oxidation (Figure I.6).

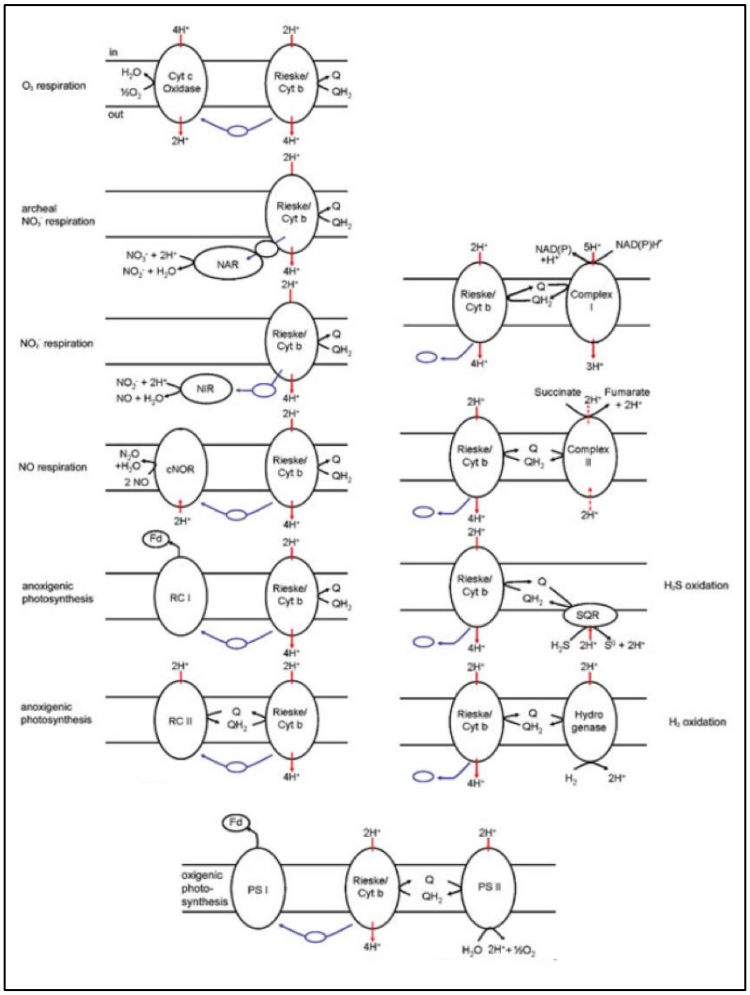

Figure I.6. Rieske/cyt *b* complexes are involved in many different bioenergetic electron transport chains. *Blue lines* represent electron transfer, *red lines* proton transfer. Modified from (ten Brink and Baymann 2014).

These multisubunit transmembrane complexes act at the junction between the two-electron/two-proton chemistry of quinones and the one-electron chemistry of the downstream redox carriers (cyt *c*/PC). Rieske/cyt *b* complexes catalyze electron transfer between these two redox carriers and exploit the difference in their redox potentials by transferring two protons across the membrane per electron transferred along the chain to generate a transmembrane electrochemical proton gradient. The free energy released by the oxidation-reduction process is therefore conserved in the form of a transmembrane electrochemical potential whose amplitude, typically 200-250 mV, drives ATP synthesis. Kramer et al. provided the following general equation for the reaction catalyzed by Rieske/cyt *b* complexes (Kramer et al. 2009):

$$\mathrm{QH_2} + 2\mathrm{C(ox)} + 2\mathrm{H^+}(n) \Leftrightarrow \mathrm{Q} + 2\mathrm{C(red)} + 4\mathrm{H^+}(p)$$

> *where QH_2 and Q are the reduced and oxidized forms of the quinone, C(ox) and C(red) are oxidized and reduced downstream electron carriers, and $H^+(p)$ and $H^+(n)$ are protons on the positively and negatively charged sides of the energy transducing membrane* (Kramer et al. 2009).

The name given to this class of transmembrane complex (Rieske/cyt *b* complexes) was proposed by Kramer et al. as a replacement of the traditional term "*bc*-complexes" (Schütz et al. 2000) which did not convey the fact that cyt *f* and cyt c_1, of the cyt b_6f and cyt bc_1 complexes respectively, share no structural homology and that the only common features of these two complexes are the cyt *b* and Rieske subunits (Kramer et al. 2009). Most of the recent work done on determining the evolutionary relationship between the various members of this family has therefore relied on phylogenetic analysis of cyt *b* sequences (Schütz et al. 2000; Xiong et al. 2000; Lebrun et al. 2006; Nitschke et al. 2010; Baymann et al. 2012; Dibrova et al. 2013; ten Brink et al. 2013; Kao and Hunte 2014) and Rieske ISP sequences (Lebrun et al. 2006).

Apart from the two core subunits having highly conserved sequence and architecture, notable similarities among Rieske/cyt *b* complexes include the geometry of *b*-hemes, which are always found to be about 20.8 Å apart, and the conformation of the quinol-oxidation (Q_o) site. The case of the Rieske ISP is more tricky due to extensive domain movement during catalysis (reviewed in (Huang and Berry 2016)), as first revealed by different conformations of this subunit in cyt bc_1 complexes crystallized in the presence of absence of inhibitors (Kim et al. 1998; Zhang et al. 1998). However, the superimposition of the *C. reinhardtii* cyt b_6f crystal structure treated with tridecyl-stigmatellin (Stroebel et al. 2003) with that of the yeast cyt bc_1 treated with

stigmatellin (Lange et al. 2001) showed very similar positioning of the 2Fe-2S clusters (Figure I.7).

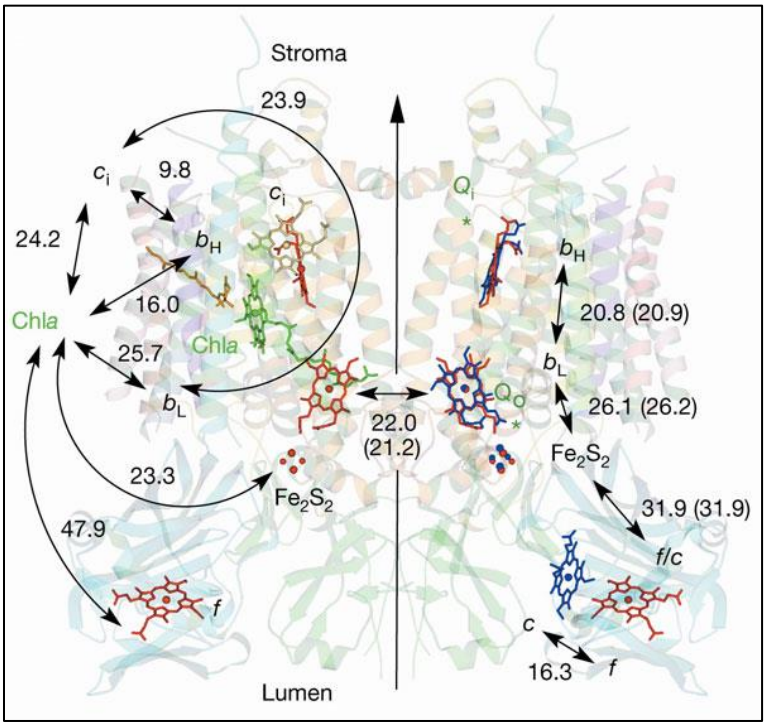

Figure I.7. Conformational similarities of cofactors in the *b_6f* and *bc_1* complexes.
Cyt *b_6f* cofactors and inter-cofactor distances (left), superimposed with cyt *bc_1* cofactors (right). The positioning of core subunits and cofactors is highly conserved between *b_6f* and *bc_1* complexes. From (Stroebel et al. 2003).

Despite a high degree of conservation and the predominance of vertical transfer of Rieske/cyt *b* sequences, several features show some variability and serve as evolutionary marker traits to classify these complexes into families or "clades". For example, the phylogenetic tree of cyt *b* sequences revealed that cyanobacteria and its green lineage descendants, as well as Heliobacteria and certain non-phototrophs, all possessed a split cyt *b*/subunit IV configuration and could be classified as a specific group, the "green clade" of Rieske/cyt *b* complexes (Nitschke et al. 2010). These marker traits can also include properties that are not directly dependent on sequence and structure, such as the redox potentials of the Rieske/cyt *b* cofactors and associated quinone species. This makes for complex phylogenetic analyses and a rich evolutionary history, of which Dibrova et al. provide an extensive review in the context of the gradual oxygenation of the atmosphere (Dibrova et al. 2013).

Important structural features (markers) that differentiate "cyanobacterial/chloroplast-type" cyt b_6f from "bacterial/mitochondrial-type" cyt bc_1 and that are later addressed in the discussion of our results include (Figure I.8):

- The split cyt b_6/subunit IV vs unsplit cyt *b* configurations.
- The number (7 or 8) of transmembrane helices spanned by the core cyt b_6/subunit IV (or unsplit cyt *b*).
- The presence of the stromal heme c_i (and its covalent cysteine partner at position 35^{b6}), as well as the peculiar chlorophyll *a* and β-carotene molecules, in cyt b_6f complexes.
- The four small peripheral subunits PetG, PetL, PetM and PetN.

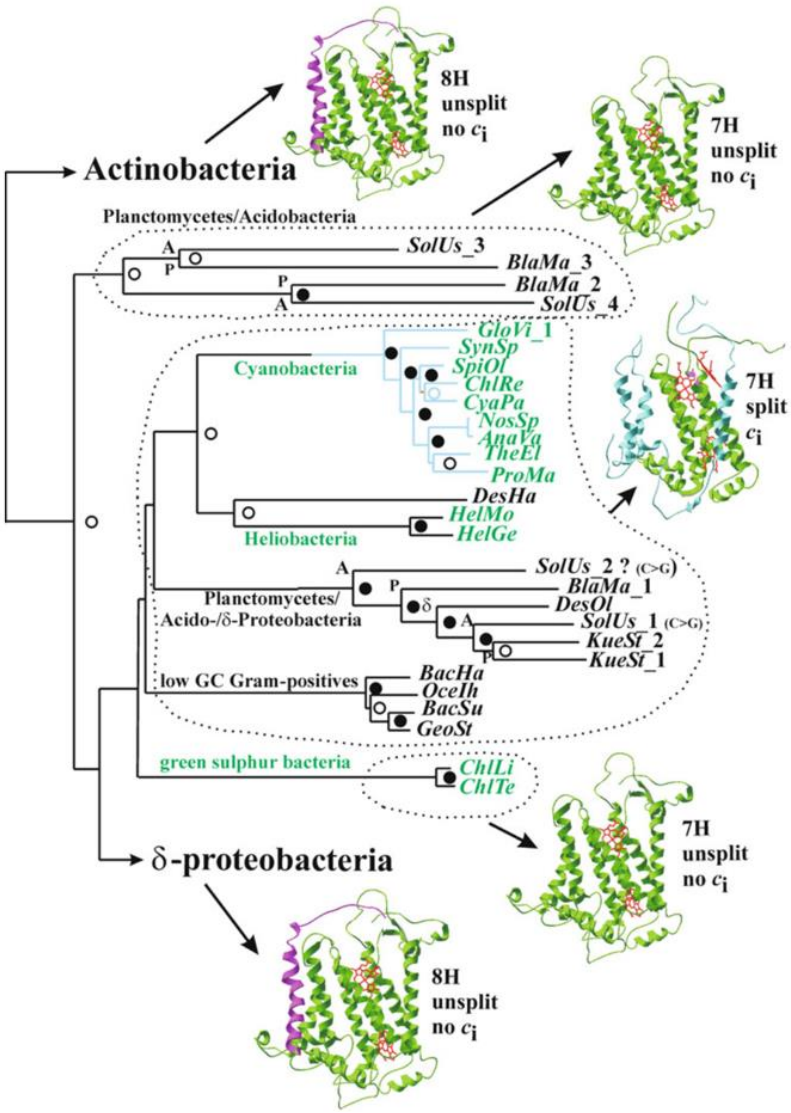

Figure I.8. The "green clade" of Rieske/cyt *b* complexes.
From (Nitschke et al. 2010): "*Phylogram of the green clade* [dotted group in the middle] *based on amino acid sequences of cytochrome b.* […] *Green species names indicate phototrophs. The structures represented next to subclades defined by common phylogenetic markers (and surrounded by dotted lines) are based on the 3D structures of the Rhodobacter capsulatus (bc_1-type) and Mastigocladus laminosus (b_6f-type) Rieske/cytb complexes and are intended to schematically indicate the global structure of cyt b in these individual subclades as deduced from the primary sequences. The purple helix indicated in these structures corresponds to the C-terminal eighth transmembrane span lost in the higher branches of the green cluster. Cyan colouring in the structure of the cyanobacterial b_6f complex is intended to differentiate the split-off SUIV-protein* […] *from the b_6-protein* […]."

2. *Structure*

The cyt b_6f (plastoquinol-plastocyanin oxidoreductase) of plants and algae is a multi-subunit transmembrane complex embedded in the thylakoid membrane (Stroebel et al. 2003). Assembled as a ~220 kDa dimer *in vivo*, each monomer is composed of four major subunits and four peripheral small subunits which altogether contain 13 transmembrane helices (Table I.1). Crystallographic structures of cyanobacterial and microalgal cyt b_6f complexes have been resolved with various bound inhibitors. The positions of stigmatellin and NQNO, which act as catalytic site inhibitors, in the resolved 3D-structures has helped define the lumenal Q_o and stromal Q_i binding pockets of quinols and quinones, respectively (Figure I.9).

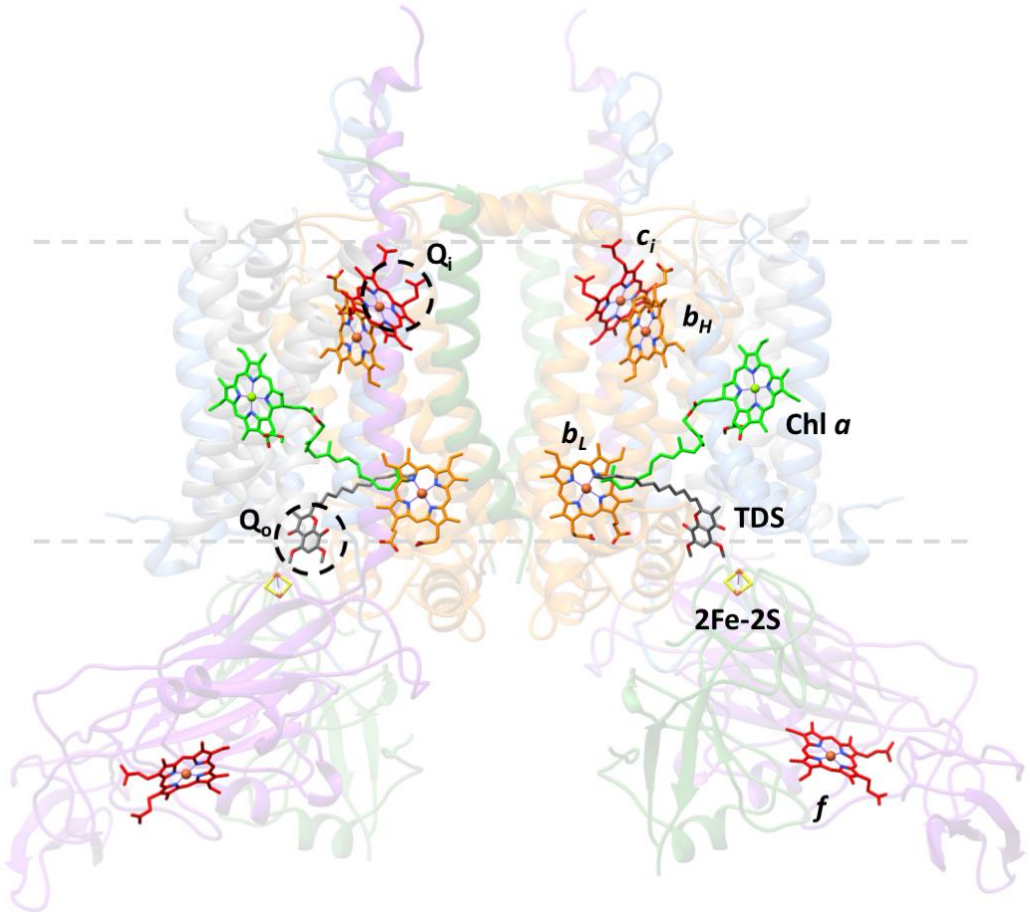

Figure I.9. Structural model of the dimeric cyt b_6f complex of *C. reinhardtii*.
View of the complex along the plane of the thylakoid membrane (dashed grey lines), with the stroma on top and lumen at the bottom. Are shown: cyt b_6 (orange), subunit IV (blue), Rieske ISP (green), cyt *f* purple), peripheral subunits (grey), *b*-hemes b_L and b_H (orange), "*c*"-hemes c_i and *f* (red), 2Fe-2S cluster (yellow), Chl *a* (green) and inhibitor tridecyl-stigmatellin (TDS, dark grey). The Q_o and Q_i pockets are marked by dashed black circles. Atomic coordinates are from PDB 1Q90 (Stroebel et al. 2003).

Table I.1. Components of the cyt *b*$_6$*f* complex and their attributes.

Subunit	Gene	Gene location	Cofactors or binding site	Mass (kDa)	TMH	$E_{m,7}$ (mV)
Cyt *f*	*petA*	Chloroplast	Heme *f*	32.2	1	+270 to +380
Cyt *b*$_6$	*petB*	Chloroplast	Heme b_L Heme b_H Heme c_i	24,7	4	-120 to -150 -30 to -50 < -50 to +100
Rieske ISP	*PETC*	Nucleus	2Fe-2S cluster	19,3	1	+300 to +320
Subunit IV	*petD*	Chloroplast	Chl *a* *β*-carotene	17,5	3	
PetG	*petG*	Chloroplast	-	4,0	1	
PetL	*petL*	Chloroplast	-	3,5	1	
PetM	*PETM*	Nucleus	-	3,8	1	
PetN	*PETN*	Nucleus	-	3,3	1	

The core of the complex is formed by the cyt *b*$_6$ subunit and subunit IV, membrane-integral subunits that both shape the Q_o and Q_i sites. The Rieske ISP has an extrinsic lumenal domain and a single transmembrane domain that crosses over to the other monomer, a key determinant of dimer stability. Its head domain contains the iron-sulfur cluster and oscillates between the proximal and distal positions during electron transfer from PQH_2 to PC. The cyt *f* subunit has a large extrinsic lumenal domain composed mostly of antiparallel *β*-sheets and a single transmembrane domain. Each of the four small subunits PetG, PetL, PetM and PetN are single transmembrane *α*-helices that together form a "picket fence" around the core subunits (Cramer et al. 2005). PetG is crucial for the assembly and stability of the complex, and Δ*petG* strains are non-phototrophic (Berthold et al. 1995; Schwenkert et al. 2007). Strains lacking the *petL* gene can grow phototrophically but show a defect in cyt *b*$_6$*f* subunit accumulation (Schwenkert et al. 2007). The PetL subunit has been implicated in electron transfer and dimer stability, probably through a stabilizing interaction with the Rieske transmembrane domain (Takahashi et al. 1996; Breyton et al. 1997; Schwenkert et al. 2007). Furthermore, the N-terminal of PetL is in the stroma and not far from the C-terminal of subunit IV (Zito et al. 2002), which gives an idea of its position with respect to the other subunits. A *petM* deletion did not affect the function of the complex but did modify the accumulation of PSI and phycobilisomes in Synechocystis, suggesting that PetM could participate in some of the regulatory functions of the cyt *b*$_6$*f* (Schneider et al. 2001). PetN was first identified in *N. tabacum* as essential for cyt *b*$_6$*f* assembly and phototrophic growth (Hager et al. 1999; Schwenkert et al. 2007), and later confirmed to be present in the complex of *C. reinhardtii* as well (Zito et al. 2002), although no clear function has been reported yet. Lastly, the nucleus-encoded 15.2 kDa PetO protein, containing a single transmembrane domain and a stromal domain, was added to the list of cyt *b*$_6$*f* subunits because

of its low accumulation in b_6f deletion mutants and its co-localization with cyt *f* (Lemaire et al. 1986; Hamel et al. 2000). It is however lost in purified cyt b_6f preparations (Pierre et al. 1995; Stroebel et al. 2003), suggesting that it is loosely bound to the complex and could participate in some of its regulatory functions (see *State transitions* section).

A monomer of cyt b_6f contains 5 redox-active prosthetic groups that function in electron transfer, as well as two pigment molecules (Chl *a* and β-carotene) whose functions are unclear. The core cyt b_6 coordinates the lumenal heme b_L (His86^{b6} and His187^{b6}) and the two stromal hemes b_H (His100^{b6} and His202^{b6}) and c_i (covalently bound to Cys35^{b6}, see dedicated section below). Several other residues, including residues from subunit IV, shape the local protein environment of the two quinone pockets and therefore play a role in the correct positioning of these three hemes. Cyt *f* contains another *c*-type heme in its lumenal domain that is covalently bound to Cys21 and Cys24 of a CXXCH motif and axially liganded by His25 and the N-terminal amino-group of this subunit. The last redox cofactor is the 2Fe-2S cluster of the Rieske-ISP lumenal domain coordinated by Cys105/His107 and Cys123/His126.

3. *Heme c_i*

As mentioned previously, one of the major features that differentiate *bf*- from *bc*-type cytochromes is the presence of a third heme in the Q_i site of the low-potential chain: heme c_i. This redox center was first identified as a new and unusual spectral component that had the properties of a high-spin *c*'-type cytochrome (Lavergne 1983b; Joliot and Joliot 1988). Based on its spectral features, it was found to be in close contact with heme b_H (Lavergne 1983b) and to change redox potential in the presence of an axial ligand (Joliot and Joliot 1988). The true nature of this signal was revealed only twenty years later when the structures of cyanobacterial and microalgal cyt b_6f were obtained (Kurisu et al. 2003; Stroebel et al. 2003), prompting further in-depth characterization (Alric et al. 2005; Baymann et al. 2007) (for a historical retrospective, see (Zito and Alric 2016)). The structures revealed that heme c_i was covalently bound by a thioether bond to a cysteine residue at position 35 of cyt b_6, highly conserved in cyt b_6f complexes of oxygenic phototrophs, classifying it as a *c*-type heme. However, several of its features were atypical for *c*-type hemes and suggested that it served specific functions related to the energetic requirement of oxygenic photosynthesis:

- The single thioether bond that it forms with Cys35^{b6} contrasts with other *c*-type hemes, which are usually bound to their protein scaffold by two cysteine residues. Furthermore, the characteristic CXXCH motif of *c*-type heme binding is not found in the cyt b_6 sequence.
- Heme c_i does not have a proteic axial ligand to its central iron atom. The latter is only coordinated by a hydroxyl ion or water molecule that forms an H-bond with one of the b_H propionates. On the other side of the heme plane, Phe40 of subunit IV lies close to the heme surface. Substitution of this phenylalanine with a tyrosine showed that the phenolic hydroxyl of the tyrosine side-chain served as an axial ligand to the heme, in tight coordination with the iron atom, resulting in a large decrease of the heme's midpoint potential and much slower kinetics of *b* hemes re-oxidation upon flash excitation (de Lacroix de Lavalette et al. 2009). The tight coordination by tyrosine contrasted with the native phenylalanine whose weaker electron density close to c_i suggested a lower occupancy and higher flexibility. The structure revealed that the Phe40^{suIV} side-chain has to move away from the heme plane to allow quinone access to the binding pocket, suggesting that this residue modulates quinone accessibility to heme c_i (de Lacroix de Lavalette et al. 2009).

Although it is positioned right between heme b_H and the site where quinones bind, leaving little doubt that it is involved in electron transfer and quinone reduction, its exact function and the reason for its recruitment in *bf* complexes are unknown. As a marker trait of *bf* complexes of oxygenic photosynthesis, it could drive an alternative mechanism of quinol reduction more suited to an oxic environment than that of *bc* complexes. One possibility is that heme c_i could reduce the life-time of the unstable, oxygen-reactive semiquinone intermediate by facilitating the simultaneous two-electron reduction of the quinone. Alternatively, it could stabilize the bound semiquinone and decrease its reactivity.

Surprisingly, heme c_i occurs also in two families of Firmicutes, namely the photosynthetic Heliobacteria and the non-photosynthetic *Bacillus* (Baymann and Nitschke 2010). Because Heliobacteria rely on cyclic electron transfer around a type-I RC (Kramer et al. 1997), like their c_i-containing oxygenic counterparts, a role of heme c_i in photosynthetic CEF was postulated (Kurisu et al. 2003; Stroebel et al. 2003). An even stronger feature shared by all c_i-containing organisms is the split of the core cyt *b* subunit into cyt b_6 and subunit IV. The hypothesis of a structural requirement of heme c_i in this split conformation is unlikely since green-sulfur

bacteria and some Haloarchaea have a split core subunit but lack heme c_i (Frauke Baymann, personal communication). Conversely, however, the split conformation could be necessary for the proper insertion of heme c_i into the complex. In this work, we shall not search for a causal explanation of the heme c_i /split subunit conformation, but rather explore the possibility that these structural attributes may have enabled the cyt b_6f to evolve new functions as the central regulator of oxygenic photosynthesis (see Chapter IV).

4. Function

Electron transfer and proton translocation: The Q-cycle

The cyt b_6f couples electron transfer from PQH_2 to PC with transmembrane proton translocation according to the Q-cycle (Q for quinone). This mechanism was initially formulated by (Mitchell 1975) while working on the cyt bc_1 complex. This came 14 years after his proposal of the chemiosmotic principle, which was still a hot topic despite the direct evidence provided by the experiments of Jagendorf et al. (Jagendorf and Hind 1963; Neumann and Jagendorf 1964). The Q-cycle mechanism not only clarified the nature of the H^+/e^- coupling sites and provided a rationale for the coupling mechanism of chemiosmosis, but also explained some peculiar observations on the kinetic behaviour of *b*- and *c*-type cytochromes of the electron transport chain (Crofts 2004). Of course, this remarkable hypothesis was made at a time when researchers relied on very few observables to describe and conceive the systems they were studying, mainly the absorbance signature and kinetics of absorbance changes of the redox species involved. His original Q-cycle was widely debated, modified and tested over the years. Notably, Peter Garland proposed a modified, self-contained Q-cycle in which the oxidizing (Q_o) site would have to turn over twice to complete the cycle. This was later incorporated into the modified Q-cycle mechanism proposed by Tony Crofts in 1983 and which still stands as reference (Crofts et al. 1983).

Figure I.10 provides equations of the Q-cycle reactions and a schematic representation of the electron transfer routes. Two catalytic sites of the cyt b_6f form the scaffold of the Q-cycle: the lumenal PQH_2 oxidation site (Q_o) and the stromal PQ reduction side (Q_i). Electrons are transferred from the first site to the second site across the membrane through the "low-potential chain". Electrons are also transferred from PSII to PSI along the "high-potential chain". Upon

flash excitation of dark-adapted cells, the PSI primary donor P_{700} is oxidized and the positive charge is sequentially transferred to the Rieske iron-sulfur cluster through PC and cyt *f* (high-potential chain). Starting from a complex with a fully oxidized low-potential chain (b_L^+ b_H^+), PQH_2 binding and oxidation at the Q_o site transfers one electron to the (2Fe-2S cyt *f*) couple of the high-potential chain and one electron to heme b_L of the low-potential chain, releasing the oxidized PQ molecule into the membrane and two protons into the lumen (Figure I.10, reaction a). Due to the more positive potential of heme b_H, the electron on b_L is then transferred to b_H, yielding a semi-reduced low-potential chain (b_L^+ b_H) (reaction b). Once the high-potential chain receives another oxidizing equivalent, a second PQH_2 molecule binds at Q_o and is oxidized. The first electron is transferred toward PSI and the second reduces heme b_L, again releasing PQ into the membrane and two protons into the lumen (reaction a'). The two electrons stored in the low-potential chain (b_L b_H) are transferred to a PQ molecule bound at the Q_i site, forming PQH_2 using two protons from the stroma (b'). The net result of a complete cycle (two turnovers) is the translocation of four protons from the stroma to the lumen and the transfer of two electrons from PSII to PSI.

$$PQH_{2\,(Q_o)} + (\text{FeS cyt } f)^+ + (b_l^+\, b_h^+) \rightarrow PQ_{(\text{membrane})} + (\text{FeS cyt } f) + (b_l\, b_h^+) + 2H^+_{(\text{lumen})} \quad \text{(a)}$$

$$(b_l\, b_h^+) \rightarrow (b_l^+\, b_h) \quad \text{(b)}$$

$$PQH_{2\,(Q_o)} + (\text{FeS cyt } f)^+ + (b_l^+\, b_h) \rightarrow PQ_{(\text{membrane})} + (\text{FeS cyt } f) + (b_l\, b_h) + 2H^+_{(\text{lumen})} \quad \text{(a')}$$

$$(b_l\, b_h) + PQ_{(Q_i)} + 2H^+_{\leftarrow \text{stroma}} \rightarrow (b_l^+\, b_h^+) + PQH_{2\,(\text{membrane})} \quad \text{(b')}$$

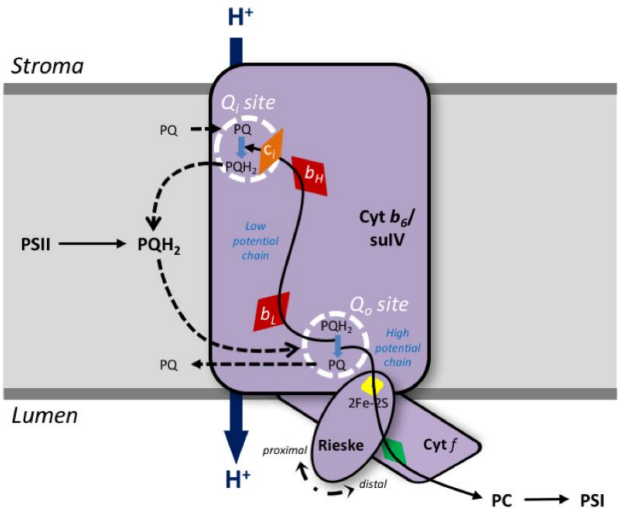

Figure I.10. The cyt *b*$_6$*f* complex drives the Q-cycle of photophosphorylation.
Equations are from (Joliot and Joliot 1998). The scheme shows that electron transfer (solid black arrows) is coupled to proton translocation (blue arrow) across the thylakoid membrane, participating in the creation of a *proton motive force*. From (Dumas et al. 2016).

Regulatory functions – Published review article: *Photosynth Res*

As the coupling component between the two photosystems, the cyt b_6f plays a crucial role in the regulation of linear and cyclic electron flows as well as in the mechanisms that depend on the establishment of a *pmf* across the membrane. It insures that all the components work together and keeps the system poised. The following review article describes the *pmf*-dependent mechanisms listed previously and tackles the various theories regarding the regulation of CEF from the point of view of the cyt b_6f. We argue that the major players are the lateral heterogeneity of membrane protein complexes, the quinone microdomains that it generates and the different regulatory working modes of the cyt b_6f in response to these local redox environments, including state transitions. The next section is then devoted entirely to state transitions and to the regulatory function of the cyt b_6f in this process.

Photosynth Res
DOI 10.1007/s11120-016-0298-y

REVIEW

Cytochrome b_6f function and localization, phosphorylation state of thylakoid membrane proteins and consequences on cyclic electron flow

Louis Dumas[1] · Marie Chazaux[1] · Gilles Peltier[1] · Xenie Johnson[1] · Jean Alric[1]

Received: 5 January 2016 / Accepted: 27 July 2016

Abstract Both the structure and the protein composition of thylakoid membranes have an impact on light harvesting and electron transfer in the photosynthetic chain. Thylakoid membranes form stacks and lamellae where photosystem II and photosystem I localize, respectively. Light-harvesting complexes II can be associated to either PSII or PSI depending on the redox state of the plastoquinone pool, and their distribution is governed by state transitions. Upon state transitions, the thylakoid ultrastructure and lateral distribution of proteins along the membrane are subject to significant rearrangements. In addition, quinone diffusion is limited to membrane microdomains and the cytochrome b_6f complex localizes either to PSII-containing grana stacks or PSI-containing stroma lamellae. Here, we discuss possible similarities or differences between green algae and C3 plants on the functional consequences of such heterogeneities in the photosynthetic electron transport chain and propose a model in which quinones, accepting electrons either from PSII (linear flow) or NDH/PGR pathways (cyclic flow), represent a crucial control point. Our aim is to give an integrated description of these processes and discuss their potential roles in the balance between linear and cyclic electron flows.

Keywords Cyclic electron flow · Cytochrome b_6f complex · Heterogeneity of thylakoid membranes · Membrane ultrastructure · Quinone microdomains · Redox sensing · State transitions

Abbreviations

PS	Photosystem
PQ	Plastoquinone
PQH_2	Plastoquinol
Cyt	Cytochrome
PC	Plastocyanin
CBB cycle	Calvin–Benson–Bassham cycle
suIV/V	Subunit IV/V
Rieske ISP	Rieske iron–sulfur protein
pmf	Proton motive force
Fd	Ferredoxin
NPQ	Nonphotochemical quenching
q_E	Energy-dependent quenching
LEF	Linear electron flow
CEF	Cyclic electron flow
DCMU	3(3,4-Dichlorophenyl)-1,1-dimethylurea
DBMIB	2,5-Dibromo-3-methyl-6-isopropyl-*p*-benzoquinone
LHC	Light-harvesting complex

Introduction

Oxygenic photosynthesis occurs within thylakoid membranes in the chloroplast of algal and plant cells and is based upon a series of oxidation–reduction reactions using water as a primary electron donor and CO_2 as a terminal electron acceptor (Ort and Yocum 1996). Several transmembrane protein complexes are involved in the conversion of light energy into chemical energy. Light-harvesting

✉ Jean Alric
jean.alric@cea.fr

[1] Laboratory of Microalgal and Bacterial Bioenergetics and Biotechnology, CEA Cadarache, CNRS, Aix-Marseille Université, UMR7161 BIAM - LB3M, 13108 Saint-Paul-lez-Durance, France

Published online: 17 August 2016

pigment–protein complexes absorb light and transfer energy quanta to photosystems, photosystem II (PSII) and photosystem I (PSI), which perform electron transfer. At the donor side of PSII, situated on the lumenal side of the membrane, water is split into oxygen and protons, while electrons are transferred to the stromal acceptor side to quinone electron acceptors denoted Q_A and Q_B. At the acceptor stromal side of PSI, electrons are transferred via ferredoxin and ferredoxin:$NADP^+$ reductase (FNR) to $NADP^+$ to form NADPH, which is ultimately used in the Calvin–Benson–Bassham (CBB) cycle for reduction of CO_2 into an organic C3 compound, 3-phosphoglycerate (Bassham 1979). Electrons are transferred from PSII to PSI by intersystem electron carriers, namely plastoquinones, cytochrome b_6f complex (cyt b_6f), and plastocyanin (PC), on which we have focused much of our attention in this review. The quinone at Q_B of PSII is doubly reduced and doubly protonated to form a quinol QH_2 that is released from its PSII binding site and exchanged for another quinone from the membrane pool. At the level of cyt b_6f, a quinol binding at the Q_o site releases two protons in the lumen (Kallas 2012) and one electron is transferred to PC which reduces $P_{700}{}^+$ at PSI, completing the chain. The other electron from the quinol at Q_o is recycled through the Q-cycle at the level of cyt b_6f, therefore increasing the number of protons transferred per electron. Proton pumping across the thylakoid membrane provides the transmembrane proton motive force (*pmf*) required for the synthesis of ATP, the other substrate of the CBB cycle.

Role of the cyt b_6f in electron transfer and regulation

Structure and function

The crystallographic structures of the cyt b_6f complex in *Chlamydomonas reinhardtii* (Stroebel et al. 2003) and *Mastigocladus laminosus* (Kurisu et al. 2003) have been resolved. Each of the two monomers in the cyt b_6f dimer comprises four major subunits (cyt *f*, cyt b_6, Rieske ISP, suIV), four minor subunits (PetG, PetL, PetM, PetN), structural lipids, as well as a β-carotene molecule and a Chl-a molecule (Stroebel et al. 2003). Another small protein (PetO or suV) was identified as a subunit of the complex (Hamel et al. 2000) but it is loosely bound to the complex (Pierre et al. 1995; Stroebel et al. 2003). In addition, four redox cofactors are present in the complex. The cyt b_6 subunit and suIV, coordinate heme b_h on the lumenal side and hemes b_l and c_i on the stromal side of the complex (Zito and Alric 2016). A 2Fe-2S cluster is present in the Rieske ISP and cyt *f* contains the last redox cofactor, a *c*-type heme, in its lumenal domain (Kurisu et al. 2003; Pierre et al. 1995; Hauska et al. 1983; Stroebel et al. 2003).

Cyt b_6 and suIV subunits coordinate the two catalytic sites of the complex: the plastoquinol (PQH_2) oxidation site (Q_o or Q_p, lumenal side) and the plastoquinone (PQ) reduction site (Q_i or Q_n, stromal side). These two quinone-binding sites are the electron ports for the Q-cycle (Crofts et al. 1983; Mitchell 1976). Mutagenesis studies have demonstrated the importance of certain residues within these sites, such as Glu78 at Q_o (Zito et al. 1998) and Phe40 at Q_i (Lavalette et al. 2009). Upon PQH_2 oxidation at the Q_o site, a reaction considered as the rate-limiting step in photosynthetic electron transport (Witt 1971), one electron from the quinol is injected into the "high-potential chain" toward PSI (Fe_2-S_2 → cyt *f* → PC → P_{700}) and the second electron into the "low-potential chain" across the membrane (b_L → b_H → c_i) toward the Q_i site on the stromal side. The release of two protons from the quinol at Q_o into the lumen and the uptake of two protons from the stroma by a doubly reduced quinone at Q_i generate a transmembrane electrochemical proton gradient also called *pmf*. The quinol produced at Q_i can be released from its site and reoxidized at Q_o, completing the Q-cycle (Fig. 1). It has been suggested that cyclic electron transport around PSI, and the corresponding formation of a PSI-LHCI/LHCII-Fd-FNR-cyt b_6f-PGRL1 supercomplex (see below), could provide a Fd-dependent reductive pathway to PQ at Q_i (possibly through heme c_i) and revive Mitchell's original Q-cycle model (Zhang et al. 2001; Kurisu et al. 2003; Stroebel et al. 2003; Iwai et al. 2010a).

At steady-state, the proton gradient across the thylakoid membrane is mainly governed by the relative contributions of the PSII oxygen evolving complex, proton pumping by cyt b_6f and proton efflux through ATP synthase. Lumen acidification triggers the protonation of the PsbS protein in higher plants (Horton et al. 2005; Li et al. 2004) and both PsbS and LHCSR3 in algae (Correa-Galvis et al. 2016; Peers et al. 2009; Tibiletti et al. 2016), and activates violaxanthin de-epoxidase which converts violaxanthin into zeaxanthin (Kramer et al. 2003). This allows for thermal dissipation of excess light energy at PSII (qE), which is the major component of nonphotochemical quenching (NPQ) (Holt et al. 2004; Niyogi 1999). This pH component is crucial for several regulations of electron flow through PSII and PSI, notably in protecting PSI against photoinhibition [reviewed in Chaux et al. (2015)]. In addition, the Q_o site of cyt b_6f responds to lumen acidification and provides a site of photosynthetic control preventing the overreduction of downstream electron carriers (Stiehl and Witt 1969). The mechanism of photosynthetic control is similar to the respiratory control whereby the proton pumping of *b*-type cytochromes (cyt b_6f or bc_1) is inhibited at low pH. Quinol binding and oxidation at the Q_o pocket of cyt b_6f depend on

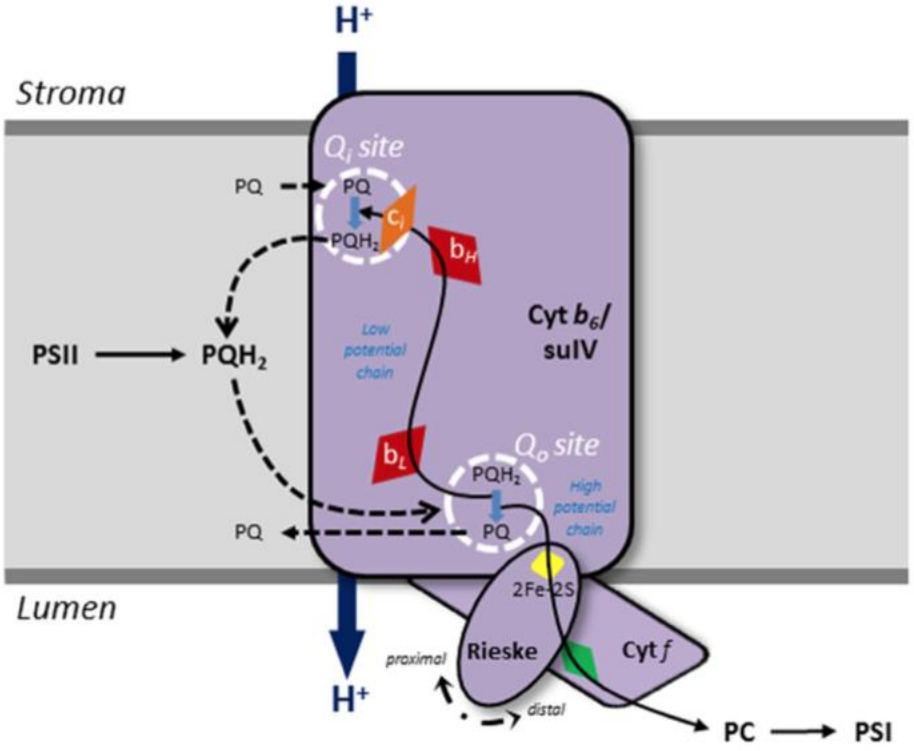

Fig. 1 The cytochrome b_6f complex drives the Q-cycle of photophosphorylation. Electron transfer (*solid black arrows*) is coupled to proton translocation (*blue arrow*) across the thylakoid membrane, establishing the *pmf*. PQH_2 oxidation occurs at the Q_o site and PQ reduction at the Q_i site. Electrons are transferred to the low-potential chain (hemes $b_L \rightarrow b_H \rightarrow c_i$) and then to the high-potential chain (Fe-S → cyt f → PC → PSI) upon PQH_2 oxidation. Movement of the Rieske ISP between proximal and distal positions is necessary for electron transfer from PQH_2 to cyt f. *Dashed black arrows* represent the movement of quinone species between the PQ pool and the two cyt b_6f catalytic sites

the formation of an H-bond between the hydroxyl group of the quinol head group and the nitrogen from the imidazole ring of His155 on the Rieske ISP (Crofts et al. 1999; Zu et al. 2003). As the lumen acidifies and the chemical environment of the Q_o pocket changes, protonation of the lone pair on the histidine residue prevents H-bond formation with the PQH_2 hydroxyl group. Cyclic electron flow (CEF) around PSI increases lumen acidification and places cyt b_6f at the crossroads of photosynthetic regulatory pathways.

Do all organisms from the green lineage walk the line?

There are many differences between plants and algae, starting from those separating multicellular from unicellular organisms. As far as chloroplast metabolism and photosynthetic electron transport are concerned, however, it is sometimes hard to clarify whether differences evidenced experimentally pertain to the very nature of the molecular mechanisms involved in a process or to differences in the experimental protocol or in the physiological state of the sample, like the redox poise of the chloroplast in the dark for example. When studying photosynthesis in plants, researchers generally focus on the source organs: photoautotrophic mature leaves where cells are dividing slowly and export sugars to support heterotrophic growth of the nonphotosynthetic plant tissues (roots, stems, and young leaves). Such metabolic differences between heterotrophic and photoautotrophic cells exist in unicellular green algae but depend on the growth media, light intensity, or phase of the cell cycle if cell growth is synchronized on the photoperiod (Chapman et al. 2015; Mettler et al. 2014; Zones et al. 2015). CO_2 availability at the vicinity of RuBisCO is a function of stomata opening and stomatal conductance in C3 plants (Evans and Loreto 2000), whereas it depends on the CCM in *Chlamydomonas* (Wang et al. 2015). Whereas C3 plants photosynthates are exported out of the chloroplast for sucrose metabolism, glycolysis and respiration, in *Chlamydomonas* the primary steps of glycolysis are exclusively localized in the chloroplast [reviewed in Johnson and Alric (2013)]. Whether such metabolic differences translate into varied regulations of CEF is still a matter of debate. To give a mechanistic description of CEF, here we have chosen to focus more on the similarities of the cyclic pathways at the molecular level.

Cyclic electron flow

A kinetic equilibration must exist between electron transfer reactions and the downstream metabolic reactions of carbon metabolism, suggesting a regulation of electron flow

through the photosynthetic apparatus to achieve balance and avoid overreduction of the electron carriers (Kramer and Evans 2011). One of the major regulations of photosynthetic electron flow relies on CEF around PSI that recycles electrons from NADPH or reduced Fd through the PQ pool, cyt b_6f complex and PC. At the level of cyt b_6f and plastoquinones, electron transfer is coupled to proton transfer. As a result, protons are pumped into the lumen and supplement ATP synthesis (Arnon et al. 1954), an important contribution to the downstream CBB cycle and CO_2-concentrating mechanism.

In plants and green algae, CEF occurs through two pathways, one that is dependent on NAD(P)H dehydrogenase, NDH-1 in plants and NDH-2 in green algae (Peltier et al. 2015), and one on the PGRL1/PGR5 couple (Peltier et al. 2010; Munekage et al. 2002). The Fd-dependent cyclic pathway requires the PGR5/PGRL1 proteins possibly in interaction with PSI subunits, Fd, NADPH reductase (FNR) and cyt b_6f complex (Terashima et al. 2012; DalCorso et al. 2008). Recombinant PGRL1 protein can reduce PQ analogues when supplied with reduced Fd in vitro, and PGRL1 also interacts with PGR5 via cysteine residues at both its C- and N-terminals. The PGRL1 protein binds iron (Petroutsos et al. 2009; Hertle et al. 2013). The PGR5/PGRL1 complex, which seems conserved throughout the green lineage, is currently considered to be the ferredoxin quinone reductase (FQR) involved in antimycin-A sensitive pathway, with mutants in *Arabidopsis thaliana*, *Oryza sativa,* and *Chlamydomonas reinhardtii* supporting this role (DalCorso et al. 2008; Petroutsos et al. 2009; Johnson et al. 2014; Munekage et al. 2002; Tolleter et al. 2011).

The contribution of CEF under steady-state conditions is highly dependent on physiological conditions. In *Chlamydomonas*, NADPH dehydrogenase may be more prevalent under aerobic and nonsaturating light conditions, while PGRL1/PGR5 may be required under strong light and air-CO_2 levels, fluctuating light or anaerobic conditions (Johnson et al. 2014). The involvement of PGR5/PGRL1 in Fd-dependent CEF fits with a redox model at steady-state (Alric 2010), probably requiring thioredoxin activation (Hertle et al. 2013; Hosler and Yocum 1987). In *Chlamydomonas*, the activity of PGR5 under conditions where stromal redox carriers are reduced also coincides with anaerobic conditions, PSI-cyt b_6f supercomplex formation (Terashima et al. 2012; Iwai et al. 2010a), PQ pool reduction, and thus the induction of a state transition.

State transitions

Besides the role that cyt b_6f plays in electron transport, it also serves as a PQ pool redox sensor involved in state transitions (Wollman and Lemaire 1988), the mechanism by which light-harvesting complexes (LHC) are redistributed between the two photosystems in order to poise the intersystem electron carriers (Wollman 2001b; Cardol et al. 2009; Lemeille and Rochaix 2010; Bonaventura and Myers 1969). The redox state of the PQ pool correlates with state transitions (Horton et al. 1981). Although the mechanistic details of the process are still unclear, we know that when excess light energy hits PSII, the PQ pool becomes more reduced and the cyt b_6f transduces the signal (Wollman and Lemaire 1988) to a specific kinase, Stt7 in *C. reinhardtii* (Depege et al. 2003; Lemeille et al. 2009) and STN7 in *A. thaliana* (Bellafiore et al. 2005). Stt7/STN7 kinases phosphorylate LHCII antenna proteins around PSII, which migrate toward PSI, thus redistributing light energy and relaxing the reducing pressure on the PQ pool. This corresponds to a transition from state 1 to state 2. State transitions are a reversible process as specific, constitutively active phosphatases such as PPH1 in *A. thaliana* (Shapiguzov et al. 2010) dephosphorylate LHCII proteins that can then reassociate with PSII.

Several lines of evidence suggest that the cyt b_6f is a central regulator of state transitions. Mutants devoid of cyt b_6f complex are blocked in state 1 in spite of a highly reduced PQ pool (Wollman and Lemaire 1988). Mutants with altered PQH_2 binding to the Q_o pocket are similarly affected for state transitions (Zito et al. 1999; Vener et al. 1995). The *C. reinhardtii* PetO (suV) protein, loosely associated with the cyt b_6f complex (Hamel et al. 2000) but found in the PSI-FNR-cyt b_6f supercomplex (Iwai et al. 2010a), becomes phosphorylated upon PQ pool reduction and could be involved in the activation of the Stt7 kinase (Hamel et al. 2000). The Stt7 kinase coimmunoprecipitates with the cyt b_6f Rieske ISP (Lemeille et al. 2009), and their putative interaction sites were mapped using the yeast two-hybrid method (Shapiguzov et al. 2016). Stt7 has a transmembrane domain with the C-terminal kinase catalytic domain located in the stroma, whereas the N-terminal region is oriented toward the lumen. Directed mutagenesis of two conserved cysteine residues in the lumenal region produced mutants blocked in state 1, with no phosphorylation of LHCII under reducing conditions (Lemeille et al. 2009). Disulfide bridge formation and transient dimerization were proposed as possible mechanisms of kinase activation, although no changes in the redox state of the two cysteine residues were observed in conditions that induce state transitions (Shapiguzov et al. 2016).

State transitions operate similarly in plants and green algae, although the increase in PSI antenna size upon state 2 formation is larger (~50 %) in *Chlamydomonas* (Le Quiniou et al. 2015) than in plants (~25 %) (Ruban and Johnson 2009). They correspond to a redistribution of light energy toward either PSI or PSII photochemistry rather than a proper quenching through energy dissipation

(Nawrocki et al. 2016). Still, state transitions are often considered as a major component of NPQ and photoprotection because when LHCII complexes are bound to PSI, PSI acts as a quencher of Chl excitation without the production of reactive oxygen species (Setif et al. 1981). An increase in PSI antenna size in state 2 favors P_{700}^{+} accumulation, an effective quencher of light energy from associated antenna complexes (Trissl 1997). Some LHCII disconnected from PSII but not associated to PSI could aggregate and self-quench (Iwai et al. 2010b; Nagy et al. 2014; Unlu et al. 2014), a situation which does not seem to occur to a significant extent in vivo (Nawrocki et al. 2016). Therefore, a central question remains as to the physiological significance of state transitions (Goldschmidt-Clermont and Bassi 2015), and their consequences on the regulation of electron transport through the relative contribution of PSII and PSI in response to various environmental cues.

Lateral distribution of photosynthetic components and ultrastructure of the thylakoid membrane

To understand the process of photosynthetic electron flow as a whole, various parameters have to be taken into consideration: the relative stoichiometry of the complexes, their distribution in the membrane, the diffusion properties of soluble electron carriers, the formation of macromolecular complexes, or the compartmentalization of biochemical reactions. These features are conserved throughout the green lineage and define certain principles of photosynthetic regulation that are integral to oxygenic photosynthesis, regardless of the variations that may exist between the molecular components of each individual species.

Stoichiometry of photosynthetic components

Spectroscopic measurements have been very useful to determine the relative stoichiometry of photosynthetic complexes and proteins. PSI concentration is generally estimated from absorbance changes related to the formation of P_{700}^{+} [$\Delta\varepsilon_{700\ nm} = -60\ mM^{-1}\ cm^{-1}$, see (Hiyama and Ke 1972)]. It ranges between 1/500 and 1/1000 of total chlorophyll (Graan and Ort 1984; Melis 1991; Neale and Melis 1986; Whitmarsh and Ort 1984). PSII:PSI ratio varies between 2:1 (in plants mostly) and 1:1 (in heterotrophic green algae). It can be measured directly comparing the contribution of both photosystems after a short and saturating single turnover flash, to the contribution of PSI alone (hydroxylamine and DCMU treatment in the light), see (Joliot and Delosme 1974). It can be deduced as well from Q_A^- formation in samples treated with DCMU ($\Delta\varepsilon_{325\ nm} = 13\ mM^{-1}\ cm^{-1}$, see (Van Gorkom 1974), and further correction for absorbance flattening at short wavelengths). A cyt b_6f content of typically 0.5–1.2 per PSI is estimated from absorbance changes of cyt f ($\Delta\varepsilon_{554\ nm} = -25\ mM^{-1}\ cm^{-1}$) see (Metzger et al. 1997) in illuminated samples treated with DBMIB (2,5-dibromo-3-methyl-6-isopropyl-p-benzoquinone), i.e., when cyt f reduction is blocked at the Q_o site, or from oxidized-minus-reduced spectra (Lee and Whitmarsh 1989). In summary, the stoichiometry of membrane-bound complexes PSI: b_6f: PSII is centered around a mean value of 1:1:1, which is generally considered acceptable for models of photosynthetic electron transfer. To this schematic unitary photosynthetic chain is associated significantly larger pools of hydro- or liposoluble electron carriers, generally 2 PCs (generally reduced in the dark) and six PQ (two-electron carriers generally oxidized in the dark) (Graan and Ort 1984). Given that the total pool-size of photo-reducible electron acceptors is around 18 (Forbush and Kok 1968), it would leave a rather small-sized pool of six oxidizing-equivalents in PSI stromal electron acceptors ferredoxin, FNR, and $NADP^+$.

Diffusion coefficients for soluble carriers

In a two-dimensional model for diffusion, which is likely to be the case for quinones/quinols in a lipid bilayer, or PC in the narrow lumenal space of thylakoids, and during a time interval τ, a carrier with a diffusion coefficient D would diffuse over average distances r with $\langle r^2 \rangle = 4\ D\ \tau$ (Whitmarsh 1986). To support photosynthetic rates of $\sim 300\ s^{-1}$ ($\tau \sim 3$ ms), D must be $\sim 8.10^{-12}\ m^2\ s^{-1}$ to transfer an electron over a ~ 100 nm distance separating PSII from cyt b_6f complex (Hope 1993). For quinols in thylakoids, estimates of diffusion coefficient of 2.10^{-12}–$3.10^{-11}\ m^2\ s^{-1}$ fall in that range (Mitchell et al. 1990). The water-soluble PC has a much larger diffusion coefficient of $8.10^{-11}\ m^2\ s^{-1}$ (Sanderson et al. 1986), allowing for its diffusion over large distances >1 μm in ~3 ms. It accounts for the submillisecond oxidation rate of cyt f following flash-excitation of PSI (Bouges-Bocquet 1977a, b). The reduction rate of cyt f and PC after a flash is correlated to quinol oxidation at the Q_o site of cyt b_6f and to an electrogenic reaction, denoting the electron transfer through the low-potential chain (hemes b_L and b_h). This latter step of cyt f reduction ~10 ms (~3 ms in uncoupled conditions) is limiting for photosynthetic electron transfer. Plastocyanin diffusion, much faster, is not limiting and serves as a long-distance electron carrier between PSII and PSI. Ferredoxin has a similarly high diffusion coefficient of 12.10^{-11}–$13.10^{-11}\ m^2\ s^{-1}$ (Yoch et al. 1975). Overall, among the different species, quinones are the least mobile electron carriers.

Structure and lateral heterogeneity of the thylakoid membrane

Whereas thylakoid membranes of most algae do not show more than 2–3 appressed layers, members of the green lineage (chlorophyta), at least for the chlorophyceae *Chlamydomonas* (Wollman and Diner 1980) and *Dunaliella* (Larkum and Barrett 1983) show stacks of 2–15 membranes, approaching plant-like granal structures. Due to hydrophobic interaction between transmembrane domains, photosynthetic complexes are densely packed in the membrane. As a result, the membrane surface adhesion depends more on the protein content than on the lipid content. Thylakoid membranes incubated in low salt completely unstack, an effect that can be reversed by the addition of cations (Izawa and Good 1966a, b), suggesting electrostatic interactions at the aqueous stromal interface. Removal or modification of the LHCII N-terminal peptide disrupts thylakoid adhesion (Mullet 1983b). The positively charged N-terminal peptides from LHCII would interact with the negatively charged LHCII surface from the facing membrane. Consistent with this, a mutant of barley deficient in LHCII shows poor stacking (Goodchild et al. 1966), while reconstitutions of LHCII proteins into membranes allow restacking (Day et al. 1984). Goodenough and Staehelin (1971) showed that the particles in the stacked regions (grana core) differ in size and density from those in the unstacked regions (grana margins, end membranes, and stroma lamellae), suggesting large differences in protein composition between these regions. For example, the ATP synthase (Andersson and Anderson 1980), NDH (Lennon et al. 2003; Berger et al. 1993), PGRL1 (Hertle et al. 2013), and PTOX (Lennon et al. 2003) have been localized at the grana margins and the stroma lamellae.

Like in plant grana, these *Chlamydomonas* appressed membranes seem to retain PSII, whereas elongated membranes contain more PSI (Vallon et al. 1985, 1986). Only in one case an absence of segregation between PSII and PSI has been reported (Bertos and Gibbs 1998), that does not seem to account for the well-established increased membrane stacking in PSI-less mutants or absence of membrane appression in mutants devoid of PSII (Goodenough and Levine 1969). The thylakoid lateral heterogeneity in *Chlamydomonas* is, very much like in plants, shown by the relatively low PSII to PSI spillover in stacked (high cation concentration) compared to unstacked membranes (low cation concentration) (Wollman and Diner 1980); for a general discussion, see (Barber 1980). PSII and PSI act in tandem for linear electron flow but are separated from each other. The functional consequence of such different localizations is still a matter of debate. Perhaps it is that PSI is a much more efficient exciton quencher than PSII, as shown for example by the quenching of Chl fluorescence observed in state 2. If PSI and PSII were linked by a strong excitonic connectivity, PSI would act as a PSII quencher (Trissl and Wilhelm 1993) and thereby decrease PSII photochemical efficiency.

Environmental cues and redox signals are major determinants for the redistribution of photosynthetic complexes. LHCII phosphorylation on a threonine residue in response to a redox signal located at the N-terminus neutralizes a positive charge and destabilizes the grana stacking (Mullet 1983a). Dynamic and reversible changes in membrane ultrastructure are observed under specific light conditions. Light treatment results in swelling of the lumenal space caused by the entrance of Cl^- and Ca^{2+} ions driven by the *pmf* (Kirchhoff et al. 2011; Ettinger et al. 1999), modifying the osmotic potential. High-light treatment also causes unstacking of the layers, as well as lateral shrinkage and reduction of the number of layers (Chuartzman et al. 2008; Nagy et al. 2014). These structural changes are caused by the migration of the phospho-LHCII from the grana stacks toward grana margins and lamellae during state transitions. Membranes look constitutively stacked in the *A. thaliana* STN7 mutant (Clausen et al. 2014), whereas grana structures of the phosphatase (*tap38*) mutant appear destabilized (Samol et al. 2012). The cyt b_6f is evenly distributed in the thylakoid membrane (Cox and Andersson 1981; Anderson 1982), although it can also migrate from appressed to nonappressed regions (Vallon et al. 1991), as a consequence of PetO, and perhaps SuIV, phosphorylation by the Stt7 kinase (Bergner et al. 2015; Hamel et al. 2000).

Another source of heterogeneity may arise from the formation of supercomplexes. Whereas no association between PSI and cyt b_6f complex was evidenced in spinach (Breyton et al. 2006), a megacomplex of ~1 500 kDa containing these two membrane complexes, plus LHCI and LHCII antenna complexes, was purified from *C. reinhardtii* cells acclimated to anaerobic conditions (Iwai et al. 2010a). Because supercomplex formation was also found in the Stt7 mutant blocked in state 1, it does not depend upon state transitions but solely on the anaerobic state of the cells (Takahashi et al. 2013). In addition to PSI-cyt b_6f-LHCI-LHCII complexes, other molecular components were retained namely FNR, PGRL1, and PetO (Iwai et al. 2010a), and also CAS (Ca^{2+} sensor) and ANR1 (Anaerobic Response 1) (Terashima et al. 2012). That PGRL1 is retained in the supercomplex without being associated to PGR5 is surprising (Iwai et al. 2010a), because the latter is found in thylakoid membranes of *C. reinhardtii* and active in CEF (Johnson et al. 2014). CAS and ANR1 knock-down lines are compromised for CEF (Terashima et al. 2012), suggesting either a direct role of these in electron transfer or in the stabilization of the supercomplex, or an indirect role in ion homeostasis in the chloroplast possibly interacting with electron and proton transfer. PetO and ANR1

proteins are not found in higher plants, perhaps the mechanism of anaerobic supercomplex formation, which seems to be found only in green algae, should be searched for in relation to these two unique players.

Kinetics consequences of lateral heterogeneities and protein packing density of the thylakoid membrane

As expected from their respective diffusion coefficients and from the presence of cyt b_6f next to PSII in the grana stacks, PC serves as the long-distance electron carrier between PSII and PSI. In plants, quinone diffusion is confined to heterogeneous membrane microdomains encompassing 3–4 PSII centers and about six PQH_2 per PSII center (Lavergne et al. 1992; Joliot et al. 1992). Upon light excitation, PSII reduces this proximal quinone pool rapidly (<100 ms), whereas full PQ reduction is only achieved after a few seconds of illumination. Such heterogeneity in quinone diffusion is also observed at the level of cyt b_6f. After cyt f oxidation by PSI, its reduction is biphasic with a fast phase likely related to the fraction of the complex localized to grana stacks, and a slow phase corresponding to a fraction of cyt b_6f disconnected from PSII and probably localized to stroma lamellae (Joliot and Joliot 1992). In *Chlamydomonas*, a kinetics analysis based on single turnover excitation of PSI showed that cyt f oxidation rate can vary from 110 to 350 µs half-time (Delosme 1991) whether cells were acclimated to anoxic or oxic conditions, respectively, but still much faster than cyt f reduction by PQH_2. This observation correlates with the preferred association of cyt b_6f with PSI in anoxic conditions (Wollman and Bulté 1989), with the migration of cyt b_6f from grana stacks to stroma lamellae upon the transition from oxic to anoxic conditions (Vallon et al. 1991; Takahashi et al. 2013), i.e., a shortening of the distance between PSI and cyt b_6f. Because CEF involves cyt b_6f complex and PSI and not PSII, it was suggested that the balance between cyclic and linear electron flows would be regulated through cyt b_6f localization in the membrane (Wollman 2001a). Further work used the postillumination reduction of cyt f, PC, and P_{700}^+ as a probe for intersystem electron transfer (Joliot and Joliot 2005; Kirchhoff et al. 2004). Kinetic heterogeneities were attributed to a restricted diffusion of PC in the lumenal space due to either molecular friction in the narrow lumenal space (Kirchhoff 2014) or bottlenecks in the interconnecting regions of the lumen (Albertsson 2001; Joliot and Joliot 2005). The first hypothesis implies that P_{700}^+ reduction by PC is somehow rate limiting. Such rate limitation would prevent the complete oxidation of cyt f under saturating illumination and that was not taken into account in the model. The bottleneck model does not face the same issues: within any given compartment PC equilibrates quickly with cyt f and P_{700}. However, it imposes rigid compartmentalization between appressed and nonappressed membranes and requires further consideration.

Structural and redox regulation of photosynthetic light reactions

Two possible regulations of cyclic flow can be considered. On the one hand, cycling of electrons around PSI is regulated by the redox poise of electron carriers involved in the cycle (Arnon and Chain 1975); on the other hand there is a possibility that some PSI are specifically engaged in cyclic (i.e., excluded from linear electron flow) (Knaff and Arnon 1969).

Early in vitro experiments showed that cyclic turnovers increased when PSI was excited more than PSII. Anaerobic conditions increased cyclic flow as well (Tagawa et al. 1963a, b). Both conditions seemed to keep Fd, added to purified thylakoid membranes, in its reduced form, while the reducing pressure of PSII on the PQ pool was restricted. PSII activity appeared to have contrasting effects, either sustaining or competing with CEF. On the one hand, when PSII turnover stopped completely, no ATP synthesis occurred, suggesting that there were no electrons available for cycling around PSI. On the other hand, when PSII was fully active, ATP synthesis was also restricted, implying that all intersystem electron carriers were reduced, leaving no electron acceptor for CEF. In between these two instances, cyclic turnovers increased and ATP formation was stimulated up to 7-fold (Tagawa et al. 1963a). This optimum condition for a proper poise of cyclic was confirmed in many other studies (Bendall and Manasse 1995; Crowther and Hind 1980; Hosler and Yocum 1987; Mills et al. 1978; Slovacek et al. 1980). Redox regulations involving thioredoxins or hydrogen peroxide may also control the threshold of activation of CEF (Hertle et al. 2013; Strand et al. 2015a, b).

The above can be considered as the "oxidoreductionist" theory of CEF, i.e., the regulation of cyclic relative to linear can be reduced to oxidation–reduction reactions. It has received very convincing support from quantitative measurements, both in vivo and in vitro. There is another point of view that can be denoted as the "ultrastructuralist" theory, i.e., the regulation of cyclic and linear electron flows depends upon the ultrastructure of the thylakoid membrane (Albertsson 2001; Joliot and Joliot 2005) and/or the formation of supercomplexes (Iwai et al. 2010a; Joliot and Joliot 2002). An important point to take into account is that heterogeneities in the electron transport chain can impact the redox equilibration between electron carriers. Practically, any deviation in the equilibrium constant of a

reaction between in vivo (or in the native membrane) and in vitro conditions (determined from the standard redox potentials) is a diagnostic for nonhomogeneity of the system (Lavergne 2009). Such heterogeneities often arise from the extremely high protein packing density found in natural biological membranes, especially in photosynthetic membranes where LHCs have to be densely packed for excitonic connectivity to the photosystems. Association of protein complexes in supercomplexes can be considered as an extreme case where the packing density and protein–protein interaction is so high that mild detergents do not destabilize the interaction between membrane protein complexes.

In the particular case of the *Chlamydomonas* "anaerobic cyclic" supercomplex containing PSI-LHCI-LHCII-FNR-cyt b_6f-PGRL1-CAS-ANR1-PetO but having lost Fd, PC, and PGR5, it is difficult to envision the function of the complex in vivo. The general expectation is that the retention of electron carriers within a confined volume would shorten the diffusion path of the electrons carriers and make the kinetics faster. It has not yet been demonstrated for the "anaerobic cyclic" supercomplex supplemented with 1 μm PC where cyt *f* oxidation is slower [>10 ms, estimated from (Iwai et al. 2010a)] than in vivo where the complexes are far more distant from each other [<0.3 ms, see (Bouges-Bocquet 1977a, b) or (Delosme 1991)]. In any case, the rate of in vivo electron transfer between cyt *f* and PSI is an order of magnitude faster than cyt *f* reduction, limiting for both LEF and CEF, so the regulation of the balance between linear and cyclic has to be searched elsewhere, perhaps on the acceptor side of PSI. On this front, the results obtained on the supercomplex were even more deceiving: 1 μm Fd added to the supercomplex slowly reduced heme b_h with a half-time of ~2 s (Iwai et al. 2010a), a reaction attributed to CEF, whereas in vitro linear double reduction of FNR with 2 μm PSI and 4 μm Fd occurred much faster ~4 ms (Cassan et al. 2005). Perhaps the slow cyclic turnover of the *C. reinhardtii* "anaerobic supercomplex" was due to the absence of PGR5, which is involved in cyclic in *A. thaliana* (Munekage et al. 2002) as well as in *C. reinhardtii* (Johnson et al. 2014). Perhaps plastoquinones were missing to accept electrons from PGRL1 and reduced Fd, a reaction that has been shown to occur in vitro (Hertle et al. 2013).

Role for plastoquinones, towards reconciliation?

An idea that has already been put forward is that the PQ pool can be an important control point for CEF (Allen 2003; Alric 2015). Plastoquinones are electron acceptors shared by PSII, the cyt b_6f and NDH, or PGR5/PGRL1. Under strong illumination PSII significantly reduces its primary quinone acceptor Q_A, and therefore the PQ pool. As a consequence, the reducing pressure from PSII on the PQ pool would oppose the NDH or PGR pathways and decrease CEF in high light. Under such conditions, however, the ΔpH-dependent qE component of NPQ of chlorophyll fluorescence is decreased in *pgr5* and *pgrl1* mutants, in *A. thaliana* (Munekage et al. 2002; Joliot and Alric 2013; DalCorso et al. 2008) as well as in *C. reinhardtii* (Johnson et al. 2014; Peers et al. 2009; Tolleter et al. 2011). It shows that CEF is important in high light and argues against a strict competition between PSII and NDH or PGR for the reduction of the PQ pool. In fact, a kinetic competition between PSII and NDH or PGR holds only for a homogenous system where plastoquinones would diffuse freely in the membrane and would accept electrons equally from any of these enzymes. We now know that such is not the case, and PTOX, NDH (Lennon et al. 2003; Berger et al. 1993), and PGRL1 (Hertle et al. 2013) are excluded from grana stacks where PSII is mostly localized, and PQ diffusion is restricted to membrane microdomains (Lavergne and Joliot 1991). In this "quinone-centric" model, the exclusion of PSII from membrane microdomains containing NDH and PGR would be more important than the association of cyt b_6f with PSI. The colocalization of NDH, PGR, PTOX, and cyt b_6f in membrane microdomains would poise CEF for action in high light by avoiding overreduction of quinones in this compartment.

In Fig. 2, we propose an illustration of the structural lateral heterogeneities of the thylakoid membrane and of the dynamic rearrangements that may occur in various conditions.

In panels (A) and (B) are schematized the dark-adapted oxidizing condition ("state 1") and reducing condition ("state 2"), respectively. In (A) the PQ pool is evenly oxidized, membrane proteins are dephosphorylated and pile up thylakoid membranes in grana stacks. In (B) the PQ pool is uniformly reduced, membrane proteins are phosphorylated and grana structures are destabilized. Under steady-state illumination, the redox poise of the PQ pool is expected to fall in between these two opposite states (A) and (B). Taking (A) as a starting point, light induced PSII activity would make the PQ pool more reduced; while starting from (B), any light intensity greater than the compensation point would restore oxygen evolution and PQ pool oxidation. In (C) are tentatively represented the redox or kinetic heterogeneities that may arise under steady-state photosynthesis, in a semiphosphorylated state such as that proposed by Goldschmidt-Clermont and Bassi (2015). In the light, PQH_2 and oxidized PC accumulate. This is usually detected as an increase of fluorescence (nonlinearly related to the reduction of Q_A) and simultaneous absorbance decay at

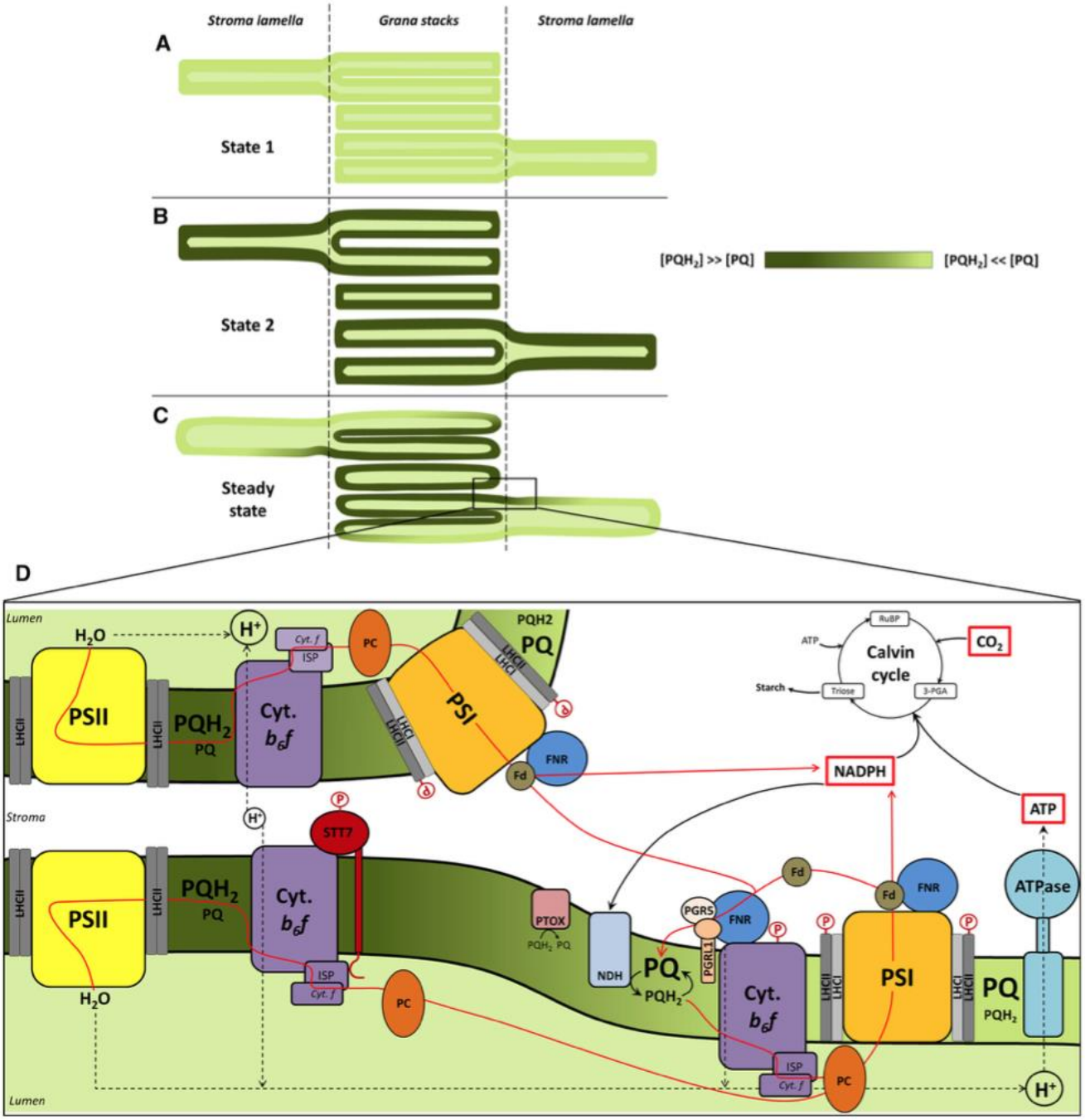

Fig. 2 Schematic representation of thylakoid ultrastructure in various conditions. **A** Oxidizing, low light, "state 1" conditions: the PQ pool is evenly oxidized (membrane colored in *light green*) as compared to the poised state. The thylakoid membranes are appressed. **B** Reducing, low light, "state 2" conditions: the PQ pool is uniformly reduced (membrane colored in *dark green*) as compared to the poised state. The thylakoid membranes are no longer appressed due to the high level of protein phosphorylation by active Stt7 kinase. A large proportion of phospho-LHCII proteins migrate toward PSI in the lamellae. **C** "Steady-state" continuous illumination, between state 1 and state 2. The redox state of plastoquinones is heterogeneous due to diffusion limited to microdomains. More quinols would be found around PSII complexes in grana stacks (*dark green*), whereas stroma lamellae, more distant from PSII and containing PTOX, would retain some significant amounts of PQ (*light green*). The ultrastructure and lateral heterogeneity of the thylakoid membrane is destabilized (protein phosphorylations and redistribution). High-light conditions also create a strong influx of protons into the lumen which induce a swelling of the thylakoids. **D** Zoom in the grana margins shows that the cyt b_6f complex is distributed homogeneously in the thylakoid membrane although it can be phosphorylated and migrate to regions lacking PSII. These membrane microdomains likely retaining oxidized quinones in high light may catalyze cyclic electron flow more efficiently. *Red arrows* electron transport; *dashed lines* proton influx and efflux

700 nm (accumulation of P_{700}^{+}). However, a more detailed in vivo kinetic analysis shows that the equilibrium constant between Q_A and the Q-pool is much smaller than estimated from equilibrium titrations of the Q_A/Q_A^- and PQ/PQH_2 redox couples (Forbush and Kok 1968; Lavergne and Joliot 1991). Such kinetic heterogeneities show that a significant reduction of Q_A does not translate into a full reduction of the PQ pool. Membrane microdomains (likely the more distant from PSII) retaining more oxidized quinones (electron acceptors for NDH and PGR) would be more efficient for CEF. When localized in membrane microdomains containing PSII (grana stacks), the cyt b_6f would oxidize PQH_2 locally produced by PSII, and would therefore be involved in LEF. When localized in membrane microdomains devoid of PSII (grana margins and lamellae) but containing NDH and PGR, the cyt b_6f would participate in the cyclic pathway. Contrary to other models of CEF, ours does not involve any assumption on electron bifurcation from Fd towards FNR or PGR nor on supercomplex formation, but only relies on the compartmentalization of plastoquinones in the membrane that would provide a regulatory control point for the balance between linear and CEFs.

Acknowledgments This work was supported by the Irtelis PhD fellowship granted to L.D. by the CEA, and by the ChloroPaths Grant ANR-14-CE05-0041 awarded to X.J. Frédéric Chaux is warmly thanked for critical reading of the manuscript.

References

Albertsson P (2001) A quantitative model of the domain structure of the photosynthetic membrane. Trends Plant Sci 6(8):349–358

Allen JF (2003) Cyclic, pseudocyclic and noncyclic photophosphorylation: new links in the chain. Trends Plant Sci 8(1):15–19

Alric J (2010) Cyclic electron flow around photosystem I in unicellular green algae. Photosynth Res 106(1–2):47–56. doi:10.1007/s11120-010-9566-4

Alric J (2015) The plastoquinone pool, poised for cyclic electron flow? Frontiers in plant science. doi:10.3389/Fpls.2015.00540

Anderson JM (1982) Distribution of the cytochromes of spinach chloroplasts between the appressed membranes of grana stacks and stroma-exposed thylakoid regions. FEBS Lett 138(1):62–66. doi:10.1016/0014-5793(82)80395-5

Andersson B, Anderson JM (1980) Lateral heterogeneity in the distribution of chlorophyll-protein complexes of the thylakoid membranes of spinach chloroplasts. Biochim Biophys Acta 593(2):427–440

Arnon DI, Chain RK (1975) Regulation of ferredoxin-catalyzed photosynthetic phosphorylations. Proc Natl Acad Sci U S A 72(12):4961–4965

Arnon DI, Allen MB, Whatley FR (1954) Photosynthesis by isolated chloroplasts. Nature 174(4426):394–396

Barber J (1980) An Explanation for the Relationship between Salt-Induced Thylakoid Stacking and the Chlorophyll Fluorescence Changes Associated with Changes in Spillover of Energy from Photosystem-Ii to Photosystem-I. FEBS Lett 118(1):1–10. doi:10.1016/0014-5793(80)81207-5

Bassham JA (1979) The Reductive Pentose Phosphate Cycle and Its Regulation. In: Latzko MGaE (ed) Photosynthesis II, Photosynthetic Carbon Metabolism and Related Processes, vol 6. Encyclopedia of Plant Physiology. Springer-Verlag, Berlin, pp 9-28

Bellafiore S, Barneche F, Peltier G, Rochaix JD (2005) State transitions and light adaptation require chloroplast thylakoid protein kinase STN7. Nature 433(7028):892–895. doi:10.1038/nature03286

Bendall DS, Manasse RS (1995) Cyclic Photophosphorylation and Electron-Transport. Bba-Bioenergetics 1229(1):23–38. doi:10.1016/0005-2728(94)00195-B

Berger S, Ellersiek U, Westhoff P, Steinmüller K (1993) Studies on the expression of NDH-H, a subunit of the NAD(P)H-plastoquinone-oxidoreductase of higher-plant chloroplasts. Planta 190(1):25–31. doi:10.1007/BF00195671

Bergner SV, Scholz M, Trompelt K, Barth J, Gabelein P, Steinbeck J, Xue H, Clowez S, Fucile G, Goldschmidt-Clermont M, Fufezan C, Hippler M (2015) STATE TRANSITION7-Dependent Phosphorylation Is Modulated by Changing Environmental Conditions, and Its Absence Triggers Remodeling of Photosynthetic Protein Complexes. Plant Physiol 168(2):615–634. doi:10.1104/pp.15.00072

Bertos NR, Gibbs SP (1998) Evidence for a lack of photosystem segregation in *Chlamydomonas reinhardtii* (Chlorophyceae). J Phycol 34(6):1009–1016. doi:10.1046/J.1529-8817.1998.341009.X

Bonaventura C, Myers J (1969) Fluorescence and oxygen evolution from *Chlorella pyrenoidosa*. Biochim Biophys Acta 189(3):366–383

Bouges-Bocquet B (1977a) Cytochrome f and plastocyanin kinetics in *Chlorella pyrenoidosa*. I. Oxidation kinetics after a flash. Biochim Biophys Acta 462(2):362–370

Bouges-Bocquet B (1977b) Cytochrome f and plastocyanin kinetics in *Chlorella pyrenoidosa*. II. Reduction kinetics and electric field increase in the 10 ms range. Biochim Biophys Acta 462(2):371–379

Breyton C, Nandha B, Johnson GN, Joliot P, Finazzi G (2006) Redox modulation of cyclic electron flow around photosystem I in C3 plants. Biochemistry 45(45):13465–13475. doi:10.1021/bi061439s

Cardol P, Alric J, Girard-Bascou J, Franck F, Wollman FA, Finazzi G (2009) Impaired respiration discloses the physiological significance of state transitions in *Chlamydomonas*. Proc Natl Acad Sci USA 106(37):15979–15984. doi:10.1073/pnas.0908111106

Cassan N, Lagoutte B, Setif P (2005) Ferredoxin-NADP + reductase. Kinetics of electron transfer, transient intermediates, and catalytic activities studied by flash-absorption spectroscopy with isolated photosystem I and ferredoxin. J Biol Chem 280(28):25960–25972. doi:10.1074/jbc.M503742200

Chapman SP, Paget CM, Johnson GN, Schwartz JM (2015) Flux balance analysis reveals acetate metabolism modulates cyclic electron flow and alternative glycolytic pathways in *Chlamydomonas reinhardtii*. Front Plant Sci 6:474. doi:10.3389/fpls.2015.00474

Chaux F, Peltier G, Johnson X (2015) A security network in PSI photoprotection: regulation of photosynthetic control, NPQ and O2 photoreduction by cyclic electron flow. Front Plant Sci 6:875. doi:10.3389/fpls.2015.00875

Chuartzman SG, Nevo R, Shimoni E, Charuvi D, Kiss V, Ohad I, Brumfeld V, Reich Z (2008) Thylakoid membrane remodeling during state transitions in *Arabidopsis*. Plant Cell 20(4):1029–1039. doi:10.1105/tpc.107.055830

Clausen CH, Brooks MD, Li TD, Grob P, Kemalyan G, Nogales E, Niyogi KK, Fletcher DA (2014) Dynamic mechanical responses of *Arabidopsis* thylakoid membranes during PSII-specific

illumination. Biophys J 106(9):1864–1870. doi:10.1016/j.bpj.2014.03.016

Correa-Galvis V, Redekop P, Guan K, Griess A, Truong TB, Wakao S, Niyogi KK, Jahns P (2016) Photosystem II subunit PsbS is Involved in the Induction of LHCSR-dependent energy dissipation in *Chlamydomonas reinhardtii*. J Biol Chem. doi:10.1074/jbc.M116.737312

Cox RP, Andersson B (1981) Lateral and transverse organisation of cytochromes in the chloroplast thylakoid membrane. Biochem Biophys Res Commun 103(4):1336–1342

Crofts AR, Meinhardt SW, Jones KR, Snozzi M (1983) The role of the quinone pool in the cyclic electron-transfer chain of *Rhodopseudomonas Sphaeroides*: a modified Q-cycle mechanism. Biochim Biophys Acta 723(2):202–218. doi:10.1016/0005-2728(83)90120-2

Crofts AR, Guergova-Kuras M, Huang L, Kuras R, Zhang Z, Berry EA (1999) Mechanism of ubiquinol oxidation by the bc(1) complex: role of the iron sulfur protein and its mobility. Biochemistry 38(48):15791–15806

Crowther D, Hind G (1980) Partial characterization of cyclic electron transport in intact chloroplasts. Arch Biochem Biophys 204(2):568–577

DalCorso G, Pesaresi P, Masiero S, Aseeva E, Schunemann D, Finazzi G, Joliot P, Barbato R, Leister D (2008) A complex containing PGRL1 and PGR5 is involved in the switch between linear and cyclic electron flow in *Arabidopsis*. Cell 132(2):273–285. doi:10.1016/j.cell.2007.12.028

Day DA, Ryrie IJ, Fuad N (1984) Investigations of the role of the main light-harvesting chlorophyll-protein complex in thylakoid membranes. Reconstitution of depleted membranes from intermittent-light-grown plants with the isolated complex. J Cell Biol 98(1):163–172

de Lavalette ADL, Barucq L, Alric J, Rappaport F, Zito F (2009) Is the redox state of the ci heme of the cytochrome b_6f complex dependent on the occupation and structure of the Qi site and vice versa? J Biol Chem 284(31):20822–20829. doi:10.1074/jbc.M109.016709

Delosme R (1991) Electron transfer from cytochrome f to photosystem I in green algae. Photosynth Res 29(1):45–54. doi:10.1007/BF00035205

Depege N, Bellafiore S, Rochaix JD (2003) Role of chloroplast protein kinase Stt7 in LHCII phosphorylation and state transition in *Chlamydomonas*. Science 299(5612):1572–1575. doi:10.1126/science.1081397

Ettinger WF, Clear AM, Fanning KJ, Peck ML (1999) Identification of a Ca2+/H+ antiport in the plant chloroplast thylakoid membrane. Plant Physiol 119(4):1379–1386

Evans JR, Loreto F (2000) Acquisition and diffusion of CO_2 in higher plant leaves. In: Leegood RC, Sharkey TD, von Caemmerer S (eds) Photosynthesis: physiology and metabolism, advances in photosynthesis and respiration. Kluwer Academic Publishers, Dordrecht, pp 321–351. doi:10.1007/0-306-48137-5_14

Forbush B, Kok B (1968) Reaction between primary and secondary electron acceptors of photosystem II of photosynthesis. Biochim Biophys Acta 162(2):243–253

Goldschmidt-Clermont M, Bassi R (2015) Sharing light between two photosystems: mechanism of state transitions. Curr Opin Plant Biol 25:71–78. doi:10.1016/j.pbi.2015.04.009

Goodchild DJ, Highkin HR, Boardman NK (1966) The fine structure of chloroplasts in a barley mutant lacking chlorophyll B. Exp Cell Res 43(3):684–688

Goodenough UW, Levine RP (1969) Chloroplast ultrastructure in mutant strains of *Chlamydomonas reinhardi* lacking components of the photosynthetic apparatus. Plant Physiol 44(7):990–1000

Goodenough UW, Staehelin LA (1971) Structural differentiation of stacked and unstacked chloroplast membranes. Freeze-etch electron microscopy of wild-type and mutant strains of *Chlamydomonas*. J Cell Biol 48(3):594–619

Graan T, Ort DR (1984) Quantitation of the rapid electron donors to P700, the functional plastoquinone pool, and the ratio of the photosystems in spinach chloroplasts. J Biol Chem 259(22):14003–14010

Hamel P, Olive J, Pierre Y, Wollman FA, de Vitry C (2000) A new subunit of cytochrome b_6f complex undergoes reversible phosphorylation upon state transition. J Biol Chem 275(22):17072–17079. doi:10.1074/jbc.M001468200

Hauska G, Hurt E, Gabellini N, Lockau W (1983) Comparative aspects of quinol-cytochrome c/plastocyanin oxidoreductases. Biochim Biophys Acta 726(2):97–133

Hertle AP, Blunder T, Wunder T, Pesaresi P, Pribil M, Armbruster U, Leister D (2013) PGRL1 is the elusive ferredoxin-plastoquinone reductase in photosynthetic cyclic electron flow. Mol Cell 49(3):511–523. doi:10.1016/j.molcel.2012.11.030

Hiyama T, Ke B (1972) Difference spectra and extinction coefficients of P 700. Biochim Biophys Acta 267(1):160–171

Holt NE, Fleming GR, Niyogi KK (2004) Toward an understanding of the mechanism of nonphotochemical quenching in green plants. Biochemistry 43(26):8281–8289. doi:10.1021/bi0494020

Hope AB (1993) The chloroplast cytochrome bf complex: a critical focus on function. Biochim Biophys Acta 1143(1):1–22

Horton P, Allen JF, Black MT, Bennett J (1981) Regulation of phosphorylation of chloroplast membrane polypeptides by the redox state of plastoquinone. FEBS Lett 125(2):193–196. doi:10.1016/0014-5793(81)80716-8

Horton P, Wentworth M, Ruban A (2005) Control of the light harvesting function of chloroplast membranes: the LHCII-aggregation model for non-photochemical quenching. FEBS Lett 579(20):4201–4206. doi:10.1016/j.febslet.2005.07.003

Hosler JP, Yocum CF (1987) Regulation of cyclic photophosphorylation during ferredoxin-mediated electron transport: effect of DCMU and the NADPH/NADP ratio. Plant Physiol 83(4):965–969

Iwai M, Takizawa K, Tokutsu R, Okamuro A, Takahashi Y, Minagawa J (2010a) Isolation of the elusive supercomplex that drives cyclic electron flow in photosynthesis. Nature 464(7292):1210–1213. doi:10.1038/nature08885

Iwai M, Yokono M, Inada N, Minagawa J (2010b) Live-cell imaging of photosystem II antenna dissociation during state transitions. Proc Natl Acad Sci USA 107(5):2337–2342. doi:10.1073/pnas.0908808107

Izawa S, Good NE (1966a) Effect of salts and electron transport on the conformation of isolated chloroplasts. I. Light-scattering and volume changes. Plant Physiol 41(3):533–543

Izawa S, Good NE (1966b) Effect of salts and electron transport on the conformation of isolated chloroplasts. II. Electron microscopy. Plant Physiol 41(3):544–552

Johnson X, Alric J (2013) Central carbon metabolism and electron transport in *Chlamydomonas reinhardtii*: metabolic constraints for carbon partitioning between oil and starch. Eukaryot Cell 12(6):776–793. doi:10.1128/EC.00318-12

Johnson X, Steinbeck J, Dent RM, Takahashi H, Richaud P, Ozawa S, Houille-Vernes L, Petroutsos D, Rappaport F, Grossman AR, Niyogi KK, Hippler M, Alric J (2014) Proton gradient regulation 5-mediated cyclic electron flow under ATP- or redox-limited conditions: a study of DeltaATpase pgr5 and DeltarbcL pgr5 mutants in the green alga *Chlamydomonas reinhardtii*. Plant Physiol 165(1):438–452. doi:10.1104/pp.113.233593

Joliot P, Alric J (2013) Inhibition of CO2 fixation by iodoacetamide stimulates cyclic electron flow and non-photochemical quenching upon far-red illumination. Photosynth Res 115(1):55–63. doi:10.1007/s11120-013-9826-1

Joliot P, Delosme R (1974) Flash-induced 519 nm absorption change in green algae. Biochim Biophys Acta Bioenerg 357(2):267–284. doi:10.1016/0005-2728(74)90066-8

Joliot P, Joliot A (1992) Electron-transfer between photosystem-Ii and the cytochrome-B/F complex—mechanistic and structural implications. Biochim Biophys Acta 1102(1):53–61. doi:10.1016/0005-2728(92)90064-9

Joliot P, Joliot A (2002) Cyclic electron transfer in plant leaf. Proc Natl Acad Sci USA 99(15):10209–10214. doi:10.1073/pnas.102306999

Joliot P, Joliot A (2005) Quantification of cyclic and linear flows in plants. Proc Natl Acad Sci USA 102(13):4913–4918. doi:10.1073/pnas.0501268102

Joliot P, Lavergne J, Beal D (1992) Plastoquinone compartmentation in chloroplasts. 1. Evidence for domains with different rates of photo-reduction. Biochim Biophys Acta 1101(1):1–12. doi:10.1016/0167-4838(92)90460-U

Kallas T (2012) Cytochrome b_6f complex at the heart of energy transduction and redox signaling. In: Eaton-Rye JJ, Tripathy BC, Sharkey TD (eds) Photosynthesis. advances in photosynthesis and respiration. Springer, Houten, pp 501–560. doi:10.1007/978-94-007-1579-0_21

Kirchhoff H (2014) Diffusion of molecules and macromolecules in thylakoid membranes. Biochim Biophys Acta 1837(4):495–502. doi:10.1016/j.bbabio.2013.11.003

Kirchhoff H, Schottler MA, Maurer J, Weis E (2004) Plastocyanin redox kinetics in spinach chloroplasts: evidence for disequilibrium in the high potential chain. Biochim Biophys Acta 1659(1):63–72. doi:10.1016/j.bbabio.2004.08.004

Kirchhoff H, Hall C, Wood M, Herbstova M, Tsabari O, Nevo R, Charuvi D, Shimoni E, Reich Z (2011) Dynamic control of protein diffusion within the granal thylakoid lumen. Proc Natl Acad Sci USA 108(50):20248–20253. doi:10.1073/pnas.1104141109

Knaff DB, Arnon DI (1969) A concept of three light reactions in photosynthesis by green plants. Proc Natl Acad Sci USA 64(2):715–722

Kramer DM, Evans JR (2011) The importance of energy balance in improving photosynthetic productivity. Plant Physiol 155(1):70–78. doi:10.1104/pp.110.166652

Kramer DM, Cruz JA, Kanazawa A (2003) Balancing the central roles of the thylakoid proton gradient. Trends Plant Sci 8(1):27–32

Kurisu G, Zhang H, Smith JL, Cramer WA (2003) Structure of the cytochrome b_6f complex of oxygenic photosynthesis: tuning the cavity. Science 302(5647):1009–1014. doi:10.1126/science.1090165

Larkum AWD, Barrett J (1983) Light-harvesting processes in algae. In: Woolhouse HW (ed) Advances in botanical research. Academic Press, New York, pp 1–219. doi:10.1016/S0065-2296(08)60260-8

Lavergne J (2009) Clustering of electron transfer components: kinetic and thermodynamic consequences. In: Laisk A, Nedbal L, Govindjee (eds) Photosynthesis in silico. Advances in photosynthesis and respiration. Springer, Houten, pp 177–205. doi:10.1007/978-1-4020-9237-4_8

Lavergne J, Joliot P (1991) Restricted diffusion in photosynthetic membranes. Trends Biochem Sci 16(4):129–134. doi:10.1016/0968-0004(91)90054-Y

Lavergne J, Bouchaud JP, Joliot P (1992) Plastoquinone compartmentation in chloroplasts. 2. Theoretical aspects. Biochim Biophys Acta 1101(1):13–22. doi:10.1016/0167-4838(92)90461-L

Le Quiniou C, Tian L, Drop B, Wientjes E, van Stokkum IH, van Oort B, Croce R (2015) PSI-LHCI of *Chlamydomonas reinhardtii*: increasing the absorption cross section without losing efficiency. Biochim Biophys Acta 4–5:458–467. doi:10.1016/j.bbabio.2015.02.001

Lee WJ, Whitmarsh J (1989) Photosynthetic apparatus of pea thylakoid membranes : response to growth light intensity. Plant Physiol 89(3):932–940

Lemeille S, Rochaix JD (2010) State transitions at the crossroad of thylakoid signalling pathways. Photosynth Res 106(1–2):33–46. doi:10.1007/s11120-010-9538-8

Lemeille S, Willig A, Depege-Fargeix N, Delessert C, Bassi R, Rochaix JD (2009) Analysis of the chloroplast protein kinase Stt7 during state transitions. PLoS Biol 7(3):e45. doi:10.1371/journal.pbio.1000045

Lennon AM, Prommeenate P, Nixon PJ (2003) Location, expression and orientation of the putative chlororespiratory enzymes, Ndh and IMMUTANS, in higher-plant plastids. Planta 218(2):254–260. doi:10.1007/s00425-003-1111-7

Li XP, Gilmore AM, Caffarri S, Bassi R, Golan T, Kramer D, Niyogi KK (2004) Regulation of photosynthetic light harvesting involves intrathylakoid lumen pH sensing by the PsbS protein. J Biol Chem 279(22):22866–22874. doi:10.1074/jbc.M402461200

Melis A (1991) Dynamics of photosynthetic membrane-composition and function. Biochim Biophys Acta 1058(2):87–106. doi:10.1016/S0005-2728(05)80225-7

Mettler T, Muhlhaus T, Hemme D, Schottler MA, Rupprecht J, Idoine A, Veyel D, Pal SK, Yaneva-Roder L, Winck FV, Sommer F, Vosloh D, Seiwert B, Erban A, Burgos A, Arvidsson S, Schonfelder S, Arnold A, Gunther M, Krause U, Lohse M, Kopka J, Nikoloski Z, Mueller-Roeber B, Willmitzer L, Bock R, Schroda M, Stitt M (2014) Systems analysis of the response of photosynthesis, metabolism, and growth to an increase in irradiance in the photosynthetic model organism *Chlamydomonas reinhardtii*. Plant Cell 26(6):2310–2350. doi:10.1105/tpc.114.124537

Metzger SU, Cramer WA, Whitmarsh J (1997) Critical analysis of the extinction coefficient of chloroplast cytochrome f. Biochim Biophys Acta 1319(2–3):233–241

Mills JD, Slovacek RE, Hind G (1978) Cyclic electron transport in isolated intact chloroplasts. Further studies with antimycin. Biochim Biophys Acta 504(2):298–309

Mitchell P (1976) Possible molecular mechanisms of the protonmotive function of cytochrome systems. J Theor Biol 62(2):327–367

Mitchell R, Spillmann A, Haehnel W (1990) Plastoquinol diffusion in linear photosynthetic electron transport. Biophys J 58(4):1011–1024. doi:10.1016/S0006-3495(90)82445-0

Mullet JE (1983) The amino-acid-sequence of the polypeptide segment which regulates membrane adhesion (grana stacking) in chloroplasts. J Biol Chem 258(16):9941–9948

Munekage Y, Hojo M, Meurer J, Endo T, Tasaka M, Shikanai T (2002) PGR5 is involved in cyclic electron flow around photosystem I and is essential for photoprotection in *Arabidopsis*. Cell 110(3):361–371

Nagy G, Unnep R, Zsiros O, Tokutsu R, Takizawa K, Porcar L, Moyet L, Petroutsos D, Garab G, Finazzi G, Minagawa J (2014) Chloroplast remodeling during state transitions in *Chlamydomonas reinhardtii* as revealed by noninvasive techniques in vivo. Proc Natl Acad Sci USA 111(13):5042–5047. doi:10.1073/pnas.1322494111

Nawrocki WJ, Santabarbara S, Mosebach L, Wollman F-A, Rappaport F (2016) State transitions redistribute rather than dissipate energy between the two photosystems in *Chlamydomonas*. Nat Plants 2(4):16031. doi:10.1038/nplants.2016.31

Neale PJ, Melis A (1986) Algal photosynthetic membrane complexes and the photosynthesis-irradiance curve: a comparison of light-adaptation responses in *Chlamydomonas reinhardtii* (chlorophyta). J Phycol 22(4):531–538. doi:10.1111/j.1529-8817.1986.tb02497.x

Niyogi KK (1999) Photoprotection revisited: genetic and molecular approaches. Annu Rev Plant Physiol Plant Mol Biol 50:333–359. doi:10.1146/annurev.arplant.50.1.333

Ort DR, Yocum CF (1996) Electron transfer and energy transduction in photosynthesis: an overview. In: Ort DR, Yocum CF (eds)

Oxygenic photosynthesis: the light reactions, vol 4. Kluwer Academic Publishers, Dordrecht, pp 1–9

Peers G, Truong TB, Ostendorf E, Busch A, Elrad D, Grossman AR, Hippler M, Niyogi KK (2009) An ancient light-harvesting protein is critical for the regulation of algal photosynthesis. Nature 462(7272):518–521. doi:10.1038/nature08587

Peltier G, Tolleter D, Billon E, Cournac L (2010) Auxiliary electron transport pathways in chloroplasts of microalgae. Photosynth Res 106(1–2):19–31. doi:10.1007/s11120-010-9575-3

Peltier G, Aro EM, Shikanai T (2015) NDH-1 and NDH-2 plastoquinone reductases in oxygenic photosynthesis. Annu Rev Plant Biol. doi:10.1146/annurev-arplant-043014-114752

Petroutsos D, Terauchi AM, Busch A, Hirschmann I, Merchant SS, Finazzi G, Hippler M (2009) PGRL1 participates in iron-induced remodeling of the photosynthetic apparatus and in energy metabolism in *Chlamydomonas reinhardtii*. J Biol Chem 284(47):32770–32781. doi:10.1074/jbc.M109.050468

Pierre Y, Breyton C, Kramer D, Popot JL (1995) Purification and characterization of the cytochrome b6 f complex from *Chlamydomonas reinhardtii*. J Biol Chem 270(49):29342–29349

Ruban AV, Johnson MP (2009) Dynamics of higher plant photosystem cross-section associated with state transitions. Photosynth Res 99(3):173–183. doi:10.1007/s11120-008-9387-x

Samol I, Shapiguzov A, Ingelsson B, Fucile G, Crevecoeur M, Vener AV, Rochaix JD, Goldschmidt-Clermont M (2012) Identification of a photosystem II phosphatase involved in light acclimation in *Arabidopsis*. Plant Cell 24(6):2596–2609. doi:10.1105/tpc.112.095703

Sanderson DG, Anderson LB, Gross EL (1986) Determination of the redox potential and diffusion coefficient of the protein plastocyanin using optically transparent filar electrodes. Biochim Biophys Acta Bioenerg 852(2):269–278. doi:10.1016/0005-2728(86)90232-X

Setif P, Hervo G, Mathis P (1981) Flash-induced absorption changes in photosystem I, radical pair or triplet state formation? Biochim Biophys Acta Bioenerg 638(2):257–267. doi:10.1016/0005-2728(81)90235-8

Shapiguzov A, Ingelsson B, Samol I, Andres C, Kessler F, Rochaix JD, Vener AV, Goldschmidt-Clermont M (2010) The PPH1 phosphatase is specifically involved in LHCII dephosphorylation and state transitions in *Arabidopsis*. Proc Natl Acad Sci USA 107(10):4782–4787. doi:10.1073/pnas.0913810107

Shapiguzov A, Chai X, Fucile G, Longoni P, Zhang L, Rochaix JD (2016) Activation of the Stt7/STN7 kinase through dynamic interactions with the cytochrome b_6f complex. Plant Physiol. doi:10.1104/pp.15.01893

Slovacek RE, Crowther D, Hind G (1980) Relative activities of linear and cyclic electron flows during chloroplast CO_2-fixation. Biochim Biophys Acta 592(3):495–505

Stiehl HH, Witt HT (1969) Quantitative treatment of the function of plastoquinone in photosynthesis. Z Naturforsch B 24(12):1588–1598

Strand DD, Fisher N, Davis GA, Kramer DM (2015a) Redox regulation of the antimycin A sensitive pathway of cyclic electron flow around photosystem I in higher plant thylakoids. Biochim Biophys Acta 1:1–6. doi:10.1016/j.bbabio.2015.07.012

Strand DD, Livingston AK, Satoh-Cruz M, Froehlich JE, Maurino VG, Kramer DM (2015b) Activation of cyclic electron flow by hydrogen peroxide in vivo. Proc Natl Acad Sci USA 112(17):5539–5544. doi:10.1073/pnas.1418223112

Stroebel D, Choquet Y, Popot J-L, Picot D (2003) An atypical haem in the cytochrome b_6f complex. Nature 426:413–418

Tagawa K, Tsujimoto HY, Arnon DI (1963a) Role of chloroplast ferredoxin in the energy conversion process of photosynthesis. Proc Natl Acad Sci USA 49:567–572

Tagawa K, Tsujimoto HY, Arnon DI (1963b) Separation by monochromatic light of photosynthetic phosphorylation from oxygen evolution. Proc Natl Acad Sci USA 50:544–549

Takahashi H, Clowez S, Wollman FA, Vallon O, Rappaport F (2013) Cyclic electron flow is redox-controlled but independent of state transition. Nat Commun 4:1954. doi:10.1038/ncomms2954

Terashima M, Petroutsos D, Hudig M, Tolstygina I, Trompelt K, Gabelein P, Fufezan C, Kudla J, Weinl S, Finazzi G, Hippler M (2012) Calcium-dependent regulation of cyclic photosynthetic electron transfer by a CAS, ANR1, and PGRL1 complex. Proc Natl Acad Sci USA 109(43):17717–17722. doi:10.1073/pnas.1207118109

Tibiletti T, Auroy P, Peltier G, Caffarri S (2016) *Chlamydomonas reinhardtii* PsbS protein is functional and accumulates rapidly and transiently under high light. Plant Physiol. doi:10.1104/pp.16.00572

Tolleter D, Ghysels B, Alric J, Petroutsos D, Tolstygina I, Krawietz D, Happe T, Auroy P, Adriano JM, Beyly A, Cuine S, Plet J, Reiter IM, Genty B, Cournac L, Hippler M, Peltier G (2011) Control of hydrogen photoproduction by the proton gradient generated by cyclic electron flow in *Chlamydomonas reinhardtii*. Plant Cell 23(7):2619–2630. doi:10.1105/tpc.111.086876

Trissl HW (1997) Determination of the quenching efficiency of the oxidized primary donor of photosystem I, P700(+): implications for the trapping mechanism. Photosynth Res 54(3):237–240. doi:10.1023/A:1005981016835

Trissl HW, Wilhelm C (1993) Why do thylakoid membranes from higher-plants form grana stacks. Trends Biochem Sci 18(11):415–419. doi:10.1016/0968-0004(93)90136-B

Unlu C, Drop B, Croce R, van Amerongen H (2014) State transitions in *Chlamydomonas reinhardtii* strongly modulate the functional size of photosystem II but not of photosystem I. Proc Natl Acad Sci USA 111(9):3460–3465. doi:10.1073/pnas.1319164111

Vallon O, Wollman FA, Olive J (1985) Distribution of intrinsic and extrinsic subunits of the Ps–Ii protein complex between appressed and non-appressed regions of the thylakoid membrane—an immunocytochemical study. FEBS Lett 183(2):245–250. doi:10.1016/0014-5793(85)80786-9

Vallon O, Wollman FA, Olive J (1986) Lateral distribution of the main protein complexes of the photosynthetic apparatus in *Chlamydomonas reinhardtii* and in spinach—an immunocytochemical study using intact thylakoid membranes and a Ps–Ii enriched membrane preparation. Photobiochem Photobiophys 12(3–4):203–220

Vallon O, Bulte L, Dainese P, Olive J, Bassi R, Wollman FA (1991) Lateral redistribution of cytochrome b6/f complexes along thylakoid membranes upon state transitions. Proc Natl Acad Sci USA 88(18):8262–8266

Van Gorkom HJ (1974) Identification of the reduced primary electron acceptor of photosystem II as a bound semiquinone anion. Biochim Biophys Acta Bioenerg 347(3):439–442. doi:10.1016/0005-2728(74)90081-4

Vener AV, Van Kan PJ, Gal A, Andersson B, Ohad I (1995) Activation/deactivation cycle of redox-controlled thylakoid protein phosphorylation. Role of plastoquinol bound to the reduced cytochrome bf complex. J Biol Chem 270(42):25225–25232

Wang Y, Stessman DJ, Spalding MH (2015) The CO_2 concentrating mechanism and photosynthetic carbon assimilation in limiting CO_2: how *Chlamydomonas* works against the gradient. Plant J Cell Mol Biol 82(3):429–448. doi:10.1111/tpj.12829

Whitmarsh J (1986) Mobile electron carriers in thylakoids. In: Staehelin LA, Arntzen CJ (eds) Photosynthesis ill, photosynthetic membranes and light harvesting systems. Encyclopedia of plant physiology. Springer-Verlag, Berlin, pp 508–527

Whitmarsh J, Ort DR (1984) Stoichiometries of electron transport complexes in spinach chloroplasts. Arch Biochem Biophys 231(2):378–389

Witt HT (1971) Coupling of quanta, electrons, fields, ions and phosphorylation in the functional membrane of photosynthesis. Results by pulse spectroscopic methods. Q Rev Biophys 4(4):365–477

Wollman FA (2001a) State transitions reveal the dynamics and flexibility of the photosynthetic apparatus. EMBO J 20(14):3623–3630. doi:10.1093/emboj/20.14.3623

Wollman FA (2001b) State transitions reveal the dynamics and flexibility of the photosynthetic apparatus. EMBO J 20:3623–3630

Wollman FA, Bulté L (1989) Towards an understanding of the physiological role of state transitions. In: Hall DO, Grassi G (eds) Photoconversion processes for energy and chemicals: proceedings of the 3rd EEC workshop on photochemical, photoelectrochemical and photobiological research and development, Taylor & Francis Group, London, 18–21 April 1989. pp 198–207

Wollman FA, Diner BA (1980) Cation control of fluorescence emission, light scatter, and membrane stacking in pigment mutants of *Chlamydomonas reinhardi*. Arch Biochem Biophys 201(2):646–659

Wollman F-A, Lemaire C (1988) Studies on kinase-controlled state transitions in photosystem II and b_6f mutants from *Chlamydomonas reinhardtii* which lack quinone-binding proteins. Biochim Biophys Acta Bioenerg 933(1):85–94

Yoch DC, Arnon DI, Sweeney WV (1975) Characterization of two soluble ferredoxins as distinct from bound iron–sulfur proteins in the photosynthetic bacterium *Rhodospirillum rubrum*. J Biol Chem 250(21):8330–8336

Zhang H, Whitelegge JP, Cramer WA (2001) Ferredoxin: NADP + oxidoreductase is a subunit of the chloroplast cytochrome b_6f complex. J Biol Chem 276(41):38159–38165. doi:10.1074/jbc.M105454200

Zito F, Alric J (2016) Heme ci or cn of the cytochrome b_6f complex, a short retrospective. In: Cramer AW, Kallas T (eds) Cytochrome complexes: evolution, structures, energy transduction, and signaling. Springer, Dordrecht, pp 295–306. doi:10.1007/978-94-017-7481-9_15

Zito F, Finazzi G, Joliot P, Wollman FA (1998) Glu78, from the conserved PEWY sequence of subunit IV, has a key function in cytochrome b_6f turnover. Biochemistry 37(29):10395–10403. doi:10.1021/bi980238o

Zito F, Finazzi G, Delosme R, Nitschke W, Picot D, Wollman FA (1999) The Qo site of cytochrome b_6f complexes controls the activation of the LHCII kinase. EMBO J 18(11):2961–2969. doi:10.1093/emboj/18.11.2961

Zones JM, Blaby IK, Merchant SS, Umen JG (2015) High-resolution profiling of a synchronized diurnal transcriptome from *Chlamydomonas reinhardtii* reveals continuous cell and metabolic differentiation. Plant Cell 27(10):2743–2769. doi:10.1105/tpc.15.00498

Zu Y, Couture MM, Kolling DR, Crofts AR, Eltis LD, Fee JA, Hirst J (2003) Reduction potentials of Rieske clusters: importance of the coupling between oxidation state and histidine protonation state. Biochemistry 42(42):12400–12408. doi:10.1021/bi0350957

C. State transitions

Whether motile (bacteria and algae) or sessile (land and marine plants), photosynthetic organisms are subject to significant environmental changes induced by abiotic factors. The most significant of these are variations in light quality and quantity which can have direct effects on the components and function of the electron transport chain. Any departure from redox equilibrium along the chain can lead to energy loss through thermal dissipation (q_E), photoinhibition (q_I) and protein degradation, and therefore to a decrease in the maximal quantum yield of photosynthesis. Because quantum efficiency and electron transfer chain integrity are important determinants of growth and reproductive success, photosynthetic organisms possess regulatory mechanisms that enable acclimation responses to changing light conditions (Figure I.11.).

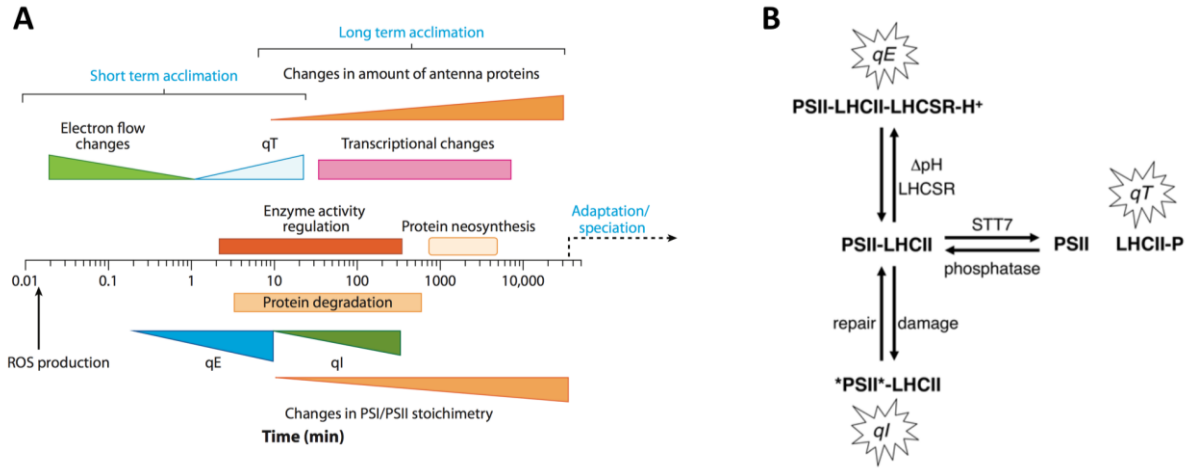

Figure I.11. Mechanisms of acclimation to changing abiotic conditions.
(A) Time scale of major acclimation processes in organisms of the green lineage (Eberhard et al. 2008). **(B)** Diagram of relationships between NPQ mechanisms that participate in photoprotection in Chlamydomonas (Erickson et al. 2015).

All descendants of cyanobacteria that perform oxygenic photosynthesis use two photosystems, with their respective light-absorbing antenna systems, working in parallel at either end of a chain of redox species acting as electron carriers. A consequence of this setup is that photochemical and redox events happening at one end of the chain can have consequences on redox reactions all along the chain and up to the other reaction center. Differences in pigment composition between the two photosystem antenna systems lead to differences in light absorption, PSII absorbing maximally at 680 nm and PSI at 710 nm. Under changing light conditions, these differences can lead to an unbalanced excitation of the two photosystems. Within minutes, as part of the short-term acclimation response, this imbalance can be

neutralized through the mechanism of state transitions (q_T). This mechanism was discovered almost 50 years ago by two teams working on unicellular green and red algae (Bonaventura and Myers 1969; Murata 1969). It was described as a process that enables and controls the transfer of excitation between the two photosystems. About a decade later, the phosphorylation of LHCII proteins was found to be part of the mechanism (Bennett 1977) and to be correlated with the redox state of the PQ pool (Allen et al. 1981). The model established then still holds, and states that a reduction of the PQ pool induces the phosphorylation and lateral redistribution of LHCII proteins from PSII to PSI, thus re-equilibrating the excitation and keeping the chain under redox poise (Figure I.12.). In the last few decades, several teams have contributed to our current understanding of this complex process (for reviews, see (Wollman 2001; Lemeille and Rochaix 2010)).

After the initial findings of the early 1980's, research efforts were directed toward identifying the state transition kinase and understanding the redox-dependency of the process. Using Chlamydomonas, an elegant genetic screen was developed to isolate state transition mutants generated by insertional mutagenesis, yielding a mutant (*stt7*, for state transition-deficient) that did not phosphorylate LHCII proteins in reducing conditions (Fleischmann et al. 1999). Identification of the crippled gene revealed that it coded for a conserved putative serine/threonine kinase localized in the thylakoid membrane, and characterization showed that it was required for the phosphorylation of antenna proteins (Depege et al. 2003). In trying to understand the redox-control of state transitions, several studies pointed to a role of the cyt b_6f in the process. Mutants lacking cyt b_6f complex were unable to transit from State I to State II in conditions where the PQ pool was reduced (Wollman and Lemaire 1988). Later, this finding was clarified by the fact that mutants lacking PQH_2 binding to the lumenal Q_o site were similarly affected for state transitions (Vener et al. 1995; Zito et al. 1999). A new protein, PetO, was found to be associated but loosely-bound to the cyt b_6f complex and to be phosphorylated upon PQ pool reduction (Hamel et al. 2000). It was unknown whether the elusive LHCII kinase was also responsible for the phosphorylation of PetO, until a very recent phosphoproteomics study confirmed it (Bergner et al. 2015). Once the two determinants had been clearly identified, their distinct role and concerted action in the mechanism of state transitions were scrutinized.

The characterization of the Stt7 kinase revealed that it contained a membrane-spanning domain, an N-terminal domain in the lumen and a C-terminal region containing the kinase domain in the stroma (Lemeille et al. 2009). The Stt7-dependent LHCII phosphorylation sites were

mapped in the stroma as well (Lemeille et al. 2010). Co-immunoprecipitation and pull-down experiments showed that the kinase interacted specifically with the lumenal Rieske ISP subunit of cyt *b*$_6$*f* (Lemeille et al. 2009). Furthermore, single amino acid substitutions of two conserved cysteine residues in the lumenal N-terminal domain abolished the activity of the kinase. Redox changes of these residues caused by Q_o site catalysis were later suggested to induce Stt7 activation through transient dimerization (Shapiguzov et al. 2016) or conformational changes of its transmembrane domain (Singh et al. 2016).

On the cyt *b*$_6$*f* side, the major unknown was how the signal of PQH_2-binding at the lumenal Q_o site could be transmitted across the membrane and activate the stromal kinase domain. The peculiar Chl *a* molecule was probed for a potential role in this signal transduction (de Lacroix de Lavalette, Finazzi, et al. 2008; Hasan and Cramer 2012) because of its position in the 3D structure (Stroebel et al. 2003). Its phytyl chain protrudes into the Q_o site and its porphyrin ring sticks out toward the exterior of the complex between helices F and G of subunit IV. This peripheral region accommodates the 8th helix of the cyt *b* subunit of cyt *bc*$_1$ complexes or the synthetic DOPC lipid used to stabilize the cyt *b*$_6$*f* complex during isolation from *M. laminosus* and crystallization (Kurisu et al. 2003). Furthermore, fusion of the subunit IV C-terminal (end of helix G) to the N-terminal of the small transmembrane PetL subunit inhibited state transitions without affecting the electron transfer capacity of the complex. This further suggested that the transmembrane domain of Stt7 would bind in the vicinity of helix G, not far from the Chl *a* molecule. As such, it was proposed that the latter could transmit the signal of PQH_2-binding at Q_o by modifying the lipid-mediated interaction of the Stt7 transmembrane domain with the subunit IV niche, thereby activating the kinase (Hasan and Cramer 2014). However, the authors specified that the concentration of synthetic DOPC had to be close to saturation in the protein buffer to maintain a stable dimeric complex, and there is no telling whether similar lipid binding at the subunit IV niche is found in the native context. Another candidate for signal transduction was the lumenal head domain of the Rieske ISP, which oscillates between the Q_o-proximal and Q_o-distal positions during electron transfer along the high-potential chain of cyt *b*$_6$*f* (Breyton 2000). The Δ*petC* deletion strain that accumulated a modified cyt *b*$_6$*f* lacking the Rieske protein and unable to oxidize PQH_2 was also impaired for state transitions (de Vitry et al. 1999). It was proposed that conformational changes of the lumenal domain could participate in kinase activation (Zito et al. 1999; Finazzi et al. 2001). However, mutants with truncated versions of the hinge region and 10-fold reduction in the plastoquinol oxidation rate did not show any alteration in the kinetics of transition from State I to State II (de Vitry et al. 2004).

Many other questions on the mechanism of state transitions have fueled recent research efforts: is Stt7 the only state transition kinase or is it part of a phosphorylation cascade? What is the sequence of phosphorylation events? Which LHCII proteins are phosphorylated and how exactly? What effects does it have on thylakoid ultrastructure, on their migration and on their association to PSI? What are the other substrates of Stt7? How do state transitions (q_T) relate to other mechanisms of NPQ (like q_E) and the establishment of safety valves through alternative electron flows? Can we find links between the short-term acclimation responses and the longer-term regulations of transcription and protein synthesis? These questions are inter-linked and show the complexity and centrality of the topic of state transitions in the larger scope of photosynthesis research.

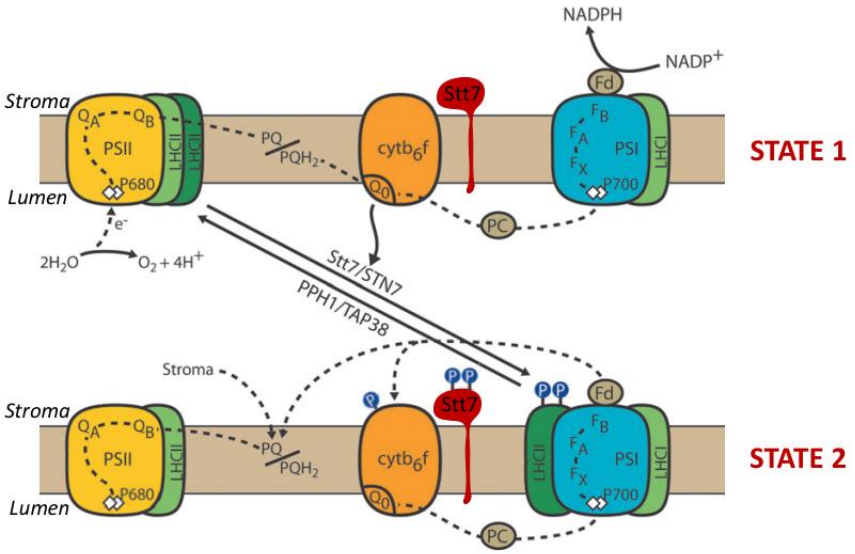

Figure I.12. Model of state transitions in Chlamydomonas.
Two redox-dependent states can be distinguished and induced in order to study the mechanism of state transitions. In State I, the excitation is either in favor of PSI or balanced between the two photosystems, the PQ pool is oxidized or poised, Stt7 is inactive and associated with the cyt b_6f and LHCII proteins are associated with PSII. Upon a change in light conditions that leads to an over-excitation of PSII with respect to PSI, the PQ pool becomes over-reduced, a PQH_2 is bound to the Q_o site of the cyt b_6f, which transmits this redox signal and activates Stt7*. The kinase becomes phosphorylated*, phosphorylates PetO and its target LHCII proteins, which dissociate from PSII, migrate out of the grana region and associate with PSI, forming State II. The increased PSI antenna size re-equilibrates the excitation energy and poises the redox state of the PQ pool. Stt7 is inactivated by the constitutive action of a phosphatase and re-associates with the cyt b_6f. Adaptet from (Rochaix 2011).

*Marks the major questions that we set out to answer in this work.

D. Structure-function study of the regulatory roles of the cyt b_6f in state transitions

As detailed in the previous sections, an extensive literature exists on the evolution, structure and function of Rieske/cyt *b* complexes, and in particular on cyt bc_1 of bacteria and mitochondria and cyt b_6f of cyanobacteria and chloroplasts. Before the structures of the chloroplast (Stroebel et al. 2003) and cyanobacterial (Kurisu et al. 2003) cyt b_6f complexes were obtained, most studies aiming at characterizing this complex used the homologous and better-known cyt bc_1 as a structural framework. Time-resolved spectroscopy and structure-function studies using site-directed mutagenesis were instrumental in building our understanding of the similarities and differences between *bc* and *bf* complexes in terms of structure and function in electron transfer and catalysis. This in turn nourished the discussion on the evolutionary history of Rieske/cyt *b* complexes. What people soon realized was that the structural core (Rieske ISP, cyt *b* subunit(s) and their respective co-factors) and functional core (electron transfer, Q-cycle, proton translocation) of the complex were highly conserved and not very robust to change. However, because Rieske/cyt *b* complexes are ubiquitous and arise in a variety of biological contexts, it seems logical to look for functional variability behind any structural differences observed between complexes of different phyla. The various structural differences found in Rieske/cyt *b* complexes and detailed in the previous section on their evolution can be viewed as markers of their molecular adaptation to different biological and chemical environments.

The cyt b_6f complex found in cyanobacteria and chloroplasts is unique in that it serves as the coupling component between two reaction centers that capture light energy and perform charge separation, in an electron transfer chain that can operate in both linear and cyclic electron transfer modes. A long-standing question in oxygenic photosynthesis research has therefore been to understand the role played by the cyt b_6f in keeping the system close to an equilibrium state, in terms of energy capture and flow, that insures maximal efficiency and integrity of the photosynthetic apparatus. This balance is entirely dependent on redox poise along the chain and maintaining a proper ATP/NAPDH ratio, two parameters that are controlled by state transitions and the relative contributions of linear and cyclic electron flows. In this work, we have focused our attention on the mechanism of state transitions.

The absence of a crystallographic structure of the state transition kinase, whether in plants or in algae, has greatly hampered our ability to decipher how it interacts with the cyt b_6f and how its activity is regulated. Of particular interest is the question of how the prerequisite step of plastoquinol binding at the lumenal Q_o site participates in the activation of the kinase whose catalytic domain is in the stroma. To overcome the missing structural information and address this question, we devised a novel experimental strategy combining random mutagenesis, chloroplast transformation and chlorophyll fluorescence emission imaging. Leaning on seminal studies that identified subunit IV as a candidate in the interaction of cyt b_6f with Stt7, we defined the region of subunit IV starting from the PEWY motif of the Q_o site and extending to its C-terminal along two peripheral transmembrane helices F and G as the target sequence for random mutagenesis. **Chapter II** describes results from this first attempt at combining the random mutagenesis of a chloroplast-encoded gene with chloroplast transformation and selection on phototrophy. We present an analysis of the sequencing data and discuss some aspects of the robustness and function of the cyt b_6f complex. In **Chapter III**, we show that, combined with a functional screen on state transitions based on chlorophyll fluorescence emission imaging, this unbiased and "large-scale" mutagenesis approach enabled us to identify a "state transition hotspot" on the stromal side of cyt b_6f where point mutations impaired state transitions. Results of the characterization of random and site-directed mutants of this region are presented, along with results that confirmed that a crucial residue, Arg125, participates in the activation of the Stt7 kinase. **Chapter IV** provides additional results and analyses that are used to build a model describing both the interaction between the cyt b_6f and Stt7 and the redox signal transduction mediated by the cyt b_6f and leading to kinase activation.

CHAPTER II – A new tool for the study and engineering of chloroplast-encoded proteins

The mutagenesis of discrete nucleotide position(s) along a gene sequence is a powerful tool for the study of protein structure and function through genetic screens. Many applications have been derived from this general concept. Organism-wide (*in vivo*) mutagenesis using ultraviolet (UV) light (Witkin 1969), chemical mutagens (Hayatsu and Miura 1970) or mutator plasmids (Selifonova et al. 2001; Badran and Liu 2015) provide ways to study processes involving many interacting parts, like metabolic pathways, or to perform directed evolution using a well-defined selective pressure. Other methods, such as error-prone PCR (epPCR) (Zakour and Loeb 1982; Leung et al. 1989; Cadwell and Joyce 1992) and DNA shuffling (Crameri et al. 1998), are used *in vitro* to target the mutagenesis to specific DNA sequences. In addition to being non-invasive, these latter methods insure a better control on mutation rate and mutational spectrum while staying compatible with large-scale approaches such as directed evolution. Two determinants in these kinds of genetic screens are the compatibility of the target organism with high-throughput methods and the selection or screening techniques used to isolate and identify a lost, affected or evolved phenotype.

Microalgae, like bacteria and yeast, are well suited as hosts of randomly mutagenized DNA sequences because of their fast generation time and the ease with which they can be phenotyped. Their photosynthetic fluorescence emission provides a functional and endogenous phenotypic probe. Heterotrophic microalgae possess the additional advantage of being able to harbor deletions of essential photosynthetic genes, yielding non-phototrophic, acetate-requiring strains. These can be used as host strains for complementation, allowing selection of transformants in the light on their ability to recover and sustain photosynthetic growth. Furthermore, the chloroplast genome contains all the elements and machinery to perform homologous recombination. All these factors are especially valuable for *in vitro* random mutagenesis by error-prone PCR because one can remove an essential gene from the chloroplast while maintaining the strain heterotrophically, and replace it with random mutagenized copies of the gene in order to look for affected or evolved phenotypes.

In the past, several groups have applied the principles of random mutagenesis to the study of photosynthetic organisms, mainly using chemical mutagens. The vast majority of studies

focused on cyanobacteria (Ermakova-Gerdes et al. 1996; Wu et al. 1999; Yamasato et al. 2002) and purple bacteria (Wang and Liao 2001; Barahona et al. 2016). Studies using organisms of the green lineage are scarce (Sakuraba et al. 2008; Cordero et al. 2011) and targeted random mutagenesis was only performed using degenerate oligonucleotides (Fischer et al. 1998; Naver et al. 2001). Here we show results of the first random mutagenesis by error-prone PCR of a chloroplast-encoded gene coupled to chloroplast complementation. Using this tool, we analyze the robustness and plasticity of subunit IV in the context of a multi-subunit transmembrane complex. Finally, we provide an example of its application to the study of a photosynthetic function and suggest some perspectives for its future uses.

A. Random mutagenesis of a chloroplast gene by error-prone PCR – Robustness and plasticity of cyt b_6f subunit IV. Submitted article: *Plant Physiology*

Authors:

Louis Dumas[1], Francesca Zito[2], Pascaline Auroy[1], Xenie Johnson[1], Gilles Peltier[1], Jean Alric[1]

Affiliations:

[1]Laboratoire de Bioénergétique et Biotechnologie des Bactéries et Microalgues, CEA, CNRS, Aix-Marseille Université, UMR 7265, BIAM, CEA Cadarache, Saint-Paul-lez-Durance, France

[2]Laboratoire de Biologie Physico-Chimique des Protéines Membranaires, Institut de Biologie Physico-Chimique, CNRS, UMR7099, University Paris Diderot, Sorbonne Paris Cité, PSL Research University, Paris, France, 13 rue Pierre et Marie Curie, F-75005 Paris, France

Corresponding author:

Jean Alric

jean.alric@cea.fr

+33 4 42 25 78 63

LB3M, BIAM, CEA Cadarache, 13108 Saint-Paul-lez-Durance, France

Keywords: random mutagenesis, error-prone PCR, chloroplast biotechnology, directed evolution of enzymes, redesigning photosynthesis.

Abbreviations

FdUrd	5-fluorodeoxyuridine
PCR	Polymerase Chain Reaction
epPCR	error-prone PCR
rcPCR	reconstruction PCR
seqPCR	sequencing PCR
cyt	cytochrome
TAP	Tris-Acetate-Phosphate
TP	Tris-Phosphate
SNP	Single Nucleotide Polymorphism
WT	Wild-Type
bp	base-pair
RM	random mutagenesis

Abstract

Site-directed mutagenesis of chloroplast genes was developed about three decades ago and has greatly advanced the field of photosynthesis research. Here we describe a new approach combining error-prone PCR of a gene of interest and chloroplast complementation of the knock-out mutant for the generation of random mutants. We targeted the *petD* gene, coding for subunit IV of the thylakoid membrane-bound cytochrome b_6f complex, and show the proof-of-concept that this method is adapted to the study of highly hydrophobic, multi-subunit and chloroplast-encoded proteins containing cofactors such as hemes, iron-sulfur clusters and chlorophyll pigments. We show that screening for mutants and sequencing can be used to study photosynthetic mechanisms or probe the mutational robustness of chloroplast-encoded proteins, and suggest that this method will be a valuable tool for the directed evolution of enzymes in the chloroplast.

Introduction

The isolation of chloroplast mutations has been sought after for decades, for chloroplast biology and for photosynthesis studies. A plant cell contains up to a hundred chloroplasts, each containing up to a hundred copies of the chloroplast genome encompassing about one hundred genes (Shinozaki et al. 1986). At variance with plant cells, the unicellular algae *C. reinhardtii* contains only one chloroplast with around eighty copies of the chloroplast genome. This genome is sequenced and chloroplast transformation techniques are widely available, making this model organism fully amenable to genetic analysis. Various chemicals have been found to increase the rate of random mutations in the chloroplast genome, like the mutagen ICR-191 (Huang et al. 1981), or the thymidine analog 5-fluorodeoxyuridine (FdUrd) that reduces the number of chloroplast DNA molecules (Wurtz et al. 1979). FdUrd facilitates the dissemination of mutations throughout the plastid genomes that otherwise would have been counter-selected against wild-type copies. Other agents like metronidazole are toxic to the photosynthesizing cell and allow enrichment in mutants null for photosynthetic electron transport (Schmidt et al. 1977). These random mutagenesis techniques proved very useful throughout the years despite their mutational effects being random. As almost all the loci on the chloroplast genome became characterized, new techniques were developed such chloroplast transformation by biolistics (Boynton et al. 1988) and homologous recombination of a transgene in the chloroplast genome, and it became possible to target a specific plastid genome locus and introduce site-directed mutations. Selection on antibiotic-containing medium allowed markers (such as the spectinomycin resistance marker (Goldschmidt-Clermont 1991) to insert in every copy of the chloroplast genome).

These latter techniques are thus specific to a genome locus, and have been used to introduce selected deletions, promoter swaps or point-mutations in the chloroplast genome. Here we thought that it would be highly valuable to have a technique for random mutagenesis of a specific gene in the chloroplast. It would allow revisiting structure-function studies of chloroplast proteins, testing protein-protein interactions or even directing the evolution of exogenous enzymes in the chloroplast, as is currently done in other biological hosts like *E. coli* or *S. cerevisiae*. At variance with those organisms, the chloroplast appears as an excellent chassis for the production and analysis of highly hydrophobic compounds such as membrane proteins or liposoluble pigments and chemicals because the thylakoids form abundant compartmentalized membrane systems with high packing densities.

A first attempt at randomly mutating a targeted chloroplast gene fragment was contributed by Fischer et al. who succeeded in randomly mutagenizing a short region of PsaC (a peripheral subunit of photosystem I) to probe electron transfer reactions between PSI and Fd (Fischer et al. 1998). The degenerate oligonucleotide-directed mutagenesis used in that study (and the subsequent study by (Naver et al. 2001)) was however very limiting because of the length restriction in the target sequence (42-mer oligonucleotides, with only 5 wobbles giving one substitution each). Here, we adapted error-prone PCR (epPCR) to the random mutagenesis of a chloroplast gene, and focused on a core, highly hydrophobic protein subunit of the cytochrome (cyt) b_6f complex, which binds several cofactors (hemes, iron-sulfur cluster, chlorophyll and carotenoid). Our method has virtually no other limitation than the maximal length of amplification by PCR. This approach is potentially a game changer for photosynthesis and chloroplast biotechnology studies.

Materials and methods

Strains and media – A non-phototrophic strain of *C. reinhardtii* deleted for the chloroplast *petD* gene coding for subunit IV of the cyt b_6f complex (Δ*petD*) was used as a host strain for complementation (Kuras and Wollman 1994). The strain was maintained on Tris-Acetate-Phosphate (TAP) medium in dark or very low light (~10 $\mu mol_{photons}.m^{-2}\ s^{-1}$) whereas complemented lines were selected on photoautotrophic growth in Tris-Phosphate (TP) medium under 100 $\mu mol_{photons}.m^{-2}\ s^{-1}$ illumination in air supplemented with 2% CO_2.

Plasmids and primers – Plasmid $pWQH_6$ described previously (Choquet et al. 2003; de Lacroix de Lavalette, Barbagallo, et al. 2008) was used as epPCR template (see annotated map in Figure A2). Table A2 lists the primers used for epPCR. Both primer pairs define the 5' and 3' boundaries of the sequence targeted for random mutagenesis, in this case going from bp4109 to bp4465 following $pWQH_6$ map numbering or from bp199 to bp483 (3' stop codon) following *petD* gene numbering.

Random mutagenesis – Two molecular biology kits were used for random mutagenesis by epPCR: the GeneMorph® II EZClone Domain Mutagenesis Kit (Agilent Technologies) and the Diversify® PCR Random Mutagenesis Kit (Clontech). These rely on two different techniques to control the error rate of the polymerase. The first technique (Agilent kit) uses a high error-rate DNA polymerase with a low mutational bias and the mutation frequency is adjusted by

varying the amount of template DNA and the number of epPCR cycles. The second technique (Clontech kit) acts directly on the fidelity of a *Taq* DNA polymerase. Manganese (in the form of $MnSO_4$) is added to the epPCR reaction and increases the mutation frequency in a concentration-dependent manner by binding to the DNA template and decreasing the fidelity of the enzyme. The mutation frequency can be further increased by rising the dGTP concentration in order to skew the relative dNTP concentrations. Table M2 shows the epPCR conditions used for each kit. The epPCR products were loaded on a 2% agarose gel and the 750 bp fragment of interest purified using the NucleoSpin® Gel and PCR cleanup kit (Macherey-Nagel). Purified fragments were used as "megaprimers" in a reconstruction PCR (rcPCR) (conditions detailed in Table M2). The reaction products were treated with 10 units of *DpnI* restriction enzyme and left to incubate at 37°C for 2 hours. 2 µL of this reaction was used to transform 50 µl XL10-Gold® Ultracompetent *E. coli* cells by heat-shock. 10% of the transformation mixture was plated on LB-agar medium containing 100 $\mu g.mL^{-1}$ ampicillin and incubated at 37°C over-night. Ampicillin-resistant clones were counted and a subset was sequenced using the Pseq-f primer after colony growth in liquid culture and plasmid DNA recovery. The rest of the transformation mixture was used to amplify the plasmid library by inoculating either 5 mL or 200 mL LB batch cultures containing 100 $\mu g.mL^{-1}$ ampicillin and growing the cells over-night (37°C, 180 rpm). The amplified plasmid DNA library was recovered either by mini-prep (for 5 mL cultures) using the NucleoSpin® Plasmid kit (Macherey-Nagel) or by midi-prep (for 200 mL cultures) using the NucleoBond® Xtra Midi kit (Macherey-Nagel) and DNA concentration was measured on a NanoDrop spectrometer (GE). When the concentration was below 0.5 $\mu g.\mu L^{-1}$, the DNA preparation was concentrated on a SpeedVac (Servant ISS110, Thermo Scientific) to ≥ 0.5 $\mu g.\mu L^{-1}$.

Biolostic transformation – The S550d Seashell Technology kit was used for transformation of *C. reinhardtii* chloroplasts following a protocol adapted from the original technique described by Boynton et al. (Boynton et al. 1988). This kit contains 550 nm gold carrier particles at 50 $mg.mL^{-1}$ and binding and precipitation buffers. Additional materials to be supplied include autoclaved membrane holders and a bombardment chamber to which a partial vacuum and a high-pressure helium pulse can be applied. A freshly inoculated 200 mL TAP culture containing Δ*petD* cells in exponential phase (between $1x10^6$ and $4x10^6$ $cells.mL^{-1}$) was used for chloroplast transformation. Δ*petD* cells in TAP medium were centrifuged and re-suspended in TP medium to a concentration of $200x10^6$ $cells.mL^{-1}$. 100 µl of this suspension was plated on TP-agar plates

to give $20x10^6$ cells per plate and per transformation. 5 µL of a 0.5 $\mu g.\mu L^{-1}$ $pWQH_6$ plasmid DNA preparation containing the randomly mutated *petD* genes was added to 50 µL of binding buffer in a sterile Eppendorf tube. 60 µL S550d gold carrier particles at 50 $mg.mL^{-1}$ were added and the tube was left to incubate on ice for 1 minute. 100 µL of precipitation buffer was added and incubated on ice for 1 minute. The suspension was vortexed 5 seconds and centrifuged at 13000 rpm for 30 seconds. The pellet was washed with 500 µL ice-cold 100% EtOH and centrifuged at 13000 rpm for 30 seconds. 50 µL ice-cold 100% EtOH was added to the pellet which was then resuspended with a brief sonication (1-5 seconds, 25V, 25-30% amplitude) to avoid particle aggregation. 10 µL of gold particles coated with plasmid DNA were spread on a membrane holder which was then placed inside a vacuum sealed bombardment chamber along with a TP-agar plate placed ~20 cm below the holder tip. The following parameters were used: 0.1 bar partial vacuum in the bombardment chamber, 7 bars helium-shot pressure. After transformation, cells were left to recover in the dark for up to one day before being transferred to phototrophic conditions (40 $\mu mol_{photons}$ m^{-2} s^{-1} and air supplemented with 2% CO_2). Once the first transformants became visible (10-14 days), light was increased to 100 $\mu mol_{photons}$ m^{-2} s^{-1} to speed up growth and subsequent analysis.

Sequencing – petD sequences of *E. coli* transformants were obtained as described previously. The Chelex® method was used to extract DNA from cells of *C. reinhardtii* transformants and this DNA material was used to sequence the *petD* gene. Clones were resuspended in 15 µL H_2O so as to leave no aggregates. 10 µl 100% EtOH was added and the mix was incubated 5 minutes at RT. 80 µL of 5% Chelex® 100 solution (Bio-Rad) was added and the sample incubated 8 minutes at 95°C. The sample tube was left open at room temperature to evaporate the EtOH. 3 µL of the suspension was then used as template for PCR (seqPCR) (Table M2). and the unpurified PCR product was then sent for sequencing using the Pseq-f primer. All sequence analyses were performed with Geneious.

Statistical analysis – epPCR data can be fitted to a binomial distribution or to a Poisson distribution when the mutational frequency stays low (Drummond et al. 2005). The probability *p* of observing *k* events in an interval is given by the equation:

$$p = e^{-\lambda}\frac{\lambda^k}{k!} \quad (1)$$

where λ is the average number of mutations. The number n of mutants containing m mutations was fitted to equation:

$$n = a\, e^{-\lambda} \frac{\lambda^m}{\Gamma(m+1)} \qquad (2)$$

where Γ is the generalization of the factorial function to non-integer values, and coefficient a is used to adjust the amplitude.

Results

Error-prone PCR, library construction and amplification – petD, the chloroplast gene coding for subunit IV of the cyt b_6f complex, was chosen for random mutagenesis (RM). RM was done by error-prone PCR (epPCR) using commercially available molecular biology kits and specific primers to target the desired *petD* sequence on the pWQH$_6$ plasmid (see Figure A1 and Table A1). After the epPCR, the amplicon library of *petD* variants was inserted back into vector pWQH$_6$. The Agilent kit supplies reagents for a reconstruction PCR (rcPCR, "EZClone Reaction") which uses the epPCR products as megaprimers and the host plasmid (here pWQH$_6$) as template to reconstruct each mutagenized gene fragment into a plasmid. The ease of this technique, allowing for an efficient and reliable construction of a plasmid library without any cloning steps, prompted us to develop our own rcPCR to be used for the reconstruction of any mutagenized fragment (see optimal conditions detailed in second line of rcPCR column, Table M2). The rcPCR product was then treated with *DpnI* restriction enzyme which specifically degrades methylated and hemi-methylated DNA, in this case the non-mutated pWQH$_6$ plasmid DNA used as template for the rcPCR.

E. coli cells were transformed with the product of this reaction in order to repair the staggered nicks left on the plasmids at the rcPCR step and amplify the plasmid library. 10% of the transformed cell suspension was plated on selective medium (containing 100 µg.mL^{-1} ampicillin) to isolate clones and sequence *petD* variants. This allowed us to control the mutational frequency and assess library diversity (Table II.1). Initial trials using the Agilent kit (mutagenesis 1-3) produced a high proportion of non-mutated sequences (>50%) and up to three mutations per mutant. Reducing the amount of target DNA even 4-fold (between mutagenesis 1 and 3) did not have much effect on the mutational frequency. In mutagenesis 4, the amount

of target DNA was reduced 20-fold compared to mutagenesis 1 and thirty epPCR cycles were performed. As expected, this decreased the proportion of non-mutated sequences (41%) and generated up to six mutations per mutant. To further bring down the percentage of non-mutated fragments, the epPCR was performed using condition 9 of the Clontech mutagenesis kit (mutagenesis 5). In this condition, no WT sequences were recovered among the twelve sequenced *E. coli* clones, and up to eight mutations per mutant were introduced in the *petD* gene.

Because chloroplast transformation requires a large quantity of DNA (0.5 to 2 µg per shot, *i.e.* 2-3 orders of magnitude more than bacterial transformation), the remaining 90% of the transformation volume was used for library amplification. Although *E. coli* transformants were grown in ampicillin-containing medium and random mutations were inserted in *petD* only (and not in the Amp^R marker, so that no reduction in library diversity was expected), a loss in *petD* variant diversity at this step was observed and, later, avoided.

Table II.1. Summary of the various random mutagenesis trials performed.

Mutagenesis number	Kit used	Error-prone conditions				*E. coli* transformants					*C. reinhardtii* transformants				
		Total DNA template (μg)	Target DNA template (ng)	Buffer condition	Number of PCR cycles	Total	Sequenced	Non-mutated	Number of variant sequences	Distribution	Total	Sequenced	Non-mutated	Number of variant sequences	Distribution
1	Agilent	10	500		25	250	23	12 (52%)	11	(0-3)					
2	Agilent	5	250		30	nd	17	10 (58%)	7	(0-2)	~ 400	18	14 (78%)	3	(0-1)
3	Agilent	2.5	125		30	nd	18	10 (56%)	8	(0-2)					
4	Agilent	0.5	25		30	nd	12	5 (41%)	7	(0-6)	~ 1000	62	30 (48%)	12	(0-3)
5	Clontech			#9	25	nd	12	0%	12	(1-8)	~ 600	72	15 (21%)	40	(0-10)

Table II.2. Distribution of SNP types and effects.

	Mutation types and effects														Mutational bias	
	Transition (Ts)				Transversion (Tv)								Total	%	$\frac{Ts}{Tv}$	$\frac{AT \rightarrow GC}{GC \rightarrow AT}$
	A > G	G > A	T > C	C > T	A > T	A > C	T > A	T > G	G > C	G > T	C > G	C > A				
Non-silent	23	1	32	6	10	1	10	2	1	3	1	3	93	62.67		
Silent	14	0	24	1	4	0	10	3	0	0	0	0	56	37.33	**2.1**	**8.3**
Total	37	1	56	7	14	1	20	5	1	3	1	3	149			
%	24.67	0.67	37.33	4.67	9.33	0.67	13.33	3.33	0.67	2.00	0.67	2.00				

ΔpetD complementation and sequencing of C. reinhardtii complemented lines – The recovery of $pWQH_6$ variants by miniprep from 5 mL batch cultures yielded rather low amounts of plasmid DNA (typically 15 µg) compared to what is usually recommended for chloroplast transformation (2 µg per shot). Prior to transforming the *C. reinhardtii* Δ*petD* strain with the library of *petD* variants, we optimized the protocol for complementation using $pWQH_6$ carrying the WT *petD* gene in order to minimize the amount of plasmid DNA needed per shot. We found that doubling the number of host cells plated on the petri dish (20.10^6 instead of 10.10^6) compensated for a 4-fold decrease in the amount of plasmid DNA (500 ng per shot instead 2 µg) without compromising complementation efficiency. In summary, the product of the miniprep allowed for ~30 chloroplast transformations.

C. reinhardtii transformants were selected under photoautrophic growth conditions *i.e.* on their ability to recombine and replicate a viable version of the *petD* gene throughout the multi-copy chloroplast genome, synthesize a stable subunit IV polypeptide and assemble a functional cyt b_6f complex. Overall, 2000 transformants were obtained from mutageneses 2-5, with an average of 40 complemented clones per transformation. After 14-20 days of growth under phototrophic selection pressure, the petri dishes were placed under a chlorophyll fluorescence imaging system(Johnson et al. 2009) to assess photosynthetic electron flow and photosystem II quantum efficiency, see Figure II.1. A photochemical quenching of $q_P = 0.5 \pm 0.1$ under high light (600 $\mu mol_{photons}.m^{-2}.s^{-1}$) showed that all clones were efficient for photosynthesis. ~1-2 mm clones were chosen randomly from each transformation plate, restreaked on TP-agar medium and resuspended in 15 µL H_2O for DNA extraction using the Chelex resin. PCR products of the amplification of the recombined *petD* gene were sequenced and analyzed using Geneious (Table II.1). In sequenced clones originating from mutagenesis 1-3, the proportion of non-mutated *petD* genes was 78%, *i.e.* higher than the ~57% found in *E. coli*, and the distribution peak was shifted toward fewer mutations. The increased mutation rate induced in mutagenesis 4 was confirmed in *E. coli* as a shift of the distribution towards larger numbers of mutations (up to six per 300 bp) and fewer non-mutated copies. It was also observed after library amplification and chloroplast transformation: out of the sixty-two sequenced *C. reinhardtii* transformants, thirty contained the WT sequence (giving 48%, compared to 78% in transformants originating from mutageneses 1-3) and mutants held up to three mutations per 300 bp (compared to a maximum of one per 300 bp in mutagenesis 1-3). In the last mutagenesis trial using the Clontech kit, amongst the seventy-two *C. reinhardtii* transformants sequenced, only fifteen clones (21%) were non-mutated, the others containing up to ten mutations.

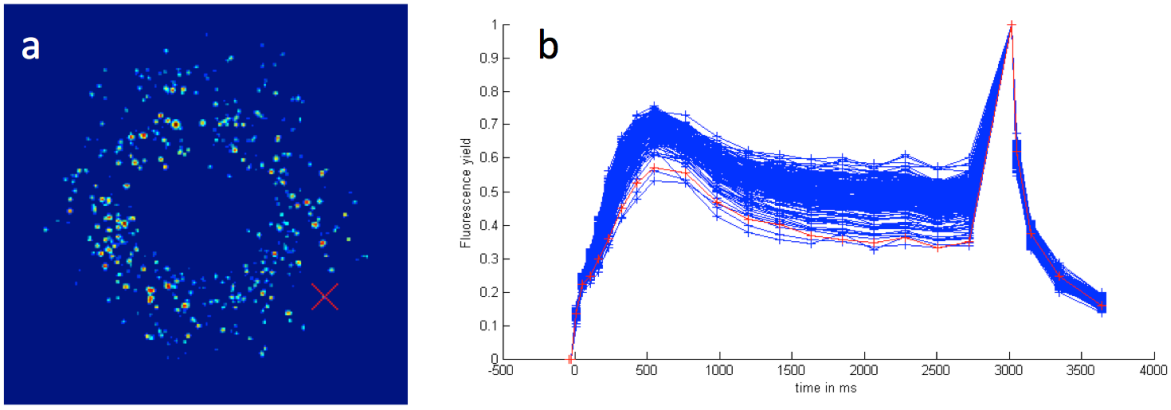

Figure II.1. Screen capture of the interactive computer interface used for screening.
(**a)** Chlorophyll fluorescence imaging of RM complementation clones selected on minimum medium. (**b)** Chlorophyll fluorescence kinetics corresponding to clones in panel (a) renormalized between F_0 shifted to zero and $F_m = 1$. Illumination protocol was 3 s at 600 $\mu mol_{photons}.m^{-2}.s^{-1}$, followed by a saturating pulse and 500 ms dark recovery. The red curve in panel (b) corresponds to the clone marked with a cross in panel (a).

Occurrence of co-transformation at the same locus – Sequencing chromatograms revealed interesting features of chloroplast transformation using a non-homogeneous pool of plasmid DNA. When complementing a knockout mutant with a homogenous population of plasmids, any copy of the plasmid is expected to recombine with the chloroplast genome and be replicated with the same efficiency, so that homoplasmy is reached eventually. For an equimolar mix of two different plasmids however, Kindle and coworkers(Kindle et al. 1991) reported the occurrence of co-transformation at two different chloroplast loci. In our experiments, *petD* variants can only recombine at one locus. In rare instances, the sequencing chromatograms of the *petD* gene recovered from our various mutants showed evidence of heteroplasmy. Figure II.2 shows a comparison of the sequencing chromatograms of the WT *petD* gene and two mutants around bp213. Mutant B has a clear double read (T and A) at that position which points to an SNP. This case corresponds to a silent mutation since ACT and ACA both code for a threonine, which may explain why this SNP was retained and not lost through counter-selection. It nevertheless suggests that at least two plasmid molecules can penetrate the same chloroplast and recombine at the same loci on two different copies of the chloroplast DNA. Such events were only rarely found because we increased the number of host cells (20.10^6 per plate) and decreased the amount of transforming DNA (0.5 µg per shot). It is probable that competition occurred between viable and non-viable *petD* variants inside a given chloroplast, and that non-viable variants were eventually counter-selected.

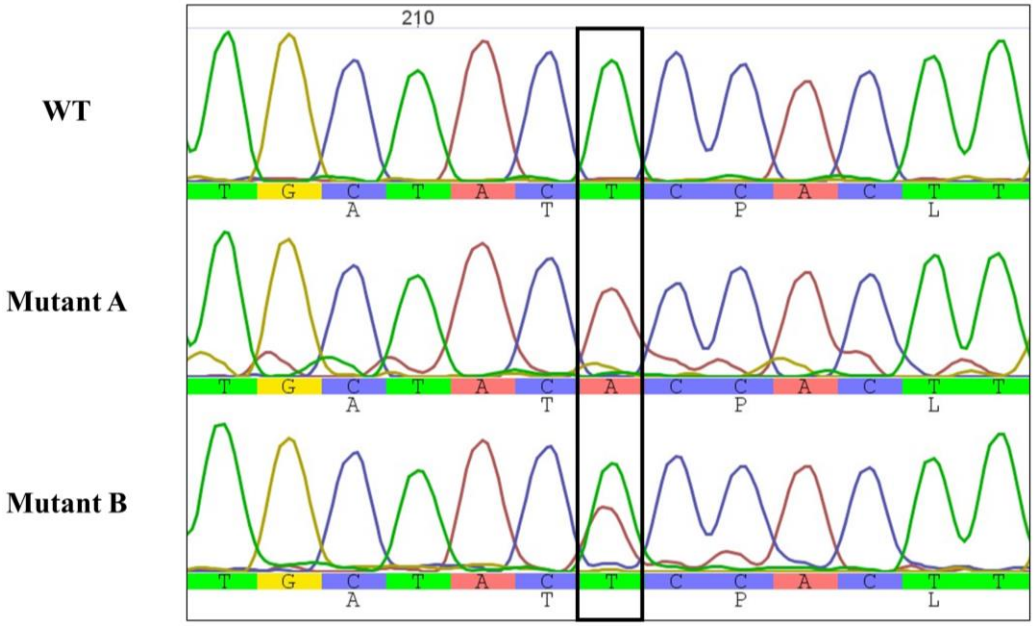

Figure II.2. Alignment of nucleotide sequences of the WT and two mutant *petD* genes around bp213. Chromatogram peaks are proportional to the relative concentration of each base at each position. Mutant A has a clear base attribution at position 213 showing a T > A substitution. Mutant B shows an ambiguous base attribution, with both T and A nucleotides having high read-out values.

Evidence for counter selection of non-viable petD copies – From our sequencing data, it clearly appeared that *C. reinhardtii* chloroplasts retained a higher proportion of non-mutated sequences and a lower number of mutations per mutant than *E. coli* cells. This is illustrated by comparing the "Non-mutated" and "Distribution" columns of Table II.1 between the two organisms. This was also visible after statistical analysis of the mutational frequency in the 114 *C. reinhardtii* transformants that were picked randomly and sequenced. 59 of these transformants did not show any mutation in the *petD* gene, while 55 transformants contained between 1 and 10 mutations. Figure II.3 shows a bar graph of the distribution of the number n of mutants containing m mutations. This graph was fitted to a Poisson distribution (Equation 2, solid line in Figure II.3). The solid curve matches satisfactorily the data for $m > 1$, showing that the Poisson model was appropriate for fitting. The fit yielded an average number of mutations of $\lambda = 3.1$ for 300 bp, i.*e*. ~10 per kb. The fit also predicts that the number of sequences retrieved with no mutations should have fallen in the range of 2 to 3, which is in stark contrast with the 59 non-mutated sequences we have obtained experimentally (grey bar in Figure II.3).

Our conclusion is that some genetic diversity of the random *petD* DNA library was lost through complementation of *C. reinhardtii*, a bias that is readily explained by the selection pressure exerted on the organism. Only a fraction of the sequence space of randomly

mutagenized *petD* genes is expected to complement photoautotrophic growth after transformation of the Δ*petD* strain. The rest of the *petD* sequence space is expected to produce non-viable subunit IV polypeptides, due for example to impaired folding of the apoprotein or insertion in the membrane, miss-assembly of the cofactors, altered redox potentials of the hemes (b_L, b_H or c_i), loss of proper interactions with the other subunits of the complex or perturbed affinity for quinones at the Q_o or Q_i sites. Such mutations, which would have impeded cyt b_6f assembly and accumulation or blocked electron and proton transfer, were not obtained after phototrophic selection.

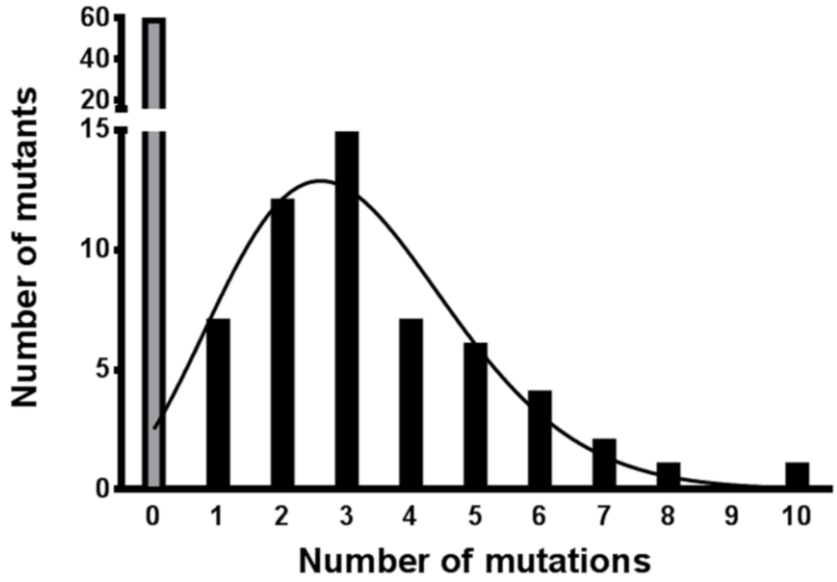

Figure II.3. Bar graph of the distribution of the number *n* of mutants against the number *m* of mutations.
A population of 114 randomly-picked *petD* mutants was sequenced and the data was fitted to a Poisson distribution (black line).

Mutation types, gene coverage and genetic saturation – All *petD* variants, generated using both random mutagenesis kits, were aligned to the reference *petD* sequence and SNP data was retrieved using Geneious software. We report 149 identified mutations in the 300 bp *petD* region targeted for random mutagenesis. The distributions of mutation types and effects are given in Table II.2, as well as two common measures of mutational bias. A to G and T to C transitions appeared largely preponderant, accounting for 25% and 37% of all mutations respectively and giving a high transition to transversion ratio (Ts/Tv = 2.1, theoretically equal to 0.5 for mutagenesis conditions completely lacking bias). The measured AT→GC to GC→AT ratio of 8.3 was also a sign of mutational bias as this ratio should equal 1 for completely unbiased epPCR conditions. We attribute these numbers to the statistical contribution of sequence variants generated with the Clontech kit. The method employed to reduce polymerase

fidelity in this kit is such that high mutation rates (as are obtained by using epPCR condition #9) and low mutational bias are mutually exclusive.

The 149 identified mutations are represented as a bar graph in Figure II.4A, which shows the number and types of SNPs at each mutated position along the *petD* sequence. The overall aspect of the graph suggests that the random mutagenesis conditions used in this study generated good sequence coverage. Mutations are equally spread along the *petD* gene, a sign that we were able to mutate equally any region of the 300 bp gene fragment. The protein sequences below show the substitutions in amino acids. Positions 87, 122, 124, 128 and 143 tolerated up to 3 different substitutions, see asterisk (*) in Figure II.4C. Figure II.4C shows an alignment of subunit IV protein sequences from organisms possessing cyt bc_1 or cyt b_6f complexes, together with the important residues for *b*-type cytochrome turnover (Brasseur, Saribas, et al. 1996). Highly conserved catalytic (PEWY) or structural (PNKL) motifs in cytochrome *b* complexes were not affected by mutations, suggesting again that the phototrophic selection pressure had discarded these mutants.

Certain residues were repeatedly substituted. It appeared in different instances. For example, the Val104Ala substitution was found in two different mutants from the same mutagenesis trial. It suggests that the mutation appeared in an early cycle of epPCR and was later combined with other random mutations eventually found in triple mutant V104A-Q121R-F149S and sextuple mutant V104A-L108H-F120L-T130S-L138F-L159S. In other cases, however, mutations were found repeatedly in mutants originating from strictly independent mutagenesis experiments. N118S was for example found on its own, but also appeared in combination with T110A and I145T in a totally independent mutagenesis round. In another instance, even more peculiar, two sextuple mutants (L95P-V104E-F120S-T130A-L132S-I145V and V104A-L108H-F120L-T130S-L138F-L159S) carried different mutations at three common loci (Val104, Phe120 and Thr130). These positions may correspond to flexible structural regions of the protein, easily tolerating substitutions, or represent tight hinges that cannot be moved independently from each other. We take these sequencing results in *C. reinhardtii*, showing a reduced sequence divergence, as a sign that genetic saturation was reached for the RM of the *petD* gene.

Robustness and plasticity of a macromolecular protein complex – Analyzing the spectrum of mutations that were introduced in *petD* and that restored phototrophy shows the robustness and plasticity of subunit IV (see Figure II.4B). Amongst the 149 mutations identified, 93 were non-silent (see Table II.2 and Figure II.4A, yellow triangles in bar graph). The alignment of these

non-silent mutations in Figure II.4B and C shows that transmembrane helices F and G tolerated few substitutions for bulky and/or charged amino acids and greatly favored substitutions that conserved amino acid property (small and/or hydrophobic). In contrast, in the inter-helix ef and fg loops and the C-terminal loop, containing more polar amino acids, substitutions modified residue polarity (Glu74Gly, Val84Glu, Gln86Arg, Lys119Glu, Gln121Arg/His, Asn122Lys, Tyr124His, Arg125Ser) more often than they conserved polarity (Glu74Asp, Arg89His, Lys94Arg). It suggests that mutations in the regions exposed to the water interface are less likely to affect the function of the complex as a whole, and that these regions are more robust and more plastic than the transmembrane regions. Expectedly, as mentioned above, catalytic and structural motifs that are generally conserved across species show lower plasticity.

When random substitutions in subunit IV, selected under photoautotrophic growth conditions, are scrutinized in the light of the 3D-structure of the macromolecular complex (see Figure II.5), some structural constraints of the *b*-type cytochromes are clearly revealed. For example, the positively charged Lys94 of subunit IV, forming an H-bond with the negatively charged Asp156 of cyt b_6, was only substituted in arginine to preserve the interaction.

Only a few substitution events were really unexpected (see **O** in Figure II.4C and Figure II.5B) where hydrophobic residues, pointing towards the core of the complex, in the vicinity of the Q_o site, were replaced by charged residues (Glu, Arg or Lys). Val84 and Met101 are situated respectively 3.9 Å and 3.7 Å from the hydrophobic tail of the stigmatellin inhibitor bound in place of the quinone at the Q_o site. The tolerance of the Q_o site to accommodate either positively charged or negatively charged residues in that pocket remains unclear and would deserve further functional analysis.

Most of the other substitutions seemed fairly acceptable at the structural level. The other three electrostatic changes (see ■ in Figure II.4C and Figure II.5B) in helices F and G concerned residues situated at the inter-helix interface (Val104Glu, Leu108His) or at the outer face of the complex (Trp142Arg). Of Val104 we know from previous studies that replacement with phenylalanine had no effect on the function of the complex (de Lacroix de Lavalette, Finazzi, et al. 2008) while replacement of Gly136 affected state transitions and electron transfer rates, a residue that was unaffected in the present study likely because of mutant selection on phototrophy. Aromatic residue Phe133 was substituted to a hydrophobic leucine, like in (Yan et al. 2008) who showed that this aromatic residue was involved in maintaining the short lifetime of Chl a^*, and polar Thr137 was changed to a hydrophobic alanine while a hydrophobic valine is found at this position in *Helibacillus mobilis*.

Of outstanding interest were the substitutions obtained in the loop linking helices F and G. Not only does the fg loop vary between cyt bc_1 and b_6f complexes, but it also easily tolerates non-conservative substitutions. From Lys119 and extending to Arg125, additions or removal of positive charges (arginine, lysine or histidine) occurred, as well as changes to opposite charge (Lys119Glu mutant) (see ◆ in Figure II.4C and Figure II.5B). Interestingly, although these substitutions did not affect the electron transfer rates of the complex, several of these impaired the mechanism of state transitions (Dumas et al. 2017) .

Discussion

Cyt *b* from mitochondria, archaea, proteobacteria and green sulfur bacteria are encoded by a single gene whereas in chloroplasts, cyanobacteria, heliobacteria, bacilli and haloarchaea, the corresponding sequence is split in two different genes, *petB* and *petD*, coding for cyt b_6 and subunit IV respectively. The complex core contains a number of transmembrane helices denoted from A to H. Cyt b_6 encompasses helices A, B, C and D and subunit IV contains E, F and G. Helix H is not found in the "green clade" of cyt *b* complexes (Nitschke et al. 2010). As noted on the list of mutants of cyt *b* complexes (Brasseur, Saribaş, et al. 1996), the distribution of point mutations affecting the catalytic turnover of the enzyme is far from being random, but rather pinpoints the regions of structural constraints for quinone binding or heme coordination. Interestingly, no mutations affecting electron or proton transfer were reported in helices F, G and H (Brasseur, Saribaş, et al. 1996), suggesting that these peripheral protein regions are more plastic than the core subunits B, C, D and E. The mutants we report in this study are no exception to this rule because they show normal turnover of the complex and allow for photoautotrophic growth. The robustness of subunit IV against mutations blocking electron transfer seemed to have allowed cyt b_6f complexes to evolve a distinctive role in the regulation of state transitions. The adaptable inter helix F and G loop has been recruited, during the course of evolution, as a binding site for the Stt7 kinase involved in LHCII phosphorylation (Dumas et al. 2017).

A technique compatible with genetic screens that opens up opportunities for the directed evolution of enzymes – When coupled to genetic screens for the study of the photosynthetic function, the epPCR of chloroplast genes can address functional questions in a straightforward manner: for example, a screen on chlorophyll fluorescence parameters was used to screen for mutants affected for state transitions (Dumas et al. 2017). Although the number of genetic

variants created in this work (~ 10^3 mutant clones) was sufficient for screening for a loss of function, we were far from having generated every possible permutation for 3 substitutions [$19 \times 3 \times 100! / (100-3)! / 3! \approx 9.10^6$], which would have been required for a gain of function (Currin et al. 2015) screen. Owing to the low efficiency of chloroplast transformation, mutant generation and screening of this amplitude would represent a very work-intensive task. Nonetheless, if photosynthesis is to be considered as the new frontier for crop improvement (Ort et al. 2015), directed evolution of chloroplast genes may very well represent a crucial step towards this grand challenge.

Acknowledgements

L.D. acknowledges the IRTELIS PhD grant from CEA, F.Z. laboratory was supported by the "Initiative d'Excellence" program (Grant "DYNAMO", ANR-11-LABEX-0011-01), X.J. acknowledges a grant from the Agence Nationale de la Recherche (ChloroPaths: ANR-14-CE05-0041-01), J.A. was supported by CNRS and INSIS Energie CNRS grant (PhotoModes 72749).

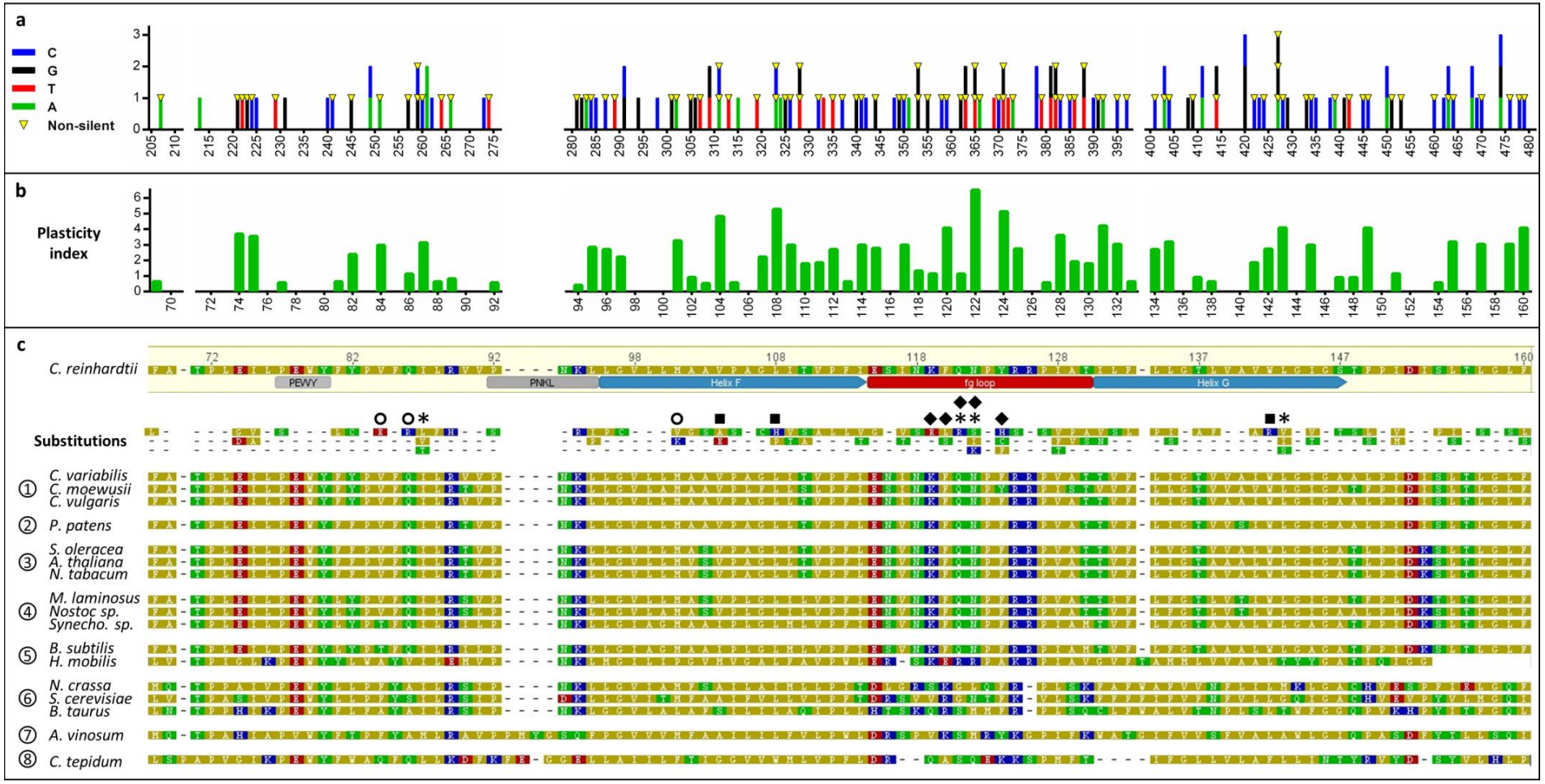

Figure II.4. Distribution of mutations along *petD* and plasticity of subunit IV.

(a) Bar graph of the distribution and types of all nucleotide substitutions introduced in the *petD* gene by random mutagenesis. Bases are color-coded and substitutions that created non-silent mutations are marked with a yellow triangle. **(b)** Index of protein plasticity calculated from the physico-chemical distances between amino acids (Miyata et al. 1979). Each position along subunit IV was attributed a plasticity value by calculating the sum of the physico-chemical distances between the original amino acid and the substituted amino acid(s). **(c)** Alignment of the subunit IV sequence from *C. reinhardtii* and all substitutions obtained at each position with other cytochrome *b* sequences. Amino acids are color-coded as follows: yellow, non-polar/hydrophobic; green, polar uncharged; blue, positively charged; red, negatively charged. Symbols are used as follows: ∗, tolerated up to 3 different substitutions; O, unexpected substitutions; ■, electrostatic charges introduced in transmembrane helices F or G; ◆, non-conservative substitutions in the subunit IV fg loop. Subunit IV is highly conserved through the green lineage green algae (1), moss (2), higher plants (3) and cyanobacteria (4). It also aligns with subunit IV from firmicutes (5) *Bacillus subtilis* and *Heliobacillus mobilis* and with the C-terminal part of cyt *b* from mitochondria (6) or purple sulfur (7) *Allochromatium vinosum* or green sulfur (8) *Chlorobaculum tepidum* bacteria.

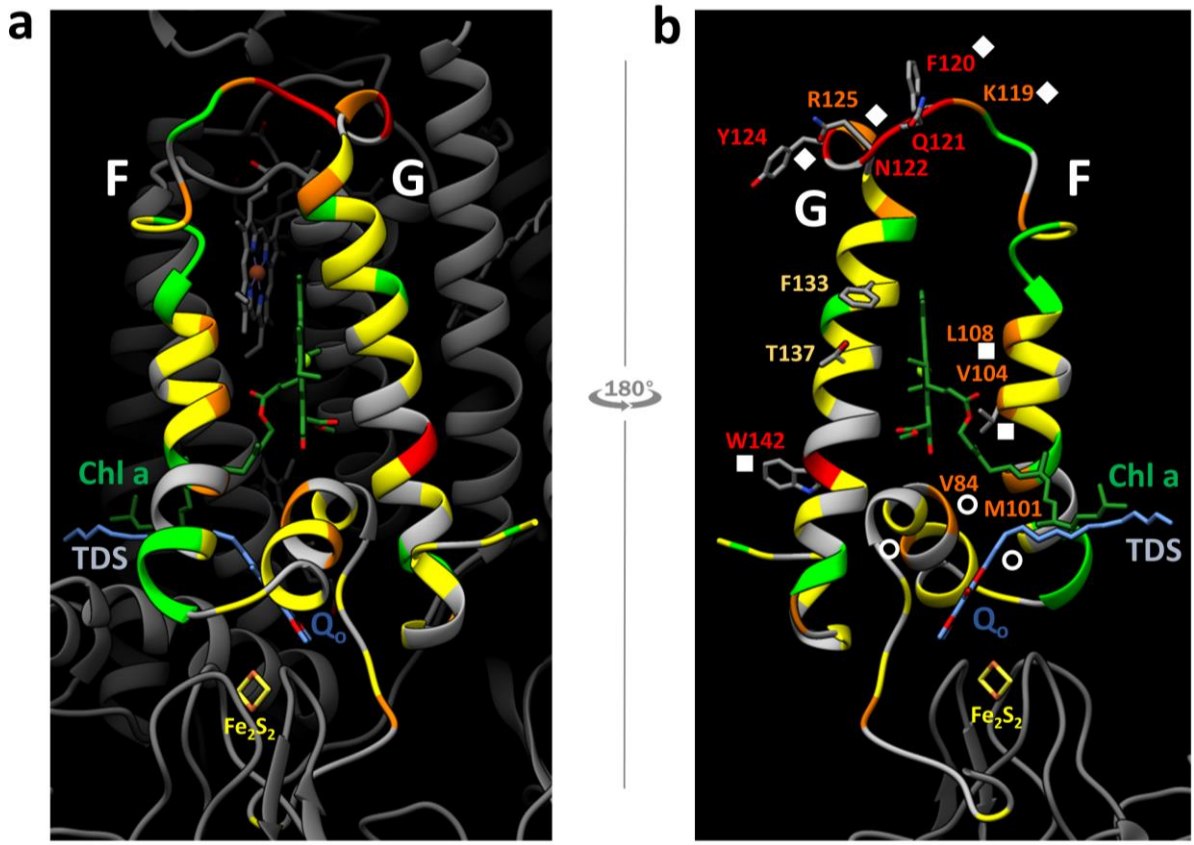

Figure II.5. Mutational robustness heatmap of subunit IV.
(a) Left panel shows an "outside" view of the cyt b_6f complex, with the peripheral region targeted for mutagenesis (helices F and G of subunit IV) colored according to the degree of variability (*i.e.* mutational robustness) at each position: from grey (no substitutions) to red (several and/or non-conservative substitutions), through green, yellow and orange (**b)** The right panel shows the 180° view of the targeted region (from the inside of the complex), showing some residues of interest and the symbols described in Figure II.4.

B. Additional results

A lot can be learned by taking one amino acid position at a time along the target mutagenized sequence and analyzing all its features: what amino acid substitutions were allowed at that position? Were they obtained from independent experiments? If not, were they caused by the same nucleotide substitutions? What other mutations were they combined with? What is the residue's position and protein environment in the 3D structure? Can we derive any principle or rationale on the function and interactions of this residue by combining all these observations? Does it relate to any function or regulation of the complex as a whole?

Here we provide a full list of all the substitutions introduced in the subunit IV sequence targeted for random mutagenesis (Table II.3). We then point out certain features of particular positions of interest along subunit IV. These include positions that were substituted but not studied further, residues that may be involved in state transitions, or highly conserved residues that were never substituted and may have functional roles.

Table II.3. List of all the substitutions obtained along the subunit IV sequence targeted by epPCR.

Residue	Substitution	Mutant	Combined with substitution(s)
Phe69	Leu	CRM11	Leu143Ile
Glu74	Gly	CRM105	-
	Asp	ARM25	Lys119Glu
Ile75	Ala	CRM36	Leu155Ile
	Val	CRM86	Ile109Val
Pro77	Ser	ARM30	Thr148Ser
Phe81	Leu	CRM62	Phe113Leu, Leu143Ser
Tyr82	Cys	CRM63	Ile87Leu, Pro105Ser, Leu155Ser
		CRM65	Ile87Leu, Leu155Ser
Val84	Glu	CRM12	Val104Ala, Phe113Leu
Gln86	Arg	CRM91	Ile87Val, Val111Ala, Ile117Thr, Ile128Thr, Val141Ala
Ile87	Thr	CRM33	-
	Leu	CRM63	Tyr82Cys, Pro105Ser, Leu155Ser
		CRM65	Tyr82Cys, Leu155Ser
	Val	CRM91	Gln86Arg, Val111Ala, Ile117Thr, Ile128Thr, Val141Ala
Leu88	Phe	CRM53	-
Arg89	His	CRM103	Leu95Pro
Pro92	Ser	ARM5	Ala102Gly
Lys94	Arg	CRM56	Met101Val, Ile109Thr
Leu95	Pro	CRM103	Arg89His
		CRM73	Val104Glu, Phe120Ser, Thr130Ala, Leu132Ser, Ile145Val
	Ile	ARM19	Ala129Val
Leu96	Pro	CRM81	-
Gly97	Cys	CRM83	Met101Lys
Met101	Val	CRM25	Ser147Thr
	Val	CRM56	Lys94Arg, Ile109Thr
	Lys	CRM83	Gly97Cys
Ala102	Gly	ARM5	Pro92Ser
Ala103	Ser	ARM31	-

Val104	Ala	CRM12	Val84Glu, Phe113Leu
		CRM22	Gln121Arg, Phe149Ser
		CRM61	Leu108His, Phe120Leu, Thr130Ser, Leu138Phe, Leu159Ser
		CRM92	Val104Ala, Gly107Cys, Leu108Pro, Ile131Val
	Glu	CRM73	Leu95Pro, Phe120Ser, Thr130Ala, Leu132Ser, Ile145Val
Pro105	Ser	CRM63	Tyr82Cys, Ile87Leu, Leu155Ser
Gly107	Cys	CRM92	Val104Ala, Leu108Pro, Ile131Val
Leu108	Pro	CRM92	Val104Ala, Gly107Cys, Ile131Val
	His	CRM61	Val104Ala, Phe120Leu, Thr130Ser, Leu138Phe, Leu159Ser
Ile109	Thr	CRM17	Phe133Leu, Ile151Met
		CRM56	Lys94Arg, Met101Val
	Val	CRM86	Ile75Val
Thr110	Ser	ARM7	Ile131Asn
	Ala	CRM78	Asn118Ser, Ile145Thr
Val111	Ala	CRM91	Gln86Arg, Ile87Val, Ile117Thr, Ile128Thr, Val141Ala
Pro112	Leu	ARM9	-
Phe113	Leu	CRM12	Val84Glu, Val104Ala
		CRM62	Phe81Leu, Leu143Ser
Ile114	Val	CRM107	-
	Thr	CRM110	Glu115Gly
Glu115	Gly	CRM110	Ile114Thr
Ile117	Val	CRM13	Gln121Arg, Asn122Ser, Leu134Pro, Phe160Ser
	Thr	CRM91	Gln86Arg, Ile87Val, Val111Ala, Ile128Thr, Val141Ala
Asn118	Ser	ARM22	Asn118Ser
		CRM78	Thr110Ala, Ile145Thr
Lys119	Glu	ARM25	Glu74Asp
Phe120	Ser	CRM64	Ser154Pro
		CRM73	Leu95Pro, Val104Glu, Thr130Ala, Leu132Ser, Ile145Val
	Leu	CRM61	Val104Ala, Leu108His, Thr130Ser, Leu138Phe, Leu159Ser
Gln121	Arg	CRM52	Tyr124His
		CRM22	Val104Ala, Phe149Ser

Gln121	Arg	CRM13	Ile117Val, Asn122Ser, Leu134Pro, Phe160Ser
Asn122	Ile	ARM10	-
	Lys	ARM21	Ile128Phe
	Ser	CRM13	Ile117Val, Gln121Arg, Leu134Pro, Phe160Ser
Tyr124	Cys	CRM109	-
	His	CRM52	Gln121Arg
		CRM82	Phe149Leu
	Phe	CRM68	Ile128Thr, Thr137Ala, Leu159Ser
Arg125	Ser	ARM42	-
Pro127	Ser	CRM21	Phe149Ser
Ile128	Val	CRM75	Trp142Arg
	Phe	ARM21	Asn122Lys
	Thr	CRM68	Tyr124Phe, Thr137Ala, Leu159Ser
		CRM91	Gln86Arg, Ile87Val, Val111Ala, Ile117Thr, Val141Ala
Ala129	Val	ARM19	Leu95Ile
	Pro	ARM17	-
Thr130	Ser	CRM61	Val104Ala, Leu108His, Phe120Leu, Leu138Phe, Leu159Ser
	Ala	CRM73	Leu95Pro, Val104Glu, Phe120Ser, Leu132Ser, Ile145Val
Ile131	Val	CRM79	Leu135Ser
		CRM92	Val104Ala, Gly107Cys, Leu108Pro
	Asn	ARM7	Thr110Ser
Leu132	Ser	CRM73	Leu95Pro, Val104Glu, Phe120Ser, Thr130Ala, Ile145Val
Phe133	Leu	CRM17	Ile109The, Ile151Met
Leu134	Pro	CRM13	Ile117Val, Gln121Arg, Asn122Ser, Phe160Ser
Leu135	Ile	ARM12	-
	Ser	CRM79	Ile131Val
Thr137	Ala	CRM68	Tyr124Phe, Ile128Thr, Leu159Ser
Leu138	Phe	CRM61	Val104Ala, Leu108His, Phe120Leu, Thr130Ser, Leu159Ser
Val141	Ala	CRM14	Ile151Val, Phe160Ser
		CRM88	-
		CRM91	Gln86Arg, Ile87Val, Val111Ala, Ile117Thr, Ile128Thr

Trp142	Arg	CRM75	Ile128Val
Leu143	Ile	CRM11	Phe69Leu
	Val	ARM13	-
		CRM18	-
	Ser	CRM62	Phe81Leu, Phe113Leu
Ile145	Val	CRM73	Leu95Pro, Val104Glu, Phe120Ser, Thr130Ala, Leu132Ser
	Thr	CRM78	Thr110Ala, Asn118Ser, Ile145Thr
Ser147	Thr	CRM25	Met101Val
Thr148	Ser	ARM30	Pro77Ser
Phe149	Ser	CRM21	Pro127Ser
		CRM22	Val104Ala, Gln121Arg
	Leu	CRM82	Tyr124His
Ile151	Val	CRM14	Val141Ala, Phe160Ser
	Met	CRM17	Ile109The, Phe133Leu
Ser154	Pro	CRM64	Phe120Ser
Leu155	Ser	CRM63	Tyr82Cys, Ile87Leu, Pro105Ser
		CRM65	Tyr82Cys, Ile87Leu
	Ile	CRM24	Leu157Ser
		CRM36	Ile75Ala
Leu157	Ser	CRM24	Leu155Ile
Leu159	Ser	CRM68	Tyr124Phe, Ile128Thr, Thr137Ala
		CRM61	Val104Ala, Leu108His, Phe120Leu, Thr130Ser, Leu138Phe
Phe160	Ser	CRM14	Val141Ala, Ile151Val
	Leu	CRM13	Ile117Val, Gln121Arg, Asn122Ser, Leu134Pro

Phe69

– Phe69Leu: found combined with the conservative Leu142Ile substitution. This aromatic residue is on the most lumenal part of the ef loop, in close contact with the Rieske protein. 5 Å away from its aromatic ring lies the cyclic pyrrolidine ring of Pro114 of the Rieske protein with which it could form an interaction due to both the hydrophobic effect and a CH/π interaction (Zondlo 2013). This interaction may play a role in regulating state transitions since this mutant showed slower state transition kinetics and since Phe69 is conserved in all b_6f but replaced by leucine or methionine in bc_1.

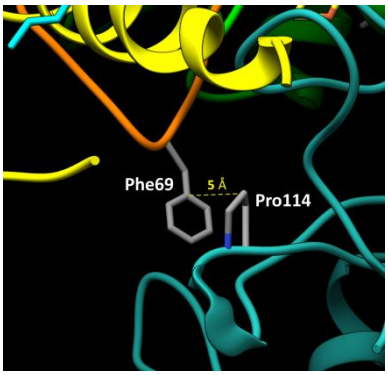

Ile75

– Ile75Ala and Ile75Val: This residue is highly conserved in both b_6f and bc_1 complexes (Figure II.4) and was only substituted for small non-charged residues (alanine and valine) by random mutagenesis. The isoleucine sticks out toward the TDS chromone ring in the Q_o site. A bulkier or charged amino acid at this position may affect quinol binding and/or oxidation and such substitutions would have been counter-selected in phototrophic conditions.

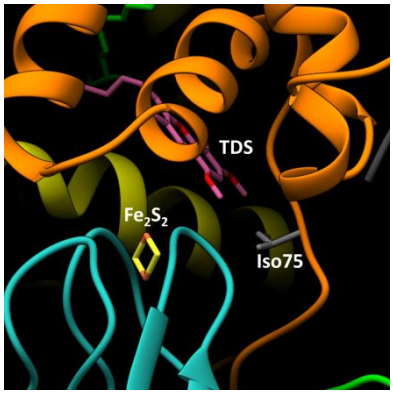

Pro77

– Pro77Ser: found combined with the conservative Thr148Ser substitution. This proline is part of the highly conserved PEWY motif that forms part the Q_o pocket and is involved in quinol oxidation (Zito et al. 1998). It is surprising that the mutant bearing a substitution at this structurally important proline was not significantly affected in b_6f turnover and was able to recover phototrophic growth after Δ*petD* complementation. However, in line with this result, the exact same substitution of the corresponding proline in the cyt bc_1 of *R. sphaeroides* (Pro294Ser) generated a "photosynthetically competent" mutant (Brasseur, Saribas, et al. 1996) albeit showing slower UQH_2 oxidation (Crofts et al. 1995).

Pro83, Phe85 and Arg89

– No amino acid substitutions were obtained at these positions, which are all highly conserved in all cyt *b* sequences shown in Figure II.4 with the exception of *H. mobilis* (Phe85 is also replaced by tyrosine in certain sequences, but the aromaticity is conserved). These residues are in the short α-helix bridge linking the PEWY motif to helix F and may be important for Q_o site structure and/or function.

Pro92

– Pro92Ser: found combined with the conservative Ala102Gly substitution. This proline is part of the PNKL motif that is annotated as a tilted alpha-helix motif and that is highly conserved among cyt *b* sequences. Surprisingly, substitution of this proline to serine did not prevent cyt b_6f assembly and function and the corresponding mutant (ARM5) was not affected for state transitions.

Lys94

– Lys94Arg: found combined with the Met101Val substitution. This lysine was only replaced by an arginine and is part of the PNKL motif, which also contains the highly conserved Asn93 residue for which no substitutions were recovered. It is likely that Lys94 forms an electrostatic interaction with Asp156 of the cyt b_6 cd loop, thus providing an attachment point between subunit IV helix F and cyt b_6 cd loop and contributing to the shaping of the Q_o pocket. The Asp156 residue is conserved or replaced by a glutamate in b_6f complexes of cyanobacteria and the green lineage. Interesting evidence of co-evolution between these two interacting residues was found by looking at the unsplit cyt *b* subunit sequence of the green sulfur bacteria *C. tepidum*: this subunit bears a lysine and a glutamate at the positions that coincide respectively with $Asp156^{b6}$ and $Lys94^{suIV}$ in b_6f complexes.

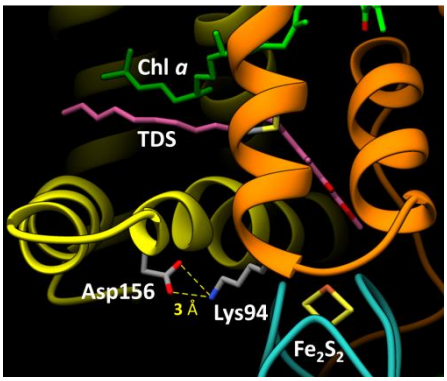

Leu95

– Leu95Pro: found in two different mutants (from the same epPCR), in one case combined with the Arg89His substitution (CRM103) and in the other with Val104Glu, Phe120Ser, Thr130Ala, Leu132Ser and Ile145Val substitutions (CRM73). Both of these showed slower state transition kinetics, possibly due to a structural change induced by the proline residue that could modify the tilt of helix F and affect Stt7 binding.

Met101

– Met101Lys: Similar case to Val84Glu, addition of a charged and bulky residue protruding into Q_o. The panel on the right shows a view of the Q_o site, with both the native Met101 residue and the highest probability lysine rotamer modelled by Chimera from the Dunbrack backbone-dependent rotamer library (Dunbrack 2002).

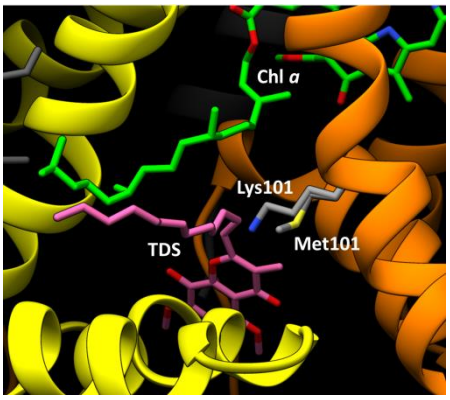

Val104

– Val104Ala and Val104Glu: The Val104Ala substitution was shared by four different random mutants (CRM12, 22, 92, 61) originating from mutagenesis #5. The corresponding base pair mutation was the same in all four *petD* sequences, suggesting that this mutation appeared in an early cycle of epPCR and was later combined to other mutations, yielding four different random mutants. The Val104Glu substitution was found in one mutant (CRM73) originating from mutagenesis #5. Three of these Val104 mutants (CRM92, 61 and 73) shared mutations at other common loci (Figure II.6). Mutants CRM92 and CRM61 both had substitutions at Leu108, namely Leu108Pro and Leu108His, respectively. Mutant CRM61 shared further mutations at two other loci with mutant CRM73, leading to substitutions Phe120Leu/Phe120Ser and Thr130Ser/Thr130Ala (for CRM61/CRM73 respectively).

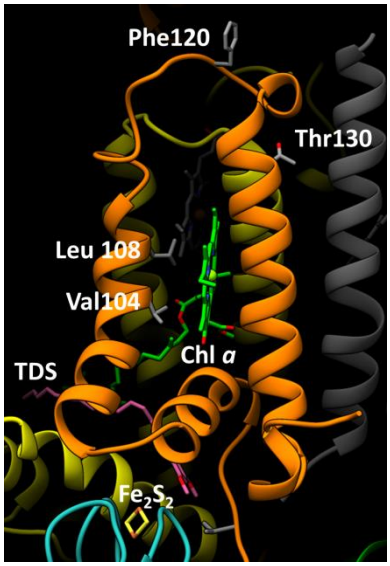

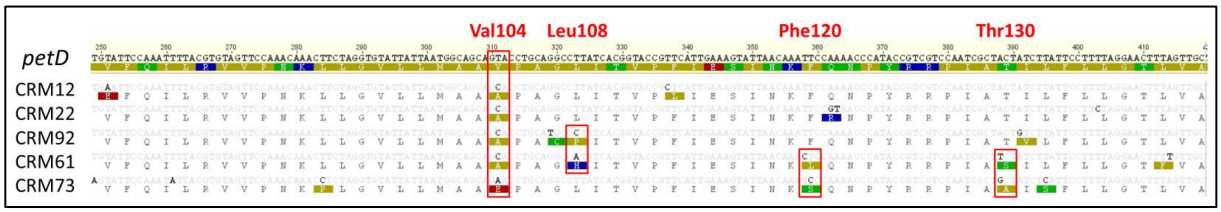

Figure II.6. Alignment of five *petD* random mutants containing a substitution at Val104.
Three of these also shared other substitutions at residues Leu108, Phe120 and Thr130.

There is a possibility that these four positions (104, 108, 120 and 130) could be structurally related and that a substitution at a given residue may affect the robustness at other positions along subunit IV. This interdependence seems especially plausible in the case of the Val104-Leu108 couple. These residues are one helix turn away from each other and both of their side-chains face the Chl *a* porphyrin ring. In line with (de Lacroix de Lavalette, Finazzi, et al. 2008) that showed that a Val104Phe substitution did not affect electron transfer, we obtained mutants with bulky and charged residues in the vicinity of the Chl *a* head (Leu108His of CRM61 and Val104Glu of CRM73) that showed normal phototrophic growth. However, these mutants did have impaired q_T, unlike the Val104Phe mutant, suggesting that introducing the charged side chains of histidine and glutamate in this region may destabilize the binding or positioning of Chl *a* enough to in turn affect the docking of the kinase. On the contrary, mutant CRM92 bore both a Val104Ala and a Leu108Pro substitution but had normal q_T.

Leu108

– Leu108Pro and Leu108His: see **Val104**

Asn118

– Asn118Ser: This substitution was found on two mutants and was caused by a mutation on the same nucleotide in two independent mutagenesis experiments (AAC > AGC). This may be explained by the high proportion of A to G transitions in the distribution of SNP types (Table II.2).

Phe120

– Phe120Leu and Phe120Ser: see **Val104**

Arg126

– No amino acid substitutions were obtained at this position. A silent mutation on the third position of the corresponding *petD* codon (CGT → CGC) was obtained in two independent random mutagenesis experiments. The arginine side chain lies very close to that of Glu115, which itself is in close contact to the Lys111 residue of the cyt b_6 subunit. An interaction between Arg126 and Glu115 may play a structural role in the conformation of the fg loop and the relative orientations of helices F and G. Residue Glu115 was only substituted once, to glycine in mutant CRM110, where it was combined with a substitution of the adjacent Ile114 residue to threonine. The threonine hydroxyl may have complemented the Glu115Gly substitution by providing a nucleophilic group that could interact with the guanidium group of Arg126, thus maintaining sufficient structural integrity of subunit IV and allowing the correct assembly and function of the complex as a whole.

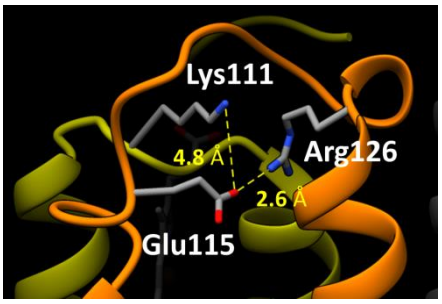

Pro127

– Pro127Ser: The only mutant bearing a substitution of Pro127 had no other non-conservative mutation and was impaired for state transitions. This residue is highly conserved in b_6f and bc_1 complexes. It is positioned at the junction between the fg loop and helix G and its high conformational rigidity is likely crucial to orient the protein backbone and initiate the tilt of the α-helix. Loss of this structural determinant in the Pro127Ser mutant may modify the conformation and orientation of helix G. As reported previously (Zito et al. 2002) and further confirmed by state transition mutants bearing substitutions of the Ile131 residue which extends toward the periphery of the complex (Ile131Asn random mutant and Ile131Asp site-directed mutant, discussed in Chapter III), modifying the steric environment of helix G seems to impede Stt7 binding (discussed in Chapter IV).

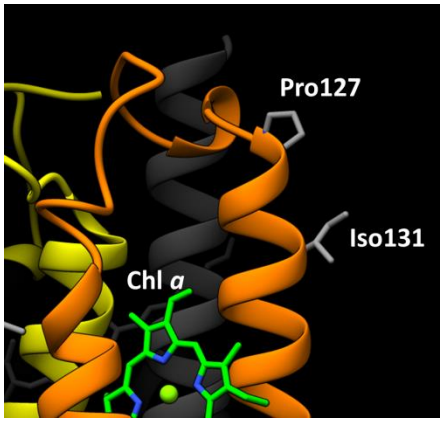

Gly136

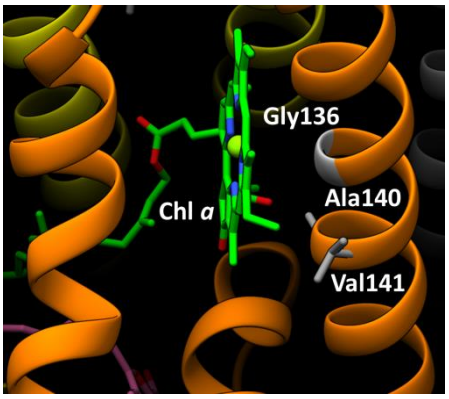

– No amino acid substitutions were obtained at this position. The only mutation found in the *petD* codon coding for this glycine was on the third base position and was silent (GGA → GGG). This is in line with a previous study that showed that replacement of this glycine with a bulky residue generated a cyt b_6f complex with much slower electron transfer rates, a lower Chl *a*/cyt *f* ratio and an increased tendency to monomerize (de Lacroix de Lavalette, Finazzi, et al. 2008). Most non-silent mutations would have been lost by counter-selection.

Asp152

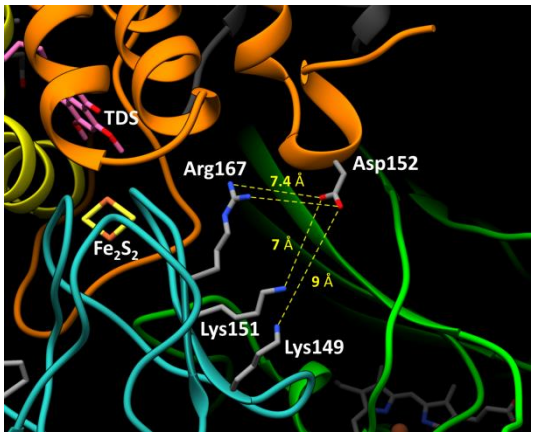

– No amino acid substitutions were obtained at this position. This residue is highly conserved in cyt b_6f and its side chain is oriented toward three basic residues of the Rieske ISP, Lys149, Lys151 and Arg167, with which it could form electrostatic interactions. Because these residues lie in the region that separates the Fe_2S_2 cluster from the *c*-type heme of cyt *f*, their putative interactions with Asp152 of subunit may play a role in the Rieske domain movements that participate in the catalysis of electron transfer from PQH_2 to cyt *f*. Loss of these interactions may affect electron transfer and phototrophic growth, which would explain why no substitutions were observed at this position in transformants selected in phototrophic conditions.

C. Concluding remarks

Our knowledge of the molecular mechanisms of photosynthesis was greatly advanced by the development of genetic and molecular biology tools that enabled the controlled modification of the chloroplast genome and the recovery of transplastomic lines using selectable markers. Several features of the plastid genome, which are actually indicators of its prokaryotic origin, rendered its genetic manipulation possible and stimulated efforts to develop the necessary tools three decades ago. One of these advantages is that transgene integration is obtained through precise homologous recombination, which prevents negative position effects and unwanted inactivation of host genes by the transgene. Moreover, unlike in the nuclear genome, no gene silencing or RNA interference mechanisms have been demonstrated on chloroplast genes. Stable chloroplast transformation was first achieved in Chlamydomonas (Boynton et al. 1988) using John Sanford's gene gun (Klein et al. 1987) and was a major breakthrough that enabled precise characterization of chloroplast gene expression and protein function. With chloroplast transformation, specific genome loci could be targeted and studied, without relying on the previously available genome-wide mutagenesis techniques. Owing to the diversity of genes and functions studied over the years, many host strains and selectable markers with various properties were developed, allowing selection on photoautotrophy, antibiotic and herbicide resistance or metabolic recovery (Day and Goldschmidt-Clermont 2011).

In this work, we report the first attempt at combining random mutagenesis and chloroplast transformation. We relied on error-prone PCR to introduce random mutations on the *petD* gene, complemented the Δ*petD* strain by biolistics and selected transformants that recovered phototrophic growth. The combination of these techniques allowed us to randomly mutate a specific sequence at the desired rate and to introduce these variants at the desired genome locus. Although we focused on a rather short (300 bp) sequence in this work, the length of the target sequence is limited only by the maximal length of amplification by PCR and much longer DNA fragments can be targeted (up to ~10 kb). As a perspective, one could aim to randomly mutate several promoter-gene sequences of interest set in series on the same construct and complement a recipient strain deleted for these same genes. In this case, the complementation efficiency would only depend on the length of the total construct. However, the native promoters of each gene would also be the target of random mutations. Another possibility would be to randomly mutate each gene on separate plasmids and attempt to complement a multi-deletion host strain by co-transformation and recombination at each locus of origin. In this situation, the mutagenesis could be targeted to the coding sequences only but the complementation efficiency

may be greatly reduced, as reported previously for the co-transformation of a phototrophic marker and an antibiotic resistance marker (Kindle et al. 1991).

This work provides a roadmap for future studies wishing to utilize random mutagenesis to study the expression of a given chloroplast gene or the function of the protein it encodes. It describes what happens when *Chlamydomonas* chloroplasts are transformed with a non-homogeneous pool of plasmid DNA. To our knowledge, we report the first evidence of co-transformation of (at least) two variant sequences at the same locus on two copies of the same chloroplast genome. We also observed extensive loss of library diversity due to strong counter-selection of non-viable *petD* variants by *Chlamydomonas* cells under phototrophic selection pressure. From a structure-function standpoint, careful analysis of the mutational spectrum and the variability at each position along the mutated sequence revealed key features of subunit IV in the context of its multisubunit complex. The mutational robustness of particular residues or motifs was assessed and helped identify regions of functional significance. In particular, the fg loop of subunit IV showed high robustness to mutations. As described in the next chapter, a functional screen of the *petD* variants revealed that this same loop contained residues involved in state transitions, a mechanism shared amongst organisms of the green lineage. It is tempting to suggest that the high evolvability of this stromal loop was a necessary factor for its recruitment as a region of interaction with the state transition kinase. This plasticity may have played a role in the evolutionary trajectory that enabled the cyt b_6f to develop regulatory functions as the coupling component between the two photosystems of oxygenic photosynthesis. As a general outlook, this example suggests that, for any given protein, if a large enough number of variant sequences are generated and if these variants are screened on a precise function, a true representation of all the structural determinants that give rise to this function can be obtained.

CHAPTER III – Probing the cyt b_6f for regions involved in the mechanism of state transitions

The first part of this work consisted in adapting the technique of error-prone PCR to the random mutagenesis of a chloroplast-encoded gene. Systematic sequencing of both *E. coli* and *C. reinhardtii* transformants allowed us to monitor the diversity introduced in the *petD* gene and adjust the mutagenesis and library amplification conditions. Indeed, there was no way of knowing *a priori* the results of transforming the chloroplast with a non-homogeneous plasmid pool and selecting transformants on their ability to recover phototrophic growth with the recombined *petD* variant(s). Although the first sequencing of *C. reinhardtii* clones revealed that our protocol was not yet optimal, it also showed that we were able to recover phototrophic cells by complementing the Δ*petD* strain with randomly mutagenized *petD* genes, and was the proof of concept of our method. This opened up many opportunities for the study of chloroplast-encoded proteins.

This chapter presents the next step in this work which consisted in applying our method to the study of a photosynthetic function. State transitions are a dynamic acclimation response that relies on the interaction and coordinated action of two transmembrane proteins: the multi-subunit cyt b_6f whose structure is known in *C. reinhardtii* (Stroebel et al. 2003) and the Stt7 kinase of which we know only the topology (Lemeille et al. 2009). The lack of this latter structure has greatly hindered our ability to orient the efforts toward understanding how these two proteins interact. The details of this interaction, as well as the signal transduction pathway from the PQ pool to the kinase, remain unknown. For instance, there is no obvious explanation as to how the pre-requisite step of plastoquinol binding at the lumenal Q_o site (Vener et al. 1995; Zito et al. 1999) can induce the activation of the kinase whose catalytic domain resides in the stroma. Understanding the role of the cyt b_6f in this process is key because state transitions determine the pigment composition and energetic coupling of two photosystems and have therefore a direct effect on the maximum quantum yield of the system, *i.e.* the number of absorbed CO_2 molecules divided by the number of absorbed photons.

The hallmarks of the cyt b_6f complex are its roles in electron transfer for the energetic coupling between photosystems and proton translocation for the establishment of a proton-motive force across the thylakoid membrane. The majority of the work that has been carried out to understand

these functions has utilized the traditional structure-function approach of site-directed mutagenesis. Before the first structures of the cyt b_6f complex were resolved, other conserved Rieske/cyt *b* sequences and structures would be used as templates to define the cyt b_6f residues or motifs that should be studied by site-directed mutagenesis. This method proved invaluable for the study of electron and proton transfer functions that are shared amongst Rieske/cyt *b* complexes. The mechanism of electron transfer at the Q_i site of the cyt b_6f is an exception to this idea due to the presence of the peculiar heme c_i that is found only in cyt b_6f complexes. Furthermore, this approach has its limitations for the study of functions that are *not* universal among this class of enzyme: one cannot hope to study the regulatory role of the cyt b_6f in state transitions or cyclic electron flow by looking for clues in its homolog mitochondrial cyt bc_1 complex. Such fast acclimation mechanisms rely on complex interactions and structural features that are specific to certain photosynthetic organisms. Moreover, even among related photosynthetic organisms that have highly homologous cyt b_6f like cyanobacteria and microalgae, the same acclimation response may not be governed by the same molecular determinants, as is the case for state transitions between these two phyla. To overcome the limitations of classical structure-function studies, we devised an experimental strategy (Figure III.1) that allowed us to probe any (chloroplast-encoded) region of the cyt b_6f for its involvement in state transitions.

The choice of the *petD* gene as the target of the epPCR random mutagenesis rested on several seminal structure-function studies of the cyt b_6f that had suggested a role for subunit IV (coded by *petD*) in state transitions. Subunit IV forms part of the Q_o site and contains the conserved PEWY motif that is critical for plastoquinol binding and oxidation (Zito et al. 1998). Plastoquinol binding at Q_o was shown to be necessary for the activation of Stt7 and induction of state transitions (Vener et al. 1995; Zito et al. 1999). In addition, the cleft between the peripheral helices F and G of subunit IV was proposed to provide a niche for the transmembrane domain of Stt7 (Zito et al. 2002; de Lacroix de Lavalette, Finazzi, et al. 2008; Hasan and Cramer 2014). We generated random variants of this peripheral subunit IV region, complemented the Δ*petD* deletion strain with these variants and simultaneously sequenced transformants and screened for mutants showing normal cyt b_6f turnover but impaired state transitions. Here are presented the results of this structure-function study.

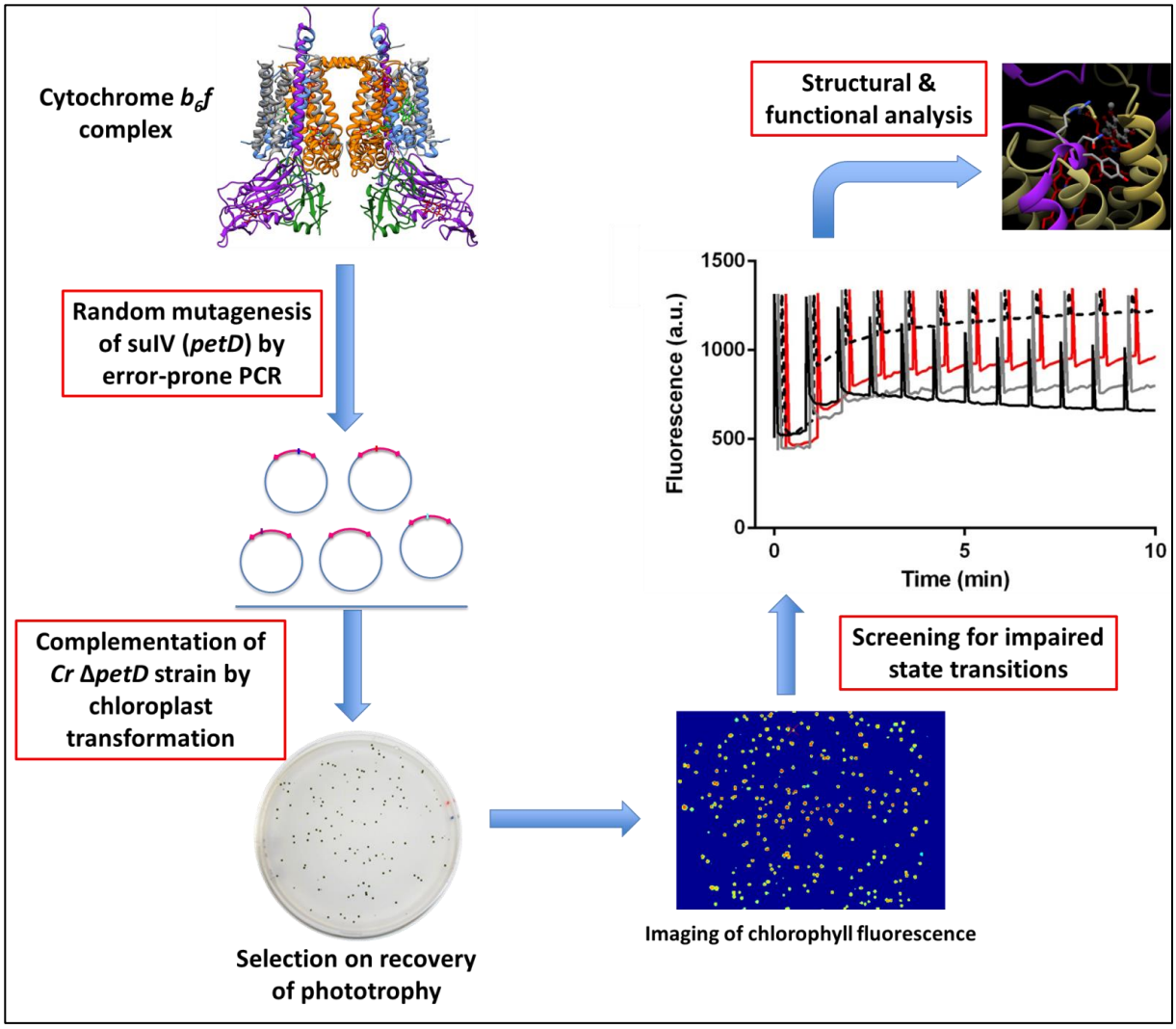

Figure III.1. Scheme of the experimental strategy used in this structure-function study of the cyt b_6f complex.

A. A stromal region of cytochrome b_6f subunit IV is involved in the activation of the Stt7 kinase in *Chlamydomonas*. Published article: *Proc Natl Acad Sci U S A*

A stromal region of cytochrome b_6f subunit IV is involved in the activation of the Stt7 kinase in *Chlamydomonas*

Louis Dumas[a], Francesca Zito[b], Stéphanie Blangy[a], Pascaline Auroy[a], Xenie Johnson[a], Gilles Peltier[a], and Jean Alric[a,1]

[a]Laboratoire de Bioénergétique et Biotechnologie des Bactéries et Microalgues, Commissariat à l'Energie Atomique et aux Energies Alternatives (CEA), CNRS, Aix-Marseille Université, UMR 7265, Institut de Biosciences et Biotechnologies d'Aix-Marseille, CEA Cadarache, F-13108 Saint-Paul-lez-Durance, France; and [b]Laboratoire de Biologie Physico-Chimique des Protéines Membranaires, Institut de Biologie Physico-Chimique, CNRS, UMR7099, University Paris Diderot, Sorbonne Paris Cité, Paris Sciences et Lettres Research University, F-75005 Paris, France

Edited by Jean-David Rochaix, University of Geneva, Geneva 4, Switzerland, and accepted by Editorial Board Member Joseph R. Ecker September 25, 2017 (received for review July 28, 2017)

The cytochrome (cyt) b_6f complex and Stt7 kinase regulate the antenna sizes of photosystems I and II through state transitions, which are mediated by a reversible phosphorylation of light harvesting complexes II, depending on the redox state of the plastoquinone pool. When the pool is reduced, the cyt b_6f activates the Stt7 kinase through a mechanism that is still poorly understood. After random mutagenesis of the chloroplast *petD* gene, coding for subunit IV of the cyt b_6f complex, and complementation of a Δ*petD* host strain by chloroplast transformation, we screened for impaired state transitions in vivo by chlorophyll fluorescence imaging. We show that residues Asn122, Tyr124, and Arg125 in the stromal loop linking helices F and G of cyt b_6f subunit IV are crucial for state transitions. In vitro reconstitution experiments with purified cyt b_6f and recombinant Stt7 kinase domain show that cyt b_6f enhances Stt7 autophosphorylation and that the Arg125 residue is directly involved in this process. The peripheral stromal structure of the cyt b_6f complex had, until now, no reported function. Evidence is now provided of a direct interaction with Stt7 on the stromal side of the membrane.

cytochrome b_6f complex | structure–function | random mutagenesis | Stt7 kinase | state transitions

Compared with other biological controls of light harvesting, such as the pH-dependent component of nonphotochemical quenching (q_E), state transitions are energy-conserving: the excess photon energy is not dissipated as heat (1, 2), but redirected from one photosystem (PS) to the other (3). State transitions therefore greatly contribute to the optimization of the maximal quantum yield of photosynthesis (4–6), probably through the poising of cyclic (PSI-dependent) vs. linear (PSI+PSII-dependent) electron flows in limiting light conditions (7, 8). In this process, the relative absorption cross-sections of PSI and PSII are dependent on the redox state of intersystem electron carriers, plastoquinones (PQ) (9), and cyt b_6f complex (10), and on the reversible phosphorylation of light harvesting complexes II (LHCII) (11, 12). Depending on their phosphorylation state, these mobile protein–pigment complexes can migrate between the stacked (grana) and nonstacked (stroma lamellae) regions of the thylakoid membrane, where PSII and PSI localize, respectively (13). LHCII migration and excitonic connectivity to either PSI or PSII therefore balance excitation between photosystems. In *Chlamydomonas reinhardtii*, when the PQ pool is reduced, the serine-threonine kinase Stt7 (14) is activated and phosphorylates LHCII, causing their migration toward nonappressed thylakoid membranes and attachment to PSI (state II). On the contrary, when the PQ pool is oxidized, LHCII are dephosphorylated by a phosphatase [protein phosphatase 1 (PPH1)/thylakoid-associated phosphatase 38 (TAP 38) in *Arabidopsis thaliana* (15, 16)] and dock to PSII (state I).

Our knowledge of the mechanism linking Stt7 kinase activation to the redox state of the PQ pool is presently incomplete, apart from certain key elements: cyt b_6f with a functional Q_o site and PQH_2 binding are required (10, 17, 18), the PetO subunit of cyt b_6f is phosphorylated by Stt7 during PQ pool reduction (19), and the lumenal domain of Stt7 interacts directly with the Rieske-ISP subunit of cyt b_6f and contains two conserved cysteine residues (20). However, the Stt7 kinase domain (20) and Stt7-dependent LHCII phosphorylation sites (21) are located on the stromal side of the membrane. Despite the recent characterization of the interaction between these two proteins (20, 22–27), the mechanism linking PQH_2 binding at the lumenal Q_o site to the activation of the stromal kinase domain of Stt7 remains unknown.

In this work, we used the technique of error-prone PCR for the mutagenesis of the chloroplast-encoded *petD* gene coding for subunit IV of cyt b_6f. We probed the regions of subunit IV putatively interacting with Stt7 (22, 24) by screening in vivo for impaired state transitions and found mutants blocked in state I. Furthermore, we show that cyt b_6f and Stt7 interact directly through their stromal domains and that $Arg125^{suIV}$ is involved in Stt7 activation.

Results

Random Mutagenesis, Chloroplast Transformation, and Sequencing of *petD* Variants. The *petD* sequence coding for the cyt b_6f subunit IV region going from the PEWY motif (28) to the C-terminal, and comprising helices F and G, was targeted for random mutagenesis (RM), whereas helix E, buried in the cyt b_6f core, remained untouched (see Fig. 5 for a structural view). This *petD* fragment was randomly mutagenized by error-prone PCR and its variants reconstructed into plasmids (*SI Appendix*, Text S1). After amplification in *Escherichia coli*, the plasmid library was

Significance

Sunlight is a powerful but fluctuating energy source used by photosynthetic organisms as a substrate for biochemistry. To optimize photosynthetic efficiency, the distribution of energy input between the two photosystems is regulated through state transitions. This mechanism is common to all organisms of the green lineage and depends on the concerted response of the cytochrome b_6f complex and the Stt7 kinase to changing redox conditions along the electron transport chain. The identification of a cytochrome b_6f stromal motif involved in state transitions gives insight into the mechanism of Stt7 kinase activation.

Author contributions: L.D., F.Z., X.J., G.P., and J.A. designed research; L.D., F.Z., S.B., P.A., and J.A. performed research; L.D., F.Z., S.B., P.A., X.J., G.P., and J.A. analyzed data; and L.D., F.Z., X.J., G.P., and J.A. wrote the paper.

The authors declare no conflict of interest.

This article is a PNAS Direct Submission. J.-D.R. is a guest editor invited by the Editorial Board.

[1]To whom correspondence should be addressed. Email: jean.alric@cea.fr.

This article contains supporting information online at www.pnas.org/lookup/suppl/doi:10.1073/pnas.1713343114/-/DCSupplemental.

used to transform the chloroplast genome of a Δ*petD* host strain. RM mutants described in this study were generated through two independent mutagenesis experiments (*SI Appendix*, Table S1). The diversity introduced in the *petD* gene was assessed by sequencing the target sequence in both *E. coli* and *C. reinhardtii*. Sequencing chromatograms did not show any SNPs or ambiguity in the *petD* sequences retrieved from *C. reinhardtii*; that is, when a mutated nucleotide appeared in the chromatogram, the signals corresponding to the other nucleotides stayed within the baseline noise (typically <1% for the sequences reported in this work; see *SI Appendix*, Fig. S1). Therefore, no *petD* sequence heterogeneity was observed, suggesting that in a given transformant, only one variant of *petD* was retained and replicated. In both rounds, no obvious bias was found in the positions of mutations along the sequence; mutations were diverse and covered the entire region of *petD* targeted for mutagenesis.

The conditions chosen for error-prone PCR (*SI Appendix*, Text S1) introduced a higher mutational frequency in trial B than in trial A. This was confirmed by counting the mutations in the *petD* fragment recovered in *E. coli* and *C. reinhardtii* clones (see "Distribution" columns in *SI Appendix*, Table S1). Expectedly, the relative amount of nonmutated sequences was also smaller in trial B than in trial A for both *E. coli* and *C. reinhardtii* (see "% Nonmutated" columns in *SI Appendix*, Table S1). Interestingly, we observed that in each of the two different RM experiments, *C. reinhardtii* cells retained mutated copies of *petD* less often than *E. coli* cells, and when they did, they contained fewer mutations. This was a result of the difference in selection pressure exerted on the two organisms. Whereas *E. coli* transformants were selected on ampicillin-containing medium after integration of an intact Amp^R cassette, *C. reinhardtii* transformants were selected on photoautotrophic growth after integration of a *petD* variant. Not all versions of randomly mutagenized *petD* genes are expected to restore a proper synthesis and folding of subunit IV and assembly of functional cyt b_6f complexes. The more mutations are introduced in an essential photosynthetic gene, the more likely they are to be deleterious and lost through phototrophic selection.

Screening for *C. reinhardtii* Transformants Impaired for State Transitions. For our screen, chlorophyll fluorescence images were recorded over the course of 10 min of anaerobic adaptation in the dark (*SI Appendix*, Fig. S2*A*), using an imaging system described in ref. 29. Anoxic reduction of the PQ pool was detected as an increase of F_0', and fluorescence quenching associated with the formation of state II (q_T) was measured as a decrease of F_m' in the WT. In the *stt7-1* strain, blocked in state I, no fluorescence quenching was observed after 10 min. All the >2,000 *C. reinhardtii* clones obtained after transformation were screened for state transitions, and most of them showed a decrease in F_m' similar to the WT. Sixteen clones, however, showed very stable F_m' values after anaerobic adaptation, as in *stt7-1*, suggesting they were affected in state transitions. *SI Appendix*, Fig. S2*A* shows a typical state transition kinetics curve for a *petD* random mutant affected for state transitions compared with the WT and *stt7-1* reference strains.

Fig. 1 illustrates some of the growth phenotypes and functional data obtained for three random *petD* mutants in comparison with the three reference strains [the site-directed (SD) *petD* mutants are discussed in *SD Mutagenesis of the Stromal fg Loop of Subunit IV*]. All strains show similar heterotrophic growth (TAP conditions) and maximal quantum efficiency of PSII photochemistry ($F_v/F_m \geq 0.7$). The host strain Δ*petD* does not grow in photoautotrophic conditions (minimum medium, MIN) and shows a very low photochemical quenching ($q_P < 0.05$) when grown in heterotrophic conditions (TAP). In all mutants selected on minimal medium, photoautotrophic growth and q_P were similar to WT ($q_P \geq 0.8$), suggesting a normal linear electron flow through PSII and downstream electron carriers in the photosynthetic chain, including the cyt b_6f complex. However, the q_T component of nonphotochemical quenching measured on anaerobic adaptation in the dark, high in the WT ($q_T \geq 0.4$), was greatly reduced in the two control strains lacking either cyt b_6f or Stt7, as well as in the three random *petD* mutants shown here ($q_T \leq 0.05$).

Among the 16 selected mutants that showed normal photochemistry but were blocked in state I, nine of them (italicized in *SI Appendix*, Table S2) were affected in the region coding for the loop linking helices F and G of cyt b_6f subunit IV (hereafter

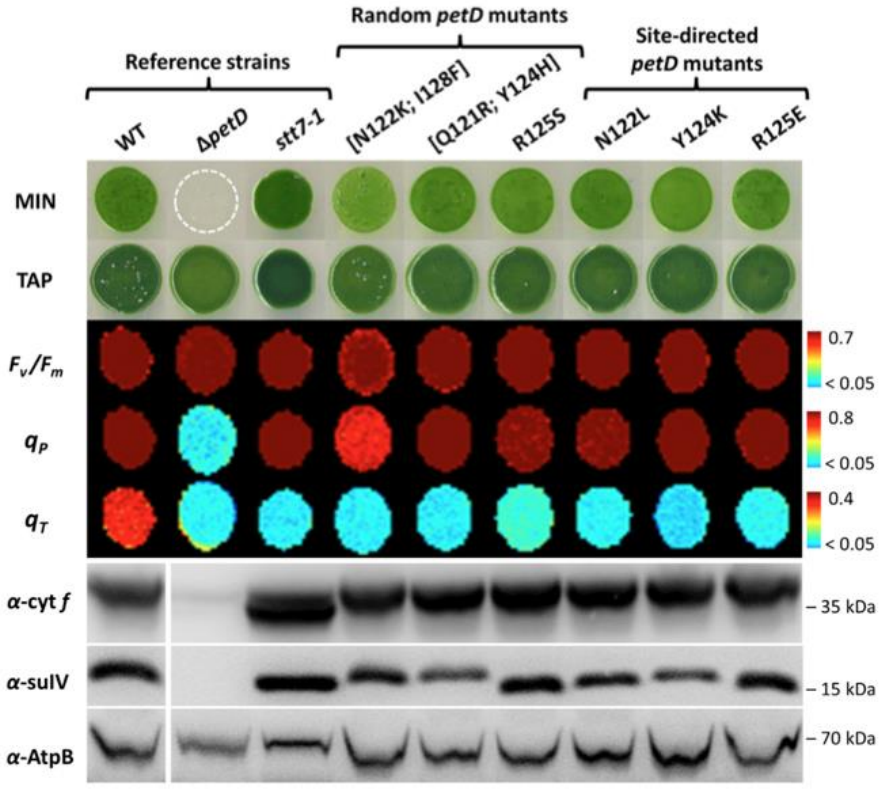

Fig. 1. Random and SD *petD* mutants are impaired for state transitions despite normal photosynthetic growth, electron transfer, and cyt b_6f subunit accumulation. Growth on minimal (MIN, 100 $\mu mol_{photons}\ m^{-2}\cdot s^{-1}$, 2% CO_2) and acetate (TAP, 20 $\mu mol_{photons}\ m^{-2}\cdot s^{-1}$) media, maximum quantum efficiency of PSII [$F_v/F_m = (F_m - F_0)/F_m$], photochemical quenching of chlorophyll fluorescence [$q_P = (F_m - F)/F_m - F_0)$], q_T component of nonphotochemical quenching measured upon anaerobic adaptation in the dark [$q_T = (F_m - F_m')/F_m'$, see *SI Appendix*, Fig. S2] and cyt b_6f subunits accumulation of the three reference strains (WT, Δ*petD*, *stt7-1*) and six *petD* mutants affected for state transitions. An antibody against AtpB was used as a loading control. *SI Appendix*, Table S2 mutants 19 ([Asn122Lys; Ile128Phe]), 13 ([Gln121Arg; Tyr124His]), and 28 (Arg125Ser) were obtained by random mutagenesis. Mutants 22 (Asn122Leu), 27 (Tyr124Lys) and 30 (Arg125Glu) were obtained by SD mutagenesis. All false color images and fluorescence parameters were calculated from chlorophyll fluorescence measurements of cells grown on MIN, except for the Δ*petD* strain grown on TAP.

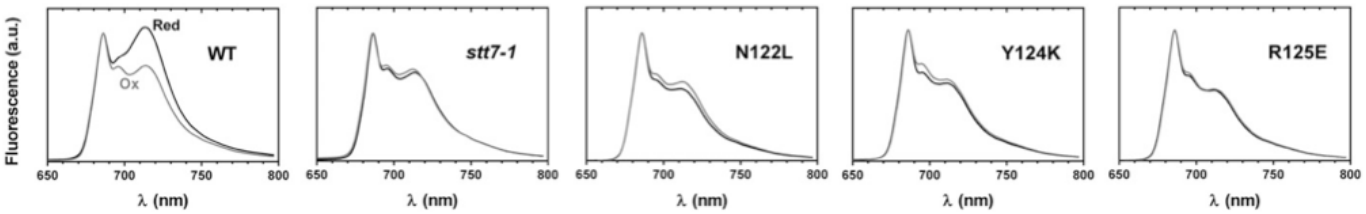

Fig. 2. Subunit IV fg loop mutants do not change photosystem antenna sizes between oxidizing and reducing conditions. Low-temperature (77 K) fluorescence emission spectra of the subunit IV mutants compared with the WT and *stt7-1* strains. Cells were placed in oxidizing (Ox, gray curve: 10 μM DCMU, moderate light, 30 min) or reducing (Red, black curve: dark anoxia, 30 min) conditions. Spectra were normalized at 685 nm on PSII contribution.

designated as fg loop), exposed at the stromal side of the membrane. These RM mutants also often contained additional mutations on either side of this stromal loop that are reported in columns 2 and 4 of *SI Appendix*, Table S2. To tease out certain phenotypic ambiguities that emerged from the comparison of the RM mutants, we generated single-point mutations along the loop (from Asn118 to Arg125) by SD mutagenesis.

SD Mutagenesis of the Stromal fg Loop of Subunit IV. Similar to RM, SD mutants were obtained by chloroplast transformation of the Δ*petD* host strain with SD mutagenized *petD*, followed by photoautotrophic selection of clones. To avoid structural destabilization of the loop, Pro123, Pro127, and residues pointing toward the core of the protein were not touched, whereas residues putatively involved in protein–protein interactions were targeted. For each residue, for example, Arg125, two amino acids with similar steric properties were substituted, bearing either a hydrophobic side chain (e.g., mutant 29 in *SI Appendix*, Table S2, Arg125Leu) or a side chain of "opposite" chemical property (e.g., mutant 30, Arg125Glu). Similar to the RM mutants, SD mutants grew under photoautotrophic conditions, and some of them, especially those containing mutations at residues Asn122, Tyr124, and Arg125, showed chlorophyll fluorescence parameters identical to the *stt7-1* strain, strongly affected in q_T, but not in q_P (Fig. 1 and *SI Appendix*, Figs. S2*B* and S4). Obtaining SD point mutants was important to discern the effect of individual mutations on the phenotype of certain RM mutants that contained more than one mutation. For example, for positions 121 and 124, although a marked decrease of q_T was observed in mutant 13 ([Gln121Arg; Tyr124His]), it was not nearly as drastic in mutant 24 ([Tyr124His; Phe149Leu]), and not observed at all in mutant 14 ([Val104Ala; Gln121Arg; Phe149Ser]; *SI Appendix*, Table S2). The Gln121Arg SD mutant 17 showed that changing Gln121 did not affect q_T, whereas SD mutant 27 (Tyr124Lys) revealed a critical role for Tyr124: substitution to Lys induced a loss of q_T, whereas substitution to the aromatic residue Phe (mutant 26, Tyr124Phe) had no effect on q_T, as observed in the RM mutant 25 ([Tyr124Phe; Ile128Thr; Thr137Ala; Leu159Ser]). Further characterization focused on SD mutants 22, 27, and 30 (Asn122Leu, Tyr124Lys, and Arg125Glu, respectively) that exhibited the most robust "locked-in-state-I" phenotype of all the SD subunit IV mutants.

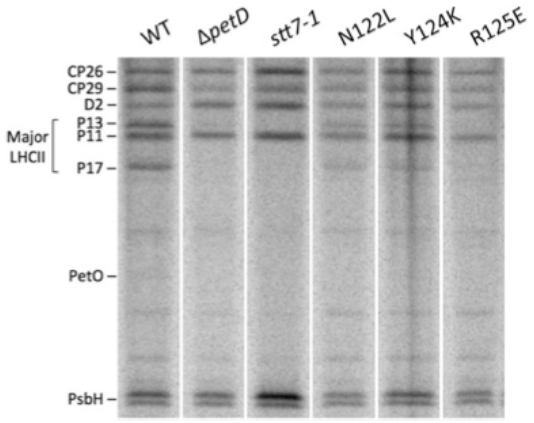

Fig. 3. Subunit IV fg loop mutants show low levels of Stt7-dependent LHCII phosphorylation. Autoradiogram of in vivo ^{33}P-labeled thylakoid polypeptides, extracted from cells placed in reducing conditions (5 μM FCCP, dark, 30 min) and separated by SDS/PAGE on an 8 M urea 12–18% gradient gel.

Characterization of Modified cyt b_6f Complexes. In Δ*petD*, totally devoid of subunit IV, the rate of synthesis of cyt *f* is strongly decreased, resulting in very little accumulation of cyt *f* (30), also observed in Fig. 1. In complemented strains, the 34.3-kDa cyt *f* subunit is tagged with 6-His at its C-terminal and shows a slower electrophoretic mobility on denaturing gels than in the *stt7-1* strain, as previously reported for the f_{297}C strain (31). Small differences are observed in the migration profiles of the 17.4-kDa subunit IV and can be attributed to slight changes in peptide mobility induced by single-point mutations. In the *petD* RM and SD mutants, the accumulation of subunit IV and cyt *f* was similar to WT levels (see *SI Appendix*, Fig. S5 for 50% and 10% loading controls).

The electron transfer rate through the cyt b_6f complex was assessed in control and mutant strains (*SI Appendix*, Figs. S6 and S7). The transmembrane electrogenic phase of electron transfer between hemes b_L and b_H, occurring after quinol oxidation at the Q_o site, was measured as an electrochromic shift of carotenoids, giving an absorbance increase at 520 nm. Electron transfer rates in mutants Asn122Leu, Tyr124Lys, and Arg125Glu were very similar to the WT.

Changes in Photosystems Antenna Size Associated with State Transitions. At 77 K, the light energy absorbed by chlorophyll in the mobile LHCII proteins is not reemitted at 682 nm, as it would be if these protein complexes were disconnected from the photosystems (32), but is transferred either to PSII and reemitted at 686 and 696 nm, or to PSI and reemitted at 713 nm. In the WT, the relative amplitudes of the fluorescence peaks change, with PSII contribution being larger in oxidizing conditions (state I) and PSI fluorescing mostly in reducing conditions (state II). It therefore reflects a change in excitonic connectivity of mobile LHCII to either PSI or PSII that depends on the Stt7 kinase. Similar to that observed in the *stt7-1* strain, the Asn122Leu, Tyr124Lys, and Arg125Glu mutants were blocked in state I despite reducing conditions, with LHCII constitutively connected to PSII (Fig. 2).

Phosphorylation of Thylakoid Polypeptides. Incorporation of radiolabeled orthophosphate [$^{33}PO_4^{3-}$] into proteins during PQ pool reduction was measured in vivo. Intact cells of SD mutants and reference strains were preincubated for 30 min under dark anoxic conditions. During nonphotochemical reduction of the PQ pool, thylakoid polypeptides incorporate radiolabeled phosphate that is detected by autoradiography after membrane preparation and fractionation by PAGE on an 8 M urea 12–18% gradient gel (Fig. 3 and see *SI Appendix*, Fig. S8 for loading controls). Contrary to the polypeptides that are constitutively phosphorylated in the various strains (CP26, CP29, D2, P11, PsbH), P13 and P17 were phosphorylated in the WT, but not in Δ*petD* or in *stt7-1*, as reported earlier (6, 10). Among the SD mutants, which accumulate WT levels of the Stt7 kinase (*SI*

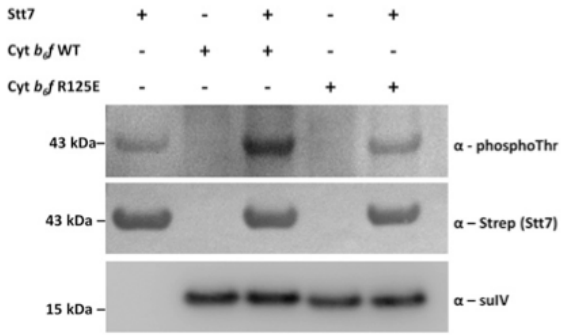

Fig. 4. Purified cyt b_6f complex increases autophosphorylation of the Stt7 kinase domain depending on the presence of $Arg125^{suIV}$. Immunoblots of Stt7-KD autophosphorylation reactions in the presence of WT or Arg125Glu cyt b_6f complex. An antibody against phospho-threonine (Cell Signaling) was used to detect Stt7-KD autophosphorylation. Antibodies against Strep-tag (recognizing the C-terminal tag of Stt7-KD) and subunit IV were used as loading and transfer controls.

Appendix, Fig. S9), Asn122Leu and Tyr124Lys showed low phosphorylation of P13 and P17, and Arg125Glu showed none. Similar phosphorylation profiles were observed in another comparative state I/state II ^{33}P-labeling experiment (*SI Appendix*, Fig. S10).

Cyt b_6f–Stt7 Interaction Studies. A GAL4-based yeast two-hybrid assay was carried out to probe the interaction between subunit IV and Stt7 (*SI Appendix*, Text S2 and Fig. S11). The WT and double-mutant ([Tyr124Lys; Arg125Glu]) subunit IV fg loops (residues 113–128) were expressed as fusions to the Gal4 DNA-binding domain and used as bait proteins. The stromal kinase domain of Stt7 was cut into four fragments that were expressed as fusions to the Gal4 activation domain and used as prey proteins: A, residues 123–238; B, 244–379; C, 397–483; and D, 484–600. Whereas no interaction was detected between the WT fg loop of subunit IV and Stt7 fragments C (397–483) and D (484–600), an interaction was detected between the WT fg loop and Stt7 fragments AB (123–379) and B alone (244–379). As expected, this interaction was lost in the double mutant ([Tyr124Lys; Arg125Glu]) fg loop. We further addressed the question of the biochemical interaction between cyt b_6f and Stt7 in a context in which the folding of subunit IV and assembly into a functional cyt b_6f complex is preserved.

Intact and functional cyt b_6f complexes were purified from *C. reinhardtii* thylakoid membranes following ref. 33. The recombinant kinase domain of Stt7 (Stt7-KD, residues 139–495) was produced in *E. coli* and purified as described in the *SI Appendix*, Text S3 and Fig. S12. Stt7-KD was active in vitro, as seen by its ATP hydrolysis activity (*SI Appendix*, Table S3). Stt7-KD was incubated for 30 min in the presence of ATP and $MgCl_2$ with either the WT or Arg125Glu purified cyt b_6f complexes. Whereas Stt7 showed a low level of autophosphorylation when incubated alone with ATP and $MgCl_2$ (Fig. 4, lane 1), addition of WT cyt b_6f greatly increased its phosphorylation (lane 3). In stark contrast, incubation of Stt7-KD with cyt b_6f containing the Arg125Glu substitution (lane 5) showed only the basal signal of Stt7 autophosphorylation, similar to lane 1. This in vitro reconstitution shows that the cyt b_6f complex and the stromal kinase domain of Stt7 interact directly and that Arg125 of subunit IV is involved in Stt7 autophosphorylation.

Discussion

Design of an Optimized Protocol for the Random Mutagenesis of Chloroplast Genes and Screening for Modified Photosynthetic Functions. We have targeted a ~300-bp fragment of *petD*, corresponding to ~100 amino acids in subunit IV. The number of single amino acid substitutions in a 100-amino acid protein is $19 \times 100 = 1{,}900$. In total, among our ~2,000 transformants, we have obtained ~1,200 random mutants bearing, on average, ≥2 mutations (rightmost column of *SI Appendix*, Table S1). When looking for a loss-of-function phenotype, single amino acid substitutions are sufficient, with no need of obtaining all possible combinations of ≥2 substitutions. Therefore, the number of genetic variants generated in this work was adequate for screening for a loss of function.

Previous studies reported the random mutagenesis of chloroplast DNA. Mutagenic agents such as 5-fluorodeoxyuridine can be used to mutagenize the entire chloroplast genome (34), and degenerate oligonucleotides can introduce a given number of mutations in the sequence spanned by the oligonucleotides (35, 36). Although both these methods contain obvious caveats, the technique described here allows for specific targeting of a chloroplast DNA sequence without any size limitation other than the maximal length of amplification by PCR. In our case, considering the rather low efficiency of chloroplast transformation, and because selection on phototrophy discards nonfunctional gene variants, we were able to increase the mutation rate of the error-prone PCR to enrich the transformation plates in putative mutant clones. We did so until we reached quite a high mutational frequency for a protein structure–function study (3.5 mutations/300 bp for RMB;

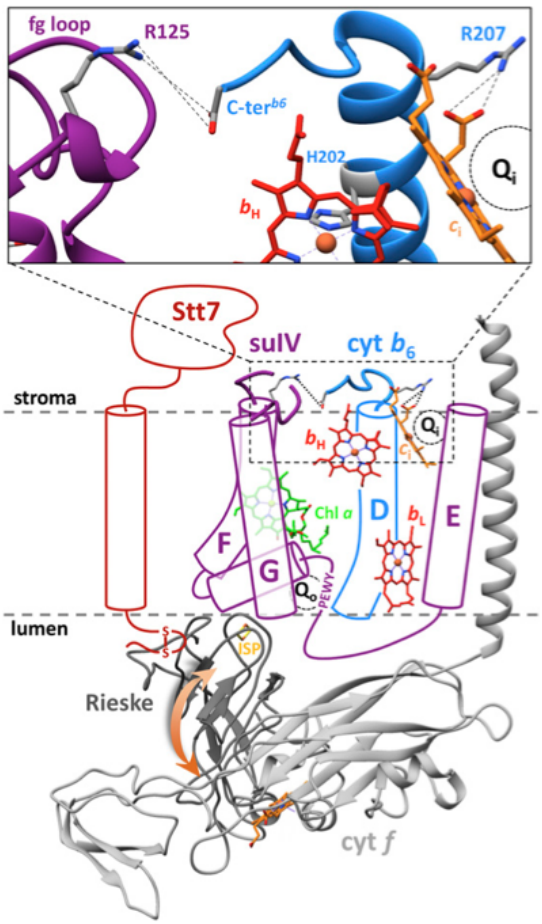

Fig. 5. Simplified drawing of the cyt b_6f monomer from *C. reinhardtii* and possible interactions with Stt7. The second cyt b_6f monomer would be located on the right-hand side of the figure. Atomic coordinates of cofactors, stromal loops and amino acid side chains shown here are from PDB 1Q90 (33). Helices A, B, and C of cyt b_6 and the transmembrane helix of the Rieske-ISP were removed for the sake of simplicity. The subunit IV (magenta) region targeted for random mutagenesis extends from the PEWY motif of the Q_o site to the C-terminal through helices F and G exposed at the periphery of the complex. The Stt7 kinase interacts with the Rieske-ISP (20), F and G helices of subunit IV (22, 27) and the stromal loop of subunit IV (this work). (*Inset*) Stromal regions of subunit IV and cyt b_6 (here in their ribbon representations), showing the structural link between $Arg125^{suIV}$ and the Q_i site through the C-terminal of cyt b_6 and the $Arg207^{cyt\ b6}$ residue that interacts with heme c_i.

see *SI Appendix*, Table S1). High mutation rates are used more often for the directed evolution of enzymes, where many substitutions can be introduced (37). As a broader perspective, this approach can be used for the study of many other chloroplast-encoded proteins and opens opportunities for the directed evolution of enzymes in transplastomic cell lines.

Identification of a cyt b_6f Stromal Loop Involved in State Transitions. After screening for a specific mutant phenotype, it was possible to gain functional insight from the comparison of sequences retrieved from the RM mutants, and we further confirmed the attribution of functional changes to point mutations by using SD mutagenesis. Given that the catalytic site of the Stt7 kinase is found in the stroma (20), we narrowed our target of investigation to the subunit IV fg loop starting from Asn118 and extending to Arg125. Protein sequence alignment showed a high degree of conservation between subunit IV from various organisms, but a strong divergence with cyt *b* from bacteria and mitochondria (*SI Appendix*, Fig. S13). We identified NKFQNPxRR as a conserved motif (where x corresponds to aromatic residues tyrosine or phenylalanine). This site, rich in lysine (K), arginine (R), and proline (P), to a lesser extent, strongly resembles a kinase binding site such as that of Stt7 (21), except that it contains no phosphorylatable residue (threonine or serine for Stt7).

Mutations at residues Asn122, Tyr124, and Arg125 produced mutants that are blocked in state I, despite a reduced PQ pool and normal cyt b_6f assembly and electron transfer activity. Upon a switch from oxidizing to reducing conditions, these mutants showed no quenching of PSII fluorescence emission associated with state transitions, no modification of the relative antenna sizes of PSII and PSI, and very low levels of phosphorylation of LHCII antenna proteins. This function was not expected for the peripheral stromal structure of the cyt b_6f complex.

Insight into the Role of cyt b_6f Complex in Stt7 Kinase Activation. The present work shows that the stromal region of cyt b_6f is involved in the activation of Stt7. Yeast two-hybrid experiments indicated that the stromal fg loop of subunit IV interacts with the kinase domain of Stt7 in the region between $Leu244^{Stt7}$ and $Pro379^{Stt7}$. Substitutions of fg loop residues $Tyr124^{suIV}$ and $Arg125^{suIV}$ abolished this interaction, showing that they are involved in the binding of the kinase to the stromal side of the complex. Furthermore, in vitro reconstitution experiments demonstrated that the autophosphorylation activity of the kinase domain was enhanced in the presence of purified cyt b_6f complex, through an interaction dependent on $Arg125^{suIV}$. The Stt7 region between $Leu244^{Stt7}$ and $Pro379^{Stt7}$ identified by two-hybrid assays contains two important kinase regulatory motifs, HRD and DLG, as well as the activation loop and the α5-hairpin (38). Several acidic Asp and Glu residues are present in this region and could form interactions with $Arg125^{suIV}$ in vivo. The absence of the lumenal domain [with the two regulatory Cys residues (20)] and the transmembrane domain of Stt7 did not prevent cyt b_6f-mediated autophosphorylation of the kinase. In our attempt to define the minimal functional length of Stt7, and going a step further than the truncation at residue 549 (27), we narrowed the kinase domain down to even before $Ser533^{Stt7}$, a phosphorylation site identified by phosphoproteomics but not involved in state transitions (20, 21). In addition to the ^{P}Thr and ^{P}Ser detected in previous phosphoproteomics studies (21, 39), our results suggest there are other phosphorylatable residues in the catalytic domain of Stt7. These residues could be important for the activation of the kinase in vivo.

On the basis of previous studies showing the crucial role of the lumenal Q_o site in state transitions (17, 28) and topology analysis showing that the kinase domain (20) and the LHCII phosphorylation sites (21) are found in the stroma, a signal transduction mechanism across the thylakoid membrane was postulated. The Chl *a* molecule, bound between helices F and G of subunit IV and protruding into the Q_o site, was proposed to play a role in this signal transduction (22, 24, 25, 40). Redox changes of the lumenal cysteine residues of Stt7, caused by Q_o site catalysis, were also suggested to induce Stt7 activation through transient dimerization (26) or conformational changes of its transmembrane domain (27). The present study identifies the stromal fg loop of subunit IV within the pattern of interactions between the cyt b_6f and Stt7. We propose that the primary activation of Stt7 depends on its interaction with the stromal side of cyt b_6f complex, whereas its release for LHCII phosphorylation could be controlled by plastoquinol occupancy and turnover at the Q_o site, as suggested previously (41).

We found here that Arg125 from the subunit IV fg loop plays a key role in the activation of the state transition kinase Stt7. The electron density map of the cyt b_6f complex from *C. reinhardtii* shows that the guanidinium group of Arg125 and the C-terminal carboxyl group of cyt b_6 are at a distance suitable to form a salt-bridge or an H-bond (see Fig. 5 and ref. 33). It suggests that $Arg125^{suIV}$ has two possible interacting partners: either the terminal carboxyl of the cyt b_6 or a negatively charged residue of Stt7 (Glu or Asp) in the region between $Leu244^{Stt7}$ and $Pro379^{Stt7}$. As shown in Fig. 5, *Inset*, the cyt b_6 C-terminal end is a short strand away from the conserved Arg207 that interacts with one of the propionates of heme c_i and shapes part of the Q_i pocket. In our previous work on heme c_i, we reported a discrepancy between its redox potentials estimated from in vivo and in vitro measurements and some peculiar electronic properties of this cofactor, depending on the pH and/or the binding of NQNO (42, 43). We attributed these unusual features to conformational heterogeneity at the stromal side of the cyt b_6f complex. It remains to be explored whether the dual interaction of $Arg125^{suIV}$ with either Stt7 or cyt b_6 could account for such structural heterogeneity.

Materials and Methods

Cell Growth Conditions. For photoautotrophic growth, *C. reinhardtii* cells were grown on Tris-phosphate (MIN, pH 7.2) medium in the light (100 $\mu mol_{photons}\ m^{-2}\cdot s^{-1}$) in air supplemented with 2% CO_2. For heterotrophic growth, cells were grown on Tris acetate-phosphate (TAP, pH 7.2) medium in very low to moderate light (10–40 $\mu mol_{photons}\ m^{-2}\cdot s^{-1}$).

Plasmids and Strains. Plasmid $pWQH_6$ (24), carrying the 3′-end sequence of *petA* with a 6-His tag, the intergenic *petA-petD* region, and the entire *petD* sequence, was used for mutagenesis and chloroplast transformation experiments. The mt^+ acetate-requiring Δ*petD* deletion strain (30) was used as the recipient strain for chloroplast transformation. The WT reference strain was obtained by chloroplast transformation of the Δ*petD* strain with plasmid $pWQH_6$ and selection on the restoration of photoautotrophic growth. The *petD* random and SD mutants were obtained the same way, apart from the use of $pWQH_6$ plasmids carrying mutations on the *petD* sequence. The WT reference strain and *petD* mutant strains therefore all express a *petA* gene coding for a His-tagged cyt *f*. The *stt7-1* strain (14), containing a deletion of the gene coding for the Stt7 kinase, was used as a control.

Mutagenesis of the *petD* Gene. Plasmid $pWQH_6$ and various primers were used for random and SD mutageneses of *petD* (*SI Appendix*, Table S4). For RM, error-prone PCR was performed using kits GeneMorph II EZClone (Agilent Technologies, "RMA" in *SI Appendix*, Table S1), and Diversify PCR (Clontech, "RMB"; see *SI Appendix*, Table S1 and see *SI Appendix*, Text S1 for details on the protocols).

Chloroplast Transformation and Mutant Selection. Plasmid DNA was precipitated on nanometer-scale gold particles using the Seashell Technology S550d gold DNA protocol. Δ*petD* cells on MIN medium were transformed by gold particle bombardment at 7 bars under vacuum. After transformation, cells were left to recover in the dark for up to 24 h and transformants were incubated in air + 2% CO_2 under low light (40–50 $\mu mol_{photons}\ m^{-2}\cdot s^{-1}$) for phototrophic selection.

Screening for State Transition Mutants. Transformation plates were left aerated in the dark for up to 15 min to induce PQ pool oxidation. The plates were then transferred to anaerobic conditions (N_2 flush) and the maximal fluorescence yield of PSII was recorded, using a fluorescence camera similar to the one described in ref. 29, during a 10-min period in the dark with 12 saturating light pulses.

PLANT BIOLOGY

77 K Chlorophyll Fluorescence Emission Spectra. Chlorophyll was excited with a LED at ~455 nm, and fluorescence was selected with a red-colored Kodak Wratten filter and collected with an Ocean Optics USB2000 CCD spectrometer. *C. reinhardtii* cells were placed in an aluminum-made sample holder and snap frozen at 77 K in liquid nitrogen. Sample, LED, and spectrometer were coupled via a Y-shaped fiberoptics.

In Vivo Phosphorylation of Antenna Proteins. Cells grown to around 2×10^6 cells·mL^{-1} were harvested and resuspended in a phosphate-depleted minimal medium containing 2 μCi mL^{-1} $^{33}P_i$. Samples were then treated as described in ref. 44, and thylakoid membranes were isolated as in ref. 45. Phosphorylation patterns of thylakoid membrane polypeptides were then analyzed on a 12–18% polyacrylamide gel containing 8 M urea, which was then dried and autoradiographed.

In Vitro Assays with Purified cyt b_6f Complexes and Recombinant Stt7-KD. Cyt b_6f complexes were purified as in ref. 33, and recombinant Stt7-KD (residues 139–495) was purified following a protocol adapted from ref. 27, as described in the *SI Appendix*, Text S3 and Fig. S12. The ADP-Glo Kinase Assay (Promega) was used to measure the in vitro activity of Stt7-KD (see *SI Appendix*, legend of Table S3). To test the interaction between the two proteins, 4.5 μM purified Stt7-KD and 1.5 μM purified WT or Arg125Glu cyt b_6f complex were incubated together with 1 mM ATP and 20 mM $MgCl_2$ for 30 min. Samples were denatured in a buffer containing LDS and DTT at 70 °C for 15 min and separated on a 10% Bis-Tris gel by SDS/PAGE. After transfer on a nitrocellulose membrane, antibodies against phospho-threonine (Cell Signaling), Strep-tag (recognizing the C-terminal tag of Stt7-KD), and subunit IV were used to detect the proteins.

ACKNOWLEDGMENTS. We are thankful for Michel Goldschmidt-Clermont's kind gift of the Stt7 antibody. We thank Daniel Picot for his structural expertise and discussion of the model. Pascal Arnoux and Bernard Genty are acknowledged for stimulating inputs. L.D. acknowledges the IRTELIS PhD Grant from CEA, the F.Z. laboratory was supported by the "Initiative d'Excellence" program (Grant "DYNAMO," ANR-11-LABEX-0011-01), X.J. acknowledges a grant from the Agence Nationale de la Recherche (ChloroPaths: ANR-14-CE05-0041-01), and J.A. was supported by CNRS and INSIS (Institut des Sciences de l'Ingénierie et des Systèmes) Energie CNRS Grant PhotoModes 72749.

1. Nagy G, et al. (2014) Chloroplast remodeling during state transitions in *Chlamydomonas reinhardtii* as revealed by noninvasive techniques *in vivo*. *Proc Natl Acad Sci USA* 111:5042–5047.
2. Ünlü C, Drop B, Croce R, van Amerongen H (2014) State transitions in *Chlamydomonas reinhardtii* strongly modulate the functional size of photosystem II but not of photosystem I. *Proc Natl Acad Sci USA* 111:3460–3465.
3. Nawrocki WJ, Santabarbara S, Mosebach L, Wollman FA, Rappaport F (2016) State transitions redistribute rather than dissipate energy between the two photosystems in Chlamydomonas. *Nat Plants* 2:16031.
4. Canaani O, Barber J, Malkin S (1984) Evidence that phosphorylation and dephosphorylation regulate the distribution of excitation energy between the two photosystems of photosynthesis *in vivo*: Photoacoustic and fluorimetric study of an intact leaf. *Proc Natl Acad Sci USA* 81:1614–1618.
5. Canaani O, Malkin S (1984) Distribution of light excitation in an intact leaf between the two photosystems of photosynthesis. Changes in absorption cross-sections following state 1-state 2 transitions. *Biochim Biophys Acta* 766:513–524.
6. Fleischmann MM, et al. (1999) Isolation and characterization of photoautotrophic mutants of *Chlamydomonas reinhardtii* deficient in state transition. *J Biol Chem* 274:30987–30994.
7. Takahashi H, Clowez S, Wollman FA, Vallon O, Rappaport F (2013) Cyclic electron flow is redox-controlled but independent of state transition. *Nat Commun* 4:1954.
8. Dumas L, Chazaux M, Peltier G, Johnson X, Alric J (2016) Cytochrome b_6f function and localization, phosphorylation state of thylakoid membrane proteins and consequences on cyclic electron flow. *Photosynth Res* 129:307–320.
9. Allen JF, Bennett J, Steinback KE, Arntzen CJ (1981) Chloroplast protein phosphorylation couples plastoquinone redox state to distribution of excitation energy between photosystems. *Nature* 291:25–29.
10. Wollman FA, Lemaire C (1988) Studies on kinase-controlled state transitions in photosystem II and b_6f mutants from *Chlamydomonas reinhardtii* which lack quinone-binding proteins. *Biochim Biophys Acta* 933:85–94.
11. Bennett J (1977) Phosphorylation of chloroplast membrane polypeptides. *Nature* 269:344–346.
12. Horton P, Allen JF, Black MT, Bennett J (1981) Regulation of phosphorylation of chloroplast membrane polypeptides by the redox state of plastoquinone. *FEBS Lett* 125:193–196.
13. Andersson B, Anderson JM (1980) Lateral heterogeneity in the distribution of chlorophyll-protein complexes of the thylakoid membranes of spinach chloroplasts. *Biochim Biophys Acta* 593:427–440.
14. Depège N, Bellafiore S, Rochaix JD (2003) Role of chloroplast protein kinase Stt7 in LHCII phosphorylation and state transition in *Chlamydomonas*. *Science* 299:1572–1575.
15. Shapiguzov A, et al. (2010) The PPH1 phosphatase is specifically involved in LHCII dephosphorylation and state transitions in *Arabidopsis*. *Proc Natl Acad Sci USA* 107:4782–4787.
16. Pribil M, Pesaresi P, Hertle A, Barbato R, Leister D (2010) Role of plastid protein phosphatase TAP38 in LHCII dephosphorylation and thylakoid electron flow. *PLoS Biol* 8:e1000288.
17. Vener AV, Van Kan PJM, Gal A, Andersson B, Ohad I (1995) Activation/deactivation cycle of redox-controlled thylakoid protein phosphorylation. Role of plastoquinol bound to the reduced cytochrome *bf* complex. *J Biol Chem* 270:25225–25232.
18. Zito F, et al. (1999) The Q_o site of cytochrome b_6f complexes controls the activation of the LHCII kinase. *EMBO J* 18:2961–2969.
19. Hamel P, Olive J, Pierre Y, Wollman FA, de Vitry C (2000) A new subunit of cytochrome b_6f complex undergoes reversible phosphorylation upon state transition. *J Biol Chem* 275:17072–17079.
20. Lemeille S, et al. (2009) Analysis of the chloroplast protein kinase Stt7 during state transitions. *PLoS Biol* 7:e45.
21. Lemeille S, Turkina MV, Vener AV, Rochaix JD (2010) Stt7-dependent phosphorylation during state transitions in the green alga *Chlamydomonas reinhardtii*. *Mol Cell Proteomics* 9:1281–1295.
22. Zito F, Vinh J, Popot JL, Finazzi G (2002) Chimeric fusions of subunit IV and PetL in the b_6f complex of *Chlamydomonas reinhardtii*: Structural implications and consequences on state transitions. *J Biol Chem* 277:12446–12455.
23. de Vitry C, Ouyang Y, Finazzi G, Wollman FA, Kallas T (2004) The chloroplast Rieske iron-sulfur protein. At the crossroad of electron transport and signal transduction. *J Biol Chem* 279:44621–44627.
24. de Lacroix de Lavalette A, Finazzi G, Zito F (2008) b_6f-associated chlorophyll: Structural and dynamic contribution to the different cytochrome functions. *Biochemistry* 47:5259–5265.
25. Hasan SS, Cramer WA (2014) Internal lipid architecture of the hetero-oligomeric cytochrome b_6f complex. *Structure* 22:1008–1015.
26. Shapiguzov A, et al. (2016) Activation of the Stt7/STN7 kinase through dynamic interactions with the cytochrome b_6f complex. *Plant Physiol* 171:82–92.
27. Singh SK, et al. (2016) Trans-membrane signaling in photosynthetic state transitions: Redox- and structure-dependent interaction *in vitro* between Stt7 kinase and the cytochrome b_6f complex. *J Biol Chem* 291:21740–21750.
28. Zito F, Finazzi G, Joliot P, Wollman FA (1998) Glu78, from the conserved PEWY sequence of subunit IV, has a key function in cytochrome b_6f turnover. *Biochemistry* 37:10395–10403.
29. Johnson X, et al. (2009) A new setup for in vivo fluorescence imaging of photosynthetic activity. *Photosynth Res* 102:85–93.
30. Kuras R, Wollman FA (1994) The assembly of cytochrome b_6f complexes: An approach using genetic transformation of the green alga *Chlamydomonas reinhardtii*. *EMBO J* 13:1019–1027.
31. Choquet Y, Zito F, Wostrikoff K, Wollman FA (2003) Cytochrome *f* translation in *Chlamydomonas* chloroplast is autoregulated by its carboxyl-terminal domain. *Plant Cell* 15:1443–1454.
32. Garnier J, Maroc J, Guyon D (1986) Low-temperature fluorescence emission spectra and chlorophyll-protein complexes in mutants of *Chlamydomonas reinhardtii*: Evidence for a new chlorophyll-*a*-protein complex related to photosystem I. *Biochim Biophys Acta* 851:395–406.
33. Stroebel D, Choquet Y, Popot J-L, Picot D (2003) An atypical haem in the cytochrome *b(6)f* complex. *Nature* 426:413–418.
34. Wurtz EA, Boynton JE, Gillham NW (1977) Perturbation of chloroplast DNA amounts and chloroplast gene transmission in *Chlamydomonas reinhardtii* by 5-fluorodeoxyuridine. *Proc Natl Acad Sci USA* 74:4552–4556.
35. Fischer N, Hippler M, Sétif P, Jacquot JP, Rochaix JD (1998) The PsaC subunit of photosystem I provides an essential lysine residue for fast electron transfer to ferredoxin. *EMBO J* 17:849–858.
36. Naver H, Boudreau E, Rochaix JD (2001) Functional studies of Ycf3: Its role in assembly of photosystem I and interactions with some of its subunits. *Plant Cell* 13:2731–2745.
37. Currin A, Swainston N, Day PJ, Kell DB (2015) Synthetic biology for the directed evolution of protein biocatalysts: Navigating sequence space intelligently. *Chem Soc Rev* 44:1172–1239.
38. Guo J, et al. (2013) Structure of the catalytic domain of a state transition kinase homolog from *Micromonas* algae. *Protein Cell* 4:607–619.
39. Bergner SV, et al. (2015) STATE TRANSITION7-dependent phosphorylation is modulated by changing environmental conditions, and its absence triggers remodeling of photosynthetic protein complexes. *Plant Physiol* 168:615–634.
40. Hasan SS, Stofleth JT, Yamashita E, Cramer WA (2013) Lipid-induced conformational changes within the cytochrome b_6f complex of oxygenic photosynthesis. *Biochemistry* 52:2649–2654.
41. Finazzi G, Zito F, Barbagallo RP, Wollman FA (2001) Contrasted effects of inhibitors of cytochrome b_6f complex on state transitions in *Chlamydomonas reinhardtii*: The role of Q_o site occupancy in LHCII kinase activation. *J Biol Chem* 276:9770–9774.
42. Alric J, Pierre Y, Picot D, Lavergne J, Rappaport F (2005) Spectral and redox characterization of the heme c_i of the cytochrome b_6f complex. *Proc Natl Acad Sci USA* 102:15860–15865.
43. Zito F, Alric J (2016) Heme c_i or c_n of the cytochrome b_6f complex, a short retrospective. *Cytochrome Complexes: Evolution, Structures, Energy Transduction, and Signaling* (Springer, Dordrecht, The Netherlands), pp 295–306.
44. Wollman FA, Delepelaire P (1984) Correlation between changes in light energy distribution and changes in thylakoid membrane polypeptide phosphorylation in *Chlamydomonas reinhardtii*. *J Cell Biol* 98:1–7.
45. Chua NH, Bennoun P (1975) Thylakoid membrane polypeptides of *Chlamydomonas reinhardtii*: Wild-type and mutant strains deficient in photosystem II reaction center. *Proc Natl Acad Sci USA* 72:2175–2179.

B. Additional results

1. Screening of C. reinhardtii transformants

Various screening procedures were tested in order to find the conditions that would produce the most drastic and reproducible difference in q_T between the WT and *stt7-1* strains. After that, transformants were screened for impaired state transition phenotypes, which would typically resemble the chlorophyll fluorescence emission kinetics shown in Figure III.2. This type of data was obtained as described in (Johnson et al. 2009) by saving the sequence recorded with the camera in a file containing each frame in an array and then using a couple of MATLAB programs to process and normalize the signal, count the number of colonies and extract all corresponding fluorescence kinetics curves. This was a remarkably efficient way of isolating transformants of interest. Once restreaked, mutants of interest could be spotted on plates containing reference strains in order to measure and compare photosynthetic parameters more precisely through simple image calculations. For example, the q_T parameter was measured and rendered as false color images as described in Figure III.3. Through successive screening rounds, the list was narrowed down to seventeen *petD* random mutants showing phototrophic growth and a blocked-in-State I phenotype (Figure III.4).

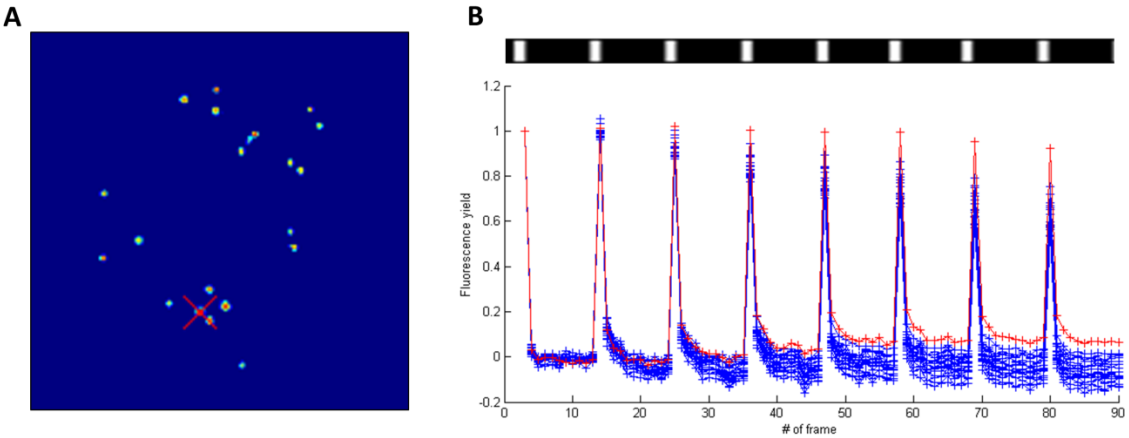

Figure III.2. Time-resolved fluorescence quenching kinetics during a switch to anaerobic conditions of *C. reinhardtii* transformants generated by random mutagenesis and chloroplast transformation.
(A) False colour fluorescence image of the ~1 mm colonies on the Petri dish. **(B)** PSII fluorescence quenching kinetics obtained from each colony over the 10 min recording sequence in the dark (dark bar) with 8 saturating flashes (2000 µE.m^{-2}.s^{-1}, white strips) and normalized on the first F_m value. The MATLAB programs used to generate this representation allows an interactive look at the data, enabling one to locate the colony of interest by clicking on a fluorescence curve.

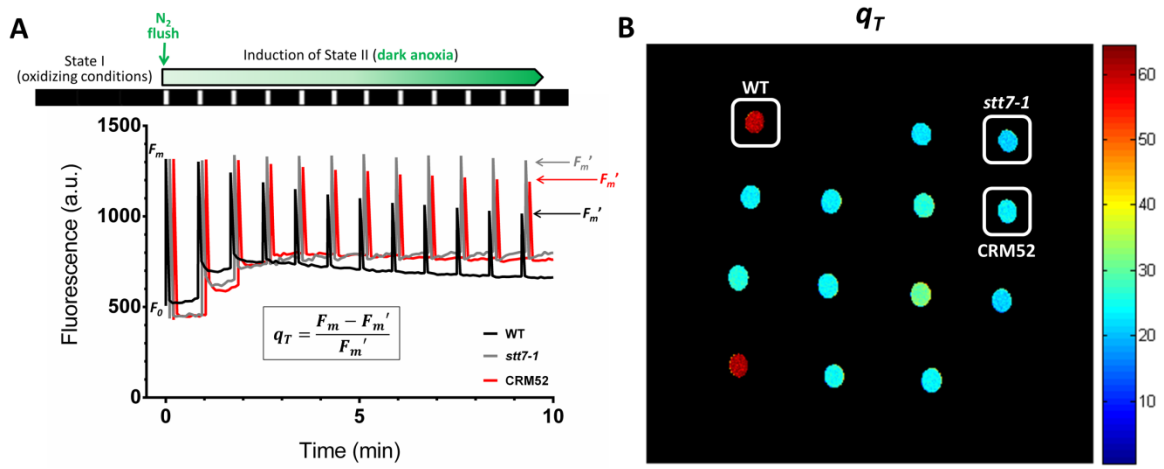

Figure III.3. Preliminary characterization of random mutants isolated from the state transition screen. **(A)** Typical fluorescence quenching curves obtained from cells spotted and grown on plates, left aerated in the dark to oxidize the PQ pool and then transferred to dark anaerobic conditions using an N_2 flush. Each white strip above the curve corresponds to a saturating flash (2000 $\mu mol_{photons}.m^{-2}.s^{-1}$). **(B)** False color image of the q_T parameter of the WT, *stt7-1* and mutant CRM52 strains, calculated as [$q_T = (F_m - F_m')/F_m'$] using maximal PSII fluorescence values of Panel A curves. Red = high q_T. Blue = low q_T and impaired state transitions.

The first nine mutants of the alignment contain mutations in the fg loop and are part of the catalog of fg loop mutants reported in Table III.1. The other eight mutants in the alignment contain mutations in other parts of the *petD* gene that also had an effect on the kinetics of maximum fluorescence yield of PSII upon a transition from dark aerobic to dark anaerobic conditions. These mutants, and the substitutions they bear, were discussed in Chapter II. Because we directed our attention toward the stromal fg loop of subunit IV that seemed to be a hotspot for state transition mutants, these additional mutants were not studied further. However, among them is mutant ARM7 which, aside from the rather conservative Thr110Ser substitution, contains the Ile131Asn substitution. This isoleucine is on the stromal edge of helix G and sticks out toward the periphery of the complex. As shown below, replacement of this residue by a charged residue such as aspartate (mutant Ile131Asp) had an effect on state transitions (Figure III.5A-B) as well as on LHCII phosphorylation (Figure III.7). The significance of this finding is discussed in Chapter IV.

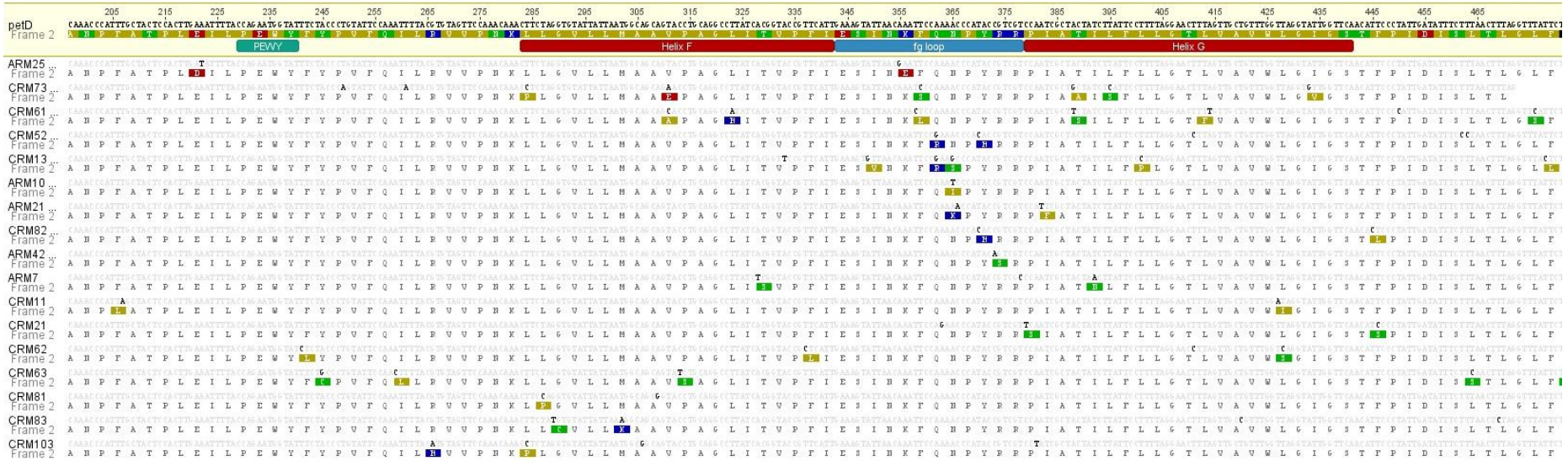

Figure III.4. Alignment of the seventeen state transition mutants obtained by random mutagenesis of *petD*.

The WT *petD* sequence was used as reference (top) and the region of the gene shown here (base 195 to terminal base 483) corresponds to the region that was targeted for random mutagenesis. Mutated nucleotides are bolded, and non-silent mutations are highlighted in color on the translated sequences shown below each corresponding nucleotide sequence.

2. *Further characterization of subunit IV fg loop mutants*

Apart from mutants Asn122Leu, Tyr124Lys and Arg125Glu that are the focus of the article, the other fg loop mutants obtained by SD and listed in Table III.1 were characterized. These were made either to reproduce some of the mutations carried by random mutants or to test the role of residues that were untouched by random mutagenesis but which could have a putative role in the interaction with Stt7. Figure III.5 shows the PSII fluorescence quenching kinetics, 77K fluorescence spectra and absorbance changes at 520 nm of all the SD mutants. Data for the three mutants presented in the article were added for the sake of comparison. The PSII fluorescence quenching kinetics and 77K fluorescence spectra were perfectly correlated and allowed an unambiguous distinction between residues whose substitution affected state transitions (Asn122, Tyr124, Arg125, Ile131) from those that were not involved in the process (Asn118, Lys119, Gln121).

Table III.1. Catalog of subunit IV fg loop mutants. RM: random mutagenesis; SD: site-directed mutagenesis; ST: state transitions

Mutant nb & origin		Helix F	Subunit IV fg loop	Helix G	ST
1	RMA		N118S		++
2	RMB	T110A	N118S	I145T	++
3	SD		N118L		++
4	SD		N118D		++
5	*RMA*	*E74D*	*K119E*		–
6	SD		K119L		++
7	SD		K119E		++
8	RMB		F120S	S154P	+
9	*RMB*	*L95P V104E*	*F120S*	*T130A L132S I145V*	– –
10	*RMB*	*V104A L108H*	*F120L*	*T130S L138F L159S*	– –
11	SD		F120L		++
12	SD		F120W		++
13	*RMB*		*Q121R Y124H*		– –
14	RMB	V104A	Q121R	F149S	++
15	*RMB*	*I117V*	*Q121R N122S*	*L134P F160L*	–
16	SD		Q121L		++
17	SD		Q121R		++
18	*RMA*		*N122I*		– –
19	*RMA*		*N122K*	*I128F*	– –
20	SD		N122T		–
21	SD		N122H		– –
22	SD		N122L		– –
23	RMB		Y124C		++
24	*RMB*		*Y124H*	*F149L*	–
25	RMB		Y124F	I128T T137A L159S	++
26	SD		Y124F		++
27	SD		Y124K		– –
28	*RMA*		*R125S*		–
29	SD		R125L		– –
30	SD		R125E		– –

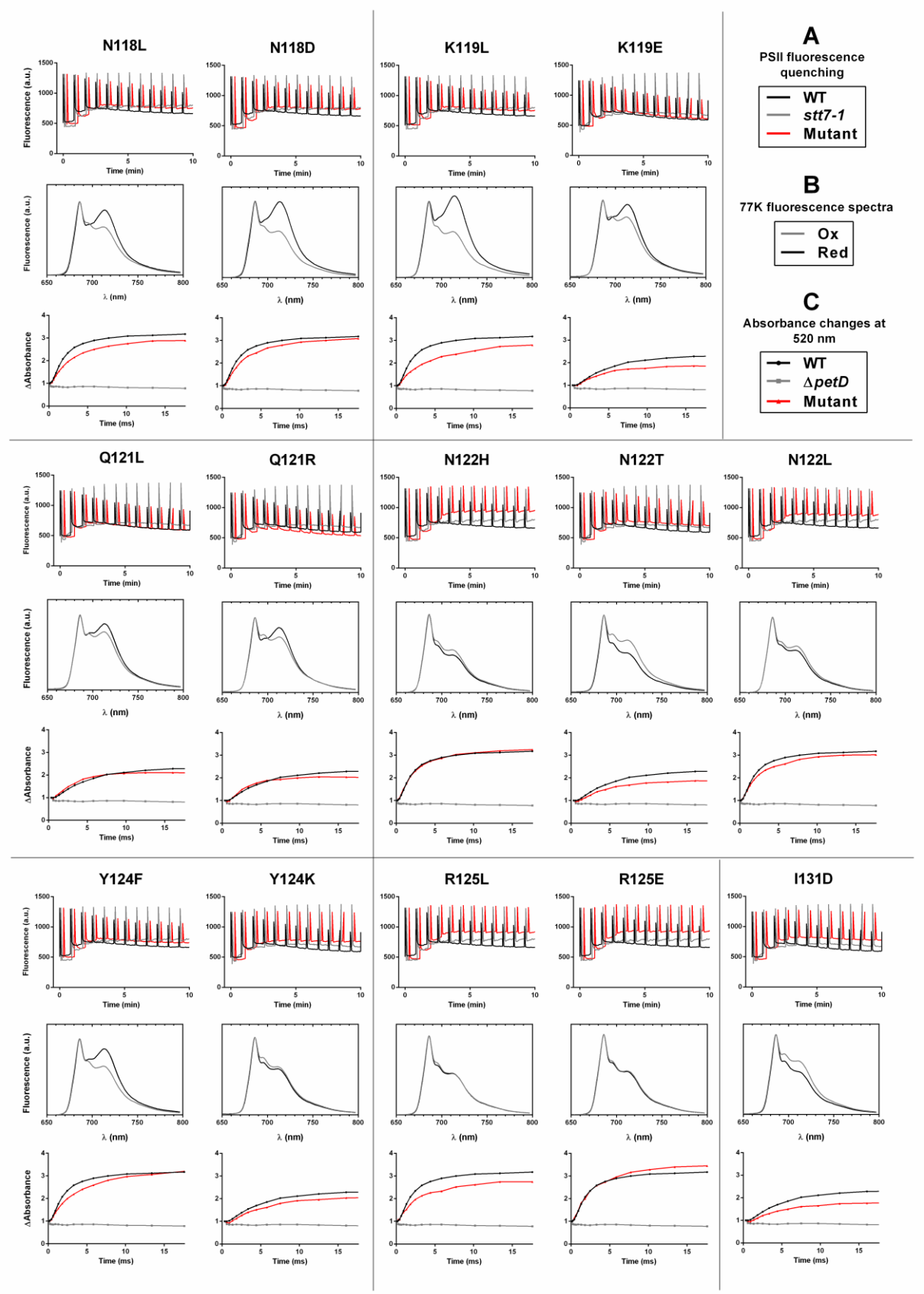

Figure III.5. Characterization of subunit IV fg loop site-directed mutant.
(A) Kinetics of PSII maximal fluorescence quenching during a transition to anaerobic conditions of the mutant compared to the WT and *stt7-1* reference strains. **(B)** 77K fluorescence spectra in oxidizing and reducing conditions. **(C)** ECS measurement associated with cyt b_6f turnover.

The only counterintuitive case were mutants of residue Tyr124, which in one case impaired state transitions (Tyr124Lys) and in the other exhibited no alteration of state transitions (Tyr124Phe) (see also phosphorylation profiles on Figure III.7). Structural and mechanistic information was obtained from this observation, which suggested that the determining factor at this position was the aromaticity of the amino acid side chain, as is discussed further in Chapter IV.

The kinetics of flash-induced absorbance changes at 520 nm correspond to the electrochromic shift (ECS) of carotenoids and reflect the transmembrane potential. A single turnover flash induces a fast electrogenic phase (phase *a*) corresponding to charge separation in the photosystems, followed by a slow electrogenic phase (phase *b*) generated by electron transfer between hemes b_L and b_H and a slower decay (phase *c*) reflecting the activity of ATPsynthase. The amplitude of phase *b* is a function of the relative rates of increase ($t½_{\text{ phase } b}$) and decrease ($t½_{\text{ phase } c}$) of membrane potential, which is itself strongly dependent on the dark-adaptation of the cells to anaerobic conditions and preactivation state of ATPase. For these reasons, and because not all data were obtained on the same day and from the same samples, some measurements showed a smaller amplitude of the phase *b*. However, in all cases, electron transfer in the mutant strains was very similar to the WT strain and much different from the Δ*petD* strain which shows no electrogenicity after a single flash.

Random (single) mutants 18 (Asn122Ile) and 28 (Arg125Ser) were blocked in State 1 in reducing conditions and suggested that mutations on the fg loop were a direct cause of the observed state transition phenotype. Point mutants were generated to verify this observation and to make sure that, for the other random mutants bearing several mutations, the observed phenotype was not solely caused by the general instability and combinatory effect of introducing several mutations on the same subunit.

Finally, the Phe120 residue, which points toward the exterior of the complex and sits right next to the Arg125 residue, was replaced with a non-aromatic (Phe120Leu, mutant 11) or bulkier aromatic (Phe120Trp, mutant 12). The quenching of PSII maximal fluorescence upon reduction of the PQ pool was not affected in these mutants (data not shown). This showed that not all substitutions of peripheral residues along the fg loop could affect state transitions, and was further proof of the specificity of the impaired phenotype in Asn122, Tyr124 and Arg125 mutants.

3. *Phosphorylation of LHCII antenna proteins*

The ^{33}P-labelling experiment result showed that mutants Asn122Leu, Tyr124Lys and Arg125Glu had low levels of Stt7-dependent LHCII phosphorylation in reducing conditions (Figure 3 in the article). This was proof that, in these mutants, the lack of PSII fluorescence quenching upon PQ pool reduction and the inability to modulate photosystem antenna size between oxidizing and reducing conditions were correlated with an impaired activity of Stt7. This result was confirmed with another ^{33}P-labelling experiment in which State II was induced by incubating the cells with 2 mg.mL^{-1} glucose oxidase and 20 mM glucose in the dark for 30 minutes (Figure III.6).

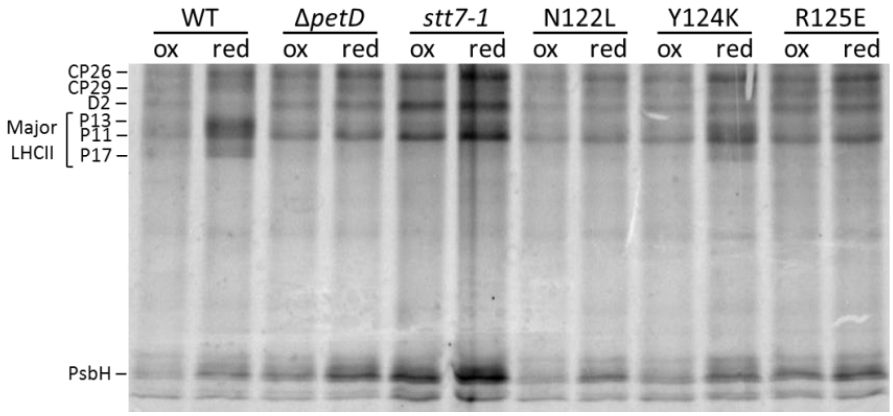

Figure III.6. Autoradiogram of *in vivo* ^{33}P-labeled polypeptides in reducing conditions.
Thylakoid proteins were extracted from cells placed in oxidizing (10 µM DCMU, moderate light, strong agitation, 30 min) or reducing (2 mg.mL^{-1} glucose oxidase, 20 mM glucose, dark, 30 min) conditions and separated by SDS-PAGE on an 8 M urea 12-18% gradient gel.

The phosphorylation profiles of the other side-directed fg loop mutants were also analyzed (Figure III.7). Similarly to the Asn122Leu strain, substitutions of Asn122 with a threonine or histidine impeded LHCII phosphorylation. The same goes for the Arg125Leu strain which showed no phosphorylation in State II, much like the Arg125Glu strain. As mentioned previously, substitution of the Ile131 residue with an aspartate created a mutant blocked in State I in reducing conditions. Of special interest is the Tyr124Phe substitution which, despite the obvious problem in State I induction (Figure III.7 lane 5), showed phosphorylation of P17 and P13, in correlation with the chlorophyll fluorescence quenching kinetics and fluorescence emission spectrum shown on Figure III.5.

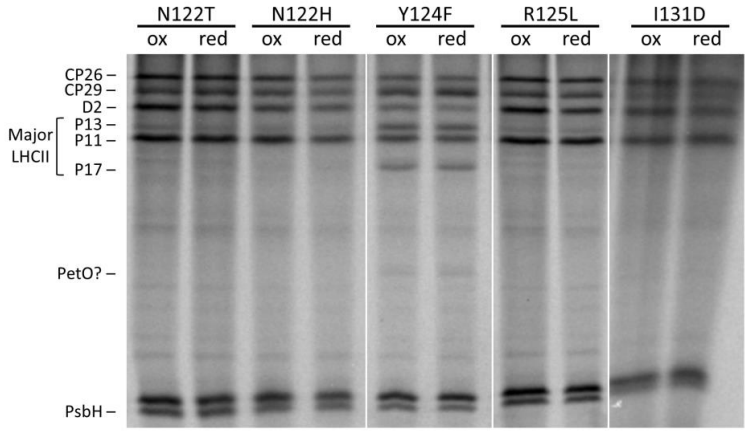

Figure III.7. Autoradiogram of *in vivo* ^{33}P-labeled polypeptides from other fg loop mutants.
Thylakoid proteins were extracted from cells placed in oxidizing (10 µM DCMU, moderate light, strong agitation, 30 min) or reducing (5 µM FCCP, dark, 30 min) conditions and separated by SDS-PAGE on an 8 M urea 12-18% gradient gel.

As an alternative to the ^{33}P-labelling experiments, phosphorylated LHCII can be detected with an antibody directed against phosphothreonine (anti-phosphoThr). In order to facilitate the subsequent attribution of phosphorylation bands, the migration profile of LHCII peptides was first obtained by running a total protein extract of the WT strain on a 6 M urea 15% gel and blotting with antibodies against the major LHCII proteins (Figure III.8A).

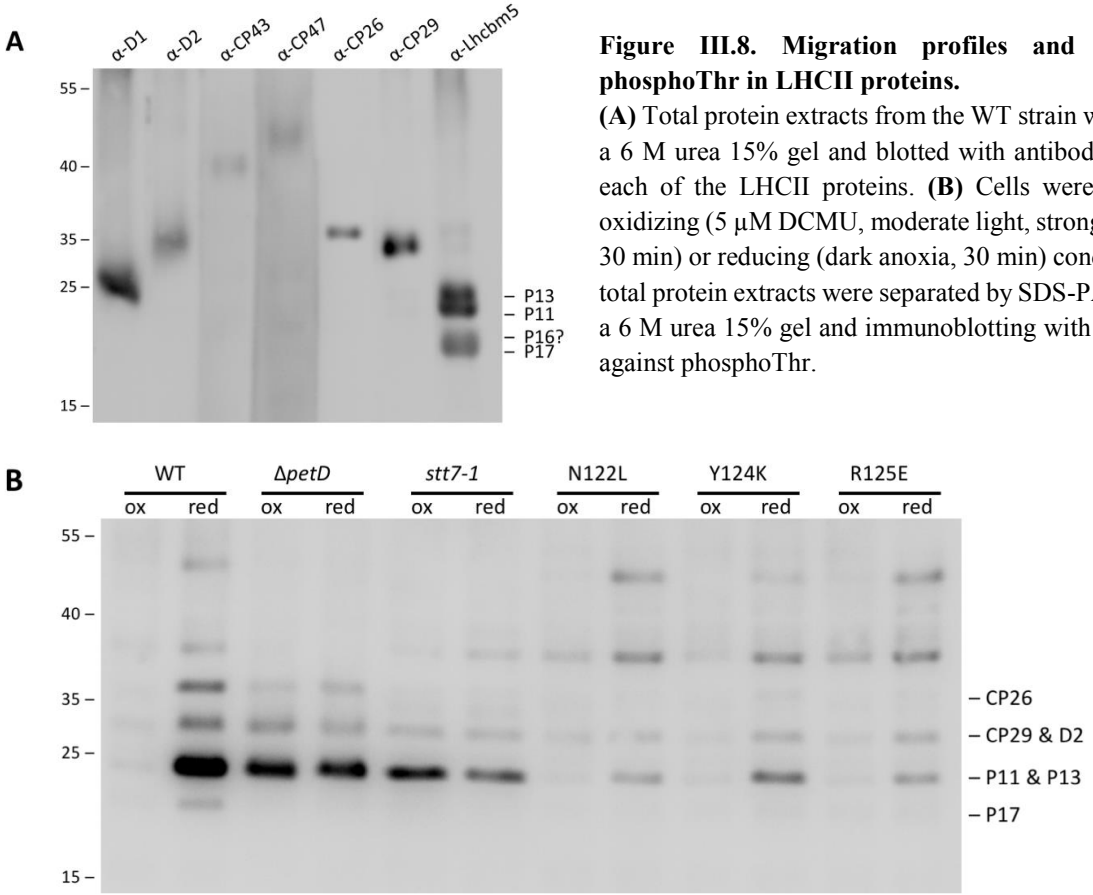

Figure III.8. Migration profiles and levels of phosphoThr in LHCII proteins.
(A) Total protein extracts from the WT strain were run on a 6 M urea 15% gel and blotted with antibodies against each of the LHCII proteins. **(B)** Cells were placed in oxidizing (5 µM DCMU, moderate light, strong agitation, 30 min) or reducing (dark anoxia, 30 min) conditions and total protein extracts were separated by SDS-PAGE using a 6 M urea 15% gel and immunoblotting with antibodies against phosphoThr.

The anti-Lhcbm5 antibody recognized three proteins that were identified as P17 (20 kDa), P11 (23 kDa) and P13 (25 kDa) based on the order of migration on 12-18% gradient gels. Antibodies against CP29, CP26, CP43 and CP47 recognized one protein each, defining distinct bands around 33, 36, 40 and 45 kDa respectively. Antibodies against D1 and D2 recognized proteins that co-migrated with P13 and CP29 at 25 and 33 kDa, respectively. It is possible that the P17 band is actually a double band composed of a lower P17 band and an upper P16 band (Type IV LHCII, coded by *LHCBM1*), as seen on the denaturating gel analysis of the PSII-LHCII supercomplex shown on Figure III.9A, which was added to provide some reference points from the literature and matches fairly with this LHCII migration analysis.

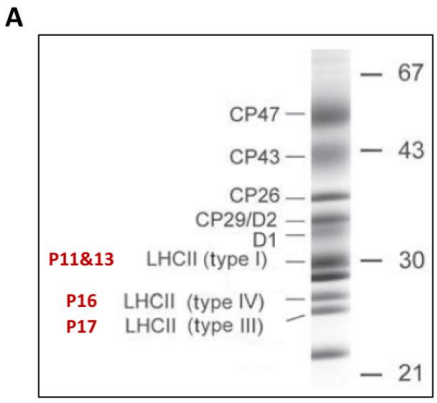

B

Protein (LHCII type)	Theoretical MW (kDa)	Approx. MW (kDa) on Fig. 8A	Gene(s)
CP47	56	45	*psbB*
CP43	50	40	*psbC*
CP26	30	36	*LHCB5*
CP29	30	33	*LHCB4*
D2	39	33	*psbD*
D1	39	25	*psbA*
P11 (I)	27	23	*LHCBM3,4, 6,8,9*
P13 (I)	27	25	
P16 (IV)	27	20	*LHCBM1*
P17 (III)	26	20	*LHCBM2,7*

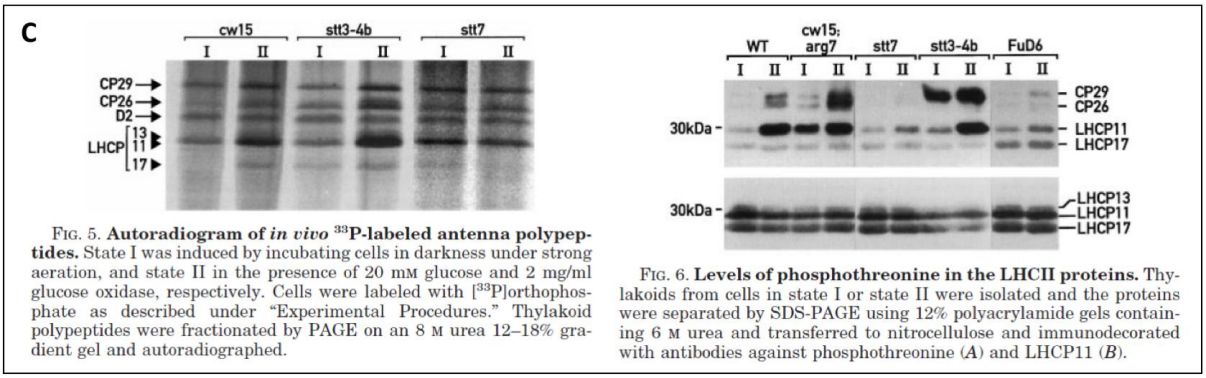

FIG. 5. **Autoradiogram of *in vivo* ^{33}P-labeled antenna polypeptides.** State I was induced by incubating cells in darkness under strong aeration, and state II in the presence of 20 mM glucose and 2 mg/ml glucose oxidase, respectively. Cells were labeled with [^{33}P]orthophosphate as described under "Experimental Procedures." Thylakoid polypeptides were fractionated by PAGE on an 8 M urea 12–18% gradient gel and autoradiographed.

FIG. 6. **Levels of phosphothreonine in the LHCII proteins.** Thylakoids from cells in state I or state II were isolated and the proteins were separated by SDS-PAGE using 12% polyacrylamide gels containing 6 M urea and transferred to nitrocellulose and immunodecorated with antibodies against phosphothreonine (*A*) and LHCP11 (*B*).

Figure III.9. Reference literature on LHCII phosphorylation.
(A) Polypeptide composition of purified PS II–LHCII supercomplex as resolved by high-resolution SDS-polyacrylamide gel electrophoresis and Coomassie blue staining (adapted from (Stern 2009), originally from Iwai and Minagawa, unpublished). (B) List of PSII core and antenna proteins, with theoretical and observed molecular weights from immunoblot on Panel A, and encoding chloroplastic (lower case) or nuclear (upper case) genes. (C) Reference autoradiogram of ^{33}P-labeled antenna proteins (left) and anti-phosphoThr immunoblot of antenna proteins (right) (from (Fleischmann et al. 1999)).

For the *in vivo* phosphorylation, *C. reinhardtii* cells were treated for 30 min to induce State I (5 µM DCMU with aeration in the light) or State II (dark anoxia). Successful induction of State I and State II was verified by measuring the 77K fluorescence spectra of the WT strain prior to protein extraction (data not shown). Total protein extracts were separated by SDS-PAGE on a 6 M urea 15% gel and analyzed by immunoblot with an anti-phosphoThr antibody (Figure III.8B). As expected, proteins P11/P13 and CP29/D2 co-migrated and formed only two bands due to the resolution of this gel electrophoresis.

In the control WT strain, all chlorophyll-binding proteins were phosphorylated in State II and almost no phosphorylation was observed in State I. The Δ*petD* and *stt7-1* strains showed phosphorylation levels intermediary between WT-State I and WT-State II for bands corresponding to CP29/D2 and P11/P13. The Δ*petD* strain had a slightly higher phosphorylation of CP26 in State II compared to State I. In the *stt7-1* strain, CP26 was not phosphorylated. Both strains showed no phosphorylation of P17. Interestingly, the phosphorylations that were present seemed completely de-correlated from the redox state of the PQ pool since their level did not change between oxidizing and reducing conditions, as reported previously for cyt b_6f mutants in (Wollman and Lemaire 1988). The strong phosphorylation signals of the CP29/D2 and P11/P13 bands in these strains were nevertheless much smaller than in the WT type and most likely correspond to the residual phosphorylation of PSII core subunits: D2 phosphorylation is Stt7- and PQ-pool-independent and has been implicated in the protection of photodamaged PSII under high light conditions (Koivuniemi et al. 1995) as well as in the regulation of its repair cycle (Tikkanen et al. 2008). The P11/P13 signals in the Δ*petD* and *stt7-1* strains may also be increased by the contribution of P11 phosphorylation which, as reported previously, stays high in both oxidizing and reducing conditions in strains inactivated for Stt7 or the cyt b_6f (Figure III.9C and (Wollman and Lemaire 1988)). These results on the phosphorylation of LHCII peptides in cyt b_6f and Stt7 deletion mutants are in agreement with previous seminal studies on this question (Wollman and Delepelaire 1984; Delepelaire and Wollman 1985; Wollman and Lemaire 1988). There seems to be different populations of LHCII proteins with different b_6f- and Stt7-dependencies for phosphorylation. The presence of phosphorylated LHCII proteins in the *stt7-1* strain is readily explained by the activity of other chloroplast kinases. Furthermore, their equal phosphorylation levels in oxidizing and reducing conditions suggest that these other kinases are not under PQ pool redox control. However, for b_6f mutants, in our case the Δ*petD* strain, this observation raises several interesting questions.

Wollman and Lemaire proposed some compelling hypotheses in their 1988 study, which we will come back to in the analysis of results obtained in an unrelated venture (see Section III.B.5).

The most striking feature about the phosphorylation pattern of the Asn122Leu, Tyr124Lys and Arg125Glu strains was the fact that they seemed to recover some kind of redox regulation and did not resemble the intermediary and redox-independent phosphorylation profiles of the two control deletion strains. Furthermore, the CP29/D2 and P11/P13 State II phosphorylation signals were greatly diminished in the mutant strains, and the residual signals can be attributed to D2 and P11 phosphorylation, respectively. No phosphorylation of CP26 and P17 was detected at all in all three strains. These site-directed mutants show a lack of Stt7-dependent phosphorylation of P17, P13, CP29 and CP26 in reducing conditions. This unambiguously demonstrates the loss of the phosphorylation signal between the reduced PQ pool and the Stt7 kinase-specific targets.

4. *Cyt b_6f – Stt7 interaction studies*

Studies have shown evidence of a direct interaction between these two proteins, either in their native state by pull down (Lemeille et al. 2009) or by yeast two-hybrid assays (Shapiguzov et al. 2016). In order to understand whether this interaction is also dependent on recognition at the stromal side of the membrane, we performed protein-protein interaction assays with purified cyt b_6f and Stt7 kinase domain (Stt7-KD), as well as yeast two-hybrid experiments.

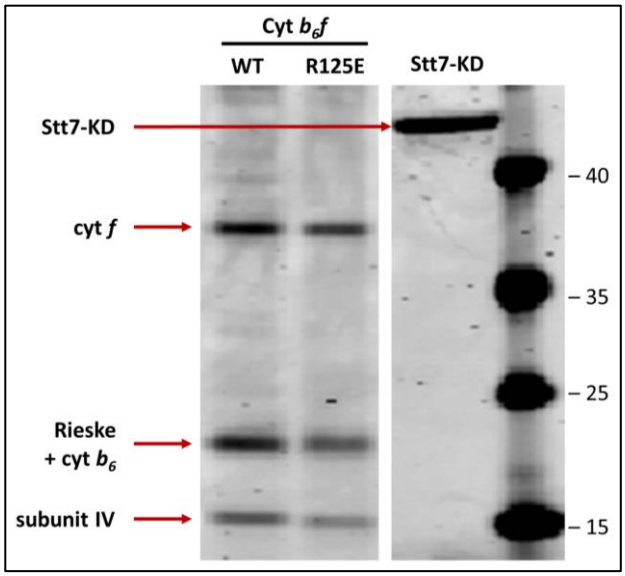

Figure III.10. SDS-PAGE analysis of purified cyt b_6f complexes and Stt7-KD.

WT and Arg125Glu cyt b_6f complexes were purified as in (Stroebel et al. 2003) and Stt7-KD was produced and purified as described in the Materials and Methods (see also Figure III.10). The formers contain His-tags and the latter both His- and Strep-tags.

Cross-linking – Stt7-KD and cyt b_6f were incubated in a 3:1 molar ratio with a 1000x molar excess of BS^2G cross-linker. Reactions were carried out over 2 hours and analyzed by taking samples at given time points, terminating the reaction with 20 mM NH_4HCO_3 and running the samples on a 4-12% denaturing gel. Figure III.11 shows the results of the Commassie blue stained gel and immunoblot using antibodies against Stt7 and subunit IV. The left lanes on Figure III.11A show the time-course of the cross-linking reaction. The Stt7-KD band signal showed that the protein gradually cross-linked during the course of the reaction (lanes 1 to 4). Apart from that, no other evidence of cross-linked peptides of interest could be obtained from this Commassie stained gel, *i.e.* no clear higher molecular weight bands appeared that were absent in the control reactions in which each protein is incubated with the cross-linker separately (lanes 5 to 8). To go further using these cross-linking samples, an immunoblot analysis was performed (Figure III.11B). When incubated for a short time (5 min) Stt7-KD and subunit IV did not crosslink and bands were detected at their expected molecular masses, 43 kDa and 15 kDa respectively (lane 1). Incubation for up to 2 hours led to a large decrease in intensity of the 43 kDa Stt7-KD band and complete disappearance of the 15kDa subunit IV

band (lane 2). The control where Stt7-KD was incubated alone with the cross-linker (lane 4) showed that the 43 kDa band also disappeared, suggesting that oligomers can be formed and that Stt7 can cross-link to one of its partners in a putative homodimer or homotetramer (see (Singh et al. 2016)) (lane 4). In the other control reaction (lane 3), subunit IV did not cross-link to other cyt b_6f subunits when incubated alone with the cross-linker (lane 3). This showed that the disappearance of the subunit IV band at 15 kDa in lane 2 was due to the presence of Stt7. However, the antibody against subunit IV did not detect any band at higher molecular masses where the cross-linking products were expected to be found, suggesting that epitopes were affected by the cross-linking reaction. This result was nevertheless strong evidence of an interaction between subunit IV and the stromal kinase domain of Stt7.

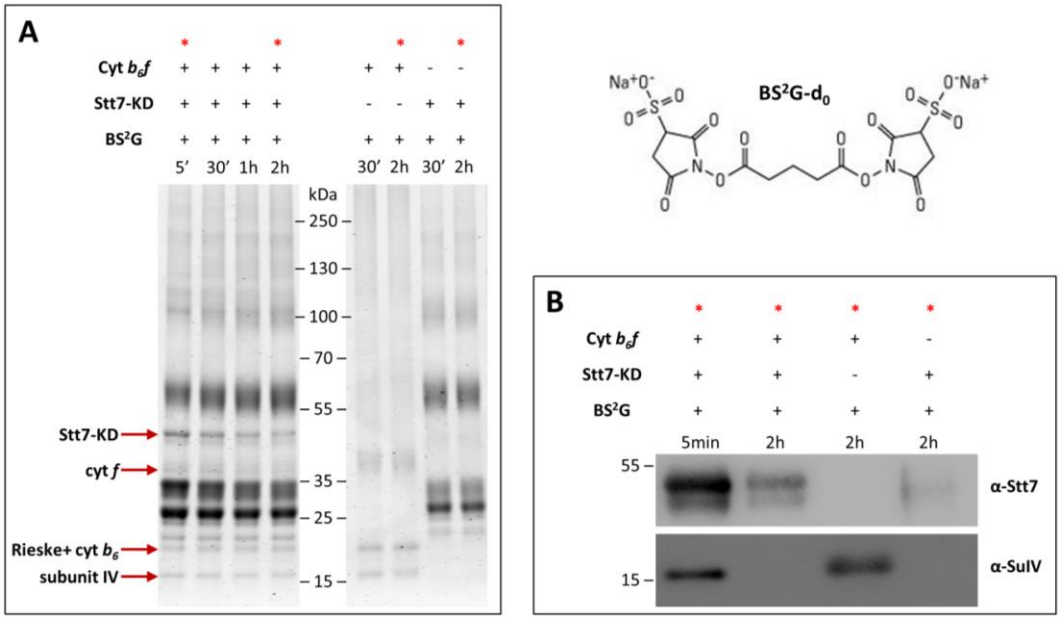

Figure III.11. Cross-linking assay between cyt b_6f and Stt7-KD.
(A) 4-12% gradient SDS-PAGE analysis of cross-linking reactions with 1.25 µM cyt b_6f, 3.75 µM Stt7-KD and 2.5 mM BS^2G. 20 mM NH_4HCO_3 was added to aliquots taken at the indicated time points to terminate the reactions. **(B)** Immunoblot of the reaction samples indicated by red asterisks in Panel A with antibodies against Stt7 and subunit IV. BS^2G is a water-soluble, 7.7 Å spacer arm cross-linker that forms stable amid bonds with primary amines (lysines).

Native-PAGE – The *in vitro* interaction between cyt b_6f and the kinase domain of Stt7 was further examined by incubating the two proteins at different molar ratios and analyzing their electrophoretic mobility on a native gel followed by an immunoblot (Figure III.12). In lane 1, the majority of cyt b_6f appeared in its dimeric form (240 kDa) although the monomeric form was also visible (120 kDa). In lane 2, a strong signal was detected at around 180 kDa which would correspond to the tetrameric form of Stt7-KD. The electrophoretic mobility of the cyt b_6f

was not affected when incubated in the presence of an equivalent molar concentration of Stt7 (lane 3). However, incubating 10x molar excess of Stt7-KD with cyt b_6f (lane 4) generated an additional band above 240 kDa which may correspond to a complex formed by the two proteins. This showed that the electrophoretic mobility of the native cyt b_6f is affected in the presence of a high molar excess of Stt7 kinase domain.

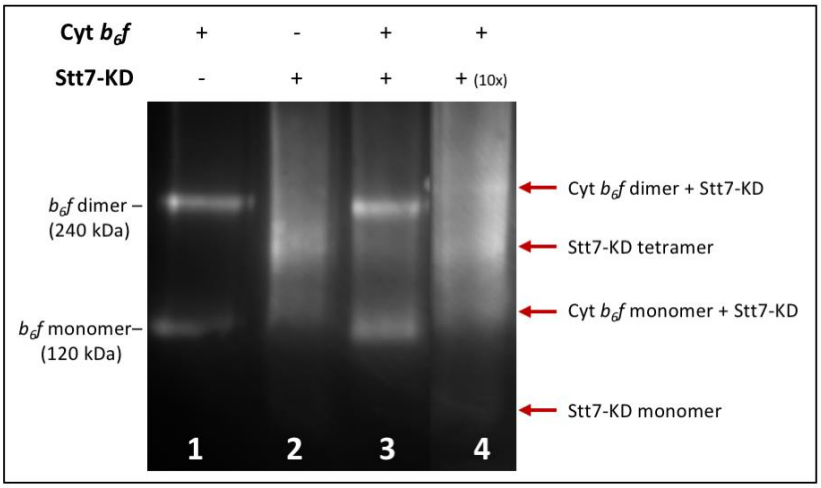

Figure III.12. Native immunoblot of cyt b_6f incubated with Stt7-KD.
Purified cyt b_6f (lane 1) and Stt7-KD (lane 2) were incubated together at room temperature for 30 minutes at 1:1 (lane 3) and 1:10 (lane 4) molar ratios. Samples were separated by native gel electrophoresis and migration profiles were visualized on a native blot using an anti-His antibody.

Yeast two-hybrid – The Matchmaker® Gold Yeast Two-Hybrid System (Clontech) was used to test the direct interaction between subunit IV and Stt7. The nucleotide sequences of the WT and [Y124K; R125E] mutant subunit IV fg loops were cloned as baits into pGBKT7 vectors and various Stt7 nucleotide sequences were cloned as preys into pGADT7 vectors. All vector constructions were verified by sequencing. Y2H Gold yeast cells were transformed with each pGBKT7-suIV vector and Y187 yeast cells were transformed with each pGADT7-Stt7 vector following the small-scale LiAc yeast transformation procedure described in the Yeast Protocols Handbook (Clontech). None of the strains transformed with pGBKT7-suIV plasmids exhibited autoactivation of the reporter genes when spotted on medium lacking Trp and containing 40 $\mu g.ml^{-1}$ X-α-Gal and 150 $ng.ml^{-1}$ Aureobasidin A. Diploids containing each bait-prey plasmid combination (Figure III.13) were obtained following the yeast mating protocol described in the Handbook and conserved on medium lacking Leu and Trp. Positives clones were selected on medium lacking Trp, Leu and His, supplemented with 40 $\mu g.ml^{-1}$ X-α-Gal with or without 150 $ng.ml^{-1}$ Aureobasidin A. The positive and negative controls were obtained as described in the Matchmaker® Gold User Manual (Clontech).

No interaction was detected between the WT fg loop of subunit IV and Stt7 fragments C (397-483) and D (484-600). An interaction was detected between the WT fg loop and Stt7 fragments AB (123-379) and B alone (244-379) in triple drop-out media (SD/-Leu/-Trp/-His) supplemented with 40 µg.ml^{-1} X-α-Gal with or without 150 ng.ml^{-1} Aureobasidin A. This interaction was lost when the WT fg loop was replaced with the double mutant [Tyr124Lys; Arg125Glu] fg loop. This experiment indicated that the stromal fg loop of subunit IV interacts with the kinase domain of Stt7 in the region between Leu244 and Pro379, which contains two important kinase regulatory motifs, HRD and DLG, as well as the activation loop and the α5-hairpin (Guo et al. 2013). Several acidic Asp and Glu residues, presented in Chapter IV, are found in this region and could form interactions with Arg125^{suIV} *in vivo*. Substitutions of fg loop residues Tyr124^{suIV} and Arg125^{suIV} abolished this interaction, showing that they are involved in the binding if the kinase to the stromal side of the complex.

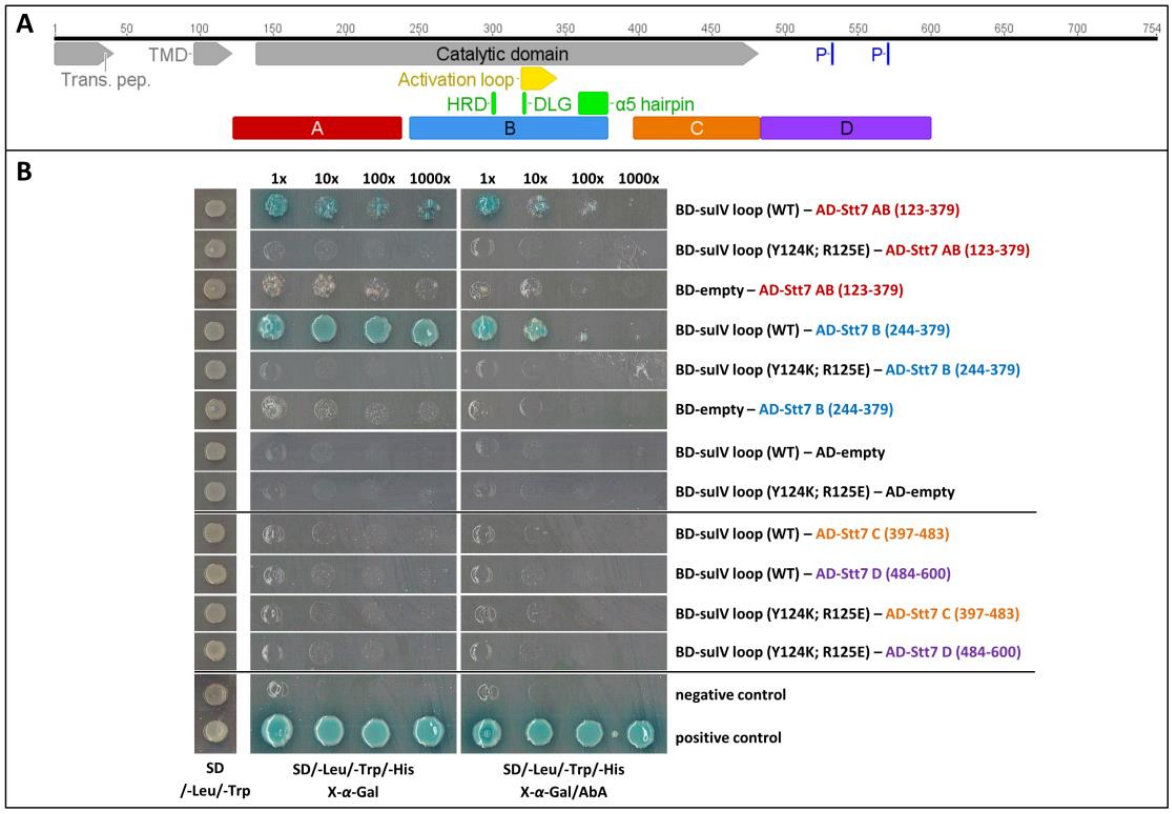

Figure III.13. Yeast two-hybrid assay of the interaction between the subunit IV fg loop and Stt7-KD.
(A) Schematic diagram of the full annotated Stt7 protein sequence. Trans. pep. = transit peptide; TMD = transmembrane domain; P = previously identified phosphorylation sites (Lemeille et al. 2010; Bergner et al. 2015). The activation loop is annotated in yellow and the catalytic motifs HRD and DLG as well as the α5-hairpin region (Guo et al. 2013) are colored in green. **(B)** Images of yeast cells spotted on various media. Double drop-out medium (SD/-Leu/-Trp) is used to select for diploids following yeast mating. Triple drop-out media (SD/-Leu/-Trp/-His) supplemented with 40 µg.ml^{-1} X-α-Gal with or without 150 ng.ml^{-1} Aureobasidin A (AbA) are used to select positive clones containing interacting peptides.

Apparent discrepancies between Stt7-KD autophosphorylation and ATP hydrolysis activities in vitro – Results of the *in vitro* autophosphorylation assay indicated that Stt7-KD phosphorylation was increased in the presence of WT cyt b_6f but not in the presence of cyt b_6f carrying the Arg125Glu mutation (Figure 4 in the article). This was proof that (i) cyt b_6f activates the stromal kinase domain of Stt7 and (ii) the Arg125^{suIV} residue is involved in this activation. As an alternative control, Stt7-KD activation was assessed by measuring its ATP hydrolysis activity in the presence of either versions of the b_6f complex (Figure III.14A). For this, we used the ADP-Glo™ Kinase Assay kit (Promega) which utilizes a reagent (Ultra-Glo™ Luciferase) containing luciferase and luciferin to generate a luminescence signal that is proportional to the amount of ADP produced during the kinase reaction and therefore correlated with Stt7-KD activity (see Figure III.14B scheme). The luminescence signals (Figure III.14A) revealed that Stt7-KD had a constitutive *in vitro* ATP hydrolysis activity (bar 1) which was stimulated in the presence of WT cyt b_6f (bar 2), in correlation with the results of the autophosphorylation assay (Figure III.14C, lanes 1 & 2). Surprisingly, whereas the Arg125Glu substitution impeded cyt b_6f-mediated autophosphorylation of Stt7-KD (Figure III.14C, lane 3), it did not prevent an increase in its ATP hydrolysis activity (Figure III.14A, bar 3). This demonstrates that ATP hydrolysis and autophosphorylation activities are not strictly correlated. Furthermore, it suggests that the cyt b_6f, WT or Arg125Glu, stabilize an active state of Stt7-KD. In this conformation, the kinase has an enhanced ATPase activity and is primed to receive the autophosphorylation signal that was shown to be (at least in part) dependent on the Arg125 residue of subunit IV. This alternative activity assay is another clue that points to the specificity of the Arg125-dependent mechanism that we elucidated. It remains to be explored whether the autophosphorylation of the kinase domain of Stt7 is required for its activity *in vivo*, *i.e.* whether it is a necessary step in state transitions. This would require identification and site-directed mutagenesis of the phosphorylation sites in the kinase domain.

Using samples from the autophosphorylation assays, we attempted to identify these phosphorylation sites by phosphoproteomics (Figure III.14D). SDS-PAGE gel bands corresponding to bands 1 and 2 on the immunoblot of Figure III.14C (Stt7-KD with basal and induced phosphorylation levels, respectively) were cut out, trypsin-digested and analyzed on by LC-MSMS on a Q-Exactive™ Hybrid Quadrupole-Orbitrap Mass Spectrometer (ThermoFisher). The SwissProt database was interrogated without species restriction with a maximum error of 1 ppm. Although both samples were identified as Stt7, the protein sequence yielded long tryptic peptides that were not detected by the spectrometer, giving poor sequence

coverage in both cases. The more sensitive and higher resolution Orbitrap Fusion™ Lumos™ Tribrid™ Mass Spectrometer was also tested and generated a slightly better sequence resolution (peptides highlighted in green in Figure III.14D). The only phosphorylation sites that have been reported and that are included in our Stt7-KD construct are $T_{489}AS_{491}LQHS_{495}$ (Bergner et al. 2015). However, these were classified as ambiguous by Bergner et al. due to PhosphoRS site probabilities below the cut-off value of 95%. In line with these results, the *TASLQHS* peptide (red brackets in Figure III.14D) was detected in its non-phosphorylated form in both samples 1 and 2. No other phosphorylation sites, out of the other 13 threonine and 18 serine residues of our construct, were detected. Indeed, most of these residues reside on peptides that could not be detected by the spectrometer. Unexpectedly, the Thr152 residue (Thr37 in Figure III.14D numbering, red arrows) that aligns perfectly with the Thr185 autophosphorylated residue of the Stt7 homolog in *Micromonas sp.* RCC299 (Guo et al. 2013), was not detected in its phosphorylated form.

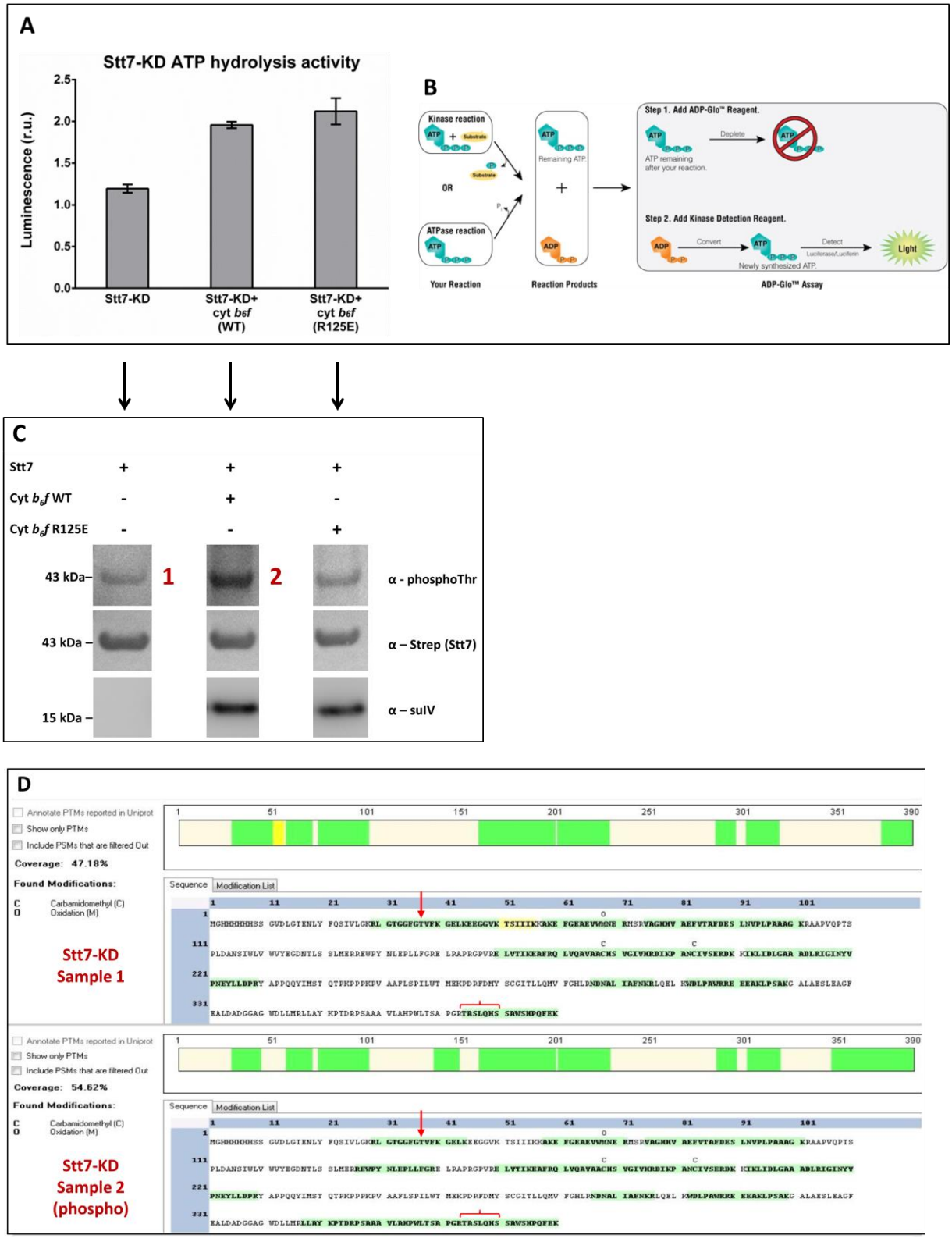

Figure III.14. Stt7-KD ATP hydrolysis *vs* autophosphorylation activities.
(A) ADP-Glo™ Kinase Assay used to measure the ATP hydrolysis activity of Stt7-KD alone or in the presence of WT or Arg125Glu cyt b_6f. The luminescence value for the control experiment (ATP alone, to measure background spontaneous ATP hydrolysis) was subtracted from the luminescence values of the experiment shown here. Three independent kinase reactions were carried out for the calculation of mean values and standards deviations. (B) Principle of the ADP-Glo™ kit (promegaconnections.com/the-ideal-kinase-assay). (C) Adapted from Figure 4 of the article. (D) Phosphoproteomics results of samples corresponding to Stt7-KD bands 1 and 2 of Panel C.

5. *Genetic suppressor approach*

Attempts & failures…

The success of the random mutagenesis of *petD* in finding state transitions mutants prompted us to try a genetic suppressor screen using the same technique on Stt7. The idea was to locate the Stt7 region in interaction with the subunit IV fg loop by randomly mutating Stt7 and finding suppressor(s) of the *petD*-Tyr124Lys mutation. The goal was to introduce this mutation in the *stt7-1* (or *stt7-9*) strain by chloroplast transformation, randomly mutate *STT7* by error-prone PCR using the pSLX-Stt7 construct (see Materials and Methods), and complement the deletion strains with randomly mutated versions of *STT7*. Transformants would then be screened on their recovered ability to perform a transition from State I to State II using the same screening procedure as described in this chapter but looking for the opposite outcome. State transition-proficient mutants would then be sequenced to find the mutation that suppressed the *petD*-Tyr124Lys mutation, thus establishing a region of interaction.

The first step was to build the tools needed for this experiment: plasmid pWQA-Y124K to transform the chloroplasts of the *stt7* deletion strains and replace the WT *petD* gene with one coding for the Tyr124Lys substitution, and plasmid pSLX-Stt7 as the template for random mutagenesis and as the complementation vector. The next step was to succeed in complementing the *stt7* deletion strains with the non-mutated *STT7* construct present on plasmid pSLX-Stt7. Various nuclear transformation protocols were tested and optimized for the *stt7-1* and *stt7-9* strains. Initial screenings of transformants did seem to show that some of them had recovered the ability to perform a state transition. However, this phenotype was systematically lost after the first re-streaking of clones on selective medium. This may have been due to gene silencing in the nucleus. A more stable phenotype might be obtained if the endogenous 1 kb sequence used as promoter region in the pSLX-Stt7 construct was replaced by the *PSAD* promoter sequence (Fischer and Rochaix 2001) or the *HSP70A-RbcS2* hybrid promoter sequence (Schroda et al. 2000). Because of time constraints and this failure to obtain stable complementants of the *stt7* deletions, the genetic suppressor approach was not pursued further.

…lead to unexpected findings

During the construction of vector pSLX-Stt7 and verification of several clones by sequencing, we noticed that a 33 bp sequence was systematically missing in the Stt7 cDNA region compared to the reference Stt7 sequence. This sequence corresponds to the 5'-end of the 14th (penultimate) exon of the Stt7 CDS and codes for the following 11 amino acids: DPYGAAPSAMQ. This meant that there are (at least) two alternative Stt7 RNA transcripts and that the cDNA preparation used to amplify the Stt7 cDNA contained only, or at least in majority, the sequence without the 33 bp. Plasmid pSLX-Stt7+33 containing this sequence was constructed and used to complement the *stt7* deletion strains, to no better avail. As suggested before, the endogenous promoter sequence should be replaced by a strong promoter in the two plasmids carrying the two *STT7* versions in order to generate stable complementants of the *stt7* deletion strains. Once this is accomplished, the functional significance of the alternative splicing we observed can be assessed by comparing strains complemented with either versions of *STT7*.

In relation to this, an interesting result was obtained in a separate experiment. Figure III.15 shows a Western Blot of the accumulation of Stt7 in various strains used in this study. The band below 70 kDa corresponds to a non-specific cross-reaction of the antibody against Stt7. The theoretical molecular mass of Stt7 is 80 kDa and a signal is visible in all strains except the *stt7-1* strain between the 70 kDa and 100 kDa molecular weight markers. In the WT, two distinct bands are visible, at around 80 kDa and 100 kDa, while only one band is visible in the Δ*petD* strain, at around 90 kDa. In the three *petD* mutants shown here, the signal corresponding to Stt7 appears smeary and likely corresponds to two indistinct bands that cover the 70-100 kDa region. This result confirmed that Stt7 accumulates in the *petD* deletion and site-directed mutant strains.

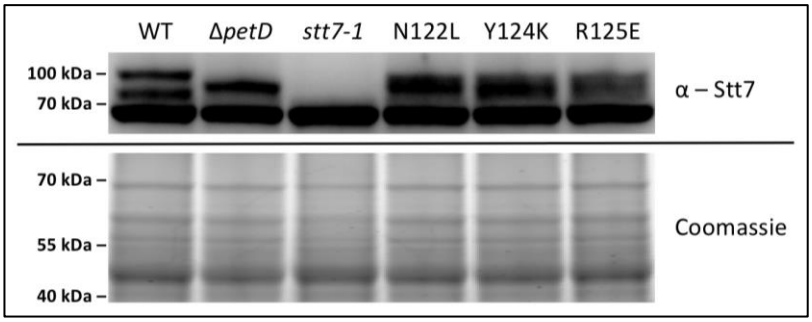

Figure III.15. Accumulation of Stt7 in reference and *petD* mutant strains.
Total protein extracts were loaded at equal protein concentration on a 3-12% gradient Bis-Tris gel and separated by SDS-PAGE. Proteins were transferred to a PVDF membrane and blotted with an antibody against Stt7 (top). A Coomassie stained gel is shown as loading control (bottom).

It is surprising to observe two clearly distinct bands in the WT sample. Although the experiment has to be reproduced to confirm these results, it suggests that there may be two forms of Stt7 in the thylakoid membrane. These may correspond to the products of the two alternative transcripts discussed above, to two forms of Stt7 with different phosphorylation states, or a combination of these features. Even more surprising is the fact that only one band is visible in the Δ*petD* strain, and that it appears at an intermediate molecular weight from the two bands of the WT sample. This suggests that the accumulation of the cyt b_6f complex may affect the accumulation of the Stt7 kinase at the transcriptional or translational level. Furthermore, this result may provide new grounds for understanding the heterogeneous phosphorylation of LHCII proteins and their different dependencies on cyt b_6f accumulation (Figure III.8B). As shown previously, only LHCII P13 and P17 phosphorylation follows closely the redox- and b_6f/Stt7-dependent pattern of state transitions. As proposed in (Wollman and Lemaire 1988):

> *The distinct phosphorylation characteristics of these two families of LHC subunits demonstrates a b_6f-complex-dependent heterogeneity within LHC for the kinase system. This heterogeneity could involve two LHC-kinases with different specificities* […]. *Alternatively, it could result from a conformational change between two states of the LHC or from two different locations of the complex in the membrane. In these hypotheses, the phosphorylation sites on polypeptides 13 and 17 would be accessible to the kinase only upon an association between LHC and b_6f complexes.*

From the blot of Stt7 accumulation (Figure III.15), we can suggest that these "*two LHC-kinases with different specificities*" may actually be two forms of Stt7, and further that these two forms could originate from alternative splicing of the *STT7* mRNA transcript. One version would be closely associated with cyt b_6f and part of the redox- and cyt b_6f-dependent pathway that phosphorylates the state-transition-specific peptides P13 and P17. The other would be free of b_6f- and redox-control and involved in other phosphorylating activities. If the residual band in the Δ*petD* mutant is indeed this second, b_6f-independent form of Stt7, there is yet no telling why it appears at a different molecular weight than either of the two bands present in the WT. The authors go further and suggest that "*different locations of the* [b_6f] *complex in the membrane*" could also account for the heterogeneity of LHCII phosphorylation, and that only kinases associated with cyt b_6f in close contact to P13 and P17 can lead to their phosphorylation. The discussion in (Dumas et al. 2016) on the importance of quinone microdomains and cyt b_6f working modes for the regulation of state transitions and cyclic electron flow should support this hypothesis: only cyt b_6f in close contact with PSII, *i.e.* in the grana region of thylakoids where the reducing pressure on the PQ pool is high, can lead to P13 and P17 phosphorylation.

The redox state of the PQ pool in these regions, and these regions only, promotes b_6f-mediated activation of Stt7. The authors propose that

> […] *kinase activation could depend on the redox state of an electron carrier, other than the plastoquinones, but associated with the b_6f complex. Our experiments showed that neither plastocyanin nor the Rieske protein was part of the regulation process. However the redox carrier, G, which interacts with the b_6f complex [35] as well as the two b cytochromes, b_H and b_L, become reduced upon the aerobic to anaerobic transitions in darkness used in the present study. The midpoint potential of G and b_H is at about 0 mV [35,36], which is consistent with the titration of kinase activation performed by Horton et al. [37]. In addition, changes in the redox state of these components may still occur via the Q_c site upon illumination of higher plant chloroplasts in the presence of DBMIB, an experiment which has been taken as indicative of the involvement of the PQ pool in the activation process [1].*

In the last chapter, we shall explore why we have reasons to believe that this redox carrier G, *i.e.* heme c_i, is a key player in the activation of Stt7. To conclude this last section, all these elements, although still tentative, suggest that many conditions need to be met to enable state transitions, and that they act as security valves on the "state transition activity" of Stt7.

C. Concluding remarks

In this work, we used a structure-function approach to identify key regions of the cyt b_6f complex that could be involved in the mechanism of state transitions, either as part of a direct interaction with the state transition kinase Stt7 or involved in the redox signal transduction for its activation. The strategy chosen was to create random mutants of the peripheral region of subunit IV (coded by *petD* gene), containing helices F and G. By error-prone PCR, the region going from the PEWY motif to the C-terminal of suIV was randomly mutated and mutants were screened specifically for their ability to perform state transitions. Comparison of state transition phenotypes with sequencing data of the cyt b_6f variants revealed that mutations impairing state transitions concentrated in the stromal loop connecting helices F and G. Key residues inside that loop were targeted for directed mutagenesis in order to confirm or disprove the results obtained from the random mutants. Modification of residues Asn122, Tyr124 and Arg125 produced mutants that are blocked in State I independently of the redox state of the PQ pool and with no adverse effect on cyt b_6f assembly and electron transfer activity. Upon a switch from oxidizing to reducing conditions, these mutants showed (i) no quenching of PSII fluorescence emission associated with state transitions, (ii) no modification of the relative antenna sizes of PSII and PSI, and (iii) very low levels of phosphorylation of LHCII antenna proteins. *In vitro* cross-linking experiments with the purified Stt7 kinase domain and cyt b_6f complex, as well as yeast-two hybrid assays, suggest that subunit IV interacts with Stt7, and *in vitro* reconstitution assays with ATP show that the cyt b_6f induces Stt7 autophosphorylation and that Arg125 is involved in this process.

This work reports the first point mutations of the cyt b_6f that specifically impair state transitions without affecting the electron transfer function of the complex. It is the first function for an acclimation mechanism of the photosynthetic apparatus to be assigned to a peripheral structure of the cyt b_6f complex. Moreover, it is the first body of results that implicates a stromal region of the cyt b_6f in state transitions, which depend on a kinase whose catalytic domain resides in the stroma.

Our reverse-genetics method proved to be very efficient for the study of the complex interplay between two transmembrane proteins. Two main aspects of our experimental setup can account for this efficiency. First, using an acetate-requiring deletion strain and selecting on the recovery of phototrophy circumvented the use of an antibiotic resistance cassette. Second, both the

selection and screening procedures relied on functional criteria that were compatible: non-phototrophic mutants were discarded and therefore did not appear as "false positives" in the state transition screen, and state transition mutants were not selected against since impairing this function does not affect phototrophic growth.

Our results are compatible with previous studies that showed that the lumenal domains of cyt b_6f are also involved in the interaction with the kinase. What we show is an additional level of complexity in its activation, which may depend entirely on the stromal mechanism that we have unveiled. In the next chapter, we will present additional findings and ideas that complement these results and propose a model for the cyt b_6f-mediated activation of the Stt7 kinase.

CHAPTER IV – Elucidating the mechanism

The goal of this final chapter is to present all additional data that can help elucidate the mechanism of interaction and signal transduction between the stromal domains of the cyt b_6f and the Stt7 kinase. A brief summary of the results presented in previous sections will first be provided as context. The second part will be devoted to the analysis of a collection of rather disparate results, most of which contribute to the construction of an interaction and activation model, which will be presented in the third and last section.

The random mutagenesis of subunit IV enabled us to locate a state transition hotspot located on the stromal fg loop. Characterization of single mutants in this region revealed that modifying residues Asn122, Tyr124 or Arg125 specifically impaired state transitions without having any effect on the electron transfer function of the complex or the phototrophic ability of the strains. Tyr124 and Arg125 were shown to be involved in the interaction with Stt7 by double-hybrid, and a role of Arg125 in Stt7 activation through autophosphorylation was evidenced. This is the first function reported for a stromal region of the cyt b_6f, and the first evidence that kinase activation depends on its docking to the stromal side of the complex. Hypotheses of a transmembrane signal transduction originating from PQH_2 binding to the Q_o site and leading to kinase activation have to be revised in light of these new results. Although the exact mechanism of activation is not known, a model will be proposed based on these results and the ones presented in this chapter.

As mentioned in the previous chapter, the electron density map of cyt b_6f complex from *C. reinhardtii* shows that the guanidinium cation of $Arg125^{suIV}$ forms a salt bridge with the carboxylate anion of the cyt b_6 C-terminal leucine. Only a few residues away from this leucine along the cyt b_6 C-terminal strand lies the Q_i site and the conserved Arg207 residue that interacts with heme c_i. Because the results of the spectroscopic characterization of heme c_i suggested a certain degree of structural heterogeneity of the Q_i site (Alric et al. 2005), we proposed the following hypothesis: conformational changes of the Q_i pocket and Arg207 interaction with heme c_i, induced by changes in the heme's redox state, protonation or quinone binding, may modify the $C\text{-}ter^{b6}$– $Arg125^{suIV}$ interaction and induce kinase activation. The main tenet of this hypothesis is that the $C\text{-}ter^{b6}$– $Arg125^{suIV}$ salt-bridge has a functional role. Here, we will first

present analyses and experiments carried out to test this tenet, and then provide further results that participate in the building of an interaction and activation model.

A. Preliminary clues…

1. … from phylogenetics

As discussed in the Introduction, there is a strong correlation in Rieske/cyt *b* complexes between the presence of heme c_i and the split conformation of the core cyt *b* subunit into cyt b_6 and subunit IV. The model of kinase activation proposed here requires both of these structural features, since the putative regulatory C-ter^{b6}– Arg125^{suIV} interaction is only realized if a carboxyl group is available in the vicinity of the Arg125 side chain, *i.e.* in the split conformation. It further depends on the presence of a basic side chain at position 125 of subunit IV, so that another factor can be added to the correlation analysis of the two structural features mentioned above (Table IV.1, kindly communicated by Frauke Baymann).

Table IV.1. Correlation between three structural features of Rieske/cyt *b* complexes.

Phylum		Split cyt *b*	Heme c_i	Position 125$^{suIV/b}$
Chloroplasts		+	+	R
Cyanobacteria		+	+	R
Heliobacteria		+	+	K
Bacili		+	+	K/R
Nitrospiraceae		+/-	+/-	R/K
Planctomycetes		+/-	+/-	R/K/N/W
Chlorobiaceae		+	-	K/E
Haloarchaea		+/-	-	R/A
Acidobacteria		-	-	R/E/Q
Thermus/Deinococcus		-	-	E
Aquificales		-	-	R/H
Actinobacteria		-	-	D/Q/E
Proteobacteria	*g-*	-	-	Y/T
	e-	-	-	K/R/E
	d-	-	-	A/R/D/K
	b-	-	-	Y
	a-	-	-	Y/F/S
Mitochondria		-	-	F
Crenarachaeota		-	-	K/R/E/D/S/M/N
Euryarchaeota		-	-	D/E

Whereas a wide variety of amino acids are found at position 125 in organisms that possess an unsplit cyt *b* subunit and/or no heme c_i, strictly basic residues arginine or lysine are found in those that possess both of these features. Without drawing hasty or deterministic conclusions, let us simply say that the correlation between the split conformation and the presence of heme c_i may be further extended to the type of residue found at position 125. Of course, the (Stt7- and LHCII-dependent) mechanism of state transitions considered here is shared only by organisms of the green lineage, whereas the split/c_i/R-K^{125} configuration was already present in some more ancient organisms. However, it is not unreasonable to suggest that a given sequence and structure can be recruited for a new function in a given organism even if its closest ancestor did not share this function. After the split of the ancestral cyt *b*, subunit IV and cyt b_6 may have evolved new structural features and functions in relation to state transitions.

2. *... and from a structure-function analogy with hemoglobin*

An analogy to the electrostatic interaction between the C-terminal carboxyl of cyt b_6 subunit and Arg125 of subunit IV can be found in the $\alpha_1\alpha_2\beta_1\beta_2$ complex of horse hemoglobin where the terminal carboxyl of the β subunits interact with the amino group of Lys40 in the α subunits (Perutz 1970) (Figure IV.1). Interestingly, a hydrogen bond is formed between these groups only in deoxyhemoglobin, which represents the "Tense" (T) form of the protein. When oxygen is bound to the heme iron (oxyhemoglobin), the protein is in its "Relaxed" (R) form and the C-terminal residues of all four chains have complete freedom of movement. These subunits interactions and structural changes account for the cooperative effect of oxygen binding observed in hemoglobin, which differentiates it from myoglobin. Reciprocally, the presence of a sixth axial ligand on the heme iron, an oxygen molecule in hemoglobin, induces the breakage of the salt bridges between subunits $\alpha_1\beta_2$ and $\alpha_2\beta_1$.

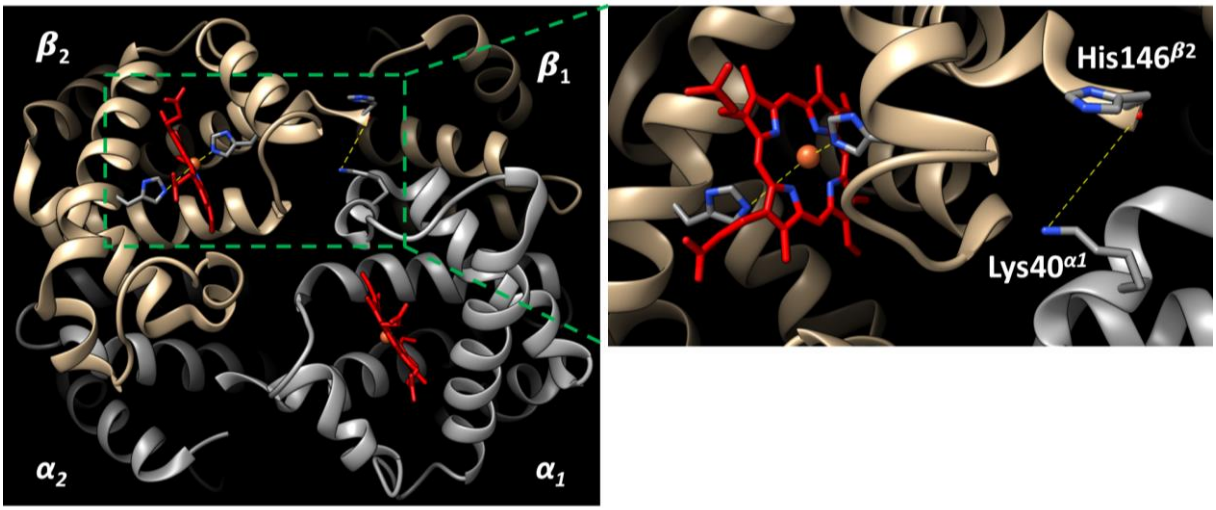

Figure IV.1. Structure of horse deoxyhemoglobin.
Atomic coordinates are from PDB 2DHB (Bolton and Perutz 1970). The inset zooms on the salt bridge formed between Lys40$^{\alpha 1}$ and the α-carboxyl of His146$^{\beta 2}$ that is central to the molecular mechanisms of hemoglobin.

It is not unlikely that similar ligand-induced conformational changes could take place in the cyt b_6f complex. The Q_i site can accommodate quinone analogs such as NQNO, or carbon monoxide (CO), to coordinate the iron of the *c*'-type heme c_i, thereby reshaping its electronic properties (Alric et al. 2005; Baymann et al. 2007; Yamashita et al. 2007). When comparing *in vivo* (Lavergne 1983a) to *in vitro* data (Alric et al. 2005), the difference observed in the equilibrium constant between heme b_H and heme c_i suggested that some kind of structural rearrangements may occur at the Q_i site or at the stromal side of the complex. Different conformations of the protein complex may be stabilized depending on experimental conditions. When the complex is embedded in the membrane and when an electrochemical proton gradient is present, the complex may be stabilized in one conformation, whereas when cyt b_6f is purified and crystalized, another slightly different state of the protein may be favored. Perhaps the most convincing indication for an equilibrium between two Q_i site conformations comes from the finding that c_i titrates in two waves in the presence of NQNO (Alric et al. 2005). The relative amplitude of these two waves is pH-dependent, suggesting that the protonation state of the complex would control the differential affinity of NQNO for the reduced/oxidized forms of c_i.

Structure-function studies of a hemoglobin variant ("*Kariya*") bearing a Lys40Glu substitution showed that the constitutive absence of a salt-bridge at the C-ter$^{\beta}$ increased hemoglobin's affinity for oxygen and decreased its cooperativity for oxygen binding (Harano et al. 1983; Imai et al. 1989). This mutation seemed to stabilize the R state that resembled the oxyhemoglobin form, in accordance with the original model proposed by (Perutz 1970). We wanted to put our

structural analogy between hemoglobin and the cyt b_6f to the test by studying the effects of breaking the C-ter^{b6}– Arg125^{suIV} salt-bridge on heme c_i's spectroscopic features. For this, we measured the EPR spectrum of the high-spin heme c_i in the Arg125Glu mutant.

B. EPR spectral analysis of heme c_i

High-spin hemes in their oxidized form display an EPR signal at $g = 6$ that can be used to describe the heme's symmetry. In turn, the symmetry of the heme can gives clues on its coordination by ligands and on the conformation of its protein environment. Increasing structural constraint around a heme favors a departure from a tetragonal symmetry toward a rhombic symmetry (Figure IV.2A) (Peisach et al. 1971).

We measured the EPR absorption derivative spectra of the high spin ferric heme c_i from thylakoid membranes of the WT and mutant strains (Figure IV.2B). EPR spectra of WT and mutant strains showed signals in the $g = 6$ region, typical of spin-5/2 species. In the WT, the spectrum of heme c_i was identical to the one reported in (Baymann et al. 2007), corresponding to a lowly (~ 3.2 %) rhombic species with $g_x \sim 6$ and $g_y \sim 5.5$. While the EPR spectrum of the Tyr124Lys mutant resembled that of the WT, the signal corresponding to heme c_i in the Arg125Glu mutant showed a decreased amplitude and a composite g_x/g_y signal. This resembled an axial species with a tetragonal coordination of the heme iron, suggesting a lower structural constraint in the vicinity of heme c_i in mutant Arg125Glu.

The EPR spectrum of heme c_i in mutant Arg125Glu differed from the WT, when that of mutant Tyr124Lys was very similar to the WT. Previous EPR studies have shown that heme c_i is in strong magnetic dipolar coupling with the neighboring heme b_H, and that its EPR signal around $g = 6$ was further distorted by structural heterogeneity of the Q_i site (Baymann et al. 2007). Here we propose that the loss of the C-ter^{b6}– Arg125^{suIV} salt-bridge in mutant Arg125Glu may be a possible source for the decreased structural constraint around heme c_i. In turn, a functional and dynamic C-ter^{b6}– Arg125^{suIV} interaction may allow the stromal fg loop to respond to local Q_i site conformational changes induced by variations in the occupancy of this site and in the redox state of the cofactors of the low-potential chain. We suggest that this mechanism may participate in the redox signal transduction for the activation of Stt7.

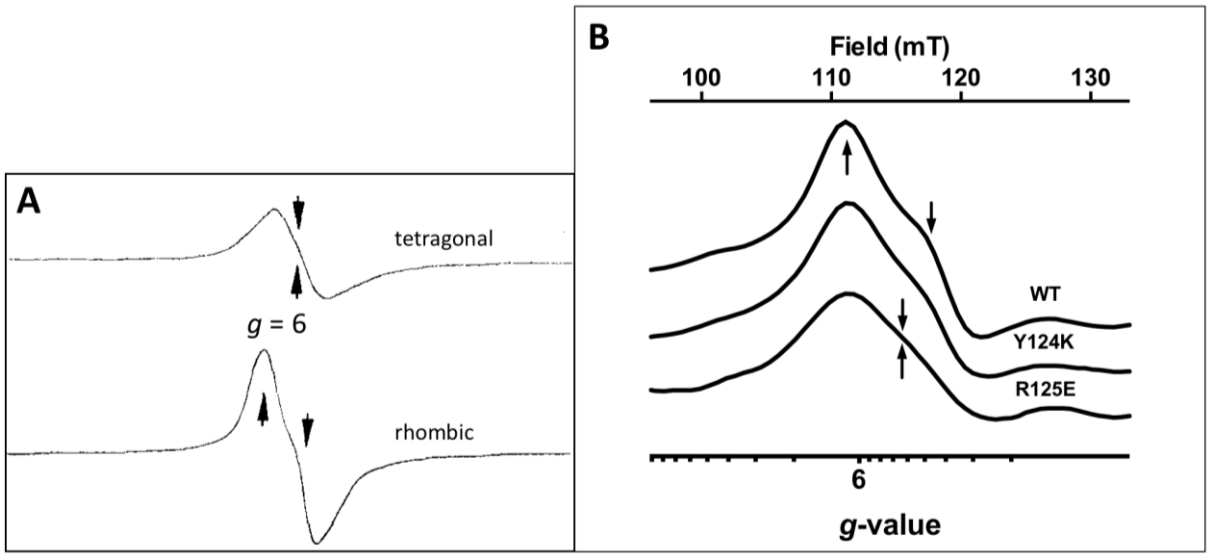

Figure IV.2. EPR spectral analysis of high-spin hemes in the region near $g = 6$.
(A) EPR absorption derivative spectra of ferrihemoglobin cyanate (top) and ferrihemoglobin thiocyanate (bottom). From (Peisach et al. 1971). **(B)** EPR absorption derivative spectra of heme c_i in WT and mutant cyt b_6f complexes. Upward and downward arrows indicate the positions at which the g_x and g_y signals were measured respectively.

C. Cyt b_6 C-terminal mutants

The Arg125 residue was shown to be involved in a direct interaction with Stt7 that participates in its activation (Chapter III). As discussed above, the role of its other putative interaction with the C-terminal carboxyl of cyt b_6 subunit was assessed by measuring the EPR spectrum of the Arg125Glu mutant where this interaction is lost. This method yielded encouraging results but was somewhat indirect since it rested on the double assumption that breaking this salt bridge would have an allosteric effect on the conformation of the Q_i pocket and that this structural rearrangement would modify heme c_i's spectral properties. In order to figure out the functional role of this interaction *in vivo*, we built mutants of the cyt b_6 C-terminal, truncating or elongating the terminal tail to either increase or decrease the distance between the carboxylate moiety and the Arg125 guanidinium group (Figure IV.3A). A mutant carrying an Arg207Lys mutation was also generated in order to test the effect of tweaking slightly this highly conserved residue that interacts with one of the propionate groups of heme c_i. *C. reinhardtii* mutants were obtained by directed mutagenesis and chloroplast transformation of a Δ*petB* strain with pWBA plasmids carrying an *aadA* resistance cassette and various mutated versions of the *petB* gene. Transformants were selected on TAP medium supplemented with spectinomycin and sequenced to verify the presence of the mutated *petB* genes. These mutants did not accumulate

the cyt b_6 subunit (Figure IV.3B) and did not grow in photoautotrophic conditions. As a control, we successfully complemented two different Δ*petB* strains with the pWBA plasmid carrying the WT *petB* gene. We concluded that the cyt b_6 C-terminal mutations specifically impeded cyt b_6 subunit accumulation and, coincidentally, cyt b_6f assembly and function.

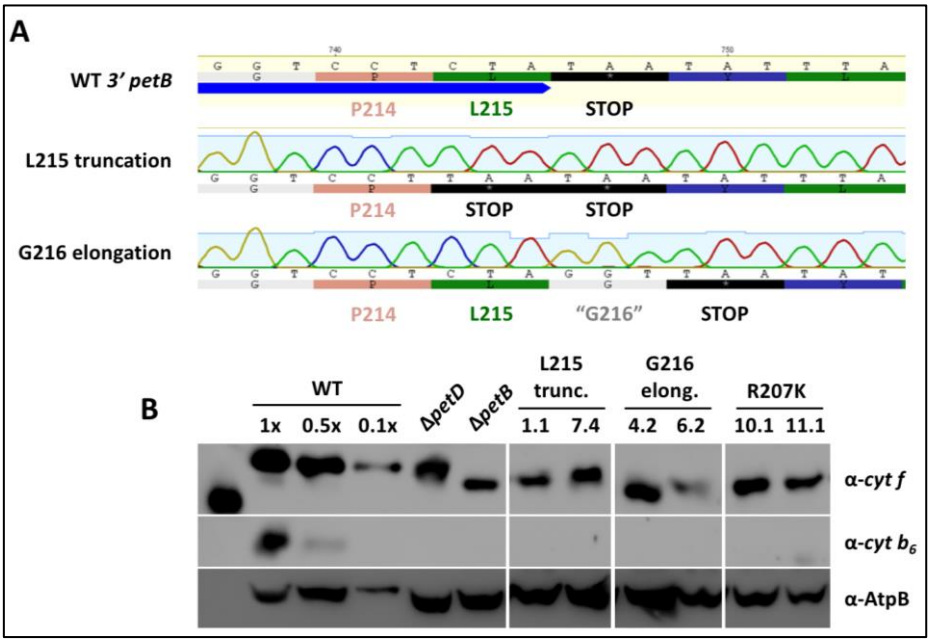

Figure IV.3. Attempt to obtain *petB* C-terminal mutants by complementing the Δ*petB* strain. **(A)** Representation of the *petB* C-terminal truncation and elongation sequences obtained by site-directed mutagenesis. **(B)** Western-Blot analysis of the accumulation of the cyt *f* and cyt b_6 subunits in the WT, Δ*petD*, Δ*petB* and *petB* C-terminal mutant strains.

The FtsH protease was shown to be involved in cyt b_6f quality control and in the degradation of misassembled complexes (Malnoe et al. 2014). We made use of the *ftsh1-1* mutant (*ftsH1-R420C*, kindly provided by Catherine de Vitry, IBPC) that displays impaired unfoldase and protease activities (Malnoe et al. 2014) to circumvent this accumulation defect. The *ftsh1-1* strain (containing the WT *petB* gene) was transformed with the pWBA plasmids carrying mutations on *petB* and transformants were selected on TAP medium containing spectinomycin. Transformants were sub-cloned on TAP-spectinomycin medium several times in order to replace every *petB* copy with its mutated version and reach homoplasmy (not checked at this point). Figure IV.4 shows the preliminary characterization of these *petB* mutants in the *ftsh1-1* genetic background. The *ftsh1-1* strain was also transformed with the WT *petB* gene to generate a control strain (*ftsh1-1*:*petB*–WT). All strains grew on minimal medium in low light (20 $\mu mol_{photons}.m^{-2}\ s^{-1}$) and 2% CO_2, attesting that their electron transfer chain was functional and that they were able to fix CO_2. However, the *ftsh1-1*:*petB*–xL215 (Leu215 truncation, denoted xL215) and *ftsh1-1*:*petB*–G216 (Gly216 elongation, denoted G216) strains, but not the *ftsh1-1*:*petB*–R027K strain (denoted R207K), grew more slowly and showed signs of photosensitivity when transferred to 50 $\mu mol_{photons}.m^{-2}\ s^{-1}$ and atmospheric-level CO_2 (data not shown). In all

strains, the maximum quantum efficiency of PSII (F_v/F_m) was similar to the WT. The xL215 and G216 strains, but not the R207K strain, showed lower photochemical quenching of chlorophyll fluorescence (q_P parameter) than the WT strain when grown on acetate. This difference was less pronounced for cells grown on minimal medium. Interestingly, the *ftsh1-1*:*petB*–WT strain seemed to have slightly slower kinetics of chlorophyll fluorescence quenching associated with state transitions (q_T parameter) than the WT. This suggests that the increased protein content in the thylakoid membrane, due to the lack of protease activity in this strain, may slow the migration of LHCII proteins from PSII to PSI. The xL215 and G216 strains exhibited q_T values similar to that of the *stt7-1* strain, suggesting that the state transition mechanism was impaired in these strains. The false color image rendition of the q_T parameter of the R207K strain grown on minimal medium gave an ambiguous result, with q_T values spanning the entire color map. From the images of cells grown on TAP, however, it seemed that q_T in the R207K strain was lower than in the WT and slightly lower than in the control *ftsh1-1*:*petB*–WT strain.

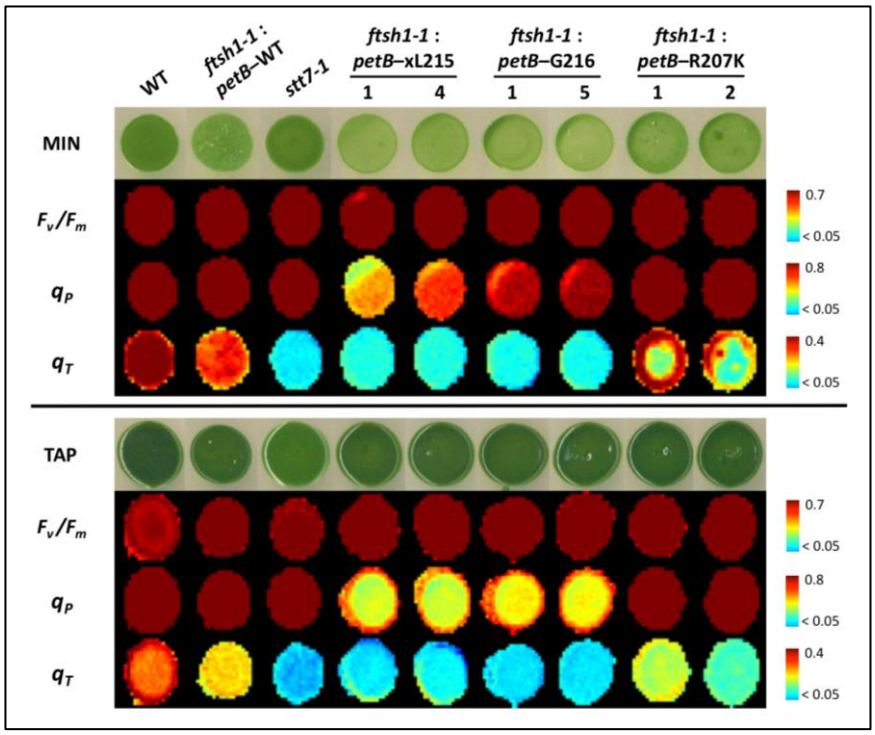

Figure IV.4. Characterization of the *petB* C-terminal mutants obtained in the *ftsh1-1* background.
Growth on minimal (MIN, 20 $\mu mol_{photons}.m^{-2}\ s^{-1}$, 2% CO_2) and acetate (TAP, 10 $\mu mol_{photons}.m^{-2}\ s^{-1}$) media, maximum quantum efficiency of PSII (F_v/F_m = (F_m – F_0)/ F_m), photochemical quenching of chlorophyll fluorescence ($q_P = (F_m - F)/F_m - F_0$)), and q_T component of NPQ measured upon anaerobic adaptation in the dark ($q_T = (F_m - F_m')/F_m'$) of the three reference strains (WT, *ftsh1-1*:*petB*–WT, *stt7-1*) and the three *petB* mutants (two clones each). False color images and fluorescence parameters were calculated from chlorophyll fluorescence measurements of cells grown on MIN (top panel) or on TAP (bottom panel).

In order to go further, these preliminary results need to be confirmed and various controls need to be obtained. In particular, the homoplasmic state of the *petB* locus needs to be verified and the accumulation of the cyt b_6 subunit needs to be assessed. However, added to the characterization of the Arg125Glu^{suIV} mutant, these results confirm that the C-terminal stromal strand of the cyt b_6 subunit and its interaction with Arg125^{suIV} are key determinants in the mechanism of activation of Stt7. Based on the previous EPR results with the Arg125Glu mutant, the modification of this interaction in mutants xL215 and G216 may induce conformational changes at the Q_i site and affect electron transfer toward quinones. This would explain the lower q_P in the cyt b_6 C-terminal mutants.

The goal of truncating or elongating the cyt b_6 C-terminal also came with the idea of stabilizing two distinct states: respectively, one where Arg125 would no longer be able to interact with the cyt b_6 terminal carboxyl and would stay in its "Stt7-activating conformation" (constitutive State II), and another where Arg125 would remain linked to the cyt b_6 terminal carboxyl and would not be able to switch to its activating conformation (constitutive State I). The truncation and elongation of the C-terminal^{b6} did not generate mutants with distinct properties but instead seemed to have the same effect on state transitions. This raises several points. First, unless a 3D structure is obtained, one can never know the exact structural changes induced by the modification, addition or subtraction of an amino acid. The theoretical idea behind the truncation or elongation may still be valid even though the new protein products obtained by mutagenesis did not produce the expected results. Second, the similarity between the truncation and elongation mutants suggests that other structural features, some which we know of, are involved in the activation of Stt7. Third, it indicates that any disturbance of the interaction between the C-terminal carboxyl and the Arg125 guanidinium group impairs the signal transduction for the activation of Stt7. This implies that these chemical groups interact in a highly dynamic manner and that this interaction is fine-tuned by various redox cues. It remains to be explored whether these cues originate from heme c_i and the Q_i pocket.

D. Structural analysis of the subunit IV fg loop and its environment

Several structural details of the cyt b_6f gain new significance in light of the results presented in Chapter III, and can help discriminate between mutations affecting mainly the interaction/docking of the kinase from mutations that also block the signal transduction from the cyt b_6f to Stt7. The Arg125Glu substitution may cause a strong impairment in state transitions because it modifies the docking site of the Stt7 stromal domain on the cyt b_6f. However, it is likely that the interaction between these two transmembrane proteins relies on many other residues. Therefore, in light of the results presented so far in this chapter, it is tempting to suggest that the Arg125Glu substitution impairs state transitions by abolishing the dynamic C-ter^{b6}– Arg125^{suIV} interaction that responds to structural rearrangements at the Q_i site and transduces the activation signal. In the case of Arg125, these two scenarios are not mutually exclusive. That is not the case for substitutions of the Asn122 residue. Its side chain extends toward the interior of the complex and should not play a direct role in the proper docking of Stt7. Yet, mutants with a substitution of Asn122 show a defect in state transitions but seem to conserve a low level of Stt7 activation as seen by their very low LHCII phosphorylation levels in reducing conditions (Figure 3 of PNAS article). Structural analysis shows that the Asn122 side chain is positioned right beneath the space where the salt bridge would be formed between Arg125^{suIV} and C-ter^{b6} (Figure IV.5). This suggests that substituting Asn122 may affect this interaction, without completely preventing it, and therefore produce a mimic of the Arg125Glu phenotype. This is further evidence of the crucial role of the C-ter^{b6}– Arg125^{suIV} interaction.

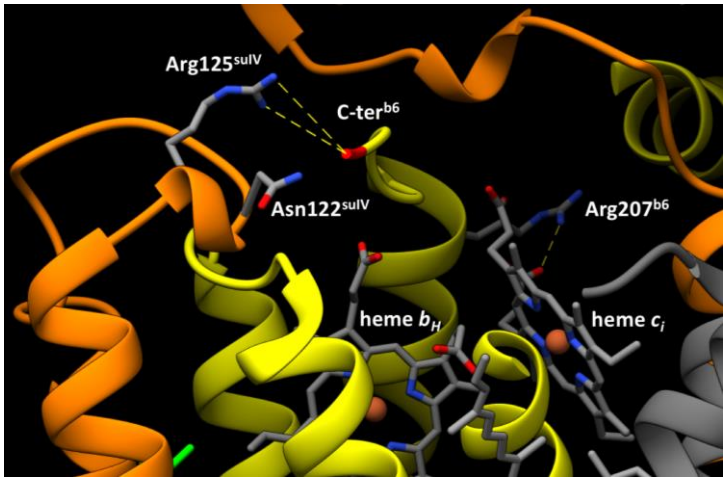

Figure IV.5. View of the relative positions of Asn122^{suIV} and the Arg125^{suIV}–COOH^{b6} salt-bridge.
Subunit IV is in orange, cyt b_6 subunit is in yellow. The Arg207^{b6} in interaction with a heme c_i propionate is visible in the background. The PetG subunit ribbon structure was removed for the sake of clarity.

Replacement of the Tyr124 residue by an amino acid with a long, basic side-chain such as that of lysine produced a strong state transition phenotype. However, mutation of the tyrosine to phenylalanine, another hydrophobic and aromatic residue, did not lead to any impairment of state transitions. In the structure, the tyrosine side chain is surrounded by three other aromatic PetG residues, Phe22, Tyr26 and Tyr29 (Figure IV.6A). Furthermore, the stromal extremity of the Stt7 transmembrane domain in *C. reinhardtii* contains two tyrosine residues and aromaticity is conserved at (at least one of) these positions in organisms of the green lineage (Figure IV.6B). It is tempting to propose that these residues (or other peripheral aromatic residues of the Stt7 stromal domain, see *Surface analyses* section below) form π-π stacking interactions with the aromatic pocket formed by subunit IV and PetG, and that they are important for Stt7 docking to this stromal region of cyt b_6f [†]. The Tyr124Lys substitution would impede proper docking of the kinase without completely abolishing its activation, as seen by the low but nevertheless visible LHCII phosphorylation in the corresponding mutant (Figure 3 of PNAS article). This is in line with the impaired state transition phenotypes of the subunit IV-PetL fusion mutant (Zito et al. 2002) and the Ile131Asp mutant (this study) that both suggest that modifying the steric environment of helix G impedes Stt7 binding. In this model, the transmembrane domain of Stt7 would dock along helix G of subunit IV on the side that is facing PetG and not helix F and Chl *a*.

[†] Aromatic residues can also form π-cation interactions with arginine and lysine side chains due to the negative electrostatic potential of their ring surface (Dougherty 2007); however, it is unlikely that positively charged lysines or arginines of Stt7 could interact with the cyt b_6f aromatic pocket described here since it is inside the membrane phase.

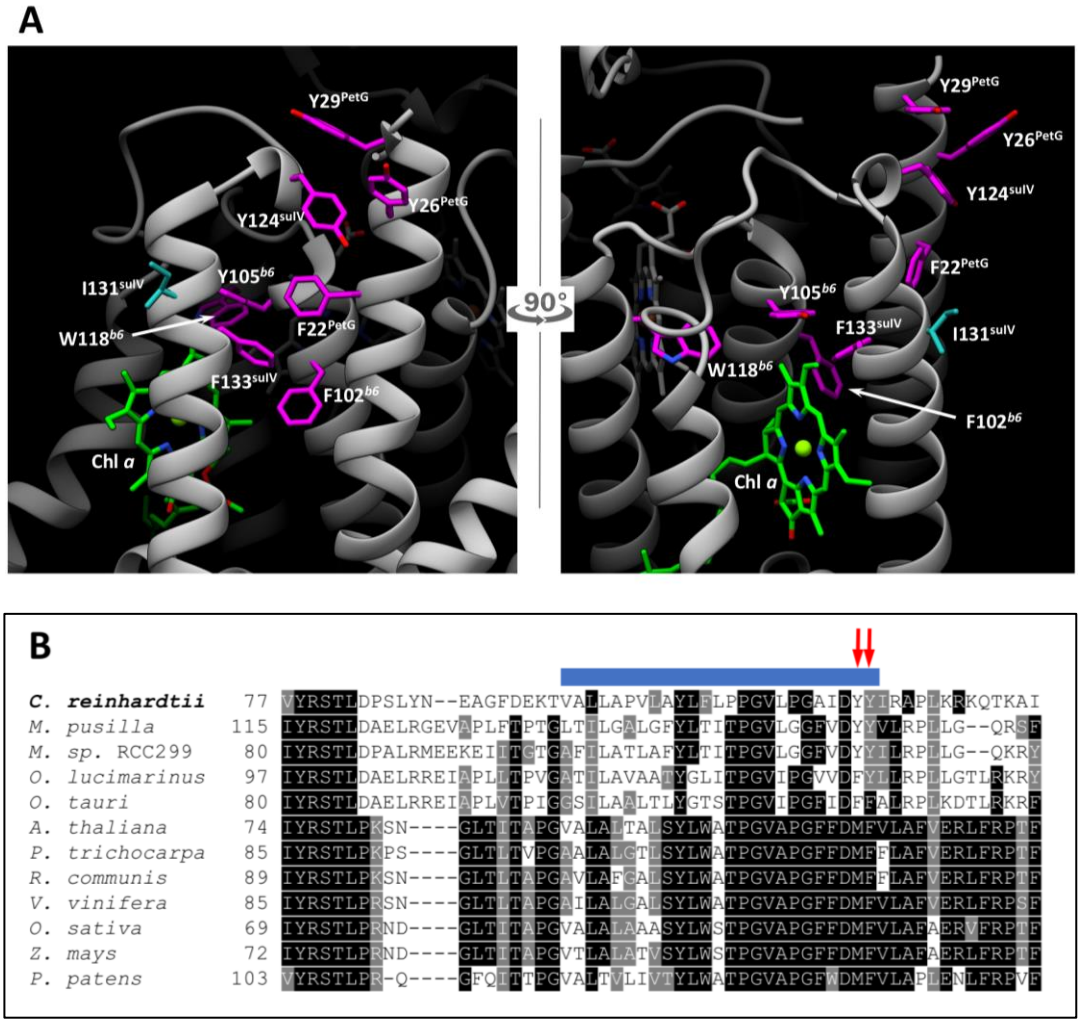

Figure IV.6. Putative aromatic interactions between stromal regions of cyt b_6f and Stt7.
(A) Structural views of the various cyt b_6f residues (magenta) forming an "aromatic pocket" or "network" that extends toward the Chl *a* molecule (green). The Ile131 side chain of subunit IV is shown in cyan. **(B)** Protein sequence alignment of *C. reinhardtii* Stt7 and its homologs in other organisms of the green lineage. Sequences were aligned with ClustalW and Boxshade. *M. pusilla* corresponds to EEH58062, *Micromonas* sp. RCC299 to XP_002499717, *O. lucimarinus* to XP_001420129, *O. tauri* to CAL56118, *A. thaliana* to STN7, *P. trichocarpa* to XP_002312380, *R. communis* to XP_002524406, *V. vinifera* to XP_002281563, *O. sativa* to NP_001056233, *Z. mays* to NP_001148075 and *P. patens* to XP_001773197. The transmembrane domain is marked by a blue box and the two conserved aromatic positions are marked by red arrows. (Adapted from https://static-content.springer.com/esm/art%3A10.1007%2Fs11120-010-9538-8/MediaObjects/11120_2010_9538_MOESM1_ESM.doc).

E. Surface analyses

This study provided proofs of a direct interaction between the cyt b_6f stromal region around the fg loop of subunit IV and the stromal kinase domain of Stt7. The acidic Arg125 residue of the fg loop was identified as a central player in this interaction. Further information can be gleaned from the analysis of the binding surfaces on each of the interacting proteins.

1. Surface analysis of the cyt b_6f subunit IV environment

Figure IV.7 shows ribbon and surface representations of the side of the complex where helices F and G of subunit IV reside. The aromatic patch surface described in the previous section is represented in yellow. The rest of the surface is colored by electrostatic potential. It appears clearly that the stromal region around the fg loop forms a surface patch of positively-charged residues (blue surface). The maximal end-to-end distance of this basic patch measured parallel to the predicted plane of the membrane is about 30 Å.

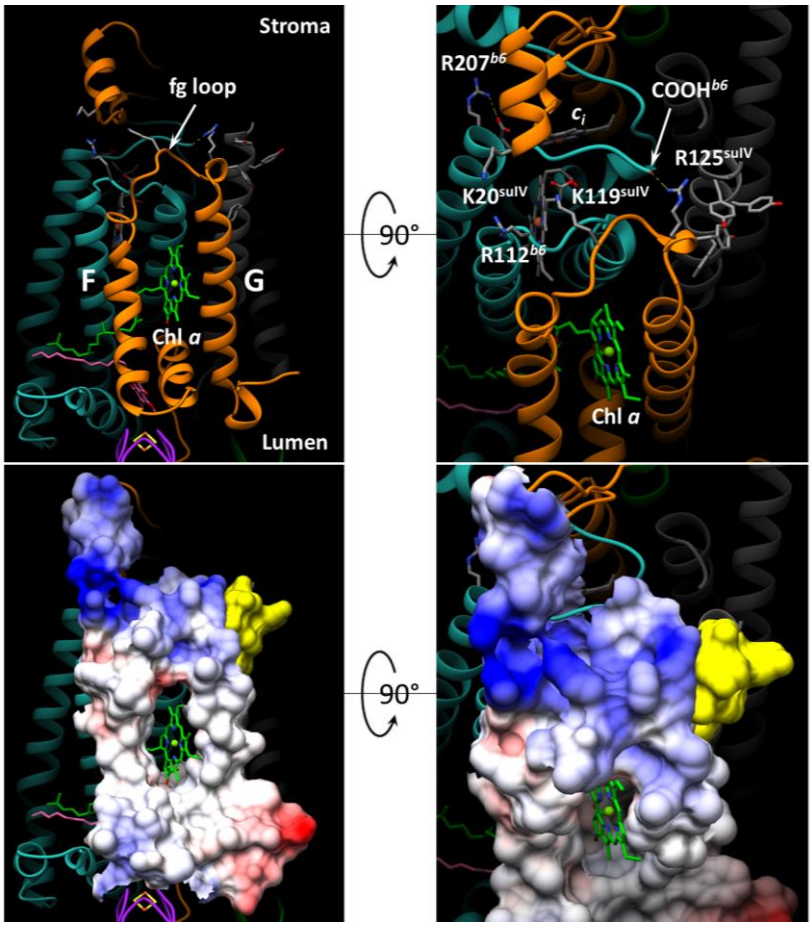

Figure IV.7. Surface analysis of the cyt b_6f stromal region surrounding the subunit IV fg loop.

2. Surface analysis of the Stt7 kinase domain model

The One-to-One threading tool of the Protein Homology/analogY Recognition Engine V 2.0 (PHYRE2, (Kelley et al. 2015)) was used to model the structure of the kinase domain of Stt7 based on the resolved structure of the kinase domain of its homolog in *Micromonas sp.* RCC299 (MsStt7d-KD, PDB 4IX6, (Guo et al. 2013)). The MsStt7d kinase domain shares 47% sequence similarity with the corresponding region of Stt7 of *C. reinhardtii* (referred to as Stt7-KD). Figure IV.8 shows the model of the structure obtained at >90% confidence, corresponding to the entire kinase domain of Stt7 (residues Val140 to Thr483). Region A (red) corresponds to the N-lobe of the kinase domain, while regions B (blue) and C (orange) make up the C-lobe. Region D (purple) was not included in the structural model. The N- and C-lobes are joined by a 6-residue hinge (grey). Important kinase catalytic motifs, DLG and HRD, as well as the α5-hairpin structure shared only by members of the Stt7/STN7 family (Guo et al. 2013), are colored in green. The activation loop extends from the DLG motif to the α5-hairpin. The coordinates of the bound ATP molecule are from PDB 4IX6, matched onto the model of Stt7-KD. All the major conserved kinase folds, motifs and residues (β-strand N-lobe, α-helix C-lobe, inter-lobe hinge, glycine-rich loop or P-loop, HRD, DLG, etc.) of the resulting model match well with other structures of kinase domains. Exceptions are the activation loop, whose variable sequence and conformations account for the specificity of a kinase's substrate recognition and activity, and the α5-hairpin that seems to be specific to the Stt7/STN7 family of kinases.

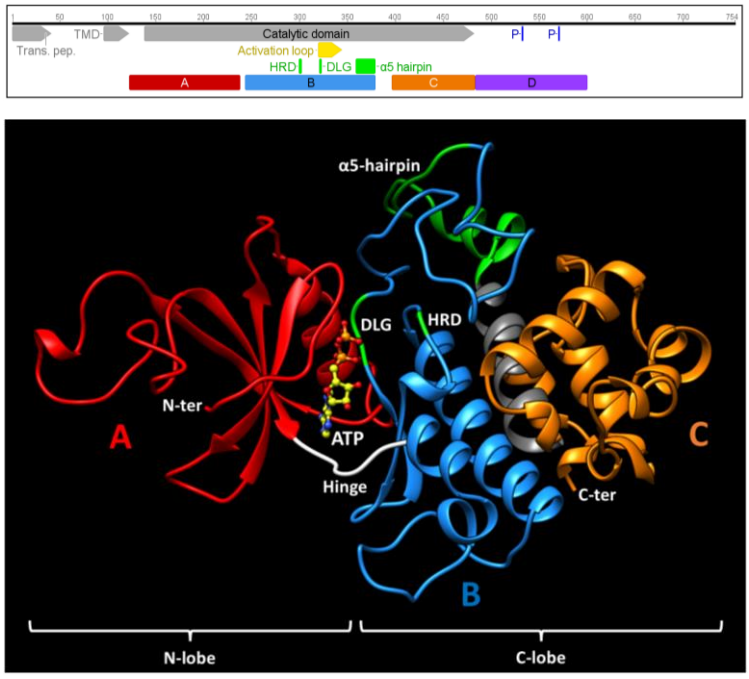

Figure IV.8. Model of the Stt7 kinase domain. See in-text legend.

Results from the yeast two-hybrid experiments (Figure III.13) indicated that the subunit IV fg loop interacted with region B and region AB. The double-substitution [Tyr124Lys;

Arg125Glu]^{suIV} abolished these interactions, showing that one or both of these residues mediate this interaction. As detailed in the previous section on the structural features of the fg loop, we expect the Tyr124^{suIV} residue, and the aromatic patch formed by the surrounding aromatic residues, to provide a docking site for one or more aromatic residues of Stt7, either the transmembrane domain tyrosines (Figure IV.6B) or a peripherally-exposed residue of the A or B regions of the kinase domain. Furthermore, we expect the Arg125^{suIV} residue, and the surrounding positively-charged stromal surface of the cyt b_6f, to interact with acidic residues of Stt7, possibly forming a negatively-charged patch on the surface of the kinase domain. Therefore, an electrostatic surface analysis of Stt7 was performed in order to search for A or B regions that combined both protruding aromatic residues and negatively charged residues.

The view of the 3D-model in Figure IV.8 shows the side of the structure that corresponds to the dimer interface observed in the crystals of MsStt7d-KD. Furthermore, this surface has an overall positive electrostatic potential and does not have any exposed aromatic residues. Therefore, we are not likely to find an interaction between this surface and the stromal region of cyt b_6f. The images of the 3D-model in Figures IV.9A1-2 were obtained by rotating the one in Figure IV.8 by 180° laterally; thus, they show the "opposite face" of the Stt7-KD structural model. Figure IV.9A2 shows a surface representation colored by electrostatic potential, with aromatic residue surfaces colored in yellow. Figures IV.9B1-2 zoom in on the only region of the structure that combines both negatively-charged residues (Glu157, Glu160, Glu161, Glu197, Glu239, Asp241, Glu265, Glu312, Asp314, red surface) and an exposed aromatic residue (Phe262, yellow surface). This region forms a pocket bordered by (mostly acidic) residues from the N-lobe, the C-lobe and the inter-lobe hinge. The maximal end-to-end distance of this acidic patch is about 28 Å. Right "behind" the hinge lies the ATP-binding pocket, which is itself part of the larger substrate-binding cleft formed by the two lobes and the activation loop (visible in the 180° view, Figure IV.8). Figures IV.9C1-2 show a 90° side-view of the hinge pocket. The Phe262 residue and the many exposed negatively-charged residues of the N- and C-lobe that make up the hinge pocket are clearly visible.

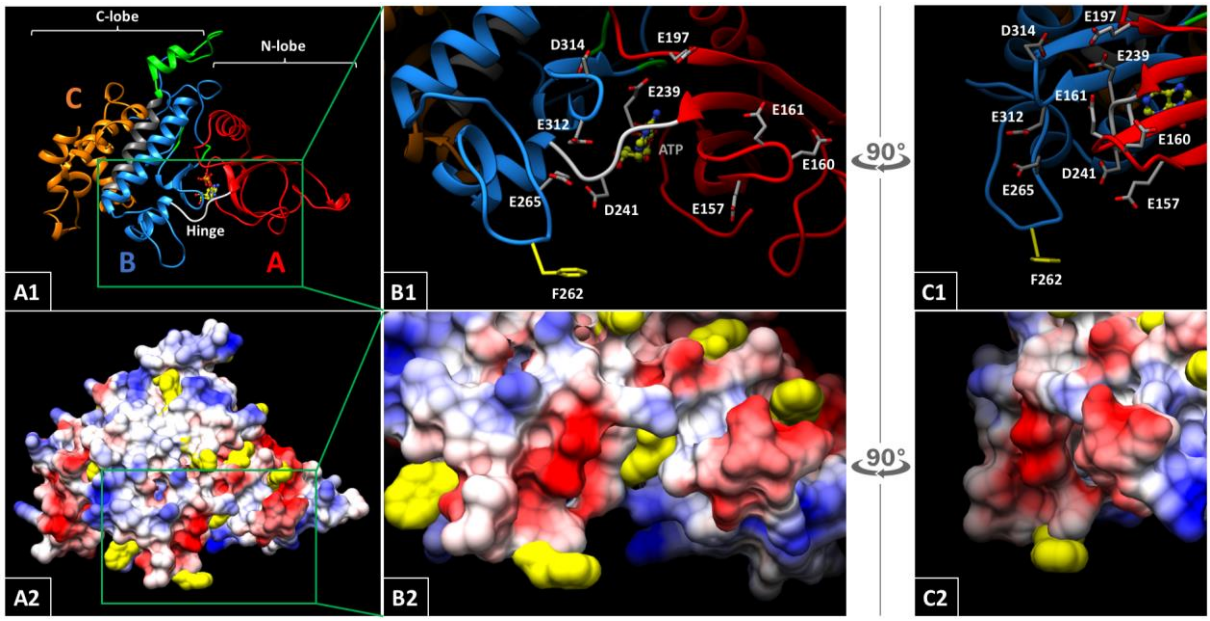

Figure IV.9. Surface analysis of the Stt7-KD model.
See in-text legend.

"Clamshell-like" or "breathing motions" of the two lobes of the kinase domain are known to be crucial for regulating the catalytic activity of many kinases (Cox et al. 1994; Nolen et al. 2004). These motions have allosteric effects that either allow or prevent local conformational changes of the substrate-binding cleft accompanying nucleotide binding and release, such as the "DFG/DLG-flip" (Shan et al. 2009). These allosterically-driven conformational changes (Masterson et al. 2008; Papaleo et al. 2016) are part of the kinase catalytic cycle and regulate ATP-binding and therefore kinase activation by phosphorylation. This phosphorylation can be catalyzed by the kinase's own active site (cis-autophosphorylation), by that of another kinase of the same type (trans-autophosphorylation, often correlated with the dimerization of the two kinase molecules) or by another kinase as part of a phosphorylation cascade (trans-phosphorylation).

Studies have shown that the inter-lobe hinge region, removed from the main catalytic pocket, can participate in the regulation of kinase activity by modulating the movement and relative positions of the two lobes. The GCN2 kinase becomes active only when it interacts with a specific histidyl-tRNA synthetase with bound tRNA; substitutions of two residues in the hinge region of this kinase in *S. cerevisiae* activate the kinase (constitutive ATP-binding and hydrolysis) in the absence of its activating partner (Qiu et al. 2002). This suggests that these residues form an inhibitory structure that rigidifies the hinge region and maintains the two lobes in a conformation that precludes ATP binding, thus keeping the kinase in an inactive

conformation (Padyana et al. 2005). Similar "molecular brakes" have been described in tyrosine kinases ZAP-70 (Deindl et al. 2007) and FGFR2 (Chen et al. 2007). In all these cases, the rigidity of the hinge region is insured by networks of H-bonds formed between charged or polar residues of the hinge motif and the surrounding N- and C-lobe structures (Figure IV.10).

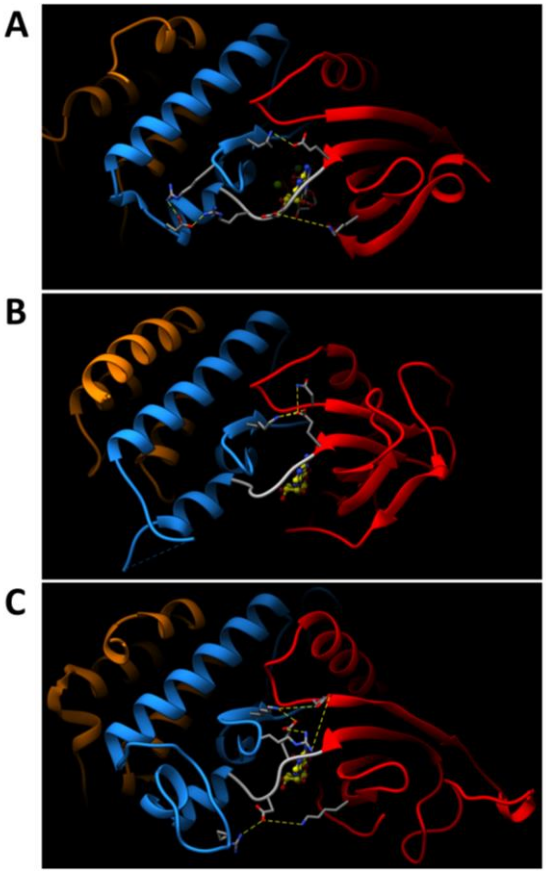

Figure IV.10. Residues of the hinge pocket can from an inhibitory "molecular brake" structure.
(A) GCN2 kinase, PDB 1ZYD (Padyana et al. 2005). **(B)** FGFR2 kinase, PDB 2PSQ (Chen et al. 2007). **(C)** Stt7-KD model, with hinge pocket residues that could form a putative inhibitory structure.

In some cases, the molecular brake function is performed by an interacting partner that binds on the same side as the hinge region and acts as a clamp, hindering the movement of the N- and C-lobes (Sicheri et al. 1997; Xu et al. 1997; Young et al. 2001; Nagar et al. 2003). Molecular dynamics simulation revealed that drastic conformational changes of the hinge region, known as hinge "cracking" (Miyashita et al. 2003), take place when an EGFR kinase interconverts between catalytically active and inactive conformations (Shan et al. 2013). Therefore, regulating the conformation and dynamics of the hinge region is a way to allosterically control catalysis at the substrate-binding cleft on the opposite face of the kinase domain.

Even more compelling evidence of the regulatory function of the hinge region is its role in the docking interaction mechanisms of kinases of the MAP family. The functions of this kinase family are mediated mainly by ERK, JNK et p38 protein kinases (Johnson and Lapadat 2002). They are part of large signaling cascades that regulate many crucial cellular processes such as cell division, apoptosis and differentiation in response to various stimuli (Pearson et al. 2001). The diversity of upstream regulators and downstream effectors/substrates in these MAPK signaling cascades, and the fact that MAPK phosphorylate any substrate containing a minimal consensus sequence (serine/threonine followed by proline), has favored the evolution of selective docking interactions away from the active site that insure the linearity and specificity of their function and maintain structured signaling networks (reviewed in (Mayor et al. 2007; Garai et al. 2012)). In MAP kinases, the docking groove involved in these interactions is located on the C-lobe and formed in part by the hinge region (Figure IV.11A). It interacts with linear docking (D) motifs that are found on various MAPK partners acting as activators, inhibitors or scaffold proteins (Figure IV.11B). The docking interactions induce local changes that can alter the kinase efficiency through allosteric effects at the catalytic site, promote or inhibit its interactions with substrates through phosphorylation, or even auto-inhibit the kinase's activity in the case of intramolecular docking motifs (Figure IV.11C). In the latter case, the kinase can then be activated by the displacement of the intramolecular inhibitory interaction by an external docking motif on an activating partner.

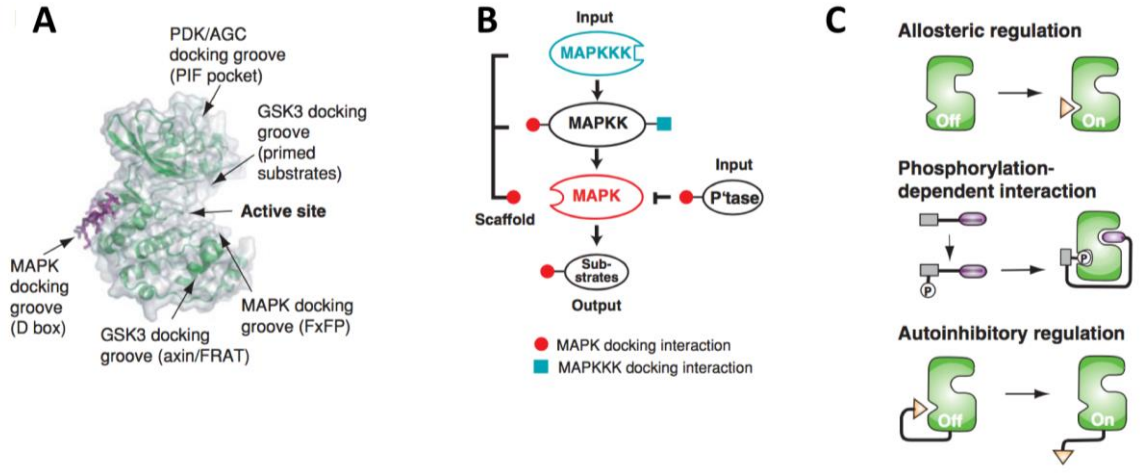

Figure IV.11. Docking interactions regulate MAP kinases and their signaling pathways.
See in-text legend (adapted from (Bhattacharyya et al. 2006)).

Most of these partners contain D motifs that fit to consensus sequences or structures showing some variability but all possessing hydrophobic residues and a patch of positively-charged residues (Figure IV.12A). Reciprocally, docking grooves on MAPK also contain consensus motifs made up of the ED and CD domains that possess hydrophobic and negatively-charged residues (Figure IV.12B).

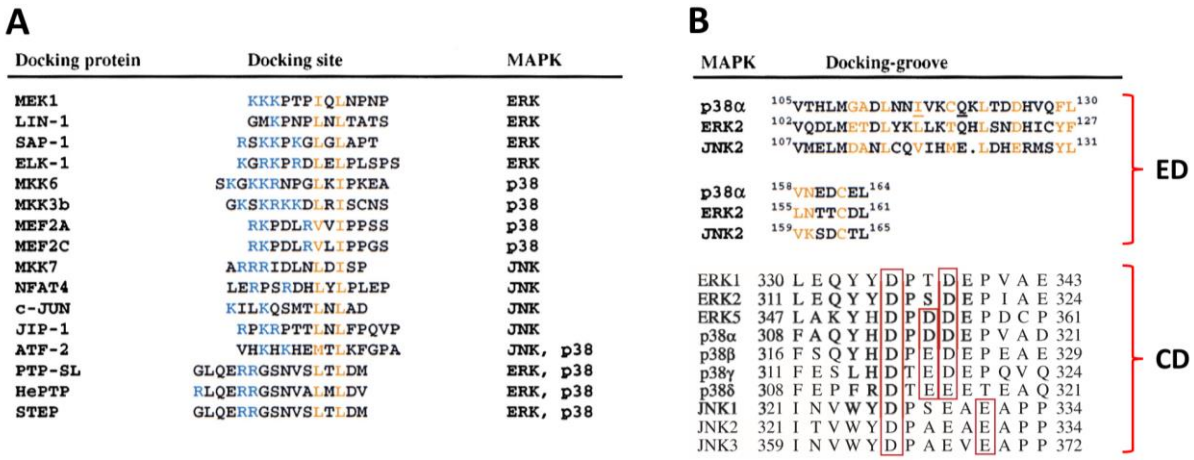

Figure IV.12. Consensus docking sequences of MAP kinases and their partners.
(A) Consensus sequences of D motifs on proteins that dock to MAP kinases. **(B)** Conserved acidic and hydrophobic residues in ED and CD domains that form the docking groove of MAP kinases. Adapted from (Chang et al. 2002) and (Tanoue and Nishida 2003).

From this analysis of the literature, it appears that the only putative region of interaction of Stt7-KD with the cyt b_6f that satisfies both the yeast two-hybrid results and the surface analysis (Figure IV.9A-C) has been described in other kinases as an important region of allosteric control of kinase activity. In MAP kinases, this regulation depends on docking interactions of the acidic hinge region with basic residues on D motifs of various partners. We propose that the positively charged surface of the cyt b_6f stromal face acts as a docking motif for the hinge region of Stt7. This interaction would modify the hinge conformation and induce allosteric effects on the kinase's oligomerization state, the relative positions of its two lobes, the conformation of the activation loop and/or the accessibility of the active site to ATP and substrates, thereby mediating its catalytic activity. If this model of Stt7 activation inspired by specificities of MAPK D motif activation turns out to be correct, then Stt7 should be classified as a MAP kinase.

F. Interaction and activation models

Several models of cyt b_6f-mediated activation of Stt7-KD can be derived from the previous description of regulatory mechanisms involving the hinge region of protein kinases. The following model (Figure IV.13) takes into account all the structural and functional data on both proteins that was presented in this work.

Stt7 is likely to form dimers or tetramers (Guo et al. 2013; Shapiguzov et al. 2016; Singh et al. 2016). Guo et al. obtained a dimeric structure of the Stt7 kinase domain of *Micromonas* and suggested that the kinase is autoinhibited in this state because the substrate-binding cleft of each monomer is obstructed by motifs of the opposite monomer. On the contrary, Shapiguzov et al. proposed that transient dimerization through intermolecular disulfide bridge formation on the lumenal side of the membrane could participate in the activation of the kinase, although no direct evidence was provided. Furthermore, Singh et al. suggested that the soluble fraction of Stt7 may be in tetrameric form and that incorporation to the membrane phase may be associated with a transition to a dimeric form. For our model, a change in the oligomerization state of Stt7 is not a determining factor in its activation but rather a consequence of the mechanisms that will be described. As such, as will be indicated, these changes may (or may not) take place at various steps along the activation pathway. Although the model would also hold if the kinase were to be always monomeric, we postulate that Stt7 forms dimers when it is free and inactive in the thylakoid membrane (Figure IV.13A).

When the kinase encounters a cyt b_6f complex (Figure IV.13B), its lumenal domain forms an interaction with the Rieske protein (Lemeille et al. 2009; Shapiguzov et al. 2016), its tilted transmembrane helix binds along helix G of subunit IV (Zito et al. 2002), and the acidic patch of its stromal hinge region (residues on the N-lobe side of the hinge pocket: Glu157, Glu160, Glu161, see Figure IV.9B1) forms electrostatic interactions with the basic surface of the cyt b_6f stromal region ($Lys20^{suIV}$, $Lys119^{suIV}$, $Arg112^{b6}$, see Figure IV.7 top right). In addition, interactions may be formed at this stage between the aromatic patch of the cyt b_6f ($Tyr124^{suIV}$, $Phe22^{PetG}$, $Tyr26^{PetG}$ and $Tyr29^{PetG}$) and aromatic residues of the stromal (Phe262) or transmembrane (Tyr120, Tyr121) domains of Stt7. This primary interaction induces slight conformational changes of the two kinase lobes that allow ATP-binding at the active site, leading to a basal ATP hydrolysis activity. These structural changes may also force the kinase to monomerize, which would participate in creating this basal activation level by allowing

access of ATP to the active site. However, this change in oligomerization may take place at later steps, as mentioned previously[‡]. This interaction can simply be viewed as the docking of the kinase to the cyt b_6f. In conditions where the redox state of the surrounding PQ pool is poised, cyt b_6f has a normal catalytic turnover and the head domain of the Rieske protein swings between the proximal and distal positions during electron transfer from PQH_2 to cyt *f*. This suggests that the kinase conformation around the cyt b_6f has to adapt to these movements and therefore that the primary docking interaction of Stt7 may be quite plastic. The kinase may even oscillate between docked and undocked/inactive forms. Note that under poised PQ pool conditions, the salt-bridge between $Arg125^{suIV}$ and $COOH^{b6}$ is formed and $Arg207^{b6}$ interacts with a propionate group of heme c_i.

This dynamic and reversible system becomes constrained upon over-reduction of the PQ pool in the vicinity of the cyt b_6f – Stt7 complex (Figure IV.13C). In this state, PQH_2 stays bound at the Q_o pocket and the Rieske head domain is stuck in its proximal position, stabilizing the docking of Stt7 close to the complex. The low-potential chain through hemes b_L and b_H is reduced and there are no oxidized quinone to bind to heme c_i. Blocked turnover at the Q_i site with a reduced and protonated heme c_i induces conformational changes of the heme and the surrounding amino acid side-chains that break its interaction with $Arg207^{b6}$ **(1)**. This redox-induced conformational change has an allosteric effect that in turn breaks the $C\text{-}ter^{b6}$ – $Arg125^{suIV}$ salt-bridge **(2)**. The released $Arg125^{suIV}$ side-chain forms an additional positive charge that extends the docking surface of Stt7 on the cyt b_6f. Acidic residues of the Stt7 docking groove (mainly Glu312) form an interaction with $Arg125^{suIV}$ **(3)**. The aromatic stacking interactions may also form at this step, if not earlier. This additional docking may lift the autoinhibiting "molecular brake" that was proposed to be formed between residues of the hinge pocket (Figure IV.10). At this stage, Stt7 is fully docked to the cyt b_6f and binding of the docking groove region further opens the inter-lobe space. This allows conformational changes of the substrate-binding cleft, including the activation loop, that yield a fully active catalytic site **(4)**. In this conformation, ATP hydrolysis leads to the activation of the kinase through autophosphorylation **(5)**.

[‡] We further propose that, regardless of when the kinase monomerizes, the interaction of one of the kinase dimer/tetramer units with a b_6f complex may release the other units in a state in which they are primed for faster activation by nearby b_6f complexes, yielding an exponential kinase activation (and state transition) response.

The autophosphorylation in Figure IV.13C is depicted as taking place on the activation loop because activation loop-phosphorylation is a well-documented mechanism of kinase activation. However, it may very well take place on residues outside the activation loop. Guo et al. found that residues Thr185 and Tyr122, both on the N-lobe and therefore not on the activation loop, are the major autophosphorylation sites in MsStt7d-KD (Guo et al. 2013). They thus proposed that MsStt7d-KD is a dual-specificity kinase with autophosphorylation activity toward both threonine and tyrosine residues. This may seem questionable knowing that its close relative Stt7 has been classified as a dual-specificity serine-threonine kinase based on the phosphorylation sites on its substrates. However, it should not be excluded that Stt7 could have distinct cis- and trans-activities, autophosphorylating on threonines and tyrosines and phosphorylating LHCII proteins and other susbstrates on serines and threonines. This feature is known among kinases, for example the MAP kinase p38α (Lochhead 2009). Interestingly, the only phosphorylatable residues on the Stt7-KD activation loop are tyrosines (Tyr339, Tyr341, Tyr351). Outside the activation loop, one other tyrosine, four threonines and only one serine line the nucleotide binding pocket and could be targets for autophosphorylation.

This model differentiates between two states of Stt7-binding to the cyt b_6f stromal region. The first is the initial docking between the N-lobe extremity of the Stt7 hinge region and one side of the basic patch of the cyt b_6f that induces slight conformational changes of the kinase domain and increases its ATP hydrolysis activity (Figure IV.13B). In the second state, a docking interaction is formed between residues of the docking groove (C-lobe extremity of the Stt7 hinge region) and Arg125^{suIV} that fully activates the kinase and induces autophosphorylation (Figure IV.13C). This distinction is based mainly on the following results. From the yeast two-hybrid assay, a stronger interaction was detected between the subunit IV fg loop and Stt7 when region B (C-lobe) was used alone as prey protein, compared to regions A and B together (N- and C-lobes, see lines 1 and 4 of Figure III.13B). This suggests that the most direct interaction of the fg loop residues (*i.e.* Arg125^{suIV}) is formed with residues of the C-lobe docking groove of Stt7. Interaction with region A (N-lobe) may depend mostly on basic residues outside the fg loop that participate in forming the positively-charged stromal surface of the cyt b_6f (Lys20^{suIV}, Arg112^{b6}, see Figure IV.7 top right). Furthermore, purified cyt b_6f with the Arg125Glu substitution impeded cyt b_6f-mediated autophosphorylation of Stt7-KD (Figure III.14C, lane 3) but did not prevent an increase in its ATP hydrolysis activity (Figure III.14A, bar 3). This demonstrated that ATP hydrolysis and autophosphorylation activities are not strictly correlated and suggested that the cyt b_6f, WT or Arg125Glu, stabilizes an active state of Stt7-KD. This

state should correspond to the initial docking of Stt7 since it does not depend on Arg125. In this conformation, the kinase has an enhanced ATPase activity and is primed to receive the autophosphorylation signal that was shown to be (at least in part) dependent on Arg125. Once the redox cue is sent, Arg125 forms an additional interaction with the regulatory docking groove of Stt7 that leads to autophosphorylation, a mechanism that is lost in the Arg125Glu mutant.

Figure IV.13. Interaction and activation models of the Stt7 kinase by the cyt *b_6f* complex.
(A) Left: stromal view of the cyt b_6f monomer with cyt b_6 in orange, subunit IV in yellow, PetG in grey, hemes b_H and c_i in red, and important residues or atoms annotated. The salt-bridges between Arg125^{suIV} and C-ter^{b6} and that between Arg207^{b6} and heme c_i are represented as dotted red lines. Right: schematic representation of an Stt7 dimer viewed from "the top", based on the dimer in the crystals of MsStt7d-KD, with the N-lobe in red, the C-lobe in blue and the hinge region in grey. The docking groove formed by C-lobe and hinge structures is depicted as a yellow half-doughnut. DLG and HRD motifs, as well as the activation loop are schematically represented. **(B)** Initial docking of the N-lobe hinge region to the stromal basic surface of cyt b_6f, inducing sufficient lobe opening for ATP binding and hydrolysis. **(C)** An over-reduction of the PQ pool modifies the coordination of heme c_i and allosterically releases the Arg125^{suIV} residue, which then forms a docking interaction with acidic residues of the Stt7 docking groove. This induces conformational changes of the kinase domain (the "DLG flip" is represented as an example) that enable its autophosphorylation and full activation.

A

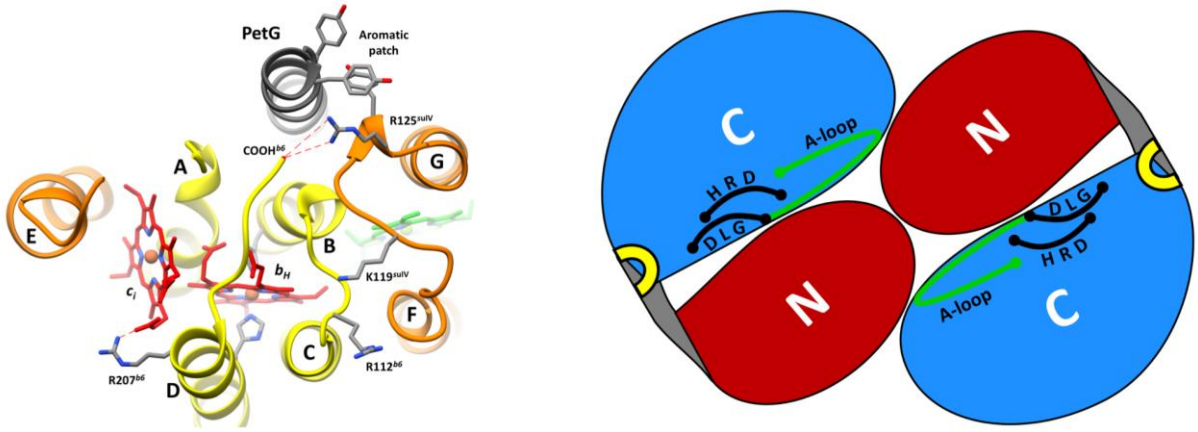
PetG
Aromatic patch
R125sulV
COOHb6
A
G
E
B
bH
K119sulV
ci
F
C
R112b6
R207b6
D
C
A-loop
H R D
D L G
N
N
D L G
H R D
A-loop
C

B

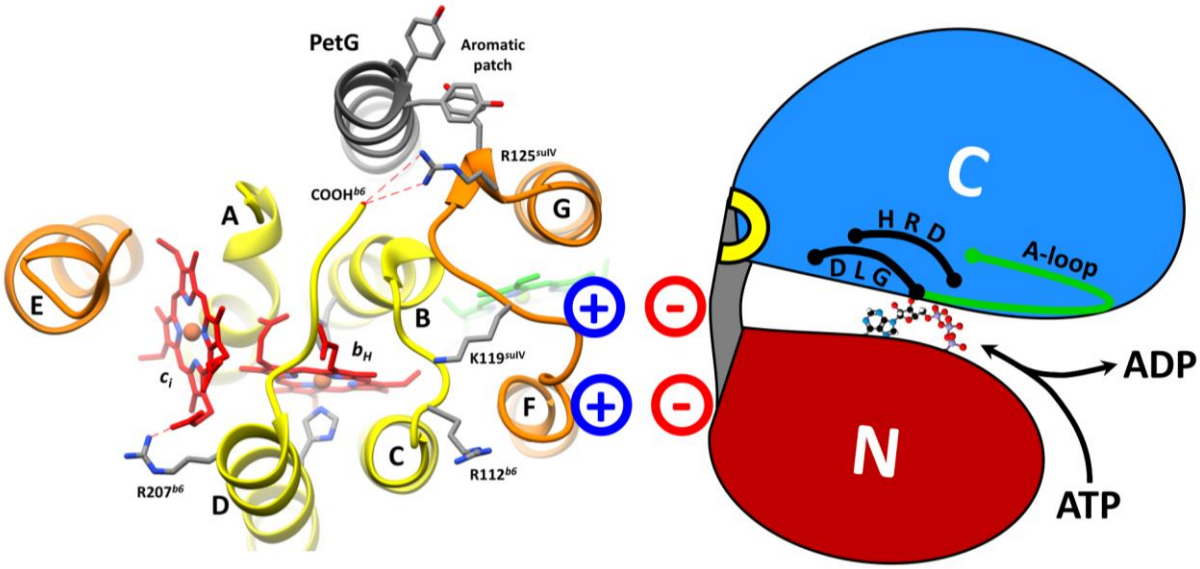
PetG
Aromatic patch
R125sulV
COOHb6
A
G
E
B
bH
K119sulV
ci
F
C
R112b6
R207b6
D
C
H R D
D L G
A-loop
ADP
N
ATP

C

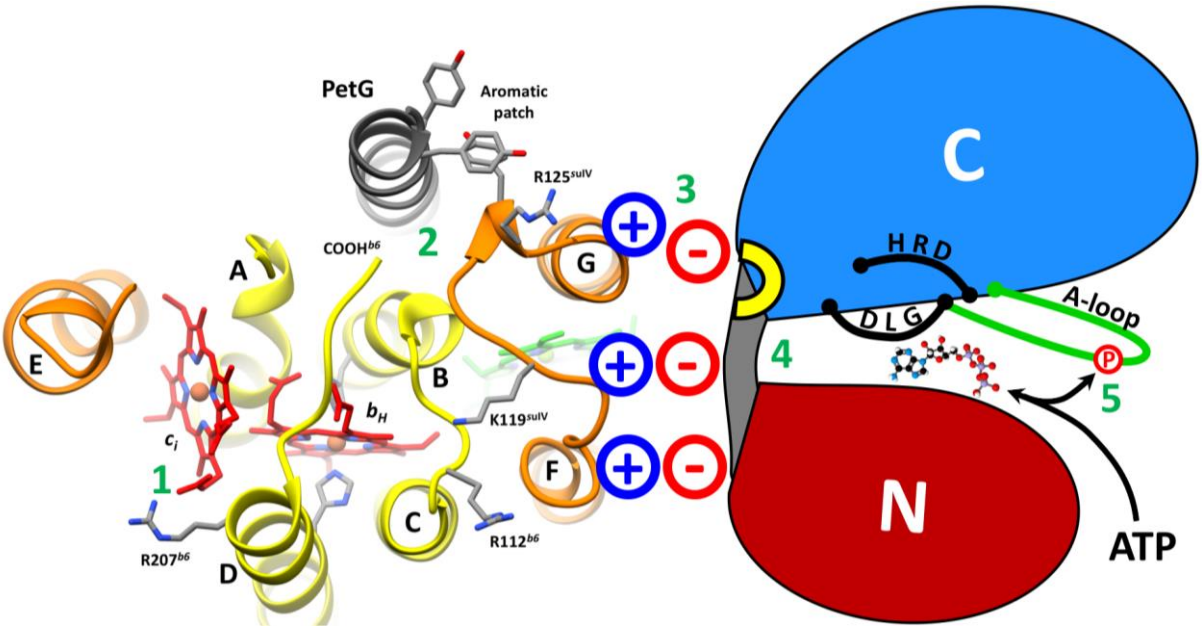
PetG
Aromatic patch
R125sulV
3
COOHb6
2
A
G
E
B
bH
K119sulV
ci
F
1
C
R112b6
R207b6
D
C
H R D
D L G
A-loop
4
P
5
N
ATP

G. Concluding remarks

In this chapter, we have provided evidence of the functional significance of the C-ter^{b6}–Arg125^{suIV} interaction and suggest that it is a strong argument for the involvement of the Q_i site and heme c_i in the mechanism of activation of Stt7. From an evolutionary point of view, we offer that the split of cyt *b* into cyt b_6 and subunit IV and the establishment of an electrostatic interaction between cyt b_6 and Arg125^{suIV} may have later on allowed the evolution of a redox sensing and transduction mechanism for the activation of Stt7 and redistribution of excitation energy between the two light-absorbing complexes of oxygenic phototrophs.

The interaction and activation model that was outlined in Figure IV.13 is very protein-centered and does not provide a rational for the physiological determinants of Stt7 activation. This work's findings prove that PQH_2 binding at Q_o is not and should not be sufficient to activate Stt7: hydrolyzing ATP at each Q_o site turnover would represent significant energy loss. Rather, we suggest a (still speculative) model describing a much more dynamic system, regulated at several levels. The sub-localization of the two protein partners along the thylakoid membrane, and therefore their exposure to different quinone microdomains, plays a role in the activation of Stt7. Only particular redox conditions set the stage for kinase activation by determining the "working mode" of cyt b_6f and inducing conformational changes. The analogy with hemoglobin can be of use here. Cyt b_6f working with a poised PQ pool turns over normally, with heme c_i binding and releasing PQ molecules rapidly. In this state, the binding and releasing of quinone species, as well as electron transfer through the high and low potential chains, induce domain movements in the cyt b_6f dimer. Indeed, movement of the Rieske head domain is well documented, and Breyton observed the following in a study comparing the projection maps of cyt b_6f and bc_1 crystals (± stigmatellin) observed by cryo-EM (Breyton 2000):

> *The two maps look quite different, which is unexpected, as there are absolutely no changes in the transmembrane region of the bc_1 complex upon binding of stigmatellin. Here* [in the b_6f map]*, the heart of the complex remains roughly unchanged, whereas differences appear further away from the dimer axis. They suggest movements in the transmembrane domains of the b_6f complex upon binding of the inhibitor, which may reflect the functional differences that distinguish the photosynthetic and respiratory complexes.*

This poised state would correspond to the "Relaxed" form of the complex. This coincides with the idea that the preliminary binding of the kinase to the complex is labile and has to

accommodate both the Rieske and peripheral transmembrane domain movements. Upon over-reduction of the PQ pool, a PQH_2 molecule stays bound at Q_o (keeping the Rieske in its proximal position and therefore stabilizing Stt7 docking to the positively-charged stromal patch), the low potential chain is reduced and heme c_i is reduced/protonated with no PQ molecule available as axial ligand (NQNO, and therefore probably PQ, binds to the oxidized form of c_i). This would correspond to the "Tense" configuration of the complex, in which domain movements would be completely halted. Upon prolonged exposure of the cyt b_6f to these conditions, the redox "strain" on the Q_i site induces conformational changes that increase the accessibility of the site and the affinity of PQ for the reduced form of heme c_i. This rearrangement, which is effectively the redox sensing function of cyt b_6f, induces the allosteric cascade schematized in Figure IV.13C that leads to kinase activation. The increased PQ affinity in turn enables a turnover at Q_i, re-oxidation of the low potential chain and a single turnover at Q_o, thereby allowing the movement of the Rieske to the distal position and the release of the kinase from its docking sites on cyt b_6f. The kinase phosphorylates LHCII proteins on nearby PSII complexes, and their migration and association to PSI lead to the re-oxidation of the locally over-reduced PQ microdomain. As the PQ pool gradually oxidizes, the cyt b_6f switches back to its steady-state "Relaxed" form and another kinase molecule eventually binds as described in the model of Figure IV.13.

In this model, the Q-cycle is the PQ pool redox sensor and the structural link between the Q_i site and Stt7 through $Arg125^{suIV}$ is the signal transducer for kinase activation.

CONCLUSIONS & PERSPECTIVES

The cytochrome b_6f complex drives electron transfer in the electron transport chain of oxygenic photosynthesis. By catalyzing reactions of quinol oxidation and quinone reduction in the Q-cycle, it is the major contributor to the *proton motive force* and the coupling component of Mitchell's chemiosmotic theory. The resolution of its crystallographic structure in 2003 both confirmed its previously-described roles in electron and proton transfer and unveiled certain peculiar features such as the presence of heme c_i in the stromal Q_i pocket. This also provided a canvas for the study of the more elusive functions of cyt b_6f in the regulation of photosynthetic electron transport. For several years, however, the question of how the complex interacts with and activates the Stt7 kinase remained a mystery.

In this work, we set out to tackle this question using a new structure-function approach. We decided to probe the cyt b_6f for regions involved in state transitions by random mutagenesis, chloroplast transformation and a state transition screen using chlorophyll fluorescence imaging. Systematic screening and sequencing revealed that there was a strong correlation between impaired state transition phenotypes and mutations on the fg loop of subunit IV, defining this region as a "state transition hotspot" that could then be characterized in depth. Several state transition mutants containing mutations outside the subunit IV fg loop were also isolated and not characterized further. These may reveal additional features of the interplay between cyt b_6f and Stt7. The success of this experimental strategy suggests that it can be applied to the structure-function study of other chloroplast-encoded proteins as long as functional selection and screening criteria are available. It is a precise and efficient way to introduce diversity in chloroplast genes and therefore a new tool in the field of chloroplast biology and engineering.

In depth characterization of site-directed mutants of the subunit IV fg loop revealed that certain point mutations completely impaired state transitions, while the accumulation and electron transfer activity of the cyt b_6f, and Stt7 accumulation, were unaffected. This suggested that specific residues were involved in the docking and/or activation of the kinase. As such, we were able to uncouple the redox state of the PQ pool from the phosphorylation of LHCII proteins through single point mutations. Of particular interest was residue Arg125, which was found to interact with Stt7 and to mediate its autophosphorylation. Furthermore, we provided strong evidence that the interaction of this arginine side chain with the carboxyl group of the cyt b_6 C-

terminal has a functional role. We proposed a mechanism for the cyt b_6f-mediated activation of Stt7 that depends on a dynamic response of this Arg125 dual interaction (the "transducer") to local redox changes detected by heme c_i and the Q_i site (the "sensor"). These results and model open up many questions and experimental perspectives that are detailed below.

A new region of interaction between two proteins playing major regulatory roles in photosynthetic electron transport has been isolated and characterized in this work. Although the exact region of interaction on Stt7 is uncertain, a rather short list of residues and motifs was provided based on sequence and surface analyses and reported mechanisms of kinase activation. Once a reliable method for complementation of the *stt7-1* or *stt7-9* deletion strains is obtained, classical site-directed mutagenesis of these residues of interest should be an efficient way to test our hypotheses. If directed mutagenesis does not yield mutants affected for state transitions, then the genetic suppressor approach described in Chapter III should be a promising alternative. Furthermore, directed mutagenesis of certain phosphorylatable residues lining the substrate-binding cleft of the Stt7 kinase domain could give insight into the requirement of autophosphorylation for Stt7 activation *in vivo*. Finally, an ambitious project would be to try co-purifying and crystallizing a complex formed by cyt b_6f and Stt7. One could substitute $Arg125^{suIV}$ and its interacting partner on Stt7 *in vivo* with residues that can be easily cross-linked. Using whole cells or thylakoid membrane preparation treated with TDS (to stabilize the docking of Stt7 to cyt b_6f), the two proteins could be cross-linked and the complex purified following the standard protocol of cyt b_6f purification. If a stable purified cyt b_6f-Stt7 complex can be obtained, efforts will no doubt follow to obtain sufficient quantities for crystallization and X-ray crystallography. Alternatively, the mutated and truncated Stt7 kinase domain with a cross-linkable residue could be expressed in and purified from *E. coli* and cross-linked *in vitro* to purified cyt b_6f bearing a matching substitution at position 125^{suIV}. This may enable better purification yields and increase the probability to crystallize a cyt b_6f-Stt7 complex, albeit incomplete.

Concerning the autophosphorylation of Stt7, one could use the *in vitro* reconstitution system developed in this study to better define the phosphorylation sites involved in its activation. By incubating Stt7-KD with either the WT or Arg125Glu version of cyt b_6f and analyzing Stt7-KD by phosphoproteomics, the site(s) responsible for the increased autophosphorylation in the presence of WT b_6f could be pinpointed and distinguished from the "basal"

autophosphorylation sites that appear phosphorylated when Stt7 and ATP are incubated alone or with Arg125Glu cyt *b*$_6$*f* (Figure 4 of PNAS article).

A major aspect of the mechanism of state transitions that was not addressed in this work is the phosphorylation of PetO, the loosely bound cyt *b*$_6$*f* subunit that is phosphorylated by Stt7 in conditions where the PQ pool is reduced. Unfortunately, the ^{33}P-labelling experiments did not generate a clear phosphorylation of PetO in the WT sample in reducing conditions, making it hard to determine whether this peptide was phosphorylated in the subunit IV mutants. Taking the Arg125Glu substitution as an example, our model predicts that since it blocks the primary activation of Stt7, PetO should not be phosphorylated in this mutant, in contrast with inhibitor studies that showed that TDS treatment allowed Stt7 and PetO phosphorylation but not LHCII phosphorylation (Finazzi et al. 2001). Further efforts to characterize the phosphorylation of PetO in subunit IV fg loop mutants may shed light on the sequence of events taking place during the cyt *b*$_6$*f*-mediated activation of the kinase. Another subunit of interest is PetG, which was proposed to form part of the docking interface of Stt7 on cyt *b*$_6$*f*. Since a knock-out mutant of *petG* is available (Berthold et al. 1995), site-directed mutagenesis of stromal residues of PetG and chloroplast transformation would provide an easy way to test its role in the interaction with Stt7.

Another point of interest would be to thoroughly compare the phenotypes of the Arg125Glu strain and the *stt7* deletion strains. Indeed, their very different phosphorylation profiles (Figure III.8.B) seem to suggest that the uncoupling between the PQ pool redox state and LHCII phosphorylation in these two strains does not lead to the same phenotypic responses. In other words, what are the long-term effects of an uncoupling between the redox state of the PQ pool and the phosphorylation of antenna proteins in a mutant where the two proteins of interest are otherwise unaffected? Going further, it may be interesting to examine whether a strain bearing the Arg125Glu substitution exhibits any long-term physiological differences in conditions of changing light quantity or quality. It may be that only having cyt *b*$_6$*f* fixed in one "working mode" instead of its dynamic WT version could, over time and in specific conditions, build up a phenotypic response. This long-term response may be elicited by slower redox poising, modified *pmf* dynamics, altered LEF/CEF regulation or changes in membrane ultrastructure and protein mobility, mechanisms that all directly or indirectly implicate the cyt *b*$_6$*f*.

Last, but not least, the functional role of the C-ter^{b6} – Arg125^{suIV} interaction should be confirmed and the hypothesis of a signal transduction from Q_i to Stt7 should be scrutinized experimentally. Redox titrations of hemes b_H and c_i, as well as EPR spectroscopy measurements of heme c_i, in the Arg125Glu^{suIV} and cyt b_6 C-terminal mutants and in the presence or absence of NQNO, should provide ways to test whether redox-induced structural changes on the stromal side of cyt b_6f could participate in the activation of Stt7. Following the logic of the model presented in the conclusions of Chapter IV, cyt b_6f with the Arg125Glu substitution should mimic the relaxation from the "Tense" form elicited by structural rearrangements at Q_i and leading to increased accessibility/affinity of PQ to heme c_i. One may test this hypothesis by first completely reducing the PQ pool and then measuring the kinetics of PQ pool re-oxidation. This should be slower in the Arg125Glu mutant because of its constitutive (and still putative) higher affinity for PQ and therefore higher ratio of PQ-reduction to PQH_2-oxidation.

To conclude, I would like to thank the members of the jury for your careful reading of this thesis manuscript. I hope I was never too cryptic and that you were able to follow my argumentation. I will be glad to discuss any aspect of this work that remains unclear and happy to correct any mistakes that I have made.

MATERIALS AND METHODS

A. Strains and culture conditions

All strains used in this work are listed in Table A1. For photoautotrophic growth, *C. reinhardtii* cells were grown on Tris-Phosphate (TP or MIN, pH 7.2) medium in the light (50-100 $\mu mol_{photons}.m^{-2}.s^{-1}$) in air supplemented with 2% CO_2. For heterotrophic growth, cells were grown on Tris-Acetate-Phosphate (TAP, pH 7.2) medium in the dark (for photosensitive strains) or low light (<40 $\mu mol_{photons}.m^{-2}.s^{-1}$). For mutant selection on phototrophy, TP medium supplemented with 2% w/v agar was used and plates were placed in a thin airtight transparent box in the light (50 $\mu mol_{photons}.m^{-2}.s^{-1}$) in air supplemented with 2% CO_2. For mutant selection on antibiotic resistance, TAP medium supplemented with 2% w/v agar and the appropriate antibiotic was used and plates were placed in the dark or dim light.

B. Molecular biology

Unless specified otherwise, all restriction enzymes were bought from NEB, gel purifications were performed using the NucleoSpin® Gel and PCR cleanup kit (Macherey-Nagel), quantification of DNA concentrations were done on gel or on a NanoDrop spectrometer (GE), mini-preps were performed using the NucleoSpin® Plasmid kit (Macherey-Nagel) and midi-preps using the NucleoBond® Xtra Midi kit (Macherey-Nagel).

All primers used in this study were synthesized by Invitrogen or Eurofins and are listed in Table A2. All plasmid maps are given in Figure A1. Plasmid $pWQH_6$ (de Lacroix de Lavalette, Finazzi, et al. 2008), carrying the 3'-end sequence of *petA* with a 6-His tag, the intergenic *petA-petD* region and the entire *petD* sequence, was used for the mutagenesis of the *petD* gene and chloroplast transformation of the Δ*petD* strain. Plasmid pWBA (Kuras and Wollman 1994) was used for the mutagenesis of the *petB* gene and chloroplast transformation of the Δ*petB* strain. Plasmid pLIC03, designed for ligation-independent cloning (LIC, (Aslanidis and de Jong 1990)), is a derivative of the pET-28a+ expression vector (Novagen) in which a cassette coding for a 6-His tag and a Tobacco etch virus (TEV) protease-cleavage site followed by the suicide gene *SacB* flanked by *BsaI* restriction sites was introduced downstream of the ATG start codon, and was used to build the pLIC03-Stt7-KD construct for expression of the recombinant Stt7

kinase domain. Plasmids pGBKT7 and pGADT7 were used for the cloning of bait and prey constructs of *petD* and *STT7*, respectively[2], for the double-hybrid experiments. Plasmid pWQA is the same as plasmid $pWQH_6$ with an added spectinomycin cassette in the region between *petA* and *petD* and was used to construct the pWQA-Y124K plasmid. Plasmid pSLX (derivative of pSL18 plasmid without the PSAD promoter) was used to build the pSLX-Stt7 constructs for complementation of the *stt7-1* and *stt7-9* strains.

1. *Site-directed mutagenesis*

Whole-plasmid PCR mutagenesis was used to introduce mutations or sequences in genes of interest. Pairs of complementary mutagenic primers (see Table A2) containing the desired nucleotide substitutions were used to amplify the entire plasmid template in a PCR (Table M1) using the Advantage® HD high-fidelity DNA polymerase (Clontech).

Table M1. PCR conditions used for whole-plasmid, site-directed PCR mutagenesis.

Reagents	**Mix**	**Cycle**		
5X Advantage HD Buffer	10 µL	98°	10 sec	
dNTP Mix (2.5 mM each)	5 µL	T_m – 3°	20 sec	x3
Plasmid template	50 ng	72°	1 min/kb	
Forward primer	125 ng	98°	10 sec	
Reverse primer	125 ng	T_m	20 sec	x22
Advantage HD Polymerase (2.5 units.µL^{-1})	0.5 µL	72°	1 min/kb	
H_2O	qsp. 50 µL	72°	10 min	

The PCR products were treated with 10 units of *DpnI* restriction enzyme and left to incubate at 37°C for 2 hours. 2 µl of this reaction was used to transform 100 µl XL10-Gold® Ultracompetent *E. coli* cells (Agilent) by heat-shock. Cells and DNA were mixed and incubated for 30 minutes on ice. The mixture was transferred to a 42°C dry-bloc for 45 seconds and back on ice for 2 minutes. The cells were supplemented with 1 mL SOC medium and incubated at 37°C for 1 hour at 180 rpm. 20% of the transformation mixture was plated on LB-agar medium containing 100 µg.mL^{-1} ampicillin and incubated at 37°C over-night. Ampicillin-resistant clones were subjected to colony-PCR and 10% of the reaction was loaded on an agarose gel to verify amplification. Successful amplification reactions containing unpurified PCR products were sent directly for sequencing with the appropriate primers (see Table A2). Plasmids from clones containing the desired mutagenized sequence were recovered by mini-prep.

2. *Random mutagenesis*

Two molecular biology kits were used for random mutagenesis by epPCR: the GeneMorph® II EZClone Domain Mutagenesis Kit (Agilent Technologies) and the Diversify® PCR Random Mutagenesis Kit (Clontech). These rely on two different techniques to control the error rate of the polymerase. The first technique (Agilent kit) uses a high error-rate DNA polymerase with a low mutational bias and the mutation frequency is adjusted by varying the amount of template DNA and the number of epPCR cycles. The second technique (Clontech kit) acts directly on the fidelity of a *Taq* DNA polymerase. Manganese (in the form of $MnSO_4$) is added to the epPCR reaction and increases the mutation frequency in a concentration-dependent manner by binding to the DNA template and decreasing the fidelity of the enzyme. The mutation frequency can be further increased by increasing the dGTP concentration in order to skew the relative dNTP concentrations. Table M2 shows the epPCR conditions used for each kit. The epPCR products were loaded on a 2% agarose gel and the 750 bp fragments of interest were gel-purified. Purified fragments were used as "megaprimers" in a reconstruction PCR (rcPCR) (conditions detailed in Table M2). The reaction products were treated with 10 units of *DpnI* restriction enzyme and left to incubate at 37°C for 2 hours. 2 µL of this reaction was used to transform 50 µl XL10-Gold® Ultracompetent *E. coli* cells (Agilent) by heat-shock (see standard protocol under "*Site-directed mutagenesis*" section). Cells and DNA were mixed and incubated for 30 minutes on ice. The mixture was transferred to a 42°C dry-bloc for 45 seconds and back on ice for 2 minutes. The cells were supplemented with 500 µL SOC medium and incubated at 37°C for 1 hour at 180 rpm. 10% of the transformation mixture was plated on LB-agar medium containing 100 $\mu g.mL^{-1}$ ampicillin and incubated at 37°C over-night. Ampicillin-resistant clones were counted and a subset was sequenced using the Pseq5-f primer after colony growth in liquid culture and plasmid DNA recovery. The rest of the transformation mixture was used to amplify the plasmid library by inoculating either 5 mL or 200 mL LB batch cultures containing 100 $\mu g.mL^{-1}$ ampicillin and growing the cells over-night (37°C, 180 rpm). The amplified plasmid DNA library was recovered either by mini-prep (for 5 mL cultures) or by midi-prep (for 200 mL cultures) and DNA concentration was measured. When the concentration was below 0.5 $\mu g.\mu l^{-1}$, the DNA preparation was concentrated on a SpeedVac (Servant ISS110, ThermoScientific) to ≥ 0.5 $\mu g.\mu l^{-1}$.

Table M2. PCR conditions used to introduce random mutations in *petD* (epPCR), reconstruct the mutated fragments into plasmids (rcPCR) and sequence *C. reinhardtii* transformants (seqPCR).

Kit used	ep-PCR		rc-PCR		seq-PCR	
	Mix	Cycle	Mix	Cycle	Mix	Cycle
GeneMorph® II (Agilent)	10X Mutazyme II buffer 5 µl $pWQH_6$ DNA template ** 10 µM P1-f primer 2,5 µl 10 µM P1-r primer 2,5 µl 40 mM dNTP mix 1 µl Mutazyme II DNA Pol. 1 µl ddH_2O qsp 50 ml	95°C 2' 95°C 30'' | x25 54°C 30'' | or 72°C 1' | x30 72°C 10'	2X EZClone mix 25 µl $pWQH_6$ DNA template 50 ng Megaprimer 250 ng EZClone solution 3 µl ddH_2O qsp 50 µl	95°C 1' 95°C 50'' | 60°C 50'' |x25 68°C 14' |		
Diversify® (Clontech)	10X TITANIUM buffer 5 µl 8 mM $MnSO_4$ 4 µl 2 mM dGTP 5 µl 50X Diversify dNTP Mix 1 µl 10 µM P2-f primer 1 µl 10 µM P2-r primer 1 µl $pWQH_6$ DNA template 1 ng TITANIUM *Taq* Pol. 1 µl ddH_2O qsp 50 µl	94°C 30'' 94°C 30'' | x25 68°C 1' | 68°C 1'	5X Advantage HD buffer 5 µl dNTP (2,5mM each) 2 µl Megaprimer 400 ng $pWQH_6$ DNA template 50 ng Advantage HD Pol. 0.25 µl ddH_2O qsp 25 µL	98°C 1' 98°C 10'' 60°C 15 '' |x25 72°C 15' |	2X Phusion® HF Mix 15 µl 10 µM Pseq-f primer 3 µl 10 µM P1-r primer 3 µl DNA (Chelex) 3 µl ddH_2O qsp 30 µl	98°C 1' 98°C 20'' | 65°C 45'' |x25 72°C 1' | 72°C 10''

**see Table II.1 for DNA template amounts used in the various mutagenesis experiments using the GeneMorph® II kit (Agilent).

3. *Cloning of the sequence coding for the Stt7 kinase domain into an E. coli expression vector*

The full-length *STT7* gene (*C. reinhardtii* accession no. Q84V18) was recoded for *E. coli* codon bias and synthesized (Invitrogen). The 1.0 kb nucleotide sequence coding for the catalytic domain of Stt7 (residues 139 to 495) with an added C-terminal Strep-tag was amplified by PCR and cloned with the InFusion® HD Cloning Kit (Clontech) into expression vector pLIC03 at the 5'- and 3'-ends of the *Bsa1* restriction sites (thus removing the *SacB* suicide gene) under the *LacZ*-inducible operon, yielding plasmid pLIC03-Stt7-KD. This plasmid was used to transform *E. coli* DH5α cells by heat-shock (see standard protocol under "*Site-directed mutagenesis*" section) for amplification and verification of the reconstructed vector by sequencing.

4. *Construction of vectors pSLX-Stt7 and pSLX-Stt7+33*

A genomic DNA preparation was used as template with primers Stt7-gDNA_fw and Stt7-gDNA_rv in a PCR (annealing T_m = 68°C) to obtain a 1.8 kb gDNA fragment containing the 1 kb sequence upstream of *STT7*, the 5'-UTR and the genomic *STT7* sequence up to the start of the 3rd exon. A cDNA preparation was used as template with primers Stt7-cDNA_fw and Stt7-cDNA_rv in a PCR (annealing T_m = 72°C) to obtain a 1.9 kb cDNA fragment going from the start of the 3rd exon to the 3' of the *STT7* CDS. A pSL18 plasmid preparation (kindly provided by Michel Goldschmidt-Clermont, Geneva) was used as template with primers Stt7-3'UTR_fw and Stt7-3'UTR_rv in a PCR (annealing T_m = 68°C) to obtain a 0.8 kb pDNA fragment

containing a 6-HA tag and 500 bp of the *STT7* 3'-UTR. PCR conditions used to amplify the three fragments are shown in Table M3.

Table M3. PCR conditions used to obtain the three fragments of the *STT7* gene construct.

Reagents	Mix	Cycle		
5X Q5 Reaction Buffer	10 µL			
dNTP Mix (2.5 mM each)	4 µL	98°	30 sec	
gDNA, cDNA or pDNA	1 µL	98°	10 sec	x35
10 µM forward primer	2.5 µL	T_m	30 sec	
10 µM reverse primer	2.5 µL	72°	30 sec/kb	
5X Q5 High GC Enhancer	10 µL	72°	2 min	
Q5 High-Fidelity DNA Polymerase (2 units.µL^{-1})	0.5 µL			
H_2O	qsp. 50 µL			

The fragments were gel-purified and quantified. 2 µg of pSLX plasmid was digested with *XbaI* and the resulting 4800 bp fragment was gel-purified and quantified. The 3-fragment In-Fusion ligation is represented in the figure opposite, with the complementary sequences of the vector and inserts shown in color. The gDNA, cDNA and pDNA inserts were mixed altogether with the digested pSLX vector each in a 2:1 molar ratio in a 10 µL reaction with 1X In-Fusion HD Enzyme Premix (Clontech) and incubated 50 min at 50°C. 2.5 µL of this In-Fusion reaction was used to transform 50 µL Stellar Competent Cells (Clontech) by heat-shock (see standard protocol under "*Site-directed mutagenesis*" section). Cells were plated on LB-ampicilin medium and colonies were screened first by colony PCR (with primers Stt7_Pseq3-f and Stt7_Pseq3-r) and then by mini-prep and *XbaI*/*StuI* double digestion. Plasmids showing the expected digestion pattern were sent for sequencing and named pSLX-Stt7.

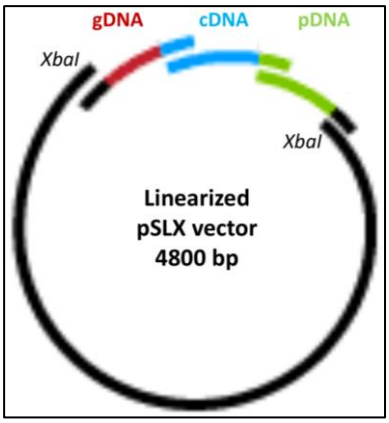

Whole-plasmid PCR mutagenesis with primers Stt7_AS-fw and Stt7_AS-rv (AS = alternative splicing) was used to introduce the 33 bp sequence into plasmid pSLX-Stt7 and yield plasmid pSLX-Stt7+33. The forward and reverse primers were first used separately in two 10-cycle PCRs (using Q5 Polymerase, see Table M3; annealing T_m = 60°C). The reactions were then pooled, supplemented with 2 µL dNTP, 5 µL Q5 Enhancer and 0.25 µL Q5 polymerase and 20 more PCR cycles were performed. 10 units of *DpnI* restriction enzyme was added and left to digest for 2 hours at 37°C. 5 µL of this reaction was used to transform 50 µL of Stellar Competent Cells (Clontech) by heat-shock (see standard protocol under "*Site-directed*

mutagenesis" section). Cells were plated on LB-ampicilin medium and colonies were screened by mini-prep and *BamHI* digestion. Plasmids containing the 33 bp sequence, which introduced an additional *BamHI* site in the plasmid, were sequenced and renamed pSLX-Stt7+33.

5. Construction of vector pWQA-Y124K

5 µg of plasmid pWQH$_6$ containing the mutated *petD* gene, coding for subunit IV with the Tyr124Lys substitution, was digested with *AvrII*, *ScaI* and *XbaI*. The 3850 bp *AvrII*/*ScaI*-digested fragment containing the mutated *petD* gene was gel-purified. 5 µg of plasmid pWQA was digested by *AvrII* and *ScaI* and the 5210 bp fragment containing the *aadA* cassette was gel-purified. The 3850 bp and 5210 bp fragments were ligated in a 3:1 molar ratio (300 ng and 100 ng, respectively) in a 10 µL reaction with 2000 units (1 µL) of T4 DNA Ligase in 1X T4 DNA Ligase Reaction Buffer at room temperature for 2 hours and 4°C over-night. The 10 µL ligation reaction was used to transform 50 µL of TOP10 Competent Cells (ThermoFisher) by heat-shock (see standard protocol under "*Site-directed mutagenesis*" section). Cells were plated on LB-ampicilin medium and colonies were screened by DNA mini-prep and *PstI* digestion. Plasmids showing the expected digestion pattern were sent for sequencing to verify the presence of both the *aadA* cassette and the Tyr124Lys substitution and renamed pWQA-Y124K.

C. Chloroplast transformation

The S550d Seashell Technology kit was used for transformation of *C. reinhardtii* chloroplasts following a protocol adapted from the original technique described by Boynton et al. (Boynton et al. 1988). This kit contains 550 nm gold carrier particles at 50 mg.mL^{-1} and binding and precipitation buffers. Additional materials to be supplied include autoclaved membrane holders and a bombardment chamber to which a partial vacuum and a high-pressure helium pulse can be applied. The Δ*petD* strain was transformed with plasmid pWQH$_6$ containing the *petD* gene (WT or mutant) and transformants were selected on photoautotrophic growth (MIN medium). The *ftsh1-1* strain was transformed with plasmid pWBA containing the *petB* gene (WT or mutant) and the *aadA* cassette and transformants were selected on their resistance to spectinomycin (TAP-spectinomycin medium, 500 mg.mL^{-1}). The *stt7-1/stt7-9* strains were transformed with plasmid pWQA-Y124K containing the mutated *petD* gene and the *aadA* cassette and transformants were selected on their resistance to spectinomycin (TAP-spectinomycin medium, 500 mg.mL^{-1}). Cells were grown over-night (25°C, 120 rpm) in 20 mL

TAP medium in 100 mL Erlenmeyer flasks. This starter culture was used to inoculate 200 mL TAP medium (in 1 L flasks) and this procedure was repeated daily for at least three consecutive days in order to keep the cells in exponential growth phase. Freshly inoculated 200 mL TAP cultures containing cells in exponential growth phase (between $1x10^6$ and $4x10^6$ cells.mL^{-1}) were used for chloroplast transformations. Cells were harvested by centrifugation and re-suspended in TP (Δ*petD*) or TAP (*ftsh1-1; stt7-1/stt7-9*) medium to a concentration of $200x10^6$ cells.mL^{-1}. 100 µL of this suspension was plated on TP-agar plates (Δ*petD*) or TAP-agar plates supplemented with 500 µg.mL^{-1} spectinomycin (*ftsh1-1; stt7-1/stt7-9*) to give $20x10^6$ cells per plate and per transformation. 5 µL of 0.5-2 µg.µL^{-1} $pWQH_6$ (Δ*petD*), pWBA (*ftsh1-1*) or pWQA-Y124K (*stt7-1/stt7-9*) plasmid DNA preparations containing WT or mutated genes was added to 50 µL of Binding Buffer in a sterile Eppendorf tube. 60 µL S550d gold carrier particles at 50 mg.mL^{-1} was added and the tube was left to incubate on ice for 1 minute. 100 µL of Precipitation Buffer was added and incubated on ice for 1 minute. The suspension was vortexed 5 seconds and centrifuged at 13000 rpm for 30 seconds. The pellet was washed with 500 µL ice-cold 100% EtOH and centrifuged at 13000 rpm for 30 seconds. 50 µL ice-cold 100% EtOH was added to the pellet which was then resuspended with a brief sonication (1-5 seconds, 25V, 25-30% amplitude) using a probe tip sonicator right before transformation to avoid particle aggregation. 10 µL of gold particles coated with plasmid DNA was spread on a membrane holder which was then placed inside the vacuum sealed bombardment chamber along with TP agar plates with Δ*petD* cells or TAP-spectinomycin agar plates with *ftsh1-1* or *stt7-1/stt7-9* cells placed ~20 cm below the holder tip. The following parameters were used: 0.1 bar partial vacuum in the bombardment chamber, 7 bars helium-shot pressure. A total of five shots (five plates, five transformations) were performed with each 50 µl plasmid preparation. After transformation, Δ*petD* cells were left to recover in the dark for up to one day before being transferred to phototrophic conditions (40 $\mu mol_{photons}\ m^{-2}\ s^{-1}$ and air supplemented with 2% CO_2). Once the first transformants became visible (10-14 days), light was increased to 100 $\mu mol_{photons}\ m^{-2}\ s^{-1}$ to speed up growth and subsequent analysis. After transformation, *ftsh1-1* cells and *stt7-1/stt7-9* cells were left in dim light until transformants colonies were large enough for restreaking and subcloning.

D. Nuclear transformation

stt7-1 and *stt7-9* cells grown in 200 mL TAP at 40 $\mu mol_{photons}.m^{-2}.s^{-1}$ to 2-4 x 10^6 cells.mL^{-1} were harvested by centrifugation (3000 rpm, 10 minutes). The pellet was resuspended in 1 mL TAP medium supplemented with 60 mM sucrose and 250 µL was aliquoted in a 0.4 cm gapped electroporation cuvette (1 cuvette per transformation). 40 µg of UltraPure Salmon Sperm DNA (ThermoFisher) was added to the cuvette. 2 µg of *XbaI*/*KpnI*-digested and purified pSLX-Stt7 or pSLX-Stt7+33 plasmid was added to the cuvette, which was mixed gently and placed on ice for 30 minutes. Cells were electroporated (9-12 ms pulse-time, 1875 $V.cm^{-1}$, 25 µF capacitance, ∞ shunt resistance), transferred to a 100 mL flask containing 20 mL TAP medium supplemented with 60 mM sucrose, and left to agitate at 100 rpm in the dark over-night. The next day, cells were harvested by centrifugation (3000 rpm, 5 minutes) and the pellet was resupsended in 500 µL TAP medium. 50 µL and 250 µL of cells were plated on TAP-agar plates supplemented with 12 $\mu g.mL^{-1}$ paromomycin (Sigma) and plates were left in dim light until colonies appeared.

E. Chlorophyll concentration measurements

Chlorophyll can easily be quantified with a spectrophotometer based on the Beer-Lambert Law and the extinction coefficient for chlorophyll. In a classic 1949 study, Arnon reported the following equations for quantification of the total chlorophyll, chlorophyll *a* and chlorophyll *b* content in an 80% acetone extract (Arnon 1949):

Chlorophyll *a* ($\mu g.ml^{-1}$) = 12.7 (A_{663}) - 2.69 (A_{645})
Chlorophyll *b* ($\mu g.ml^{-1}$) = 22.9 (A_{645}) - 4.68 (A_{663})
Total Chl ($\mu g.ml^{-1}$) = 20.2 (A_{645}) + 8.02 (A_{663})

where A_{663} is the solution absorbance at 663 nm andA_{645} is the absorption at 645.

Unfortunately, the Arnon equations are not particularly accurate (Porra 2002). Other equations have been derived that minimize the problems with the Arnon equations. For example, Lichtenthaler & Welburn report the following equations to determine chlorophyll *a*, chlorophyll *b* and carotenoid content in 80% acetone extracts (Lichtenthaler and Wellburn 1983):

Chlorophyll *a* ($\mu g.ml^{-1}$) = 12.21 (A_{663}) - 2.81 (A_{646})
Chlorophyll *b* ($\mu g.ml^{-1}$) = 20.13 (A_{646}) - 5.03 (A_{663})

Carotenoids ($\mu g.ml^{-1}$) = ($1000A_{470}$ - 3.27[Chl *a*] - 104[Chl *b*])/227

And, more recently Porra reports the following equations in buffered aqueous 80% acetone (Porra 2002):

Chlorophyll *a* ($\mu g.ml^{-1}$) = 12.25 ($A_{663.6}$) - 2.55 ($A_{646.6}$)
Chlorophyll *b* ($\mu g.ml^{-1}$) = 20.31 ($A_{646.6}$) - 4.91 ($A_{663.6}$)
Total Chl ($\mu g.ml^{-1}$) = 17.76 ($A_{646.6}$) + 7.34 ($A_{663.6}$)

If the absorbance was greater than 0.8 then the solutions were diluted with fresh 80% acetone and re-measured. All chlorophyll concentration measurements were done according to these equations.

F. *In vivo* biochemistry

1. Analysis of protein accumulation by Western-Blot

Cells grown in TAP and low light to around 2-4 x 10^6 cells.mL^{-1} were harvested by centrifugation 10 min at 2500 rpm. The supernatant was discarded and the pellet was resuspended in 1 mL of 80% acetone and incubated at -20°C for 1-2 hours. The sample was centrifuged 30-45 minutes at 4000 rpm at 4°C. The 1 mL supernatant was transferred to a clear cuvette and chlorophyll concentration was measured as described previously. A volume of loading buffer (1X NuPage LDS, 1X NuPage Reducing Agent) corresponding to ten times the $\mu g.mL^{-1}$ value was used to fully resuspended the pellet. The sample was incubated 5 minutes at 95°C, spun down and 10 µL was loaded on a 10% Bis-Tris gel, which was run at 200 V for 30 to 45 minutes. After staining of the gel with Coomassie blue, the total protein concentration was quantified on an Odyssey scanner (LI-COR Biosciences) and the relative protein concentrations of each sample adjusted.

For the analysis of protein accumulation by Western-Blot, samples were loaded at equal protein concentration on a 12% Bis-Tris gel. The electrophoresis was run at 120 V for the length of the stacking gel and 180 V for the rest of the migration. The gel was transferred to a nitrocellulose membrane using a semi-dry transfer setup (2 $mA.cm^{-2}$, 1 hour) or an iBlot Dry Blotting system (ThermoFisher). The membrane was blocked with 3% non-fat dried milk or 3% BSA in 1X

TBST over-night and then incubated for 1 hour with a primary antibody against the protein of interest in 1X TBST. The membrane was washed three times for 5 minutes in 1X TBST and then incubated with the appropriate secondary antibody for 45 minutes. After an additional washing cycle, the membrane was revealed using commercially-available HRP-reactive chemiluminescent substrates on a G:Box imager (Syngene).

2. *Phosphorylation of LHCII antenna proteins by Western Blot*

A culture containing cells grown in TAP and low light to around 2-4 x 10^6 cells.mL^{-1} was separated in two: 5 mL were transferred to a 100 mL Erlenmeyer, supplemented with 10 µM DCMU and incubated for 30 minutes at ~40 $\mu mol_{photons}.m^{-2}$ s^{-1} under strong agitation (induction of State I), 5 mL were transferred to a 5 mL syringe which was sealed and placed in the dark for 30 minutes after removal of all the air bubbles (dark anoxia, induction of State II). 3 mL of each sample was added to 12 mL of cold 100% acetone to extract proteins without affecting their phosphorylation levels, and the samples were incubated at -20°C for 1-2 hours. After centrifugation (30-45 minutes, 4000 rpm, 4°C), chlorophyll content was measured as described previously, and the pellet was resuspended in a volume of loading buffer (1X NuPage LDS, 1X NuPage Reducing Agent, 6 M urea) corresponding to 150x the chlorophyll value ($\mu g.mL^{-1}$). The sample was incubated 30 minutes at 37°C, spun down and the total protein concentration was obtained as described in the previous section. For the analysis of LHCII protein phosphorylation by Western-Blot, samples were loaded at equal protein concentration on a 15% Tris-Glycine containing 6 M urea. The electrophoresis was run at 120 V for the length of the stacking gel and up to 180 V for the rest of the migration. The proteins were transferred to a nitrocellulose membrane that was then blocked, as described in the previous section. The membrane was incubated with an anti-phosphothreonine antibody (Cell Signaling, 1/1000 in 1X TBST+3% BSA) for one hour and then revealed as described in the previous section.

3. *Phosphorylation of LHCII antenna proteins by ^{33}P-labelling and autoradiography*

Cells grown in TAP and low light to around 2 x 10^6 cells.mL^{-1} were harvested and re-suspended in a phosphate-depleted minimal medium. After 30 minutes of acclimation in moderate light (~50 $\mu mol_{photons}.m^{-2}$ s^{-1}), 2 $\mu Ci.mL^{-1}$ $^{33}P_i$ was added and samples were incubated in moderate light for 90 minutes to reach a steady-state level of phosphorylation. Samples were then divided in two and incubated for 30 to 45 minutes under conditions favoring either the oxidation (10 µM DCMU, moderate light, strong agitation) or the reduction ([2 mg/mL glucose oxidase, 20 mM glucose, dark] *or* [5 µM FCCP, dark]) of the PQ pool. The cell suspensions were transferred on ice and supplemented with 10 mM EDTA, 200 µM PMSF and 0.3 M sucrose as lysis buffer, along with 10 mM NaF to inhibit the activity of phosphatases and maintain the phosphorylation levels reached at the end of the State I/State II treatments. Thylakoid membranes were then isolated based on the protocol by (Chua and Bennoun 1975), as detailed below. HEPES solutions were prepared as follows:

Table M4. Composition of HEPES buffers used for sucrose-gradient purification of thylakoid membranes.

	HEPES III	**HEPES V**	**HEPES VI**
1 M HEPES	1 mL	2 mL	5 mL
200 mM EDTA pH 7.5	10 mL	20 mL	50 mL
2 M sucrose	180 mL	100 mL	-
H_2O	qsp. 200 mL	qsp. 400 mL	qsp. 1 L

Cells were lyzed at 400 psi with a French Press and centrifuged 20 minutes at 27000 g. The pellet was re-suspended in 4 mL HEPES III and deposited in a round-bottom tube compatible with buckets for ultracentrifugation using a swinging rotor (SW Ti Rotor type, Beckman Coulter). 8 mL of HEPES V was carefully deposited with a syringe and needle on top of the HEPES III layer containing the lyzed cells, and the sample was centrifuged 1 hour at 40000 rpm. The layer corresponding to thylakoid membranes was harvested and re-suspended in 10 mL HEPES VI. The suspension was centrifuged 20 minutes at 27000 g, re-suspended in 1 mL HEPES VI, transferred to an Eppendorf tube and centrifuged again at 13000 rpm for 2 minutes. The pellet was re-suspended in an equal volume of 0.1M DTT/carbonate. An equal total volume of 5% SDS and 30% sucrose was added and the sample was denatured at 95°C for 5 minutes. The sample was spun down, 10 µL was added to 1 mL of H_2O and the optical density (OD) was measured at 680 nm. The rest of the sample was loaded (volume in µL = 1.64/OD) on a large 12-18% polyacrylamide gradient gel containing 8 M urea (see Table M5 for gel preparation guidelines). The gel electrophoresis was run at 20 mA over-night (initial voltage 100 V, final voltage ~350 V). The gel was stained with Coomassie blue for 1 hour in order to visualize the

migration and de-stained with 40% AcOH, 20% EtOH and 2% glycerol for 1 hour. It was then dried and exposed on a Phosphor Screen enclosed in a cassette for at least 2 days. Laser-induced stimulation with a Typhoon scanner (GE) was used to detect light emission from the screen, which was proportional to the amount of radioactivity in the gel samples. The digitized signal was analyzed with ImageJ (Rasband 1997).

Table M5. Composition of gels and buffers for large, IBPC-style 12-18% gradient gels

RUNNING GEL	18%	12%
Urea (8 M final)	19.4 g	19.4 g
40% Acrylamide	9 mL	6 mL
40% Acrylamide/Bis 37.5:1	9 mL	6 mL
3 M Tris-HCl pH 8.8 (375 mM final)	5 mL	5 mL
Sucrose	5.3 g	-
H_2O	1 mL	8.8 mL
	Low heat & stir	
TEMED	8.4 µL	9.6 µL
10% APS	24 µL	24 µL
STACKING GEL		
30% Acrylamide/ Bis 37.5:1 (5% final)	5 mL	
0.5 M Tris-HCl pH 6.8 (125 mM final)	7.5 mL	
H_2O	17.3 mL	
TEMED	20 µL	
10% APS	200 µL	
RUNNING BUFFERS	Bottom	Top
5X Tris-Glycine	100 mL	180 mL
0.2 M EDTA pH 7.5	100 mL	4.5 mL
20% SDS	100 mL	4.5 mL
H_2O	qsp. 500 mL	qsp. 900 mL

G. *In vitro* biochemistry

1. Purification of cyt b_6f complexes

The cyt *b_6f* complex was purified based on the protocol that enabled the resolution of its crystal structure (Stroebel et al. 2003). All work was done on ice or at 4°C. A tube containing 5 mL of thylakoid membrane preparation (2-3 mg.mL^{-1} of chlorophyll) kept at -80°C was thawed in water. 5 mL of solubilisation buffer (40 mM Tris-HCl, 24 mM *n*-Dodecyl β-D-maltoside (DDM), pH 8) was added and the preparation was agitated in a beaker with a magnetic stirrer for 10 minutes. The sample was transferred to a round-bottom centrifuge tube compatible with buckets for ultracentrifugation using a swinging rotor and centrifuged 10 min at 347500 *g* (SW

70 Ti, Beckman Coulter). The supernatant containing the solubilized proteins was recovered and loaded on a 5 mL HiTrap Q HP column linked to an ÄKTA-Purifier chromatography system and pre-equilibrated in buffer A14 (20 mM Tris-HCl, 1 mM DDM, pH 8). The column was washed first with buffer A14 and then with 70 mM NaCl with buffer A16 (20 mM Tris-HCl, 0.5 mM DDM, pH 8) supplemented with 7% buffer B2 (20 mM Tris-HCl, 1 M NaCl, 0.4 mM DDM, pH 8). The column was eluted with 220 mM NaCl with buffer A16 supplemented with 22% buffer B2. The elution fraction was loaded on a 1 mL HisTrap HP column pre-equilibrated in buffer A12 (20 mM Tris-HCl, 250 mM NaCl, 0.3 mM DDM, pH 8). The column was washed with buffer A12 supplemented with 2,5% and then 5% buffer B1 (20 mM Tris-HCl, 250 mM NaCl, 400 mM imidazole, 0.3 mM DDM, pH 8) and cyt b_6f complexes were eluted with buffer A12 supplemented with 75% buffer B1. The elution fractions were pooled, transferred to Buffer D (20 mM HEPES-KOH, 250 mM NaCl, 0.2 mM DDM, pH 8.0) using a Zeba™ Spin Desalting column (7K MWCO, ThermoFisher) and concentrated (Amicon® Ultra Filter, Millipore).

2. *Purification of Stt7*

As reported previously (Singh et al. 2016), the kinase domain of Stt7 is not easily expressed and purified as a soluble protein. Several Stt7 gene fragments, *E. coli* expression vectors and purification protocols were tested with the aim of obtaining a pure, soluble, active and sufficiently concentrated protein. The following is an account of all the significant observations that were made during this process:

- *Stt7 fragment* – Best results were obtained when expressing the shortest functional fragment of Stt7 corresponding to its kinase domain (residues 139 to 495). Attempts at expressing the kinase domain along with the N-terminal and transmembrane domains did not yield better results, unlike what was reported in (Singh et al. 2016) about transmembrane helices stabilizing the protein as a tetramer. Similarly, expression of the entire stromal domain (residues 123 to 754), including regions of predicted structural instability (like between residues 634 to 651), did not facilitate the purification procedure.

- *E. coli expression vectors* – pET28-derived vectors pLIC03 and pLIC07 were used primarily. Owing to the presence of contaminants in the initial purification experiments (see "Purification protocol" section below), a pET22 vector containing a periplasm targetting peptide was also used. However, this method was discarded because small amounts of protein were recovered following periplasmic extraction, either due to a faulty expression of Stt7 in

that compartment or to a loss of protein during the extraction procedure. The pLIC07 vector contains a thioredoxin domain fused to the N-terminal of the protein of interest and its use seemed to improve the folding and solubility of Stt7. The downside of this system is that it adds wasteful steps to the procedure, namely an incubation with the TEV protease to cleave off the thioredoxin domain and a nickel affinity purification to remove the His-tagged thioredoxin and protease and recover the free protein in the column flow-through. Although this method may work well for easily expressed and fully soluble proteins, it did not yield satisfactory results in the tricky case of Stt7. As described below, the best results were obtained when using vector pLIC03 with a His-tag and a Strep-tag at the N- and C-terminals of Stt7, respectively.

- *Purification protocols* – Many factors determine the success or failure of the lysis and purification steps: the components and pH of the lysis and purification buffers, the method used to lyze the cells and recover the proteins, the type, volume and order of use of the chromatography columns, the choice of additives (salts, detergents, glycerol, metal chelators, reducing agents), etc. The choice of purification technique and steps was therefore made by trial and error. Despite the addition of DNase in the lysis buffer, DNA or RNA contamination of the supernatant after the lysis step prompted us to add an incubation step in the presence of 0.05% polyethyleneimine (PEI) to precipitate the nucleic acids, which were effectively removed after a second centrifugation with no loss of Stt7 (see anti-His and anti-Strep immunoblots for sample P2, Figure M1C). Addition of a reducing agent to all buffers, either 2-Mercaptoethanol (βME) or tris(2-carboxyethyl)phosphine (TCEP), greatly improved the purification, possibly by increasing the stability of the kinase. We first followed a rather common purification protocol that consisted in a 5mL nickel immobilized metal affinity chromatography column (Ni-IMAC column) followed by a 300 mL size exclusion chromatography column (SEC column, or gel filtration column, GF). Comparing the anti-His and anti-Strep immunoblot signals of the B7 elution fraction (Figure M1C-D), we noticed that the anti-Strep antibody recognized Stt7-KD and a smaller peptide that was most likely an N-terminal degradation product. We also observed that loading the crude supernatant directly on a 5mL Ni-IMAC systematically resulted in contamination by two *E. coli* proteins that were identified by MS as the 50S ribosomal protein L2 (RL2) and the SlyD isomerase (Figure M1C).

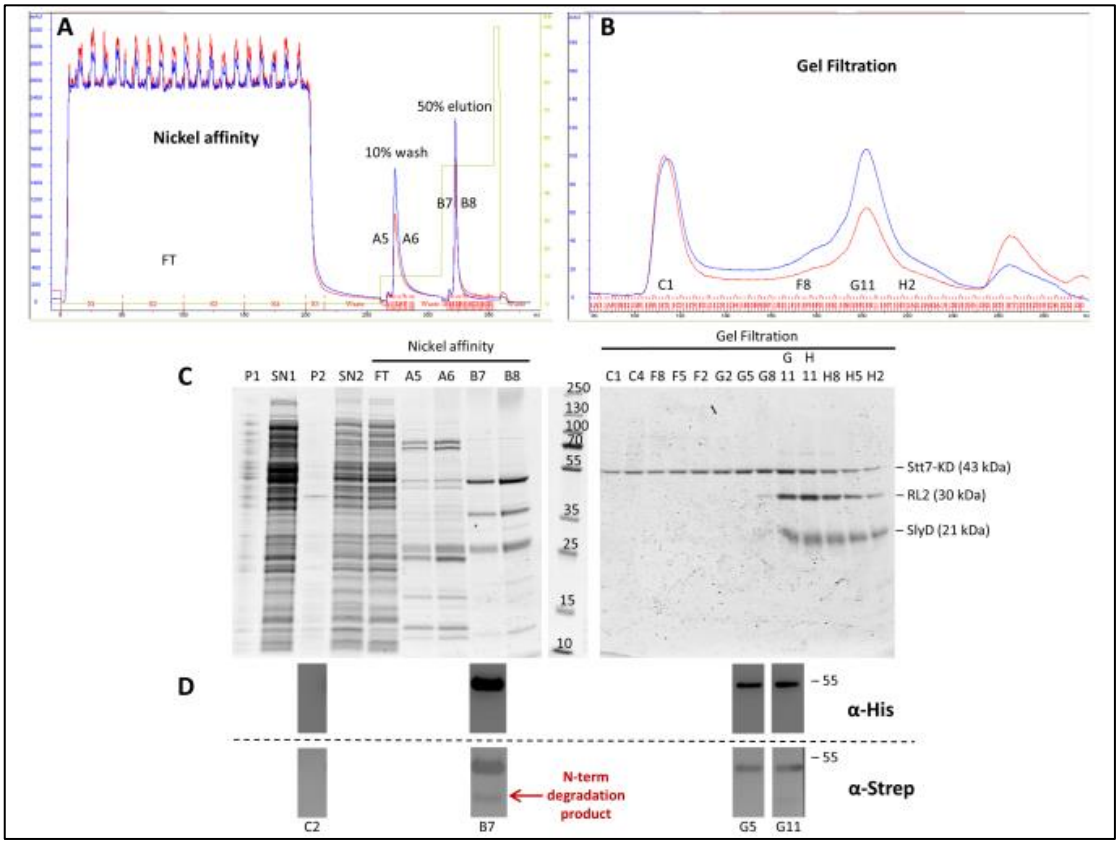

Figure M1. Typical result of initial Stt7-KD purification procedures.
Absorbance chromatograms showing the elution profiles of the Ni-IMAC **(A)** SEC columns **(B)**. Wash and elution steps are depicted by the green curve. Representative elution fractions were analyzed by SDS-PAGE **(C)** and Western Blot with antibodies recognizing the N-terminal His-tag and C-terminal Strep-tag **(D)**. P: pellet; SN: supernatant; FT: flow- through.

The prolyl isomerase SlyD is involved in metal homeostatis in *E. coli* and specifically binds divalent metal ions such as nickel along a C-terminal patch that contains 28 metal-binding amino acids including 15 histidines (Roof et al. 1994; Hottenrott et al. 1997; Weininger et al. 2009; Kaluarachchi et al. 2011). This can result in significant SlyD contamination of Ni-IMAC preparations of heterologously expressed His-tagged proteins (Bolanos-Garcia and Davies 2006). *E. coli slyD* mutant and knockout strains have been engineered but show significant growth defect (Wulfing et al. 1994; Roof et al. 1997), which prompted other groups to try engineering strains with reduced SlyD affinity for divalent metal ions (Robichon et al. 2011; Andersen et al. 2013). Aware of its lower affinity for cobalt (Kaluarachchi et al. 2011), we tried to replace the nickel column with a cobalt column (TALON) but did not obtain better results. These options were of no help for the other less known contaminant, the 50S ribosomal protein L2. Instead, we noticed that Stt7-KD, RL2 and SlyD had theoretical isolelectric points (pI) of 7.9, 10.9 and 4.9, respectively, and attempted to separate the three proteins by anion exchange chromatography at pH 9.0 after the Ni-IMAC step. Although we did manage to elute the three

proteins differentially, Stt7 could not be recovered in sufficient quantity and purity. Finally, we decided to make use of the C-terminal Strep-tag that had been included in the Stt7-KD construct to clarify the total protein extract on a streptavidin column prior to loading on the Ni-IMAC column Due to the strength and specificity of interaction between the Strep peptide and the streptavidin protein, this step was very effective in removing all the major *E. coli* contaminants and enriching the protein extract in Stt7-KD. Furthermore, the protein would be eluted in ~25 mL which permitted the use of a more resolutive 1 mL Ni-IMAC column and recovery of the pure Stt7-KD in ≤ 4 mL. Minimizing the final elution volume was a great advantage as the protein showed no tolerance to concentration by centrifugation and would often go out of solution at this step. The following optimized protocol (see corresponding purification results shown in Figure M2) typically allowed the recovery of ~100 µg of Stt7-KD (~ 0.5 µL @ 5 µM) from a 2 L *E. coli* culture grown to an $OD_{600\ nm}$ of ~7 in TB medium over-night:

> Cultures of *E. coli* Rosetta cells transformed with plasmid pLIC03-Stt7KD were grown at 37°C, induced at an optical density of 0.6-0.8 with 400 µM IPTG and grown overnight at 17°C. Cells were harvested by centrifugation (4000 *g*, 20 min, 4°C), resuspended in lysis buffer (50 mM Tris Buffer, 300 mM NaCl, 2.5 mM *β*ME, 0.25 $mg.mL^{-1}$ lysozyme, 5% glycerol, protease inhibitor cocktail (pH 8.0)) and frozen at -80°C. The thawed cells were then lyzed by sonication and centrifuged (15000 *g*, 40 min, 4°C). The supernatant was incubated with 0.05% PEI for 30 min at 4°C to precipitate contaminating DNA molecules. The suspension was centrifuged (15000 *g*, 40 min, 4°C) and Stt7-KD was then purified on an ÄKTA-Purifier chromatography system. The clear supernatant was loaded on a hand-packed column containing Streptavidin Sepharose™ HP beads (5 mL, GE) pre-equilibrated with Buffer A (50 mM Tris Buffer, 300 mM NaCl, 2.5 mM *β*ME (pH 8.0)). Unbound or weakly bound proteins were washed with Buffer A and bound proteins eluted with Buffer A supplemented with 2.5 mM desthiobiotin (Figure M2A). The elution fractions were pooled and loaded on a HisPur™ Ni-NTA column (1 mL, ThermoFisher) pre-equilibrated with Buffer B (50 mM Tris Buffer, 300 mM NaCl, 2.5 mM *β*ME, 10 mM imidazole (pH 8.0)). Unbound or weakly bound proteins were washed with Buffer B. The column was washed with Buffer B containing 34 mM imidazole and His-tagged Stt7-KD was eluted with Buffer B containing 250 mM imidazole (Figure M2B). The pooled elution fractions were transferred to Buffer C (20 mM HEPES-KOH, 300 mM NaCl, 2.5 mM TCEP

(pH 8.0), Zeba™ Spin Desalting 7K MWCO, ThermoFisher) and concentrated (Amicon® Ultra Filter, Millipore) for subsequent *in vitro* experiments. Figure M2C shows SDS-PAGE analysis of the purification procedure.

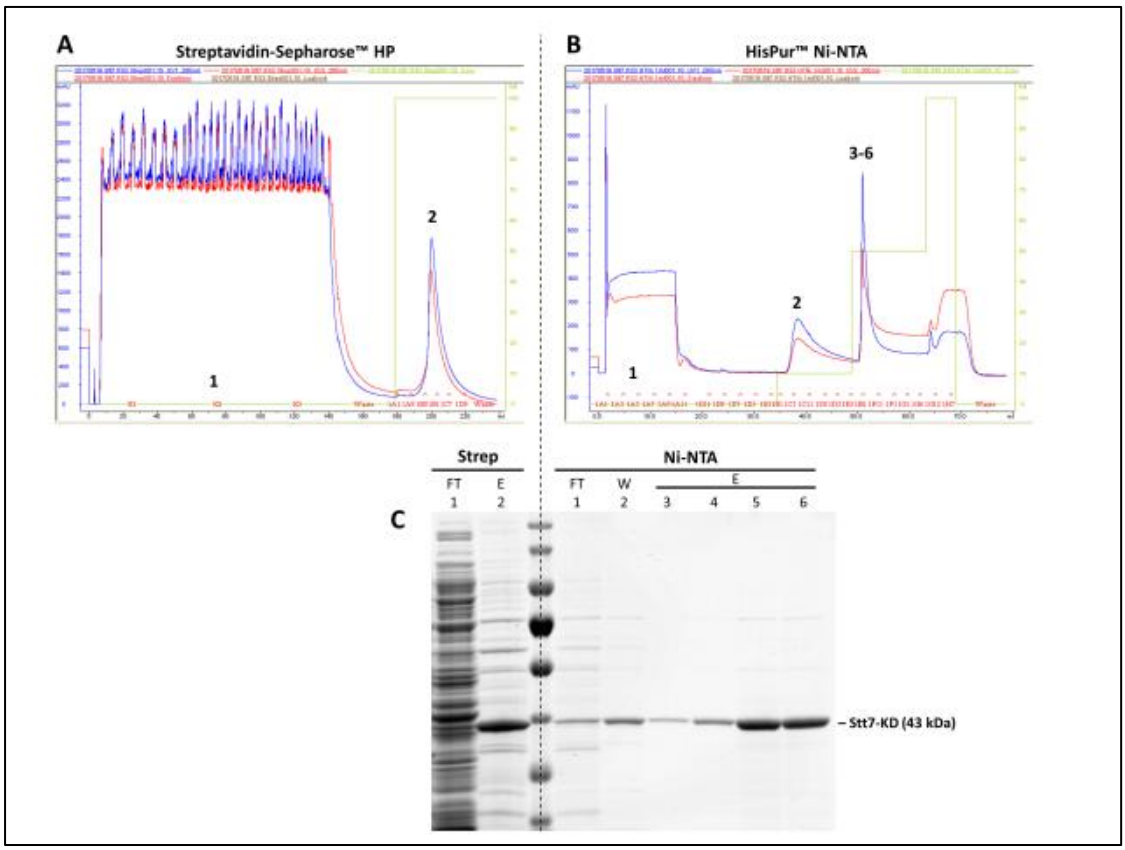

Figure M2. Purification of Stt7 kinase domain.
(A) Absorbance chromatograms showing the elution profiles of the Streptavidin Sepharose™ HP column and **(B)** the HisPur™ Ni-NTA column. Wash or elution steps are depicted by the green curves. **(C)** Representative elution fractions were analyzed by SDS-PAGE. FT: flow- through; W: wash; E: elution.

3. *Cross-linking*

The water-soluble, homobifunctional, amine-reactive, non-deuterated cross-linker Bis(sulfosuccinimidyl) 2,2,4,4-glutarate-d0 (BS^2G, ThermoFisher) was aliquoted into 5 mg in vials that were flushed with argon, sealed and stored at -20°C with a dessicant. Right before use, 15 µL of DMSO was added to the vial to dissolve the powder and obtain a concentration of 625 mM. Two other BS^2G stock solutions at 125 mM and 62.5 mM were prepared by dilution. Total reaction volumes (100 µL) were calculated so as to allow sampling and quenching of 19 µL of the cross-linking reaction with 20 mM NH_4HCO_3 at five different time points over the 2-hour total reaction time. All reactions were carried out on ice. 5 µM cyt b_6f complex and 5 µM Stt7-KD, both in 20 mM HEPES-KOH pH 8, were mixed together in 1:1 or 1:3 molar ratios or with HEPES buffer for the control reactions. 2 µL of 62.5 mM, 125 mM or

625 mM BS^2G was added to reactions to obtain final concentrations of 1.25 mM, 2.5 mM and 12.5 mM, respectively, corresponding to 500x, 1000x and 5000x molar excess of cross-linker. The quenched reaction samples were supplemented with loading buffer, denatured 5 min at 95°C and loaded on 4-12% gradient gels for SDS-PAGE and immunoblot analysis with antibodies against Stt7 and subunit IV.

4. Native-PAGE

1 µM cyt b_6f complex and 1 µM Stt7-KD were incubated for 30 minutes at room temperature at 1:1, 1:5 and 1:10 molar ratios. 1X NativePAGE Sample Buffer and NativePAGE 5% G-250 Sample Additive (Thermo Fisher) were added and samples were run on a 4-16% NativePAGE Bis-Tris gel (30 min 150V Dark Blue, 1 h 150 V Light Blue). The gel was rinsed in TGS buffer and proteins were transferred to a PVDF membrane, pre-soaked in 100% EtOH or MetOH and rinsed with water, using a wet transfer setup in TGS buffer (15 mA over-night). An HRP-conjugated antibody recognizing the His-tags of cyt *f* and Stt7-KD was used to detect the proteins on the membrane.

5. Autophosphorylation assays

4.5 µM of purified Stt7-KD and 1.5 µM of purified WT or Arg125Glu cyt b_6f complex were incubated together with 1 mM ATP and 20 mM $MgCl_2$ for 30 minutes. Samples were denatured in a buffer containing LDS and DTT at 70°C for 15 min and separated on a 10% Bis-Tris gel by SDS-PAGE. After transfer on a nitrocellulose membrane, antibodies against phospho-threonine (Cell Signaling), Strep-tag (recognizing the C-terminal tag of Stt7-KD) and subunit IV were used to detect the proteins.

6. ATP hydrolysis assays

Following the protocol of the ADP-Glo™ Kinase Assay kit (Promega), 1 µM purified Stt7-KD was incubated with 1 mM ATP, with or without purified WT or Arg125Glu cyt b_6f complex, in a 25 µL kinase reaction containing 40 mM Tris-HCl, 20 mM $MgCl_2$ and 0.1 mg/mL BSA at room temperature for 30 minutes. An equal volume of ADP-Glo™ Reagent was added to the reaction and left to incubate at room temperature for 40 min to deplete the residual unconsumed ATP. 50 µL of Kinase Detection Reagent containing luciferase and luciferin was then added to convert ADP to ATP and generate a stable luminescence signal, proportional to the amount of

ADP produced during the kinase reaction and therefore correlated with Stt7-KD activity. After incubation at room temperature for one hour, the luminescence signal was measured on an Infinite M200 luminometer (TECAN).

H. Yeast two-hybrid assays

The Matchmaker® Gold Yeast Two-Hybrid System (Clontech) was used to test the direct interaction between subunit IV and Stt7. The nucleotide sequences of the WT and [Y124K; R125E] mutant subunit IV fg loops were cloned as baits into pGBKT7 vectors and various Stt7 nucleotide sequences were cloned as preys into pGADT7 vectors. All vector constructions were verified by sequencing. Y2H Gold yeast cells were transformed with each pGBKT7-suIV vector and Y187 yeast cells were transformed with each pGADT7-Stt7 vector following the small-scale LiAc yeast transformation procedure described in the Yeast Protocols Handbook (Clontech). None of the strains transformed with pGBKT7-suIV plasmids exhibited autoactivation of the reporter genes when spotted on medium lacking Trp and containing 40 $\mu g.mL^{-1}$ X-α-Gal and 150 $ng.mL^{-1}$ Aureobasidin A. Diploids containing each bait-prey plasmid combination were obtained following the yeast mating protocol described in the Handbook and conserved on medium lacking Leu and Trp. Positives clones were selected on medium lacking Trp, Leu and His, supplemented with 40 $\mu g.mL^{-1}$ X-α-Gal with or without 150 $ng.mL^{-1}$ Aureobasidin A. The positive and negative controls were obtained as described in the Matchmaker® Gold User Manual (Clontech).

I. Biophysics

1. Chlorophyll fluorescence emission kinetics

Absorbed light energy can give rise to charge separation, thermal dissipation (q_E component of NPQ) or chlorophyll fluorescence emission. In light conditions that do not induce q_E, the fluorescence yield is therefore inversely proportional to the rate of photosynthetic electron transfer and serves as an endogenous, non-invasive probe of the status of the electron transport chain. The setup described in (Johnson et al. 2009) was used to measure the kinetics of PSII chlorophyll fluorescence emission yield. To screen for state transition mutants, clones on a Petri dish were left aerated in the dark to oxidize the PQ pool and then transferred to a flat box with a transparent lid hooked up to a nitrogen tank. Upon starting the nitrogen flush, a 10-min

sequence in the dark with 12 saturating flashes (2000 $\mu E.m^{-2}.s^{-1}$) giving the maximum fluorescence yield of PSII (F_m) was launched. The increase of the fluorescence yield in the dark (F'_0) showed that the switch to anaerobic conditions induced the reduction of the PQ pool. The fluorescence curves were normalized on the value of the maximum fluorescence yield measured after the first saturating flash and q_T parameters were calculated: $q_T = (F_m - F_m')/F_m'$. For the calculation of other photosynthetic parameters (q_P, F_v/F_m, ΦPSII), a 3 second illumination at 600 $\mu mol_{photons}.m^{-2}.s^{-1}$ was used.

2. *Chlorophyll fluorescence emission spectra*

Chlorophyll was excited with a LED at ~ 455 nm and fluorescence was selected with a red colored Kodak Wratten filter and collected with an Ocean Optics USB2000 CCD spectrometer. *C. reinhardtii* cells were placed in an aluminum-made sample holder and snap frozen at 77K in liquid nitrogen. Sample, LED and spectrometer were coupled *via* a Y-shaped fiberoptics.

3. *Absorbance spectroscopy*

The transmembrane electrogenic phase *b* of electron transfer between b_L and b_H, occurring after quinol oxidation at the Q_o site, was measured as an electrochromic shift (ECS) of carotenoids giving an absorbance increase at 520 nm (Joliot and Joliot 1998). The signal was measured using a Joliot-type spectrophotometer/fluorimeter (JTS-10, Bio-Logic). Electron transfer reactions were measured under anaerobic conditions following a single-turnover of PSI (10 ns flash, 10 mM hydroxylamine and 10 µM DCMU added to inhibit PSII) and normalized on PSI contribution at 100 µs. Changes in the redox states of heme within the cyt b_6f were probed by measuring the kinetics of absorbance changes following a single turnover of PSI (PSII was inhibited by 1 mM hydroxylamine and 10 µM DCMU, excitation is a very short laser flash of 10 ns) obtained in whole cells suspensions adapted under dark-anaerobic conditions. Kinetics were obtained at two different detecting wavelengths, 554 nm for cyt *f* and 563 nm for the *b*-hemes, with or without addition of NQNO.

4. *EPR spectroscopy*

EPR spectra of heme c_i were recorded on purified thylakoid membranes on a Bruker Elexsys E500 X-band spectrometer fitted with an Oxford Instrument He-cryostat ESR900 and temperature control system. The instrument settings were: temperature, 6 K; microwave power,

65 mW; microwave frequency, 9.48 GHz; modulation amplitude, 3 mT. Membrane samples were oxidized with 3 mM ferricyanide, and then washed with 5mM EDTA and MOPS 50 mM pH 7. EPR spectra were normalized between WT and mutants on the g_y contribution of the Rieske protein at $g = 1.89$ after addition of ascorbate.

J. Bioinformatics

Molecular biology and sequence data analyses were done using the Geneious software (Biomatters, (Kearse et al. 2012)). Structural analyses were performed using the UCSF Chimera software (Pettersen et al. 2004). The One-to-One threading tool of the Protein Homology/analogY Recognition Engine V 2.0 (PHYRE2, (Kelley et al. 2015)) was used to model the structure of the kinase domain of Stt7 based on the resolved structure of the kinase domain of its homolog in *Micromonas sp.* RCC299 (MsStt7d, PDB 4IX6).

Appendix

Table A1. *C. reinhardtii* strains used in this work.

Strains	Characteristics	Origin
Δ*petD*	mt^+ acetate-requiring strain deleted for the chloroplast gene *petD* coding for subunit IV of the cyt b_6f.	(Kuras and Wollman 1994)
"WT"	Reference WT strain isolated by complementing the Δ*petD* strain by the WT *petD* gene; contains a His-tag at the 3'-end of the *petA* gene (cyt *f*).	This study
stt7-1	Strain deleted for the nuclear gene *STT7* coding for the Stt7 kinase.	(Depege et al. 2003)
stt7-9	Clone allelic to *stt7-1* with residual Stt7 activity ("leaky" *stt7-1*).	(Depege et al. 2003)
ftsh1-1	Strain expressing an inactive FtsH protease due to a mutation on the nuclear gene *FTSH1* leading to an Arg420Cys substitution.	

Table A2. Oligonucleotides used in this work.

Name	Sequence	Target gene/plasmid; Use
Pseq5_f	TCCGAAATAGAACAAATGCCA	$pWQH_6$; PCR amplification for sequencing of *petD*
P1_f	ACCCATTTGCTACTCCACTTG	pWQH6/*petD*; random mutagenesis (Agilent kit)
P1_r	TGACAGAACTCAGTTTTCCCC	
P2_f	TGGGTGAGCCAGCAAACCCATTTGCTACTCCACTTG	pWQH6/*petD*; random mutagenesis (Clontech kit)
P2_r	TGACAGAACTCAGTTTTCCCCCTTCAGGGTTGC	
T4S_f	TAAATAAATATGTCAGTTAGTAAAAAACCTGATTTA	*petD*; site_directed mutagenesis*
T4V_f	TAAATAAATATGTCAGTTGTTAAAAAACCTGATTTA	
N118D_f	CCGTTCATTGAAAGTATTGACAAATTCCAAAACCCATAC	
N118L_f	CCGTTCATTGAAAGTATTCTCAAATTCCAAAACCCATAC	
K119E_f	TTCATTGAAAGTATTAACGAATTCCAAAACCCATACCGT	
K119L_f	TTCATTGAAAGTATTAACCTATTCCAAAACCCATACCGT	
F120L_f	ATTGAAAGTATTAACAAATTACAAAACCCATACCGTCGT	
F120W_f	ATTGAAAGTATTAACAAATGGCAAAACCCATACCGTCGT	
Q121L_f	GAAAGTATTAACAAATTCCTAAACCCATACCGTCGTCCA	
Q121R_f	GAAAGTATTAACAAATTCCGAAACCCATACCGTCGTCCA	
N122H_f	AGTATTAACAAATTCCAACACCCATACCGTCGTCCAATC	
N122L_f	AGTATTAACAAATTCCAACTCCCATACCGTCGTCCAATC	
N122T_f	AGTATTAACAAATTCCAAACCCCATACCGTCGTCCAATC	
Y124F_f	AACAAATTCCAAAACCCATTCCGTCGTCCAATCGCTACT	
Y124K_f	AACAAATTCCAAAACCCAAAGCGTCGTCCAATCGCTACT	
Y124K; R125E_f	AACAAATTCCAAAACCCAAAGGAGCGTCCAATCGCTACTATC	
R125E_f	AAATTCCAAAACCCATACGAACGTCCAATCGCTACTATC	
R125L_f	AAATTCCAAAACCCATACCTTCGTCCAATCGCTACTATC	
I131D_f	CGTCGTCCAATCGCTACTGACTTATTCCTTTTAGGAACT	
xL215_f	CAAGGTATTTCAGGTCCTTAATAATATTTAATATCCATT	pWBA/*petB*; site_directed mutagenesis*
G216_f	GGTATTTCAGGTCCTCTAGGTTAATATTTAATATCCATT	
R207K_f	ATGCACTTCTTAATGATTAAGAAACAAGGTATTTCAGGT	
Pseq2_f	TCTTAAGAAAGCCTAATGGTC	pWBA; PCR amplification and sequencing of *petB*
Pseq2_r	GAAACTTACGTAGCAGCCT	
Homo-xL215_f	CAAGGTATTTCAGGTCCTTAA	PCR check of *petB* homoplasmy
Homo-WT_f1	CGTAAACAAGGTATTTCAGGTCCTCTA	

Homo-G216_f	GGTATTTCAGGTCCTCTAGGTTAA	PCR check of *petB* homoplasmy (cont.)
Homo-WT_f2	AAACAAGGTATTTCAGGTCCTCTATAA	
Homo-R207K_f	TTAATGCACTTCTTAATGATTAAG	
Homo-WT_f3	ATGTTAATGCACTTCTTAATGATTCGT	
Homo-pWBK1_r	ACCAAGGTAGTCGGCAAATAACTGCAG	
Homo-pWBK2_r	TACTTCGGCGATAACCGCTTCACGAGC	
pLIC03-Stt7_f	GTACTTCCAATCAATGATTGTGCTGGGTAAACGTCTGG	pLIC03; Amplification and cloning of the *STT7* sequence coding for the kinase domain of Stt7 into pLIC03 to express recombinant Stt7-KD
pLIC03-Stt7_r	CGTATCCACCTTTACTGTTATTATTTTTCGAACTGCGGGTGGC TCCAAGCGCTGCTATGCTGCAGGCTTGCGGTA	
b6f-Loop_f	TTCGTCTCGATTCTTCATTGAAAGTATTAACAA	pGBKT7; Amplification and cloning of *petD* sequences to serve as baits in the Y2H experiments
b6f-Loop_r	TTCGTCTCGCCCATTAGATTGGACGACGGTATGGGT	
b6f-Lykre_r	TTCGTCTCGCCCATTAGATTGGACGTTCCTTTGGGT	
Stt7-A_f	TTCGTCTCGATTCCGTGCACCGCTGAAACGCAA	pGADT7; Amplification and cloning of *STT7* sequences to serve as preys in the Y2H experiments
Stt7-A_r	TTCGTCTCGCCCATTAATAAACCCAAACCAGCCAAA	
Stt7-B_f	TTCGTCTCGATTCCTGAGCAGCCTGATGGAACG	
Stt7-B_r	TTCGTCTCGCCCATTATTTTTCCATGGTCCACAGAA	
Stt7-C_f	TTCGTCTCGATTCGGTCATCTGCGTAATGATAA	
Stt7-C_r	TTCGTCTCGCCCATTAGGTCAGCCACGGATGTGCCA	
Stt7-D_f	TTCGTCTCGATTCAGCGCACCGGGTCGTACCGC	
Stt7-D_r	TTCGTCTCGCCCATTAATACGGATCGCTTTCGCTCA	
Stt7-gDNA_fw	ATCCACTAGTTCTAGCATACGCGAAGCGGTTCTAGTGGAGT	pSLX; Amplification and InFusion cloning of the various *STT7* fragments to obtain plasmid pSLX-Stt7
Stt7-gDNA_rv	TAGTCGATGGCGCCTGGTAGCAC	
Stt7-cDNA_fw	AGGCGCCATCGACTATTACATTCGC	
Stt7-cDNA5'_fw	ATGGCTCTGGCCCAGCGC	
Stt7-cDNA_rv	CCGCCGAAAGACTCCCAGCA	
Stt7-3'UTR_fw	GTCTTTCGGCGGGATCGATA	
Stt73'UTR_rv	CGGTGGCGGCCGCTCTAGAAGGCTACAGCGCCAAAGAAA	
Stt7_Pseq2-f	CGTGCTTGCGTATCTCTTCCTCCCA	pSLX-Stt7; Sequencing primers to verify pSLX-Stt7 constructs (to be used along with the seven primers above)
Stt7_Pseq2-r	TGAGGATGGCCTCCTCCATTGACG	
Stt7_Pseq3-f	AGCAGGAGACCGCTTCCAAG	
Stt7_Pseq3-r	AGCATTCTCATAGGAAGCTTGA	
Stt7_Pseq4-f	CGTCAATGGAGGAGGCCATCCTCA	
Stt7_Pseq5-f	CGGCCCCATCCGCAATGCA	
Stt7_AS-fw	GGATCCATACGGTGCGGCCCCATCCGCAATGCAGGTCGGCTC GGCGATCAACA	pSLX-Stt7; Insertion of the 33 bp sequence by whole-plasmid PCR mutagenesis
Stt7_AS-rv	TGCATTGCGGATGGGGCCGCACCGTATGGATCCGACTCCGAC ATGGCCTCCCG	
Stt7_P1-f	CCAAGGCCATTGACAAAAATGACATTGTCCT	pSLX-Stt7; Random mutagenesis of the *STT7* sequence coding for the kinase domain of Stt7 by error-prone PCR
Stt7_P1-r	CGAAGCTGCCGCTGAGGCTGTGCTGCAGGC	
Stt7_P1-r2	TGGACACGGTGGCCTCGAAGCT	
Pseq2-f	ACCCTGCTCGTATTCAAGGT	pWQA-Y124K; In *petA* gene, upstream of *aadA* cassette, used for sequencing of construct (with Pseq5-f to check Y124K mutation)
Homo-Y124K-stt7-1_f	ATTAACAAATTCCAAAACCCAAAG	PCR check of homoplasmy of the *petD*-Y124K mutation in the *stt7-1* strain
Homo-WTpetD-stt7-1_f	ATTAACAAATTCCAAAACCCATAC	

*The reverse complements of the forward primers listed here were used as reverse primers.

Figure A1. Annotated maps of all plasmids used or constructed in this work.

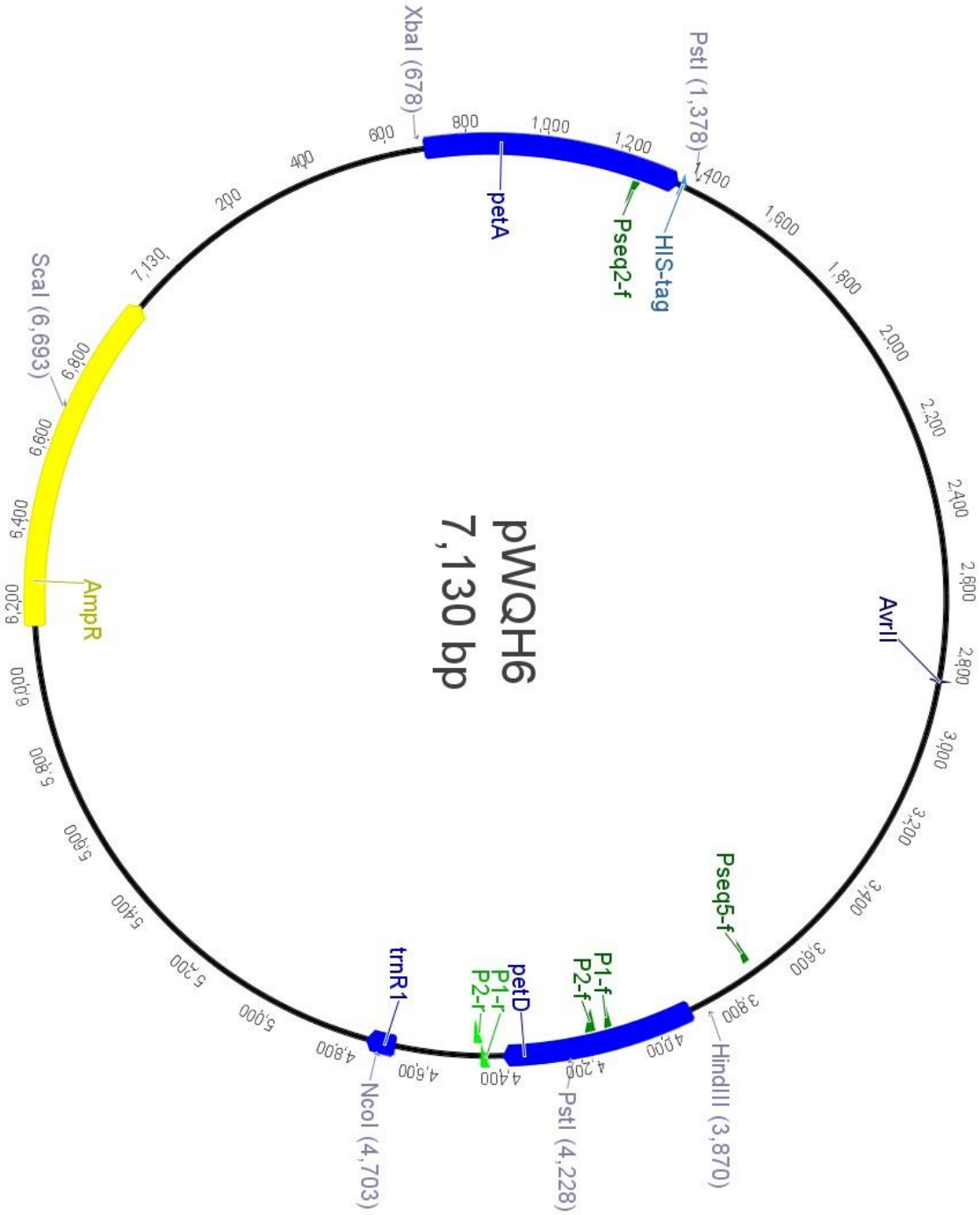
pWQH6
7,130 bp
XbaI (678)
PstI (1,378)
petA
Pseq2-f
HIS-tag
AvrII
Pseq5-f
P1-f
P2-f
petD
P1-r
P2-r
trnR1
NcoI (4,703)
PstI (4,228)
HindIII (3,870)
ScaI (6,693)
AmpR
200
400
600
800
1,000
1,200
1,400
1,600
1,800
2,000
2,200
2,400
2,600
2,800
3,000
3,200
3,400
3,600
3,800
4,000
4,200
4,400
4,600
4,800
5,000
5,200
5,400
5,600
5,800
6,000
6,200
6,400
6,600
6,800
7,130

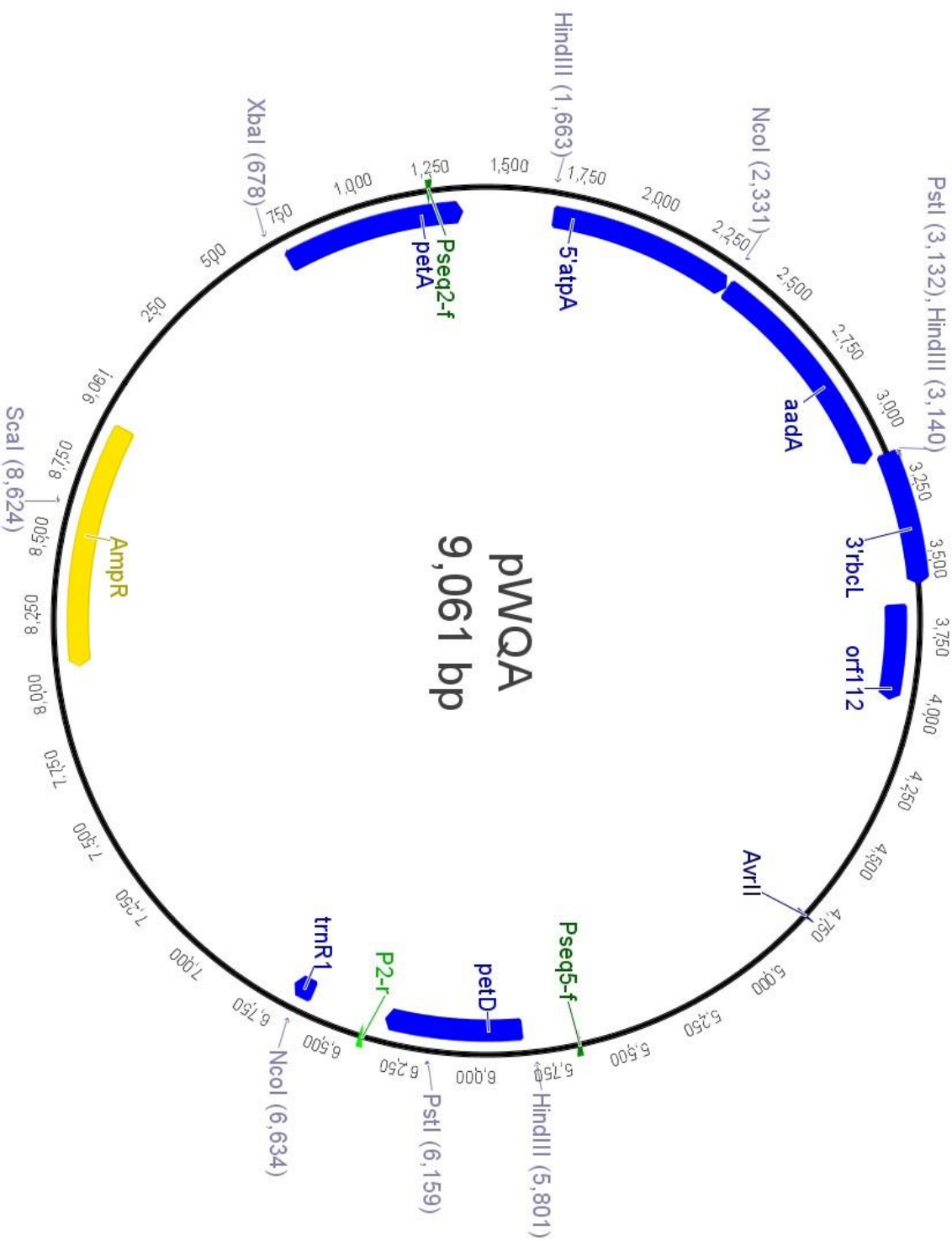
pWQA
9,061 bp
PstI (3,132), HindIII (3,140)
HindIII (1,663)
NcoI (2,331)
XbaI (678)
ScaI (8,624)
AvrII
NcoI (6,634)
PstI (6,159)
HindIII (5,801)
5'atpA
aadA
3'rbcL
orf112
Pseq2-f
petA
Pseq5-f
petD
P2-r
trnR1
AmpR

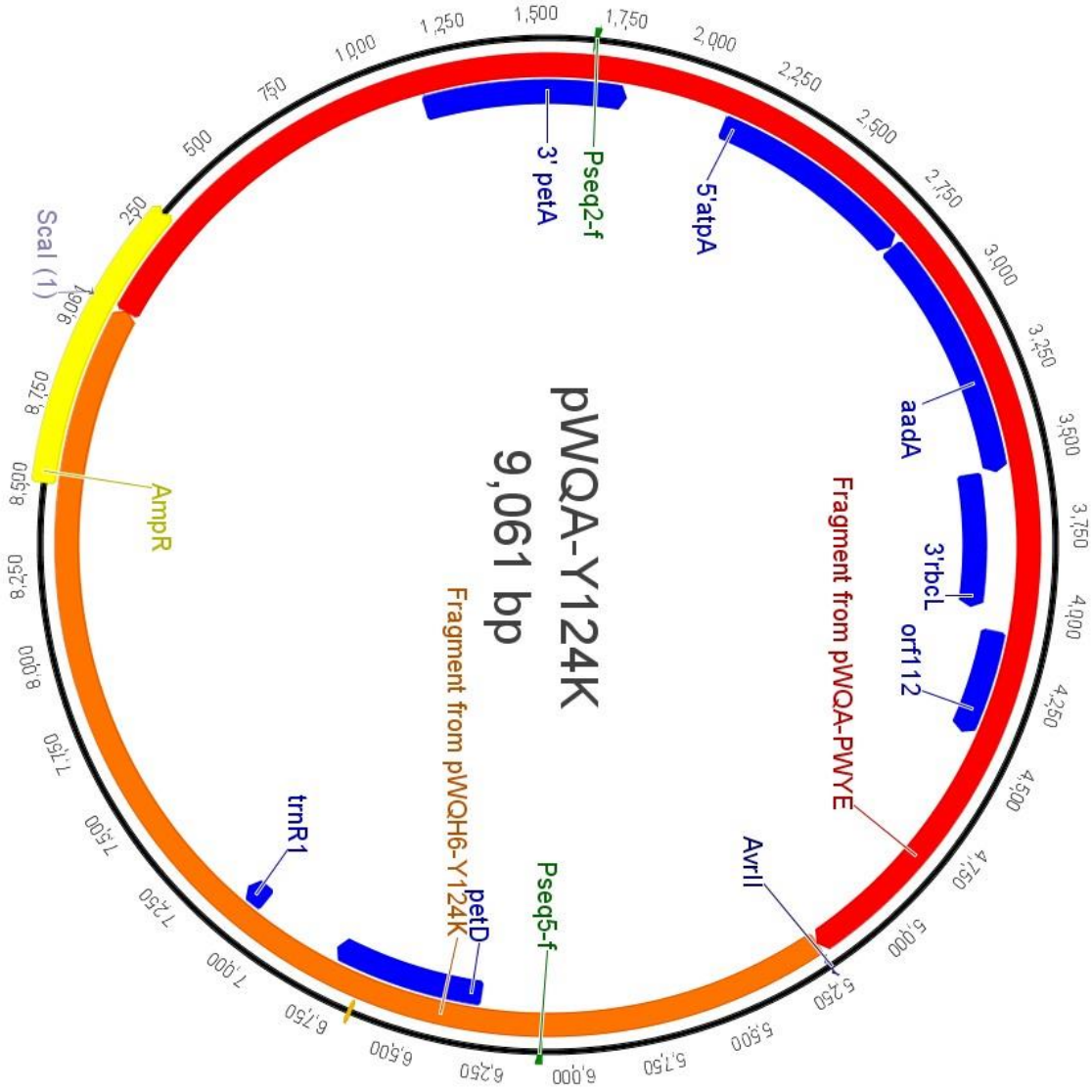
pWQA-Y124K
9,061 bp
1,500
1,750
2,000
2,250
2,500
2,750
3,000
3,250
3,500
3,750
4,000
4,250
4,500
4,750
5,000
5,250
5,500
5,750
6,000
6,250
6,500
6,750
7,000
7,250
7,500
7,750
8,000
8,250
8,500
8,750
9,000
250
500
750
1,000
1,250
3' petA
Pseq2-f
5'atpA
aadA
3'rbcL
orf112
Fragment from pWQA-PWYE
AvrII
Pseq5-f
petD
Fragment from pWQH6-Y124K
trnR1
AmpR
ScaI (1)

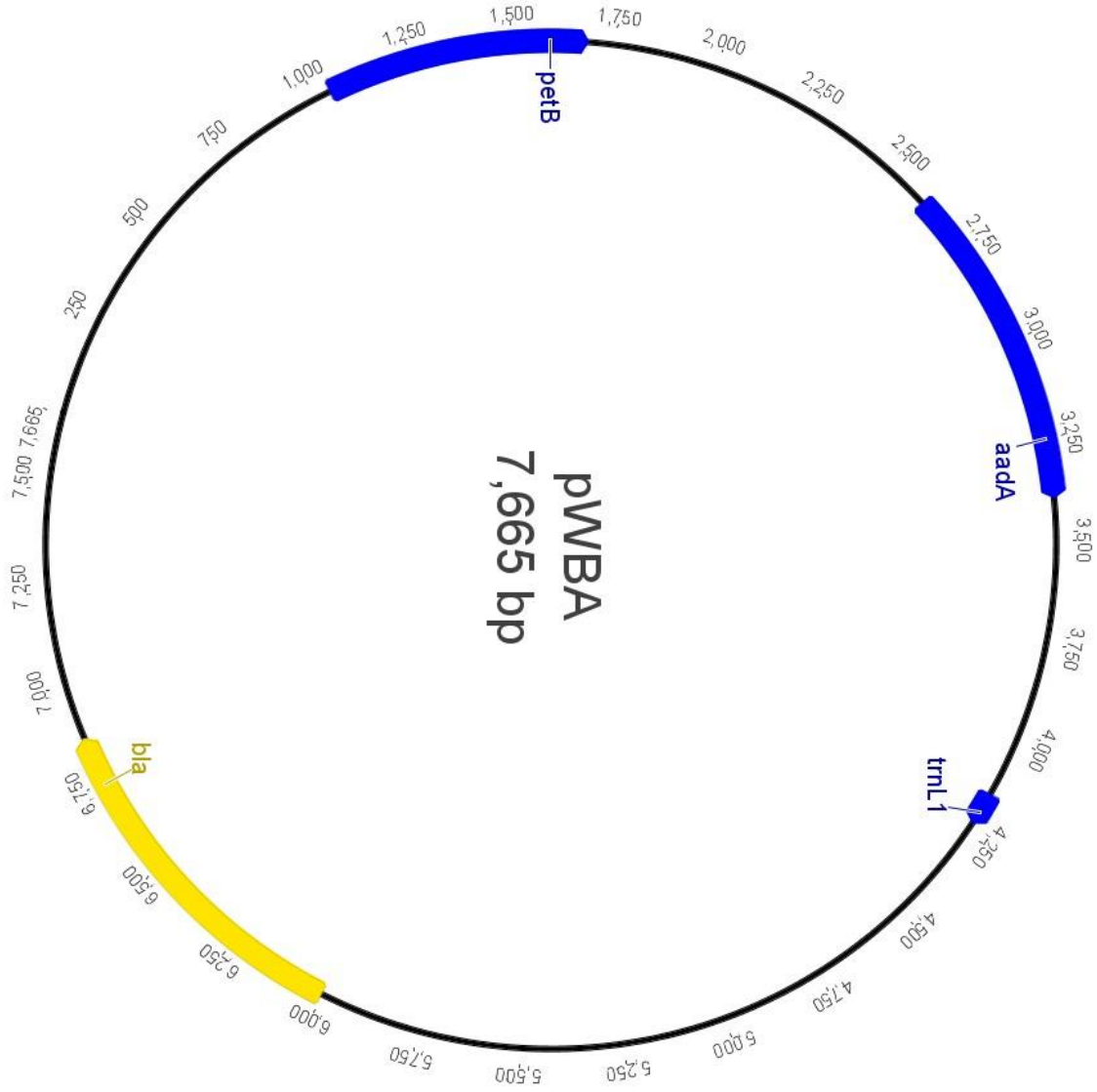
pWBA
7,665 bp
petB
aadA
trnL1
bla
1,000
1,250
1,500
1,750
2,000
2,250
2,500
2,750
3,000
3,250
3,500
3,750
4,000
4,250
4,500
4,750
5,000
5,250
5,500
5,750
6,000
6,250
6,500
6,750
7,000
7,250
7,500
7,665
250
500
750

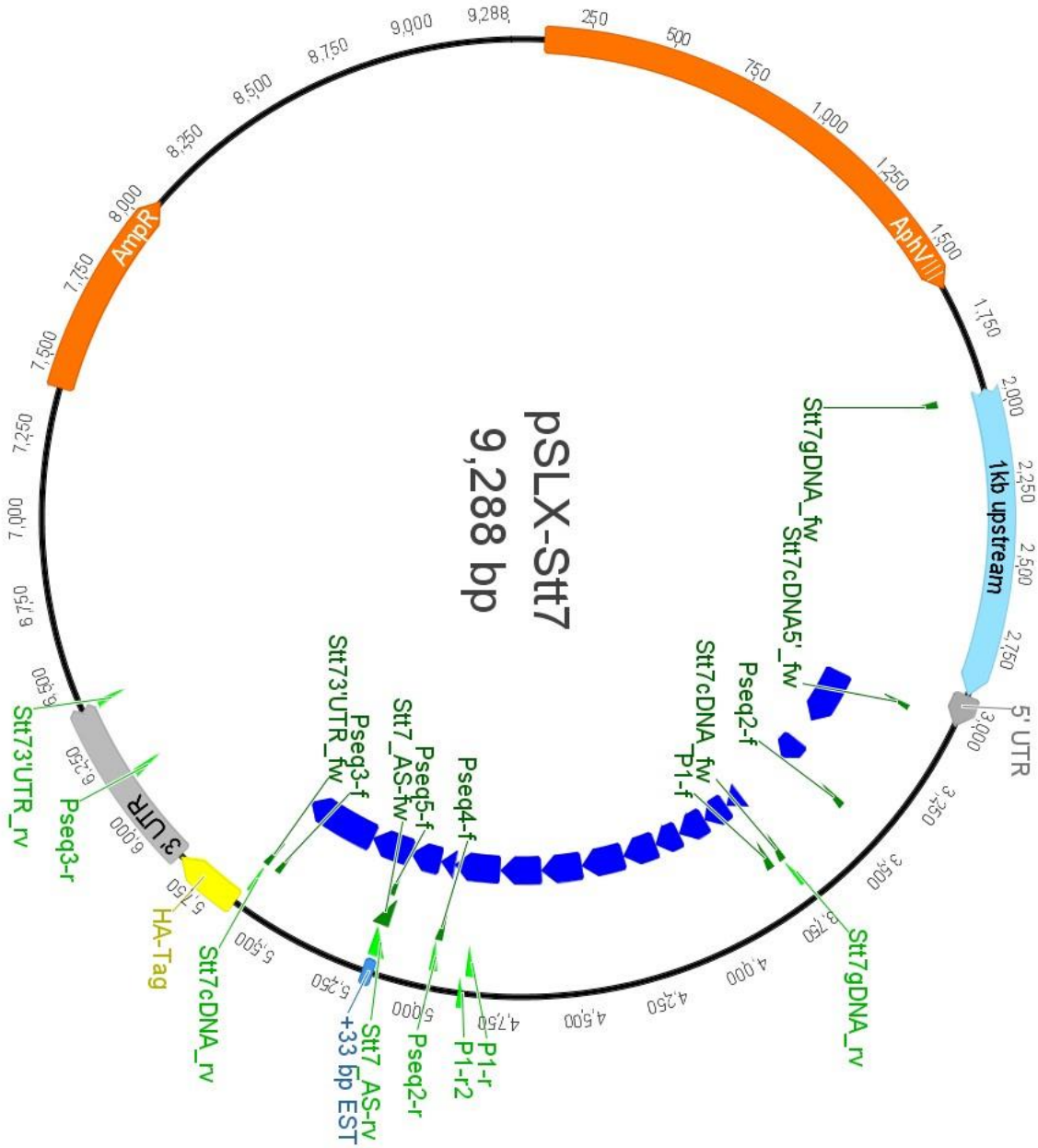
pSLX-Stt7
9,288 bp
1kb upstream
5' UTR
AphVIII
AmpR
3' UTR
Stt7gDNA_fw
Stt7cDNA5'_fw
Pseq2-f
Stt7cDNA_fw
P1-f
Pseq4-f
Pseq5-f
Stt7_AS-fw
Pseq3-f
Stt73'UTR_fw
Stt7gDNA_rv
P1-r
P1-r2
Pseq2-r
Stt7_AS-rv
+33 bp EST
Stt7cDNA_rv
HA-Tag
Pseq3-r
Stt73'UTR_rv

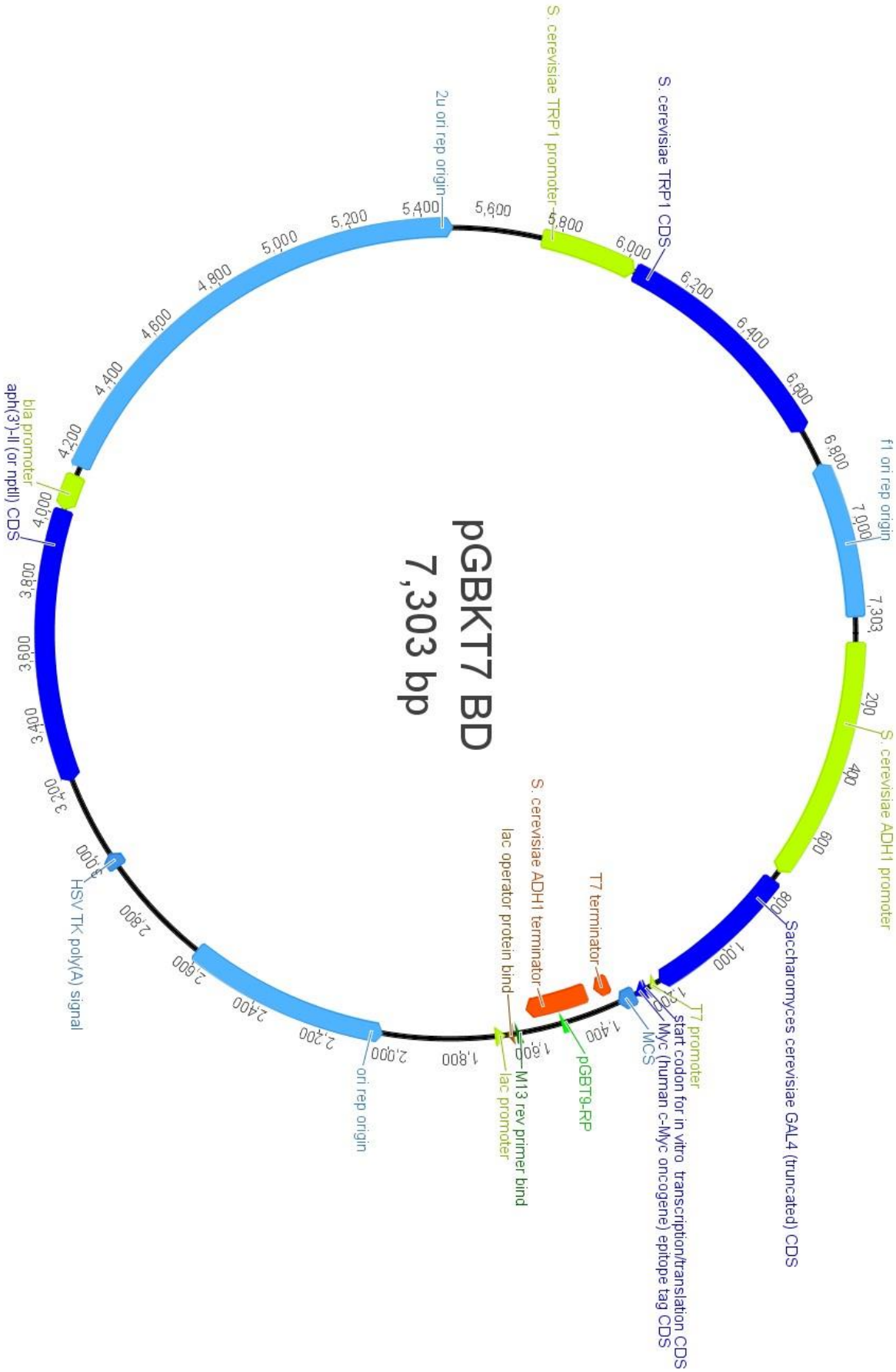
pGBKT7 BD
7,303 bp
f1 ori rep origin
S. cerevisiae ADH1 promoter
Saccharomyces cerevisiae GAL4 (truncated) CDS
T7 promoter
start codon for in vitro transcription/translation CDS
Myc (human c-Myc oncogene) epitope tag CDS
MCS
pGBT9-RP
M13 rev primer bind
lac promoter
ori rep origin
HSV TK poly(A) signal
aph(3')-II (or nptII) CDS
bla promoter
2u ori rep origin
S. cerevisiae TRP1 promoter
S. cerevisiae TRP1 CDS
S. cerevisiae ADH1 terminator
lac operator protein bind
T7 terminator

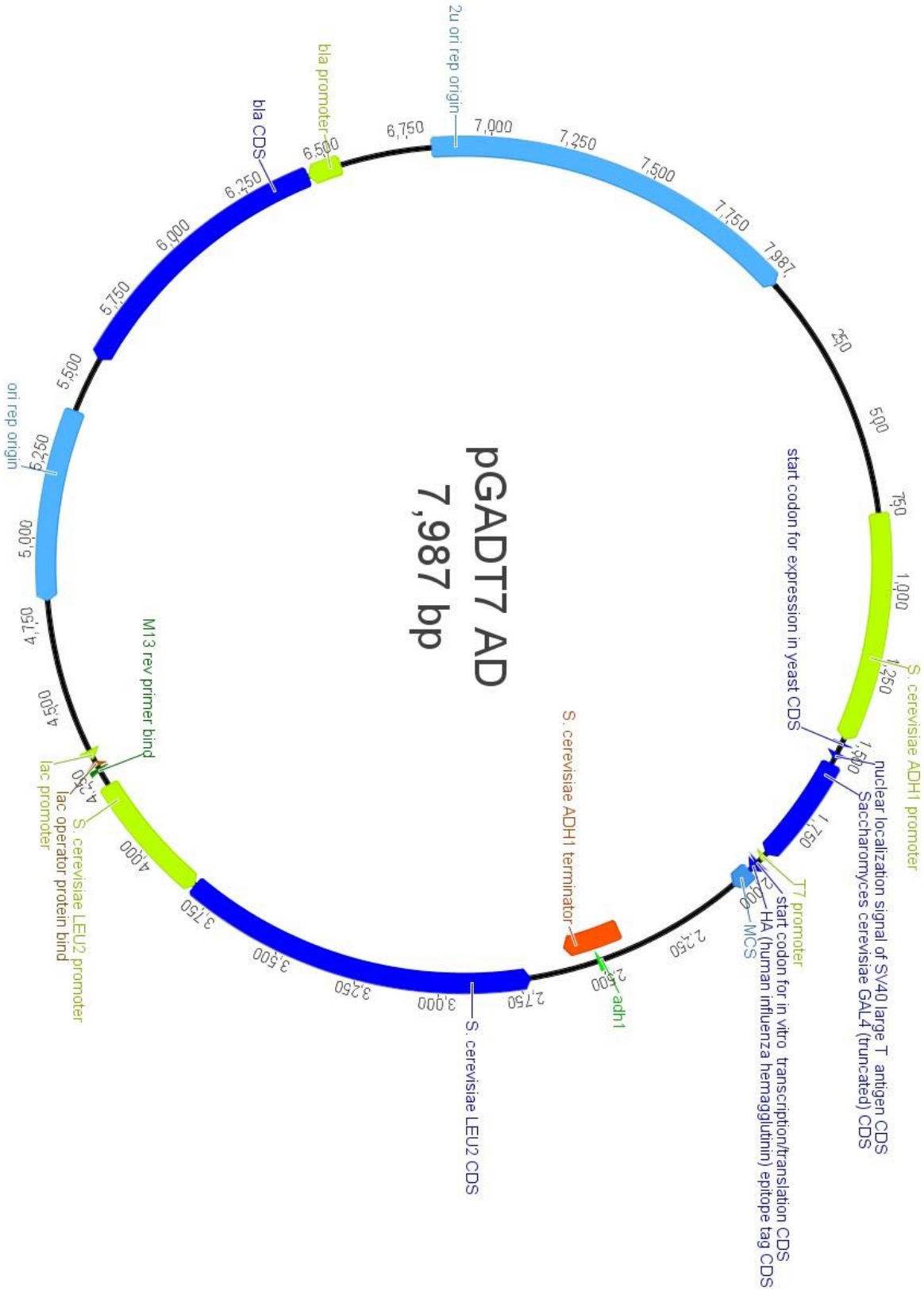
pGADT7 AD
7,987 bp
S. cerevisiae ADH1 promoter
nuclear localization signal of SV40 large T antigen CDS
Saccharomyces cerevisiae GAL4 (truncated) CDS
start codon for expression in yeast CDS
T7 promoter
start codon for in vitro transcription/translation CDS
HA (human influenza hemagglutinin) epitope tag CDS
MCS
S. cerevisiae ADH1 terminator
adh1
S. cerevisiae LEU2 CDS
M13 rev primer bind
S. cerevisiae LEU2 promoter
lac operator protein bind
lac promoter
ori rep origin
bla CDS
bla promoter
2u ori rep origin

Index of Figure and Tables

References

Allen JF. 2003. Cyclic, pseudocyclic and noncyclic photophosphorylation: new links in the chain, *Trends Plant Sci*, 8: 15-9.

Allen JF, Bennett J, Steinback KE, and Arntzen CJ. 1981. Chloroplast protein phosphorylation couples plastoquinone redox state to distribution of excitation energy between photosystems, *Nature*, 291: 25-9.

Allen JF, de Paula WB, Puthiyaveetil S, and Nield J. 2011. A structural phylogenetic map for chloroplast photosynthesis, *Trends Plant Sci*, 16: 645-55.

Alric J, Pierre Y, Picot D, Lavergne J, and Rappaport F. 2005. Spectral and redox characterization of the heme ci of the cytochrome b6f complex, *Proc Natl Acad Sci U S A*, 102: 15860-5.

Andersen KR, Leksa NC, and Schwartz TU. 2013. Optimized E. coli expression strain LOBSTR eliminates common contaminants from His-tag purification, *Proteins*, 81: 1857-61.

Antal TK, Kovalenko IB, Rubin AB, and Tyystjarvi E. 2013. Photosynthesis-related quantities for education and modeling, *Photosynth Res*, 117: 1-30.

Arnon DI. 1949. Copper Enzymes in Isolated Chloroplasts. Polyphenoloxidase in Beta Vulgaris, *Plant Physiol*, 24: 1-15.

Arnon DI, Allen MB, and Whatley FR. 1954. Photosynthesis by isolated chloroplasts, *Nature*, 174: 394-6.

Aslanidis C, and de Jong PJ. 1990. Ligation-independent cloning of PCR products (LIC-PCR), *Nucleic Acids Res*, 18: 6069-74.

Badran AH, and Liu DR. 2015. Development of potent in vivo mutagenesis plasmids with broad mutational spectra, *Nat Commun*, 6: 8425.

Barahona E, Jimenez-Vicente E, and Rubio LM. 2016. Hydrogen overproducing nitrogenases obtained by random mutagenesis and high-throughput screening, *Sci Rep*, 6: 38291.

Baymann F, Giusti F, Picot D, and Nitschke W. 2007. The c(i)/b(H) moiety in the b(6)f complex studied by EPR: A pair of strongly interacting hemes, *Proc Natl Acad Sci USA*, 104: 519-24.

Baymann F, and Nitschke W. 2010. Heliobacterial Rieske/cytb complex, *Photosynth Res*, 104: 177-87.

Baymann F, Schoepp-Cothenet B, Lebrun E, van Lis R, and Nitschke W. 2012. Phylogeny of Rieske/cytb complexes with a special focus on the Haloarchaeal enzymes, *Genome Biol Evol*, 4: 720-9.

Bennett J. 1977. Phosphorylation of chloroplast membrane polypeptides, *Nature*, 269: 344-6.

Bergner SV, Scholz M, Trompelt K, Barth J, Gabelein P, Steinbeck J, Xue H, Clowez S, Fucile G, Goldschmidt-Clermont M, Fufezan C, and Hippler M. 2015. STATE TRANSITION7-dependent phosphorylation is modulated by changing environmental conditions, and its absence triggers remodeling of photosynthetic protein complexes, *Plant Physiol*, 168: 615-34.

Berthold DA, Schmidt CL, and Malkin R. 1995. The deletion of petG in Chlamydomonas reinhardtii disrupts the cytochrome bf complex, *J Biol Chem*, 270: 29293-8.

Bhattacharyya RP, Remenyi A, Yeh BJ, and Lim WA. 2006. Domains, motifs, and scaffolds: the role of modular interactions in the evolution and wiring of cell signaling circuits, *Annu Rev Biochem*, 75: 655-80.

Bjorn L-O. 2015. "Photobiology: The Science of Light and Life." In.: Springer-Verlag New York Inc.

Blankenship RE. 2013. *Molecular mechanisms of photosynthesis* (John Wiley & Sons).

Bolanos-Garcia VM, and Davies OR. 2006. Structural analysis and classification of native proteins from E. coli commonly co-purified by immobilised metal affinity chromatography, *Biochim Biophys Acta*, 1760: 1304-13.

Bolton W, and Perutz MF. 1970. Three dimensional fourier synthesis of horse deoxyhaemoglobin at 2.8 Angstrom units resolution, *Nature*, 228: 551-2.

Bonaventura C, and Myers J. 1969. Fluorescence and oxygen evolution from Chlorella pyrenoidosa, *Biochim Biophys Acta*, 189: 366-83.

Boynton JE, Gillham NW, Harris EH, Hosler JP, Johnson AM, Jones AR, Randolph-Anderson BL, Robertson D, Klein TM, Shark KB, and et al. 1988. Chloroplast transformation in Chlamydomonas with high velocity microprojectiles, *Science*, 240: 1534-8.

Brasseur G, Saribas AS, and Daldal F. 1996. A compilation of mutations located in the cytochrome *b* subunit of the bacterial and mitochondrial bc_1 complex, *Biochim Biophys Acta*, 1275: 61-9.

Brasseur G, Saribaş AS, and Daldal F. 1996. A compilation of mutations located in the cytochrome b subunit of the bacterial and mitochondrial bc1 complex, *Biochim Biophys Acta*, 1275: 61-9.

Breyton C. 2000. The cytochrome b(6)f complex: structural studies and comparison with the bc(1) complex, *Biochim Biophys Acta*, 1459: 467-74.

Breyton C, Tribet C, Olive J, Dubacq JP, and Popot JL. 1997. Dimer to monomer conversion of the cytochrome b6 f complex. Causes and consequences, *J Biol Chem*, 272: 21892-900.

Bryant DA, Costas AMG, Maresca JA, Chew AGM, Klatt CG, Bateson MM, Tallon LJ, Hostetler J, Nelson WC, and Heidelberg JF. 2007. Candidatus Chloracidobacterium thermophilum: an aerobic phototrophic acidobacterium, *Science*, 317: 523-6.

Cadwell RC, and Joyce GF. 1992. Randomization of genes by PCR mutagenesis, *PCR Methods Appl*, 2: 28-33.

Chang CI, Xu BE, Akella R, Cobb MH, and Goldsmith EJ. 2002. Crystal structures of MAP kinase p38 complexed to the docking sites on its nuclear substrate MEF2A and activator MKK3b, *Mol Cell*, 9: 1241-9.

Chaux F, Peltier G, and Johnson X. 2015. A security network in PSI photoprotection: regulation of photosynthetic control, NPQ and O2 photoreduction by cyclic electron flow, *Front Plant Sci*, 6: 875.

Chen H, Ma J, Li W, Eliseenkova AV, Xu C, Neubert TA, Miller WT, and Mohammadi M. 2007. A molecular brake in the kinase hinge region regulates the activity of receptor tyrosine kinases, *Mol Cell*, 27: 717-30.

Choquet Y, and Wollman F-A. 2009. The CES process, *The Chlamydomonas sourcebook*, 2: 1027-63.

Choquet Y, and Wollman FA. 2002. Translational regulations as specific traits of chloroplast gene expression, *FEBS Lett*, 529: 39-42.

Choquet Y, Zito F, Wostrikoff K, and Wollman FA. 2003. Cytochrome *f* translation in *Chlamydomonas* chloroplast is autoregulated by its carboxyl-terminal domain, *Plant Cell*, 15: 1443-54.

Chua NH, and Bennoun P. 1975. Thylakoid membrane polypeptides of C*hlamydomonas reinhardtii* - Wild-type and mutant strains deficient in Photosystem II reaction center, *Proc Natl Acad Sci USA*, 72: 2175-9.

Cordero BF, Obraztsova I, Couso I, Leon R, Vargas MA, and Rodriguez H. 2011. Enhancement of lutein production in Chlorella sorokiniana (Chorophyta) by improvement of culture conditions and random mutagenesis, *Mar Drugs*, 9: 1607-24.

Cox S, Radzio-Andzelm E, and Taylor SS. 1994. Domain movements in protein kinases, *Current Opinion in Structural Biology*, 4: 893-901.

Cramer WA, Yan J, Zhang H, Kurisu G, and Smith JL. 2005. Structure of the cytochrome b6f complex: new prosthetic groups, Q-space, and the 'hors d'oeuvres hypothesis' for assembly of the complex, *Photosynth Res*, 85: 133-43.

Crameri A, Raillard SA, Bermudez E, and Stemmer WP. 1998. DNA shuffling of a family of genes from diverse species accelerates directed evolution, *Nature*, 391: 288-91.

Crofts A, Barquera B, Bechmann G, Guergova M, Salcedo-Hernandez R, Hacker B, Hong S, and Gennis R. 1995. Structure and function in the bc_1 complex of *Rb. sphaeroides*, *Photosynthesis: from light to biosphere*, 2: 493ñ500.

Crofts AR. 2004. The Q-cycle - A Personal Perspective, *Photosynth Res*, 80: 223-43.

Crofts AR, Meinhardt SW, Jones KR, and Snozzi M. 1983. The Role of the Quinone Pool in the Cyclic Electron-Transfer Chain of Rhodopseudomonas Sphaeroides: A Modified Q-Cycle Mechanism, *Biochim Biophys Acta*, 723: 202-18.

Currin A, Swainston N, Day PJ, and Kell DB. 2015. Synthetic biology for the directed evolution of protein biocatalysts: navigating sequence space intelligently, *Chem Soc Rev*, 44: 1172-239.

Day A, and Goldschmidt-Clermont M. 2011. The chloroplast transformation toolbox: selectable markers and marker removal, *Plant Biotechnol J*, 9: 540-53.

de Lacroix de Lavalette A, Barbagallo RP, and Zito F. 2008. Why is it so difficult to construct Q(i) site mutants in Chlamydomonas reinhardtii?, *C R Biol*, 331: 510-7.

de Lacroix de Lavalette A, Barucq L, Alric J, Rappaport F, and Zito F. 2009. Is the redox state of the ci heme of the cytochrome b6f complex dependent on the occupation and structure of the Qi site and vice versa?, *J Biol Chem*, 284: 20822-9.

de Lacroix de Lavalette A, Finazzi G, and Zito F. 2008. b_6f-associated chlorophyll: structural and dynamic contribution to the different cytochrome functions, *Biochemistry*, 47: 5259-65.

de Vitry C, Finazzi G, Baymann F, and Kallas T. 1999. Analysis of the nucleus-encoded and chloroplast-targeted rieske protein by classic and site-directed mutagenesis of Chlamydomonas, *The Plant Cell*, 11: 2031-44.

de Vitry C, Ouyang Y, Finazzi G, Wollman FA, and Kallas T. 2004. The chloroplast Rieske iron-sulfur protein - At the crossroad of electron transport and signal transduction, *J Biol Chem*, 279: 44621-7.

Deindl S, Kadlecek TA, Brdicka T, Cao X, Weiss A, and Kuriyan J. 2007. Structural basis for the inhibition of tyrosine kinase activity of ZAP-70, *Cell*, 129: 735-46.

Delepelaire P, and Wollman FA. 1985. Anaerobic adaptation and state transitions - Correlations between fluorescence and phosphorylation changes in thylakoid membranes of Chlamydomonas reinhardtii in vivo: a kinetic analysis.

Depege N, Bellafiore S, and Rochaix JD. 2003. Role of chloroplast protein kinase Stt7 in LHCII phosphorylation and state transition in *Chlamydomonas*, *Science*, 299: 1572-5.

Dibrova DV, Cherepanov DA, Galperin MY, Skulachev VP, and Mulkidjanian AY. 2013. Evolution of cytochrome bc complexes: from membrane-anchored dehydrogenases of ancient bacteria to triggers of apoptosis in vertebrates, *Biochim Biophys Acta*, 1827: 1407-27.

Dougherty DA. 2007. Cation-pi interactions involving aromatic amino acids, *J Nutr*, 137: 1504S-8S; discussion 16S-17S.

Drummond DA, Iverson BL, Georgiou G, and Arnold FH. 2005. Why high-error-rate random mutagenesis libraries are enriched in functional and improved proteins, *J Mol Biol*, 350: 806-16.

Dumas L, Chazaux M, Peltier G, Johnson X, and Alric J. 2016. Cytochrome b_6f function and localization, phosphorylation state of thylakoid membrane proteins and consequences on cyclic electron flow, *Photosynth Res*, 129: 307-20.

Dumas L, Zito F, Blangy S, Auroy P, Johnson X, Peltier G, and Alric J. 2017. A stromal region of cytochrome b6f subunit IV is involved in the activation of the Stt7 kinase in Chlamydomonas, *Proc Natl Acad Sci U S A*, 114: 12063-8.

Dunbrack RL. 2002. Rotamer Libraries in the 21st Century, *Current Opinion in Structural Biology*, 12: 431-40.

Eberhard S, Finazzi G, and Wollman FA. 2008. The dynamics of photosynthesis, *Annu Rev Genet*, 42: 463-515.

Erickson E, Wakao S, and Niyogi KK. 2015. Light stress and photoprotection in Chlamydomonas reinhardtii, *The Plant Journal*, 82: 449-65.

Ermakova-Gerdes S, Shestakov S, and Vermaas W. 1996. Random chemical mutagenesis of a specific psbDI region coding for a lumenal loop of the D2 protein of photosystem II in Synechocystis sp. PCC 6803, *Plant Molecular Biology*, 30: 243-54.

Finazzi G, Zito F, Barbagallo RP, and Wollman FA. 2001. Contrasted effects of inhibitors of cytochrome b_6f complex on state transitions in *Chlamydomonas reinhardtii* - The role of Q_o site occupancy in LHCII kinase activation, *J Biol Chem*, 276: 9770-4.

Fischer N, Hippler M, Setif P, Jacquot JP, and Rochaix JD. 1998. The PsaC subunit of Photosystem I provides an essential lysine residue for fast electron transfer to ferredoxin, *EMBO J*, 17: 849-58.

Fischer N, and Rochaix JD. 2001. The flanking regions of PsaD drive efficient gene expression in the nucleus of the green alga Chlamydomonas reinhardtii, *Mol Genet Genomics*, 265: 888-94.

Fischer WW, Hemp J, and Johnson JE. 2016. Evolution of Oxygenic Photosynthesis, *Annual Review of Earth and Planetary Sciences*, 44: 647-83.

Fleischmann MM, Ravanel S, Delosme R, Olive J, Zito F, Wollman FA, and Rochaix JD. 1999. Isolation and characterization of photoautotrophic mutants of *Chlamydomonas reinhardtii* deficient in state transition, *J Biol Chem*, 274: 30987-94.

Garai A, Zeke A, Gogl G, Toro I, Fordos F, Blankenburg H, Barkai T, Varga J, Alexa A, Emig D, Albrecht M, and Remenyi A. 2012. Specificity of linear motifs that bind to a common mitogen-activated protein kinase docking groove, *Sci Signal*, 5: ra74.

Goldschmidt-Clermont M. 1991. Transgenic expression of aminoglycoside adenine transferase in the chloroplast: a selectable marker of site-directed transformation of chlamydomonas, *Nucleic Acids Res*, 19: 4083-9.

Govindjee, Shevela D, and Bjorn LO. 2017. Evolution of the Z-scheme of photosynthesis: a perspective, *Photosynth Res*.

Guo J, Wei X, Li M, Pan X, Chang W, and Liu Z. 2013. Structure of the catalytic domain of a state transition kinase homolog from Micromonas algae, *Protein Cell*, 4: 607-19.

Guskov A, Kern J, Gabdulkhakov A, Broser M, Zouni A, and Saenger W. 2009. Cyanobacterial photosystem II at 2.9-A resolution and the role of quinones, lipids, channels and chloride, *Nat Struct Mol Biol*, 16: 334-42.

Hager M, Biehler K, Illerhaus J, Ruf S, and Bock R. 1999. Targeted inactivation of the smallest plastid genome-encoded open reading frame reveals a novel and essential subunit of the cytochrome b(6)f complex, *EMBO J*, 18: 5834-42.

Haldane JS. 1929. Claude Bernard's Conception of the Internal Environment, *Science*, 69: 453-4.

Hamel P, Olive J, Pierre Y, Wollman FA, and de Vitry C. 2000. A new subunit of cytochrome b_6f complex undergoes reversible phosphorylation upon state transition, *J Biol Chem*, 275: 17072-9.

Harano T, Harano K, Shibata S, Ueda S, Imai K, Tsuneshige A, Yamada H, Seki M, and Fukui H. 1983. Hemoglobin Kariya [alpha 40 (C5) Lys leads to Glu]: a new hemoglobin variant with an increased oxygen affinity, *FEBS Lett*, 153: 332-4.

Hasan SS, and Cramer WA. 2012. Lipid functions in cytochrome bc complexes: an odd evolutionary transition in a membrane protein structure, *Philos Trans R Soc Lond B Biol Sci*, 367: 3406-11.

Hasan SS, and Cramer WA. 2014. Internal lipid architecture of the hetero-oligomeric cytochrome b6f complex, *Structure*, 22: 1008-15.

Hayatsu H, and Miura A. 1970. The mutagenic action of sodium bisulfite, *Biochem Biophys Res Commun*, 39: 156-60.

Hill R, and Bendall F. 1960. Function of the two cytochrome components in chloroplasts: a working hypothesis, *Nature*, 186: 136-7.

Hohmann-Marriott MF, and Blankenship RE. 2011. Evolution of photosynthesis, *Annu Rev Plant Biol*, 62: 515-48.

Hottenrott S, Schumann T, Pluckthun A, Fischer G, and Rahfeld JU. 1997. The Escherichia coli SlyD is a metal ion-regulated peptidyl-prolyl cis/trans-isomerase, *J Biol Chem*, 272: 15697-701.

Huang B, Piperno G, Ramanis Z, and Luck DJ. 1981. Radial spokes of Chlamydomonas flagella: genetic analysis of assembly and function, *J Cell Biol*, 88: 80-8.

Huang L-s, and Berry E. 2016. Rieske iron-sulfur protein movement and conformational changes in cytochrome bc–bf complexes. in, *Cytochrome Complexes: Evolution, Structures, Energy Transduction, and Signaling* (Springer).

Imai K, Tsuneshige A, Harano T, and Harano K. 1989. Structure-function relationships in hemoglobin Kariya, Lys-40(C5) alpha----Glu, with high oxygen affinity. Functional role of the salt bridge between Lys-40 alpha and the beta chain COOH terminus, *J Biol Chem*, 264: 11174-80.

Jagendorf A, and Hind G. 1963. Studies on the mechanism of photophosphorylation, *Photosynthetic Mechanisms of Green Plants*, 1146: 599-610.

Johnson GL, and Lapadat R. 2002. Mitogen-activated protein kinase pathways mediated by ERK, JNK, and p38 protein kinases, *Science*, 298: 1911-2.

Johnson X, Vandystadt G, Bujaldon S, Wollman FA, Dubois R, Roussel P, Alric J, and Beal D. 2009. A new setup for in vivo fluorescence imaging of photosynthetic activity, *Photosynth Res*, 102: 85-93.

Joliot P, and Joliot A. 1988. The low-potential electron-transfer chain in the cytochrome bf complex, *Biochimica et Biophysica Acta (BBA)-Bioenergetics*, 933: 319-33.

Joliot P, and Joliot A. 1998. *In vivo* analysis of the effect of dicyclohexylcarbodiimide on electron and proton transfers in cytochrome *bf* complex of *Chlorella sorokiniana*, *Biochemistry*, 37: 10404-10.

Kaluarachchi H, Siebel JF, Kaluarachchi-Duffy S, Krecisz S, Sutherland DE, Stillman MJ, and Zamble DB. 2011. Metal selectivity of the Escherichia coli nickel metallochaperone, SlyD, *Biochemistry*, 50: 10666-77.

Kao WC, and Hunte C. 2014. The Molecular Evolution of the Qo Motif, *Genome Biology and Evolution*, 6: 1894-910.

Kearse M, Moir R, Wilson A, Stones-Havas S, Cheung M, Sturrock S, Buxton S, Cooper A, Markowitz S, and Duran C. 2012. Geneious Basic: an integrated and extendable desktop software platform for the organization and analysis of sequence data, *Bioinformatics*, 28: 1647-9.

Keeling PJ. 2010. The endosymbiotic origin, diversification and fate of plastids, *Philosophical Transactions of the Royal Society of London B: Biological Sciences*, 365: 729-48.

Kelley LA, Mezulis S, Yates CM, Wass MN, and Sternberg MJ. 2015. The Phyre2 web portal for protein modeling, prediction and analysis, *Nature protocols*, 10: 845-58.

Kim H, Xia D, Yu CA, Xia JZ, Kachurin AM, Zhang L, Yu L, and Deisenhofer J. 1998. Inhibitor binding changes domain mobility in the iron-sulfur protein of the mitochondrial bc1 complex from bovine heart, *Proc Natl Acad Sci U S A*, 95: 8026-33.

Kindle KL, Richards KL, and Stern DB. 1991. Engineering the chloroplast genome: techniques and capabilities for chloroplast transformation in Chlamydomonas reinhardtii, *Proc Natl Acad Sci U S A*, 88: 1721-5.

Klein TM, Wolf E, Wu R, and Sanford J. 1987. High-velocity microprojectiles for delivering nucleic acids into living cells, *Nature*, 327: 70-3.

Koch AL, and Schmidt TM. 1991. The first cellular bioenergetic process: primitive generation of a proton-motive force, *J Mol Evol*, 33: 297-304.

Koivuniemi A, Aro EM, and Andersson B. 1995. Degradation of the D1- and D2-proteins of photosystem II in higher plants is regulated by reversible phosphorylation, *Biochemistry*, 34: 16022-9.

Kramer D, Nitschke W, and Cooley J. 2009. The Cytochrome bc 1 and Related bc Complexes: The Rieske/Cytochrome b Complex as the Functional Core of a Central Electron/Proton Transfer Complex. in C. Neil Hunter, Fevzi Daldal, MarionC Thurnauer and J. Thomas Beatty (eds.), *The Purple Phototrophic Bacteria* (Springer Netherlands).

Kramer DM, Schoepp B, Liebl U, and Nitschke W. 1997. Cyclic electron transfer in Heliobacillus mobilis involving a menaquinol-oxidizing cytochrome bc complex and an RCI-type reaction center, *Biochemistry*, 36: 4203-11.

Kuras R, and Wollman FA. 1994. The assembly of cytochrome b6/f complexes: an approach using genetic transformation of the green alga Chlamydomonas reinhardtii, *EMBO J*, 13: 1019-27.

Kurisu G, Zhang H, Smith JL, and Cramer WA. 2003. Structure of the cytochrome b6f complex of oxygenic photosynthesis: tuning the cavity, *Science*, 302: 1009-14.

Lane N, Allen JF, and Martin W. 2010. How did LUCA make a living? Chemiosmosis in the origin of life, *Bioessays*, 32: 271-80.

Lange C, Nett JH, Trumpower BL, and Hunte C. 2001. Specific roles of protein-phospholipid interactions in the yeast cytochrome bc1 complex structure, *EMBO J*, 20: 6591-600.

Lavergne J. 1983a. Membrane Potential-Dependent Reduction of Cytochrome-B-6 in an Algal Mutant Lacking Photosystem-I Centers, *Biochimica Et Biophysica Acta*, 725: 25-33.

Lavergne J. 1983b. Membrane Potential-Dependent Reduction of Cytochrome-B-6 in an Algal Mutant Lacking Photosystem-I Centers, *Biochim Biophys Acta*, 725: 25-33.

Lebrun E, Santini JM, Brugna M, Ducluzeau AL, Ouchane S, Schoepp-Cothenet B, Baymann F, and Nitschke W. 2006. The Rieske protein: a case study on the pitfalls of multiple sequence alignments and phylogenetic reconstruction, *Mol Biol Evol*, 23: 1180-91.

Lemaire C, Girard-Bascou J, Wollman F-A, and Bennoun P. 1986. Studies on the cytochrome b6/f complex. I. Characterization of the complex subunits in Chlamydomonas reinhardtii, *Biochimica et Biophysica Acta (BBA)-Bioenergetics*, 851: 229-38.

Lemeille S, and Rochaix JD. 2010. State transitions at the crossroad of thylakoid signalling pathways, *Photosynth Res*, 106: 33-46.

Lemeille S, Turkina MV, Vener AV, and Rochaix JD. 2010. Stt7-dependent phosphorylation during state transitions in the green alga *Chlamydomonas reinhardtii*, *Mol Cell Proteomics*, 9: 1281-95.

Lemeille S, Willig A, Depege-Fargeix N, Delessert C, Bassi R, and Rochaix JD. 2009. Analysis of the chloroplast protein kinase Stt7 during state transitions, *PLoS Biol*, 7: e45.

Leung DW, Chen E, and Goeddel DV. 1989. A method for random mutagenesis of a defined DNA segment using a modified polymerase chain reaction, *Technique*, 1: 11-5.

Lichtenthaler HK, and Wellburn AR. 1983. "Determinations of total carotenoids and chlorophylls a and b of leaf extracts in different solvents." In.: Portland Press Limited.

Lochhead PA. 2009. Protein kinase activation loop autophosphorylation in cis: overcoming a Catch-22 situation, *Sci Signal*, 2: pe4.
Malnoe A, Wang F, Girard-Bascou J, Wollman FA, and de Vitry C. 2014. Thylakoid FtsH protease contributes to photosystem II and cytochrome b6f remodeling in Chlamydomonas reinhardtii under stress conditions, *Plant Cell*, 26: 373-90.
Margulis L. 1981. Symbiosis in cell evolution: Life and its environment on the early earth.
Martin W, and Kowallik KV. 1999. Annotated English translation of Mereschkowsky's 1905 paper 'Über Natur und Ursprung der Chromatophoren im Pflanzenreiche', *European Journal of Phycology*, 34: 287-95.
Martin W, Stoebe B, Goremykin V, Hapsmann S, Hasegawa M, and Kowallik KV. 1998. Gene transfer to the nucleus and the evolution of chloroplasts, *Nature*, 393: 162-5.
Masterson LR, Mascioni A, Traaseth NJ, Taylor SS, and Veglia G. 2008. Allosteric cooperativity in protein kinase A, *Proceedings of the National Academy of Sciences*, 105: 506-11.
Mayor F, Jr., Jurado-Pueyo M, Campos PM, and Murga C. 2007. Interfering with MAP kinase docking interactions: implications and perspective for the p38 route, *Cell Cycle*, 6: 528-33.
Mereschkowsky C. 1905. *Über natur und ursprung der chromatophoren im pflanzenreiche*.
Mitchell P. 1961. Coupling of phosphorylation to electron and hydrogen transfer by a chemi-osmotic type of mechanism, *Nature*, 191: 144-8.
Mitchell P. 1975. The protonmotive Q cycle: a general formulation, *FEBS Lett*, 59: 137-9.
Miyashita O, Onuchic JN, and Wolynes PG. 2003. Nonlinear elasticity, proteinquakes, and the energy landscapes of functional transitions in proteins, *Proceedings of the National Academy of Sciences*, 100: 12570-5.
Miyata T, Miyazawa S, and Yasunaga T. 1979. Two types of amino acid substitutions in protein evolution, *J Mol Evol*, 12: 219-36.
Murata N. 1969. Control of excitation transfer in photosynthesis. I. Light-induced change of chlorophyll a fluorescence in Porphyridium cruentum, *Biochim Biophys Acta*, 172: 242-51.
Nagar B, Hantschel O, Young MA, Scheffzek K, Veach D, Bornmann W, Clarkson B, Superti-Furga G, and Kuriyan J. 2003. Structural basis for the autoinhibition of c-Abl tyrosine kinase, *Cell*, 112: 859-71.
Naver H, Boudreau E, and Rochaix JD. 2001. Functional studies of Ycf3: Its role in assembly of Photosystem I and interactions with some of its subunits, *Plant Cell*, 13: 2731-45.
Neumann J, and Jagendorf A. 1964. Light-induced pH changes related to phosphorylation by chloroplasts, *Arch Biochem Biophys*, 107: 109-19.
Nitschke W, van Lis R, Schoepp-Cothenet B, and Baymann F. 2010. The "green" phylogenetic clade of Rieske/cytb complexes, *Photosynth Res*, 104: 347-55.
Nolen B, Taylor S, and Ghosh G. 2004. Regulation of protein kinases: controlling activity through activation segment conformation, *Molecular cell*, 15: 661-75.
Ort DR, Merchant SS, Alric J, Barkan A, Blankenship RE, Bock R, Croce R, Hanson MR, Hibberd JM, Long SP, Moore TA, Moroney J, Niyogi KK, Parry MA, Peralta-Yahya PP, Prince RC, Redding KE, Spalding MH, van Wijk KJ, Vermaas WF, von Caemmerer S, Weber AP, Yeates TO, Yuan JS, and Zhu XG. 2015. Redesigning photosynthesis to sustainably meet global food and bioenergy demand, *Proc Natl Acad Sci U S A*, 112: 8529-36.
Padyana AK, Qiu H, Roll-Mecak A, Hinnebusch AG, and Burley SK. 2005. Structural basis for autoinhibition and mutational activation of eukaryotic initiation factor 2alpha protein kinase GCN2, *J Biol Chem*, 280: 29289-99.

Papaleo E, Saladino G, Lambrughi M, Lindorff-Larsen K, Gervasio FL, and Nussinov R. 2016. The role of protein loops and linkers in conformational dynamics and allostery, *Chemical reviews*, 116: 6391-423.

Pearson G, Robinson F, Beers Gibson T, Xu BE, Karandikar M, Berman K, and Cobb MH. 2001. Mitogen-activated protein (MAP) kinase pathways: regulation and physiological functions, *Endocr Rev*, 22: 153-83.

Peisach J, Blumberg WE, Ogawa S, Rachmilewitz EA, and Oltzik R. 1971. The effects of protein conformation on the heme symmetry in high spin ferric heme proteins as studied by electron paramagnetic resonance, *J Biol Chem*, 246: 3342-55.

Perutz MF. 1970. Stereochemistry of cooperative effects in haemoglobin, *Nature*, 228: 726-39.

Pettersen EF, Goddard TD, Huang CC, Couch GS, Greenblatt DM, Meng EC, and Ferrin TE. 2004. UCSF Chimera—a visualization system for exploratory research and analysis, *Journal of computational chemistry*, 25: 1605-12.

Pierre Y, Breyton C, Kramer D, and Popot JL. 1995. Purification and characterization of the cytochrome b6 f complex from Chlamydomonas reinhardtii, *J Biol Chem*, 270: 29342-9.

Porra RJ. 2002. The chequered history of the development and use of simultaneous equations for the accurate determination of chlorophylls a and b, *Photosynth Res*, 73: 149-56.

Prebble JN. 2010. The discovery of oxidative phosphorylation: a conceptual off-shoot from the study of glycolysis, *Studies in History and Philosophy of Science Part C: Studies in History and Philosophy of Biological and Biomedical Sciences*, 41: 253-62.

Qiu H, Hu C, Dong J, and Hinnebusch AG. 2002. Mutations that bypass tRNA binding activate the intrinsically defective kinase domain in GCN2, *Genes Dev*, 16: 1271-80.

Rasband W. 1997. "ImageJ. US National Institutes of Health, Bethesda, MD." In.

Raymond J, Zhaxybayeva O, Gogarten JP, Gerdes SY, and Blankenship RE. 2002. Whole-genome analysis of photosynthetic prokaryotes, *Science*, 298: 1616-20.

Robichon C, Luo J, Causey TB, Benner JS, and Samuelson JC. 2011. Engineering Escherichia coli BL21(DE3) derivative strains to minimize E. coli protein contamination after purification by immobilized metal affinity chromatography, *Appl Environ Microbiol*, 77: 4634-46.

Rochaix JD. 2011. Reprint of: Regulation of photosynthetic electron transport, *Biochim Biophys Acta*, 1807: 878-86.

Rochaix JD. 2013. Redox regulation of thylakoid protein kinases and photosynthetic gene expression, *Antioxid Redox Signal*, 18: 2184-201.

Roof WD, Fang HQ, Young KD, Sun J, and Young R. 1997. Mutational analysis of slyD, an Escherichia coli gene encoding a protein of the FKBP immunophilin family, *Mol Microbiol*, 25: 1031-46.

Roof WD, Horne SM, Young KD, and Young R. 1994. slyD, a host gene required for phi X174 lysis, is related to the FK506-binding protein family of peptidyl-prolyl cis-trans-isomerases, *J Biol Chem*, 269: 2902-10.

Sakuraba Y, Yamasato A, Tanaka R, and Tanaka A. 2008. Analysis of the N-Terminal Domain of Chlorophyllide a Oxygenase by Random Mutagenesis. in, *Photosynthesis. Energy from the Sun* (Springer).

Schimper AFW. 1883. Ueber die entwickelung der chlorophyllkoerner und farbkoerper.

Schmidt GW, Matlin KS, and Chua NH. 1977. A rapid procedure for selective enrichment of photosynthetic electron transport mutants, *Proc Natl Acad Sci U S A*, 74: 610-4.

Schneider D, Berry S, Rich P, Seidler A, and Rogner M. 2001. A regulatory role of the PetM subunit in a cyanobacterial cytochrome b6f complex, *J Biol Chem*, 276: 16780-5.

Schroda M, Blocker D, and Beck CF. 2000. The HSP70A promoter as a tool for the improved expression of transgenes in Chlamydomonas, *Plant J*, 21: 121-31.

Schütz M, Brugna M, Lebrun E, Baymann F, Huber R, Stetter KO, Hauska G, Toci R, Lemesle-Meunier D, Tron P, Schmidt C, and Nitschke W. 2000. Early evolution of cytochrome bc complexes, *J Mol Biol*, 300: 663-75.

Schwenkert S, Legen J, Takami T, Shikanai T, Herrmann RG, and Meurer J. 2007. Role of the low-molecular-weight subunits PetL, PetG, and PetN in assembly, stability, and dimerization of the cytochrome b6f complex in tobacco, *Plant Physiol*, 144: 1924-35.

Selifonova O, Valle F, and Schellenberger V. 2001. Rapid evolution of novel traits in microorganisms, *Appl Environ Microbiol*, 67: 3645-9.

Shan Y, Arkhipov A, Kim ET, Pan AC, and Shaw DE. 2013. Transitions to catalytically inactive conformations in EGFR kinase, *Proceedings of the National Academy of Sciences*, 110: 7270-5.

Shan Y, Seeliger MA, Eastwood MP, Frank F, Xu H, Jensen MO, Dror RO, Kuriyan J, and Shaw DE. 2009. A conserved protonation-dependent switch controls drug binding in the Abl kinase, *Proc Natl Acad Sci U S A*, 106: 139-44.

Shapiguzov A, Chai X, Fucile G, Longoni P, Zhang L, and Rochaix JD. 2016. Activation of the Stt7/STN7 kinase through dynamic interactions with the cytochrome b_6f complex, *Plant Physiol*, 171: 82-92.

Shinozaki K, Ohme M, Tanaka M, Wakasugi T, Hayashida N, Matsubayashi T, Zaita N, Chunwongse J, Obokata J, Yamaguchi-Shinozaki K, Ohto C, Torazawa K, Meng BY, Sugita M, Deno H, Kamogashira T, Yamada K, Kusuda J, Takaiwa F, Kato A, Tohdoh N, Shimada H, and Sugiura M. 1986. The complete nucleotide sequence of the tobacco chloroplast genome: its gene organization and expression, *EMBO J*, 5: 2043-9.

Sicheri F, Moarefi I, and Kuriyan J. 1997. Crystal structure of the Src family tyrosine kinase Hck, *Nature*, 385: 602.

Singh SK, Hasan SS, Zakharov SD, Naurin S, Cohn W, Ma J, Whitelegge JP, and Cramer WA. 2016. Trans-membrane signaling in photosynthetic state transitions - Redox- and structure-dependent interaction *in vitro* between Stt7 kinase and the cytochrome b_6f complex, *J Biol Chem*, 291: 21740-50.

Slater EC. 1953. Mechanism of phosphorylation in the respiratory chain, *Nature*, 172: 975-8.

Stern D. 2009. *The Chlamydomonas sourcebook: organellar and metabolic processes* (Academic Press).

Stroebel D, Choquet Y, Popot J-L, and Picot D. 2003. An atypical haem in the cytochrome b6f complex, *Nature*, 426: 413-8.

Takahashi Y, Rahire M, Breyton C, Popot JL, Joliot P, and Rochaix JD. 1996. The chloroplast ycf7 (petL) open reading frame of Chlamydomonas reinhardtii encodes a small functionally important subunit of the cytochrome b6f complex, *EMBO J*, 15: 3498-506.

Tanoue T, and Nishida E. 2003. Molecular recognitions in the MAP kinase cascades, *Cell Signal*, 15: 455-62.

ten Brink F, and Baymann F. 2014. Rieske/cytochrome b complexes: the turbo chargers of chemiosmosis. in, *The Structural Basis of Biological Energy Generation* (Springer).

ten Brink F, Schoepp-Cothenet B, van Lis R, Nitschke W, and Baymann F. 2013. Multiple Rieske/cytb complexes in a single organism, *Biochim Biophys Acta*, 1827: 1392-406.

Tikkanen M, Nurmi M, Kangasjarvi S, and Aro EM. 2008. Core protein phosphorylation facilitates the repair of photodamaged photosystem II at high light, *Biochim Biophys Acta*, 1777: 1432-7.

Vener AV, Vankan PJM, Gal A, Andersson B, and Ohad I. 1995. Activation/deactivation cycle of redox-controlled thylakoid protein phosphorylation - Role of plastoquinol bound to the reduced cytochrome *bf* complex, *J Biol Chem*, 270: 25225-32.

Wang CW, and Liao JC. 2001. Alteration of product specificity of Rhodobacter sphaeroides phytoene desaturase by directed evolution, *J Biol Chem*, 276: 41161-4.

Weininger U, Haupt C, Schweimer K, Graubner W, Kovermann M, Bruser T, Scholz C, Schaarschmidt P, Zoldak G, Schmid FX, and Balbach J. 2009. NMR solution structure of SlyD from Escherichia coli: spatial separation of prolyl isomerase and chaperone function, *J Mol Biol*, 387: 295-305.

Witkin EM. 1969. Ultraviolet-induced mutation and DNA repair, *Annu Rev Microbiol*, 23: 487-514.

Wollman FA. 2001. State transitions reveal the dynamics and flexibility of the photsynthetic apparatus.

Wollman FA, and Delepelaire P. 1984. Correlation between Changes in Light Energy Distribution and Changes in Thylakoid Membrane Polypeptide Phosphorylation in Chlamydomonas Reinhardtii.

Wollman FA, and Lemaire C. 1988. Studies on kinase-controlled state transitions in photosystem II and b6f mutants from Chlamydomonas reinhardtii which lack quinone-binding proteins, *Biochimica et Biophysica Acta (BBA)-Bioenergetics*, 933: 85-94.

Wu J, Masri N, Lee W, Frankel LK, and Bricker TM. 1999. Random mutagenesis in the large extrinsic loop E and transmembrane alpha-helix VI of the CP 47 protein of Photosystem II, *Plant Molecular Biology*, 39: 381-6.

Wulfing C, Lombardero J, and Pluckthun A. 1994. An Escherichia coli protein consisting of a domain homologous to FK506-binding proteins (FKBP) and a new metal binding motif, *J Biol Chem*, 269: 2895-901.

Wurtz EA, Sears BB, Rabert DK, Shepherd HS, Gillham NW, and Boynton JE. 1979. A specific increase in chloroplast gene mutations following growth of Chlamydomonas in 5-fluorodeoxyuridine, *Mol Gen Genet*, 170: 235-42.

Xiong J, Fischer WM, Inoue K, Nakahara M, and Bauer CE. 2000. Molecular evidence for the early evolution of photosynthesis, *Science*, 289: 1724-30.

Xu W, Harrison SC, and Eck MJ. 1997. Three-dimensional structure of the tyrosine kinase c-Src, *Nature*, 385: 595.

Yamasato A, Kamada T, and Satoh K. 2002. Random mutagenesis targeted to the psbAII gene of Synechocystis sp. PCC 6803 to identify functionally important residues in the D1 protein of the photosystem II reaction center, *Plant Cell Physiol*, 43: 540-8.

Yamashita E, Zhang H, and Cramer WA. 2007. Structure of the cytochrome b(6)f complex: Quinone analogue inhibitors as ligands of heme c(n), *Journal of Molecular Biology*, 370: 39-52.

Yan J, Dashdorj N, Baniulis D, Yamashita E, Savikhin S, and Cramer WA. 2008. On the structural role of the aromatic residue environment of the chlorophyll a in the cytochrome b6f complex, *Biochemistry*, 47: 3654-61.

Young MA, Gonfloni S, Superti-Furga G, Roux B, and Kuriyan J. 2001. Dynamic coupling between the SH2 and SH3 domains of c-Src and Hck underlies their inactivation by C-terminal tyrosine phosphorylation, *Cell*, 105: 115-26.

Zakour RA, and Loeb LA. 1982. Site-specific mutagenesis by error-directed DNA synthesis, *Nature*, 295: 708-10.

Zeng Y, Feng F, Medová H, Dean J, and Koblížek M. 2014. Functional type 2 photosynthetic reaction centers found in the rare bacterial phylum Gemmatimonadetes, *Proceedings of the National Academy of Sciences*, 111: 7795-800.

Zhang Z, Huang L, Shulmeister VM, Chi Y-I, Kim KK, Hung L-W, Crofts AR, Berry EA, and Kim S-H. 1998. Electron transfer by domain movement in cytochrome bc1, *Nature*, 392: 677-84.

Zito F, and Alric J. 2016. Heme c_i or c_n of the cytochrome b_6f complex, a short retrospective. in, *Cytochrome Complexes: Evolution, Structures, Energy Transduction, and Signaling* (Springer).

Zito F, Finazzi G, Delosme R, Nitschke W, Picot D, and Wollman FA. 1999. The Qo site of cytochrome b6f complexes controls the activation of the LHCII kinase, *EMBO J*, 18: 2961-9.

Zito F, Finazzi G, Joliot P, and Wollman FA. 1998. Glu78, from the conserved PEWY sequence of subunit IV, has a key function in cytochrome b_6f turnover, *Biochemistry*, 37: 10395-403.

Zito F, Vinh J, Popot JL, and Finazzi G. 2002. Chimeric fusions of subunit IV and PetL in the b_6f complex of *Chlamydomonas reinhardtii* - Structural implications and consequences on state transitions, *J Biol Chem*, 277: 12446-55.

Zondlo NJ. 2013. Aromatic-proline interactions: electronically tunable CH/pi interactions, *Acc Chem Res*, 46: 1039-49.

Abstract

Sunlight is a powerful but fluctuating energy source used by photosynthetic organisms to power the assimilation of atmospheric CO_2 into reduced carbon compounds. To optimize photosynthetic efficiency in ever-changing light conditions, organisms of the green lineage regulate the distribution of energy input between the two photosystems through state transitions. This process is governed by the redox state of the membrane pool of quinones, liposoluble electron carriers. Through a yet unknown mechanism, the cytochrome (cyt) b_6f complex detects these redox changes and transmits a signal to the state transition kinase Stt7 for its activation. In order to decipher the role of the cyt b_6f, we devised a novel experimental strategy in *Chlamydomonas reinhardtii* combining the random mutagenesis of a chloroplast gene (*petD* coding for cyt b_6f subunit IV) by error-prone PCR, chloroplast transformation and selection of clones on phototrophic growth. Analysis of variant sequences allowing proper assembly and function of cyt b_6f revealed some interesting features on the mutational robustness of this subunit in the context of its large transmembrane protein complex. Transformants were then screened by chlorophyll fluorescence emission imaging on their ability to perform state transitions. Several state transition mutants were isolated, and sequencing revealed that mutations concentrated in the stromal fg loop of subunit IV. Site-directed mutagenesis of key fg loop residues showed that substitutions of Asn122, Tyr124 and Arg125 produced mutants that are blocked in State I independently of the redox state of the PQ pool and with no adverse effects on cyt b_6f assembly and electron transfer activity. Protein-protein interaction studies provided evidence that the kinase domain of Stt7 interacts with the subunit IV fg loop and that its autophosphorylation activity depends on Arg125. We propose a model for the interaction between these two proteins as well as for the cyt b_6f-mediated mechanism of Stt7 activation.

Keywords: photosynthetic efficiency, Chlamydomonas reinhardtii, state transitions, Stt7 kinase, cytochrome b_6f complex, structure-function, random mutagenesis, error-prone PCR, chlorophyll fluorescence, protein interactions, kinase activation, Rieske/cyt b evolution.

Résumé

La lumière du Soleil est une source d'énergie puissante mais fluctuante utilisée par les organismes photosynthétiques pour permettre l'assimilation du CO_2 atmosphérique en espèces carbonées réduites. Pour optimiser l'efficacité photosynthétique en conditions de lumière changeantes, les organismes de la lignée verte régulent la distribution de l'excitation lumineuse entre les deux photosystèmes grâce aux transitions d'état. Ce processus est modulé par l'état redox du réservoir membranaire de quinones, des transporteurs d'électrons liposolubles. Par un mécanisme encore inconnu, le cytochrome (cyt) b_6f détecte ces changements redox et transmet un signal d'activation à la kinase des transitions d'état, Stt7. Afin de comprendre le rôle du cyt b_6f, nous avons mis au point une nouvelle stratégie expérimentale chez *Chlamydomonas reinhardtii* combinant la mutagénèse aléatoire d'un gène chloroplastique (*petD* codant pour la sous-unité IV du cyt b_6f) par PCR error-prone, la transformation chloroplastique et la sélection des clones sur leur croissance phototrophe. L'analyse des séquences variantes permettant l'assemblage et le fonctionnement du cyt b_6f a révélé certaines caractéristiques intéressantes de la robustesse de cette sous-unité aux mutations dans le contexte du complexe protéique transmembranaire auquel elle appartient. Les transformants ont ensuite été criblés par imagerie de l'émission de fluorescence de la chlorophylle sur leur capacité à réaliser des transitions d'état. Plusieurs mutants de transitions d'état ont été ainsi isolés, et le séquençage a révélé que les mutations impliquées étaient concentrées sur la boucle stromale fg de la sous-unité IV. La mutagénèse dirigée de plusieurs résidus clés de la boucle fg a montré que les substitutions des résidus Asn122, Tyr124 et Arg215 généraient des mutants bloqués à l'état I indépendamment de l'état redox du pool de quinones et sans effets défavorables sur l'assemblage et l'activité de transfert d'électrons du complexe. Des expériences d'interaction protéine-protéine ont ensuite servi à prouver que le domaine kinase de Stt7 interagit avec la boucle fg de la sous-unité IV et que son activité d'autophosphorylation dépend du résidu Arg125. Nous proposons un modèle de l'interaction entre ces deux protéines ainsi que du mécanisme d'activation de la kinase médié par le cyt b_6f.

Mots-clés : efficacité photosynthétique, Chlamydomonas reinhardtii, transitions d'état, kinase Stt7, complexe cytochrome b_6f, structure-fonction, mutagénèse aléatoire, PCR error-prone, fluorescence de la chlorophylle, interactions protéiques, activation de kinase, évolution des complexes Rieske/cyt b.